Journal of Sea Research 208 (2025) 102646

Contents lists available at ScienceDirect

Journal of Sea Research

journal homepage: www.elsevier.com/locate/seares

Feeding selectivity and gametogenic cycle of *Crassostrea madrasensis* in relation to seasonal plankton and environmental variability in the southeast coast of the Bay of Bengal, Bangladesh

Khandakar Zakir Hossain [a,b], Israt Jahan [a], Md Nayeem Hossain [a,c], Afshana Ferdous [a,d], Md. Ramzan Ali [a], Md Moshiur Rahman [e], Mohammad Sadequr Rahman Khan [a], Md Asaduzzaman [a,*]

[a] Department of Marine Bioresource Science, Faculty of Fisheries, Chattogram Veterinary and Animal Sciences University, Khulshi, 4225, Chittagong, Bangladesh
[b] Division of Post-Harvest Technology, Faculty of Fisheries, Sher-e-Kashmir University of Agricultural Sciences and Technology of Kashmir, Shalimar 190025, India
[c] Department of Marine Fisheries and Aquaculture, Faculty of Earth and Ocean Science, Bangladesh Maritime University, Dhaka, 1216, Bangladesh
[d] Department of Marine Fisheries and Oceanography, Faculty of Fisheries and Marine Science, Sher-e-Bangla Agricultural University, Dhaka, 1207, Bangladesh
[e] Fisheries and Marine Resource Technology Discipline, Khulna University, Khulna, 9208, Bangladesh

ARTICLE INFO

Keywords:
Crassostrea madrasensis
Estuarine bivalve
Selective feeding behaviors
Plankton assemblage
Eco-physiological drivers
Gametogenic cycle
Bay of Bengal

ABSTRACT

The feeding behaviour of the Indian backwater oyster (*Crassostrea madrasensis*), a key estuarine filter-feeding bivalve native to the dynamic coastal waters of the Bay of Bengal, is intricately linked to a complex interplay of external environmental conditions and internal physiological processes. This study investigated the selective feeding behaviour of *C. madrasensis* over a complete annual cycle (July 2023–June 2024) along the southeast coast of Bangladesh, employing an integrated multivariate approach to elucidate how seasonal variations in plankton assemblages and environmental conditions influence feeding selectivity and the reproductive cycle of *C. madrasensis*. Various multivariate analyses revealed that water quality parameters, plankton abundance, and ingested gut plankton exhibited significant seasonal variability, driven by monsoonal hydrodynamics and nutrient influx. Environmental parameters such as temperature and turbidity were negatively associated, while chlorophyll-a and dissolved nutrients were positively correlated with both plankton availability and ingestion. Analysis of gut contents revealed that *C. madrasensis* selectively ingested specific plankton genera/groups, with clear seasonal positive selection for 17 genera/groups, including *Amphidinium* (17.5 % of total ingestion), *Skeletonema* (15.1 % of total ingestion), *Coscinodiscus* (12.0 % of total ingestion), and *Cyclotella* (10.8 % of total ingestion) comprised the highest proportions. Cluster analyses showed peak ingestion during the post-monsoon and late autumn months, coinciding with elevated chlorophyll-a concentrations and nutrient levels in the water column. The seasonal shifts in feeding selectivity corresponded with environmental changes and gonadal development phases, indicating an adaptive response to both external ecological factors and internal physiological cues. During the post-monsoon gametogenic phase, multivariate patterns suggest greater reliance on ingested food to support gamete maturation. In contrast, patterns observed during the pre-monsoon period are consistent with increased use of stored reserves, although continued feeding on smaller planktonic cells cannot be ruled out. These findings from these broad datasets provide valuable insights into the ecological adaptability of *C. madrasensis*, informing sustainable oyster farming strategies and enhancing resilience in coastal aquaculture systems in monsoon-influenced tropical environments like the Bay of Bengal.

1. Introduction

Marine food production has increasingly emerged as a critical sector to meet the growing global demand for protein (Costello et al., 2020; Free et al., 2022). Bivalve farming has gained global prominence due to its simplicity, cost-effectiveness, and ecological sustainability, requiring

* Corresponding author at: Department of Marine Bioresource Science, Faculty of Fisheries, Chattogram Veterinary and Animal Sciences University, Khulshi 4225, Chattogram, Bangladesh.
E-mail address: a_zamanbau@yahoo.com (M. Asaduzzaman).

https://doi.org/10.1016/j.seares.2025.102646
Received 11 July 2025; Received in revised form 15 November 2025; Accepted 16 November 2025
Available online 17 November 2025

minimal infrastructure and no supplemental feed (O'Shea et al., 2019). Global mollusc aquaculture, including oysters, clams, cockles, scallops, mussels, and others, produced approximately 18.9 million tonnes in 2022 (FAO, 2024) and continues to expand owing to increasing demand for sustainable, low-trophic seafood and ecosystem services such as carbon sequestration, habitat provision, and water purification (Cabre et al., 2021; Theuerkauf et al., 2021; Willer et al., 2021). In Asia, where mariculture sustains coastal livelihoods and food security (Ahmed and Thompson, 2019; Krause et al., 2019; Smaal et al., 2019), bivalve farming offers a sustainable means to enhance seafood production without depleting wild stocks (Jacquet, 2017; Willer et al., 2021). Consequently, a thorough understanding of the feeding biology of marine bivalves is essential to provide scientifically sound recommendations for the sustainable management and commercial farming of marine bivalves.

Bangladesh's coastal and maritime waters host diverse oyster species (Siddiqui et al., 2007). Among the various species of *oysters*, *Crassostrea madrasensis,* commonly known as the Indian backwater oyster, stands out as a prominent bivalve found primarily in the estuarine and coastal waters along the Bay of Bengal, Bangladesh (Asaduzzaman et al., 2025). Like other marine bivalves, *C. madrasensis* is a filter feeder that ingests organic particles, with plankton as its main food source (Meitei et al., 2025; Thangavelu, 1988). Thus, its feeding biology is closely linked to coastal hydrodynamics and seasonal plankton dynamics, both driven by the monsoonal climate. The Bay of Bengal experiences marked shifts between wet (June–September) and dry (October–May) periods, regulated by the southwest monsoon (Sarker et al., 2021; Singh et al., 2014), which alters salinity, turbidity, nutrients, and temperature (Achary et al., 2014; Madhupratap et al., 2003). During the wet monsoon, heavy rainfall, about 80 % of the annual 3740 mm, causes strong riverine discharge, reducing salinity and water transparency but enriching surface waters with nutrients, influencing plankton abundance and composition (BMD, 2017; Das et al., 2017; Mukhopadhyay et al., 2006). Furthermore, stratification of the surface water layer during the monsoon months often limits the upward movement of nutrient-rich waters from the deeper ocean to the surface (Kumar et al., 2001). Conversely, the dry season stabilizes salinity and nutrients, promoting post-monsoon plankton growth (Choudhury and Pal, 2010; Singh and Kumar, 2021). These seasonal fluctuations in plankton communities strongly influence *C. madrasensis* feeding strategies, underscoring the need to examine how plankton dynamics shape oyster feeding behaviors.

Marine bivalves can adjust selective ingestion by modulating filtration rates in response to changing environmental conditions (Cranford et al., 2016; Rosa et al., 2018). Selective feeding is a complex eco-physiological trait, enables oysters to regulate food intake based on particle size and quality to support growth, reproduction, and health (Dupuy et al., 2000; Prasetiya et al., 2017). This ability is especially advantageous in estuarine systems associated with the Bay of Bengal, where suspended particulates include both organic nutrients (e.g., phytoplankton) and non-nutrient (e.g., inorganic silt) components. In *C. madrasensis*, feeding selectivity is mediated by labial palps and ciliated gills that sort particles by size and biochemical quality, ingesting nutritious particles and rejecting others as pseudofeces (Ward and Shumway, 2004). However, selection efficiency varies among species due to structural and behavioral differences (Hawkins et al., 1988; Ward et al., 1998). Oysters also adjust selection in response to environmental factors, including plankton quality and availability (Pales Espinosa et al., 2007). During high turbidity in the wet season, selective feeding minimizes low-quality ingestion and supports growth and reproduction. Thus, studying this behaviour under varying seasonal conditions is critical for improving oyster farming and understanding their ecological roles in the Bay of Bengal.

Eco-physiological drivers such as gametogenic cycles, metabolic rates, and stress tolerance also influence feeding behaviour (Enríquez-Díaz et al., 2009; Karray et al., 2015; Ubertini et al., 2017). The gametogenic cycle of *C. madrasensis* is energy-intensive and tightly linked to ecological cues like temperature, salinity, and phytoplankton availability (Gosling, 2003; Ojea et al., 2004). Depending on conditions, oysters may adopt opportunistic or conservative strategies for energy allocation (Bayne, 1976; Berthelin et al., 2000; Kang et al., 2000; Lopes-Lima et al., 2014; Asaduzzaman et al., 2019). It is essential to determine whether *C. madrasensis* derives energy directly from food during favourable conditions or mobilizes stored reserves during stress (Hassan et al., 2018; Pouvreau, 2000). Energy demand peaks during pre-spawning and spawning, elevating filtration rates (Li et al., 2009; Mendo et al., 2016), while post-spawning phases emphasize somatic maintenance with reduced feeding. Thus, feeding intensity and selectivity in oysters are influenced by both external food availability and internal physiological priorities throughout the reproductive season (Barr et al., 2024; Bourlès et al., 2009). Yet, the interrelations among feeding selectivity, seasonal plankton dynamics, and eco-physiological factors remain poorly understood in *C. madrasensis* and other marine bivalves (Asaduzzaman et al., 2020; Geetha et al., 2007; Noor et al., 2021; Saurel et al., 2007).

This study aimed to elucidate how seasonal variations in plankton assemblages and environmental conditions influence feeding selectivity and the reproductive cycle of *C. madrasensis* along the southeast coast of the Bay of Bengal. Year-round data were analyzed to evaluate seasonal variability in taxonomic assemblages of water and gut plankton. Selectivity indices were calculated to determine selective ingestion patterns and adaptive feeding strategies during key reproductive stages. Finally, comprehensive multivariate analyses were performed to explore the linkages among eco-physiological factors, plankton dynamics, and selective feeding behaviour. Understanding these relationships is crucial for predicting oyster responses to environmental variability and improving productivity and resilience in coastal aquaculture systems.

2. Materials and methods

2.1. Sampling strategies of C. madrasensis

Mature specimens of the Indian backwater oyster (*C. madrasensis*) were collected from two designated sampling sites within the Moheshkhali Channel, located in Cox's Bazar, Bangladesh (Fig. 1). This estuarine channel, situated along the southeastern coastline, is directly connected to the Bay of Bengal and is recognized as a natural breeding ground for *C. madrasensis*. From July 2023 to June 2024, approximately 25–30 adult oysters (shell length $>$ 80 mm) were randomly sampled each month by local tribal fishers. The collected specimens were immediately transferred to the field laboratory with sufficient seawater at the Coastal Biodiversity, Marine Fisheries, and Wildlife Research Centre, Chattogram Veterinary and Animal Sciences University (CVASU), located at Dorianagar, Cox's Bazar. Upon arrival, the oysters were thoroughly cleaned using stiff brushes to remove biofouling organisms, sediment, and other debris, followed by rinsing with clean water. For monthly gut plankton analysis, 10 individuals were randomly selected from each monthly sample. To correlate gut content with reproductive phases, the corresponding oysters were macroscopically examined to assess gonadal development. Individuals showing visible signs of gametogenesis, excluding those in resting or undifferentiated stages, were assigned unique identification codes. A small portion of gonadal tissue from each coded oyster was preserved in fixative (Bouin's solution) in labelled vials for histological examination to confirm the maturity stage. Once the maturity stage was verified, the corresponding gut plankton data for each coded individual were linked to its confirmed gonadal development stage.

2.2. Observation of environmental parameters

All water samples were collected in the morning during low tide conditions. Temperature (°C), salinity (ppt), pH, and dissolved oxygen

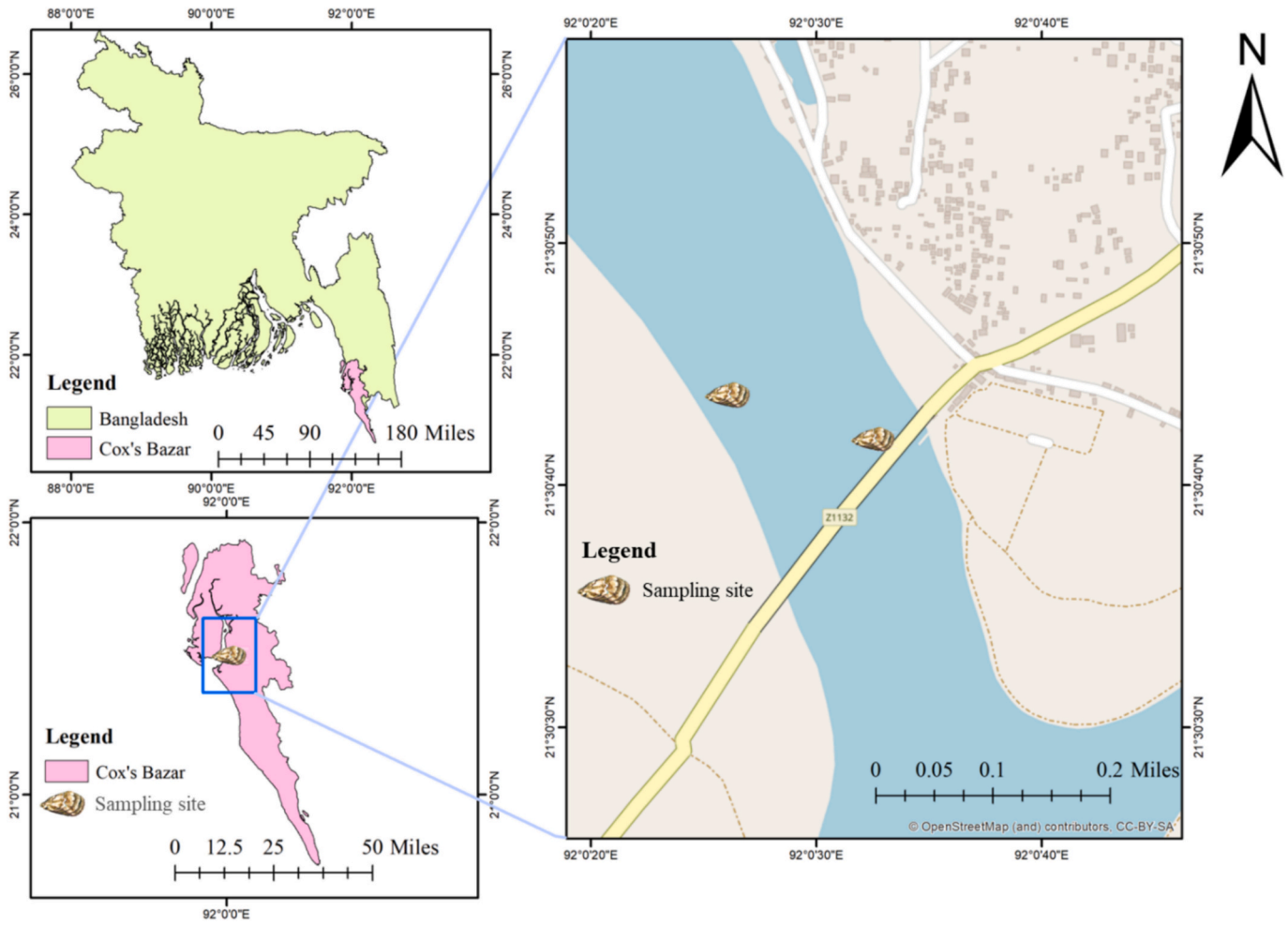

Fig. 1. Map showing the collection sites for *Crassostrea madrasensis* along the southeastern coast of the Bay of Bengal, Bangladesh.

(DO, mg/L) were recorded monthly in triplicate at each sampling site using a multifunctional environmental sensor (YSI, Loveland, CO, USA). For nutrient analysis (NO_3-N, NO_2-N, NH_3-N, and PO_4-P), triplicate water samples were collected in 500 mL plastic bottles and transported to the laboratory under ice-storage conditions. Subsamples of 10 mL were used to analyze NO_2-N, NH_3-N, and PO_4-P, while 1 mL subsamples were used for NO_3-N analysis using spectrophotometry (PhotoFlex STD, WTW, Weilheim, Germany), following APHA (1992) guidelines. Turbidity was measured in triplicate using 10 mL subsamples and a digital turbidity meter (Turb 430 IR, WTW, Weilheim, Germany). Additional water quality parameters were assessed using 1-l composite samples (collected in triplicate) obtained with a vertical water sampler (1200-E Kemmerer, WildCo, FL, USA) from each site. Total suspended solids (TSS, mg/L) were determined from 500 mL of these samples using the gravimetric method described by Wahab et al. (2018). For chlorophyll-a analysis, the remaining 500 mL of each water sample was filtered through a Whatman GF/C glass microfiber filter paper using a vacuum pressure air pump. Chlorophyll-a concentrations were then measured spectrophotometrically at wavelengths of 664, 647, and 630 nm using a calibrated spectrometer (Optizen Pop 2102, Daejeon, Republic of Korea), following the method outlined by Boyd (1979).

2.3. Qualitative and quantitative estimation of water plankton

To characterize the plankton assemblage within the particle size spectrum relevant to oyster feeding, 20 L of pooled subsurface water samples were collected monthly in triplicate from both sampling sites using a vertical water sampler (1200-E Kemmerer, WildCo, FL, USA). The collected water was filtered through a 20-μm mesh plankton net, and the resulting filtrate concentrate was collected and preserved in 150 mL plastic bottles containing 5 % buffered formalin. Samples were then transported to the Oceanography Laboratory at Chattogram Veterinary and Animal Sciences University (CVASU) for qualitative and quantitative analysis. Plankton quantification was performed using a Sedgewick-Rafter (S-R) cell containing 1000 grids, each with a volume of 1 mm^3, following the method described by Asaduzzaman et al. (2020). For each water sample, 1 mL aliquot of the sample in triplicate was loaded into the S-R cell, and plankton present in 10 randomly selected grids were counted under a binocular microscope (Optica B-190 TB, Ponteranica, Italy) equipped with a 10× ocular lens and 10 × − 40× objectives, providing total magnifications of 100× − 400×. Phytoplankton were identified to the genus level using taxonomic keys by Botes (2001) and Mitra et al. (2013). Zooplankton were further classified into major taxonomic groups according to Al-Kandari et al. (2009). The plankton abundance in water was determined using the formula: $N = (P \times C \times 100)/L$, where, N is the number of plankton cells (phytoplankton) or individual (zooplankton) per liter of original water, P is the average number of plankton measured in 10 fields, C is the volume (ml) of the final concentrate, and L is the volume (liter) of the water sample utilized. Larger meso- and macrozooplankton (> 500 μm) that could not be accommodated in the S-R cells were rare and were excluded from quantitative analyses.

2.4. Gonadal histological analyses

Gonadal tissues preserved in Bouin's solution were subjected to a graded ethanol-xylene dehydration series (ranging from 80 % to 100 % ethanol), followed by paraffin embedding using Paraplast®. The embedded tissues were then sectioned transversely at a thickness of 7 μm and mounted onto glass slides. To prepare the tissue sections for staining, a progressive alcohol dehydration protocol was applied. Slides were subsequently stained with Harris' hematoxylin and eosin following the method outlined by Pearse (1985). The stained sections were examined and photographed under a digital microscope (Optika B-190 TB, Ponteranica, Italy) at objective magnifications ranging from 10 to 40 × to assess gonadal development stages. Based on histological features, gonadal development was categorized into five distinct stages: resting, developing, mature, spawning, and spent, as described by Asaduzzaman et al. (2019).

2.5. Qualitative and quantitative estimation of gut plankton abundance

After dissection, stomach contents were collected using a glass pasteur pipette through a small slit beneath the crystalline style and diluted with a specific amount of distilled water. A 1-ml subsample was transferred to a Sedgewick Rafter Counting Cell (S–R cell), and all plankton in 10 randomly selected squares were identified up to the genus level and counted using a binocular microscope (Optica B-190 TB with digital facilities) equipped with a 10× ocular lens and 10 × − 40× objectives, providing total magnifications of 100× − 400×. Three subsamples from each gut sample were studied in the same way. Like water plankton, ingested phytoplankton in the gastrointestinal tract were also identified up to the genus level using keys by Botes (2001) and Mitra et al. (2013). Zooplankton were classified into different taxonomic groups according to Al-Kandari et al. (2009). The plankton abundance in the gut was determined using the following formula: $N = (P \times C \times 100)$, where N is the number of plankton cells (phytoplankton) or individuals (zooplankton) in the entire gut, P is the total number of plankton collected in 10 fields, and C is the volume of the sample's final concentrate in milliliters.

2.6. Determination of selective feeding indices

The feeding selectivity of oysters was assessed using the equation (Ivlev, 1961): $E' = (ag\text{-}aw)/(ag + aw)$, where E' = Ivlev's selectivity indices, ag = relative abundance (% of total plankton composition) of a plankton genus/group in the stomach content, and aw = relative abundance (% of total plankton composition) of the same plankton genus/group in the water column. The index values range from −1 (total avoidance) to +1 (complete preference), where 0 indicates random feeding.

2.7. Statistical analysis

All statistical analyses were conducted using R software, version 3.5.2 (R Core Team, 2024). Proportional data were initially expressed as percentages and subsequently transformed using the arcsine square root method to meet statistical assumptions. Normality of the data distributions was evaluated using the Shapiro–Wilk test, while homogeneity of variances was assessed through Levene's test, implemented via the 'onewaytests' package (Dag et al., 2017). To examine monthly variations across datasets, a univariate analysis of variance (ANOVA) was performed using the "car" package (Fox and Weisberg, 2019). Where significant differences were detected, Tukey's post hoc test was applied using the "multcomp" package (Hothorn et al., 2010) for multiple comparisons. All statistical inferences were made at a 95 % confidence level. Before conducting multivariate analyses, one-way ANOVA was applied specifically to the water quality data. Monthly trends in water and gut plankton composition were explored using hierarchical cluster analysis, employing Euclidean distance as the dissimilarity metric and the UPGMA (unweighted pair group method with arithmetic mean) algorithm for clustering. These analyses were performed using the 'dendextend' package (Galili, 2015). Relationships among the studied variables were assessed and visualized using correlation plots generated through the 'PerformanceAnalytics' package (Peterson and Carl, 2024). Principal component analysis (PCA) was conducted on all datasets using the 'FactoMineR' package (Lê et al., 2008), with interpretation based on the first two principal components, which accounted for the majority of the variance observed. A second PCA was applied to plankton relative abundance data to explore natural (unconstrained) patterns and seasonal overlap among communities. Canonical Variance Analysis (CVA) was carried out using the 'MASS' package (Venables and Ripley, 2002) to statistically assess and visualize group separation based on actual seasonal categories (summer, rainy, autumn, late-autumn, winter, and spring) or predefined seasonal monsoon categories (pre-monsoon, monsoon, post-monsoon). This analysis maximizes between-group variance relative to within-group variance, providing a quantitative test of distinct seasonal assemblages. All visualizations and graphical outputs were created using the 'ggplot2' package (Wickham, 2016).

3. Results

3.1. Seasonal variation in water quality parameters and plankton community dynamics

Water quality parameters at the oyster sampling sites exhibited pronounced seasonal fluctuations throughout the study period (Table 1). Temperature remained highest from July to September and gradually declined to the lowest values in December. Salinity showed an opposite pattern, increasing progressively from 12.7 ppt in July (monsoon) to peak values of 33.6 ppt during February–March (late winter to early pre-monsoon). Turbidity was extremely high during the monsoon months (July–September) and dropped sharply during post-monsoon and winter (October–January). Dissolved oxygen ranged from 6.0 to 7.4 ppm, with relatively higher levels during winter (December–February), whereas pH fluctuated moderately (7.1–8.3) without clear seasonal trends. Nutrient concentrations also showed strong seasonality; nitrate and phosphate were elevated during the monsoon and early post-monsoon. Chlorophyll-a levels followed a similar pattern, peaking during nutrient-rich post-monsoon and early winter and reaching a minimum during late pre-monsoon.

A total of 69 plankton genera/groups were identified from the coastal waters of the southeastern Bay of Bengal, comprising 61 phytoplankton and 8 zooplankton genera/groups (Fig. 2A). The phytoplankton community belonged to several taxonomic groups, including Coscinodiscophyceae (17 genera), Fragilariophyceae (5), Bacillariophyceae (21), Chlorophyceae (3), Cyanophyceae (6), and Dinophyceae (9). The zooplankton component included 8 genera/groups. Among these plankton, several genera/groups were consistently dominant across the study period, including *Bellerochea*, *Coscinodiscus*, *Cyclotella*, *Ditylium*, *Leptocylindricus*, *Melosira*, *Asterionellopsis*, *Fragilaria*, *Lioloma*, *Thalassionema*, *Chaetoceros*, *Lithodesmium*, *Nitzschia*, *Pleurosigma*, *Pseudo-nitzschia*, *Skeletonema*, *Anabaena*, *Oscillatoria*, *Ceratium*, *Protoperidinium*, *Pyrophacus*, Amphipoda, Copepoda, *Daphnia*, and *Moina* (Fig. 2A).

Multivariate analyses of plankton abundance along the southeast coast of the Bay of Bengal revealed strong seasonal dynamics in community composition (Fig. 2A). Analysis through hierarchical clustering, using Euclidean distance to assess dissimilarity, indicated January and February formed a distinct cluster with minimal diversity and dominance of a few plankton taxa. As the year progressed, especially from March to July, the community composition diversified, with increased contributions from a wider range of plankton taxa. The months from August to December displayed additional shifts, with October and December showing distinct planktonic structures, suggesting seasonal

Table 1
Monthly fluctuations in water quality parameters at sampling locations for *Crassostrea madrasensis* along the southeastern coast of the Bay of Bengal, Bangladesh. Data represent mean ± standard deviation (top row for each parameter) and observed ranges (bottom row) based on measurements from two sites. Statistical significance of one-way ANOVA is indicated by *p*-values, with asterisks denoting significance levels (***$p < 0.001$).

Water Parameters	Annual variation												Sig. level P-Value
	Jul	Aug	Sep	Oct	Nov	Dec	Jan	Feb	Mar	Apr	May	Jun	
Temp. (°C)	30.75 ± 0.11	32.53 ± 0.22	31.75 ± 0.1	28.38 ± 0.16	23.53 ± 0.38	22.3 ± 0.26	24.56 ± 0.24	25.53 ± 0.38	26.35 ± 0.25	27.27 ± 0.33	29.41 ± 0.27	29.5 ± 0.34	0.000***
	30.7–30.9	32.4–32.8	31.6–31.9	28.2–28.5	23.2–23.8	22.1–22.5	24.3–24.7	25.3–25.8	26.2–26.5	26.8–27.2	29.3–29.6	29.2–29.8	
Turbidity (NTU)	269.16 ± 5.4	334.83 ± 0.28.4	367.16 ± 5.5	71.76 ± 26.5	13.29 ± 6.1	11.6 ± 4.6	197.03 ± 77.6	119.73 ± 5.6	37.08 ± 32.3	89.03 ± 16.8	215 ± 40.9	283.16 ± 26.7	0.000***
	262–275	298–365	358–372	39.5–105	8.45–20.9	6.9–16.6	83.2–275	114–126	10.7–86	68.3–110	182–258	243–320	
DO (ppm)	6.07 ± 0.2	6.54 ± 0.1	6.10 ± 0.2	6.51 ± 0.3	7.28 ± 0.3	6.77 ± 0.3	7.29 ± 0.4	7.42 ± 0.3	6.79 ± 0.4	6.53 ± 0.4	6.68 ± 0.3	6.25 ± 0.2	0.000***
	5.84–6.33	6.04–6.72	5.88–6.24	6.14–6.90	6.8–7.48	6.4–7.12	6.94–7.78	7.02–7.81	6.28–6.94	6.12–7.00	6.14–6.90	5.98–6.42	
pH	7.633 ± 0.3	8.35 ± 0.1	8.15 ± 0.1	7.733 ± 0.2	7.633 ± 0.2	8.05 ± 0.1	7.983 ± 0.1	7.7 ± 0.3	7.9 ± 0.1	7.416 ± 0.37	7.166 ± 0.3	8.06 ± 0.1	0.000***
	7.3–7.9	8.2–8.5	8–8.3	7.5–8	7.5–7.8	8–8.1	7.9–8.2	7.0–8.0	7.8–8	7.0–8.0	7.0–7.5	8.0–8.2	
Salinity (ppt)	12.68 ± 0.2	18.53 ± 0.2	22.8 ± 0.4	26.8 ± 0.3	30.8 ± 0.7	32.85 ± 0.1	33.35 ± 0.1	33.66 ± 0.2	33.08 ± 0.2	32.15 ± 0.23	31.81 ± 0.3	28.63 ± 0.0	0.000***
	11.6–13.1	18.2–18.8	22.4–23.4	26.4–27.2	29.8–31.4	32.5–33.2	32.8–33.9	33.4–33.8	32.8–33.5	31.8–32.4	31.4–32.3	28.2–28.8	
TSS (ppm)	144.5 ± 5.4	161.4 ± 4.4	152.7 ± 6.1	85.8 ± 4.5	71.4 ± 5.4	73.8 ± 3.9	30.3 ± 2.8	55.8 ± 6.4	70.5 ± 3.8	50.5 ± 4.8	28.7 ± 1.8	41.7 ± 1.7	0.936NS
	138.8–150.5	156.8–166.5	145.4–159.7	80.4–90.3	65.6–77.2	68.9–77.4	26.9–33.5	49.6–62.7	66.2–74.8	44.8–55.4	26.5–30.8	39.4–44.4	
NO_3-N (ppm)	0.46 ± 0.1	0.49 ± 0.1	0.48 ± 0.1	0.55 ± 0.1	0.65 ± 0.1	0.52 ± 0.1	0.49 ± 0.1	0.4 ± 0.0	0.33 ± 0.1	0.29 ± 01	0.24 ± 0.0	0.20 ± 0.1	0.000***
	0.32–0.58	0.34–0.64	0.42–0.54	0.44–0.62	0.58–0.74	0.48–0.64	0.46–0.56	0.36–0.44	0.28–0.42	0.22–0.34	0.18–0.28	0.12–0.28	
PO_4-P (ppm)	1.26 ± 0.1	0.95 ± 0.1	0.83 ± 0.1	1.33 ± 0.1	1.64 ± 0.1	1.21 ± 0.1	1.31 ± 0.1	1.07 ± 0.1	0.83 ± 0.1	0.92 ± 0.1	0.70 ± 0.1	0.67 ± 0.1	0.000***
	1.12–1.52	0.84–1.04	0.74–1.02	1.14–1.64	1.48–1.74	1.03–1.48	1.24–1.38	0.98–1.12	0.68–0.98	0.84–1.02	0.64–0.88	0.62–0.78	
Chlo-a (μg/L)	6.81 ± 0.8	5.63 ± 0.3	4.78 ± 0.3	6.47 ± 0.3	7.66 ± 0.5	5.95 ± 0.3	6.54 ± 0.3	5.38 ± 0.8	5.09 ± 0.2	4.55 ± 0.5	4.01 ± 0.5	3.88 ± 0.2	0.000***
	6.12–7.74	5.27–6.02	4.38–5.20	6.12–6.76	7.02–8.45	5.58–6.25	6.12–7.12	4.88–6.01	4.86–5.27	4.12–5.58	3.45–4.88	3.58–4.22	

turnover associated with environmental transitions. (Fig. 2A). The PCA analyses supported this seasonal separation, with the first two dimensions explaining 58.8 % of the total variance in the dataset (Dim1: 37.7 %, Dim2: 21.1 %) (Fig. 2B). A clear separation was evident along the PCA axes for October, November, and December, setting them apart from the closely grouped remaining months. The PCA biplot further displayed the monthly shift of the dominant taxonomic group of water plankton (Fig. 2B). Coscinodiscophyceae, Bacillariophyceae, Chlorophyceae, and Cyanophyceae were more prevalent from October to December. In contrast, Fragilariophyceae peaked in August, while Dinophyceae showed the highest abundance in March. Notably, zooplankton reached their maximum abundance in August (Fig. 2B). The CVA analyses further clarified the seasonal clustering pattern, showing distinct month-wise groupings, with minimal overlap between certain periods such as March, August, and October (Fig. 2C). In contrast, the compact grouping of samples in some months (e.g., March, August) suggests more stable community composition during those periods (Fig. 2C).

A density plot analysis was also employed to examine seasonal trends in the abundance of various plankton groups in the water column (Fig. 3). During winter, Fragilariophyceae and zooplankton were dominant, indicating a mixed planktonic community with both diatom and zooplankton peaks. Summer exhibited an increased abundance of Chlorophyceae and Dinophyceae, with high densities of zooplankton, reflecting a nutrient-rich environment. The rainy season was characterized by the low to moderate densities of all groups of plankton. Autumn showed a diverse assemblage with an increase of Bacillariophyceae and overall total phytoplankton. Late autumn had a sharp dominance of total phytoplankton, accompanied by a resurgence in water Dinophyceae and zooplankton. These seasonal shifts highlight the dynamic nature of plankton communities, influenced by monsoonal patterns, nutrient fluxes, and hydrological conditions.

To assess how environmental factors influenced water plankton abundance, correlation analyses were conducted between ecological parameters and water plankton composition (Fig. 4). Temperature exhibited a significant negative correlation with several phytoplankton groups, including Coscinodiscophyceae ($r = -0.32$; $p < 0.001$), Chlorophyceae ($r = -0.53$; $p < 0.001$), Cyanophyceae ($r = -0.24$; $p < 0.01$), and Dinophyceae ($r = -0.19$; $p < 0.05$). Overall, phytoplankton abundance also showed inverse relationships with temperature ($r = -0.24$; $p < 0.01$). Turbidity was another factor that negatively impacted several plankton groups. Significant inverse correlations were observed for Coscinodiscophyceae ($r = -0.26$; $p < 0.01$), Bacillariophyceae ($r = -0.30$; $p < 0.001$), Chlorophyceae ($r = -0.47$; $p < 0.001$), Cyanophyceae ($r = -0.21$; $p < 0.05$), Dinophyceae ($r = -0.28$; $p < 0.01$), as well as total phytoplankton abundance ($r = -0.41$; $p < 0.001$). Conversely, salinity and dissolved oxygen (DO) showed no significant correlations with the majority of the plankton groups, except for a significant positive correlation with Chlorophyceae ($r = 0.25$; $p < 0.01$ and $r = 0.34$; $p < 0.001$, respectively). Chlorophyll-a concentration was also positively associated with the abundance of several plankton groups, including Bacillariophyceae ($r = 0.24$; $p < 0.01$), Chlorophyceae ($r = 0.37$; $p < 0.001$), Cyanophyceae ($r = 0.17$; $p < 0.05$), overall phytoplankton ($r = 0.33$; $p < 0.001$). Furthermore, concentrations of key nutrients such as nitrate (NO_3-N), nitrite (NO_2-N), and phosphate (PO_4-P) were positively correlated with the abundance of most plankton taxa, except Dinophyceae which did not exhibit significant responses to nutrient levels (Fig. 4).

A PCA analysis was further conducted to explore how environmental factors shape the plankton abundance and composition associated with the seasonal changes along the southeast coast of the Bay of Bengal, Bangladesh (Fig. 5). The analysis revealed that the first two principal components (PC1 and PC2) together accounted for 53.4 % of the total variance in the dataset. PC1 alone explained 33.9 % of the variation and was positively associated with most plankton taxa. This axis showed strong positive correlations with dissolved nutrients (NO_3, NO_2, and

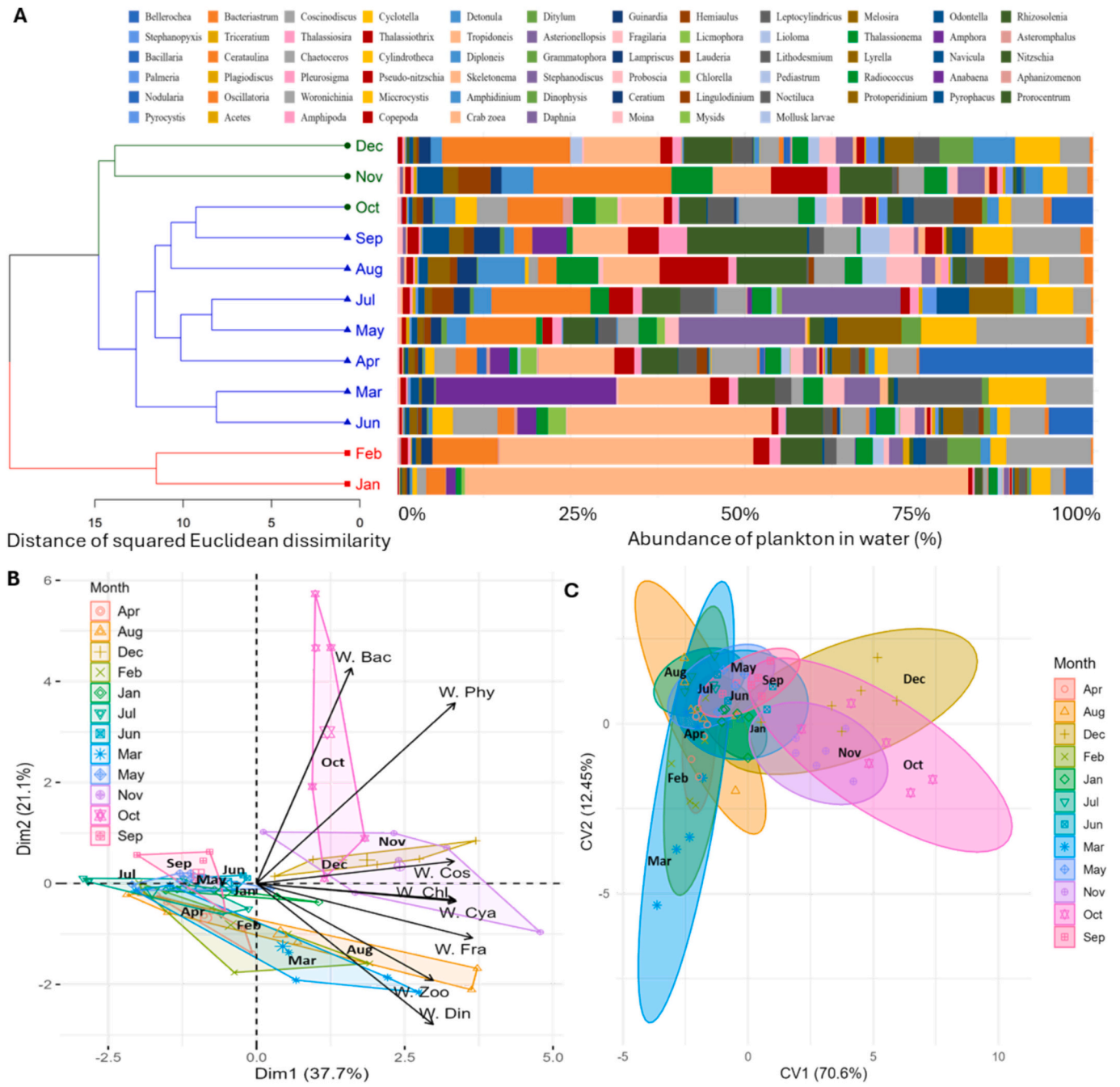

Fig. 2. Cluster and multivariate analyses depicting the monthly fluctuations in plankton abundance (cells or individuals/L) and composition in the water column at *Crassostrea madrasensis* collection sites along the southeastern coast of the Bay of Bengal, Bangladesh. (A) Dendrogram constructed using squared Euclidean distance to show dissimilarities in monthly water plankton composition (%). The sequential arrangement of groups within each stacked bar precisely mirrors their rank order as presented in the legend. (B) Principal Component Analysis (PCA) biplot illustrating variation in water plankton abundance across months. (C) Canonical Variate Analysis (CVA) biplot demonstrating monthly differences in water plankton abundance. Analyses are based on six replicates per month (3 replicates from each of 2 sampling sites) of water plankton data ($n = 72$).

PO_4), salinity, dissolved oxygen (DO), and chlorophyll-a concentrations, while being negatively correlated with temperature, turbidity, and total suspended solids (TSS). The PCA results suggested that elevated nutrient levels, particularly during October and November, were key drivers of high plankton abundance (Fig. 5). In contrast, distinct ecological conditions shaped plankton dynamics during other seasons. From April to June, species distributions were influenced by different environmental processes, while from July to August and September, elevated temperatures and turbidity levels were the dominant factors shaping plankton community structure and abundance along the Moheshkhali channel of the Bay of Bengal, Bangladesh.

3.2. Seasonal variation of ecological factors and plankton ingestion

Throughout the study period, a total of 53 plankton genera/groups were identified within the gastrointestinal tracts of *C. madrasensis*, comprising 47 phytoplankton and 6 zooplankton genera/groups (Fig. 6). These included representatives from several phytoplankton groups: Coscinodiscophyceae (14 genera), Fragilariophyceae (5), Bacillariophyceae (16), Chlorophyceae (3), Cyanophyceae (4), and

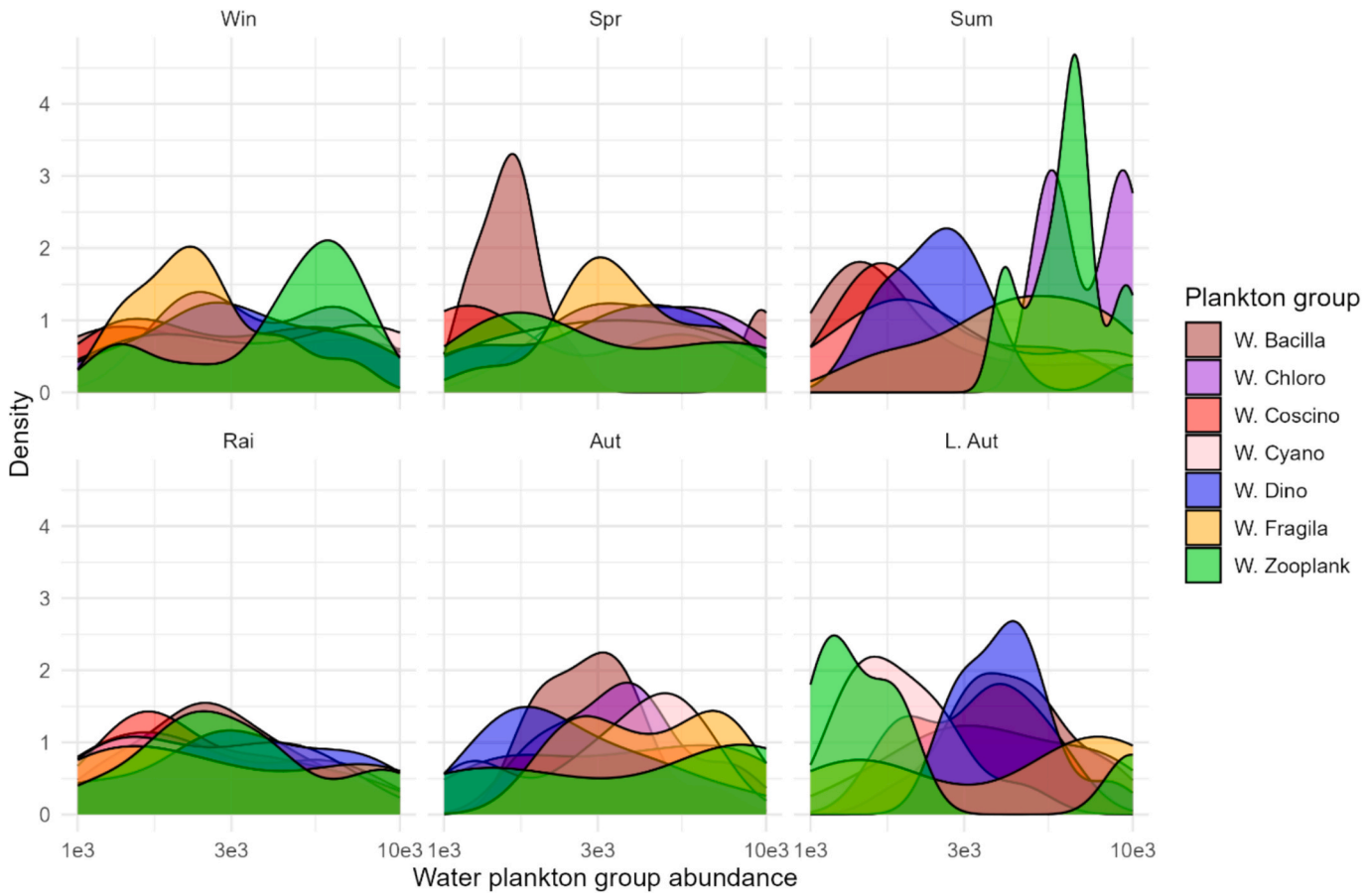

Fig. 3. Density plot of seasonal water plankton abundance at *Crassostrea madrasensis* collection sites along the southeastern coast of the Bay of Bengal, Bangladesh. The following abbreviations are used for the variables: W.Coscino – Coscinodiscophyceae in water; W.Fragila – Fragilariophyceae in water; W.Bacilla – Bacillariophyceae in water; W.Chloro – Chlorophyceae in water; W.Cyano – Cyanophyceae in water; W.Dino – Dinophyceae in water; W.Zooplank – water zooplankton, Win – Winter, Spr – Spring, Sum – Summer, Rai – Rainy, Aut – Autumn, L. Aut – Late Autumn. The scale is log10 of the actual abundance values (cells or individuals/L).

Dinophyceae (5), along with 6 genera/groups of zooplankton. The most frequently consumed genus was *Amphidinium*, which made up 17.51 % of the total ingested plankton, followed by *Skeletonema* (15.11 %), *Coscinodiscus* (11.95 %), and *Cyclotella* (10.76 %). Other notable genera/groups included *Lioloma*, *Thalassionema*, *Pleurosigma*, *Pseudo-nitzschia*, *Anabaena*, *Oscillatoria*, and members of Copepoda.

Various multivariate analyses of monthly plankton ingestion by *C. madrasensis* revealed marked temporal variations, indicating seasonal shifts in dietary composition (Fig. 6). Hierarchical clustering analysis demonstrated that January and February formed separate clusters, reflecting the dominance of a few taxa such as *Amphidinium*, *Nitzschia*, and *Skeletonema* (Fig. 6A). The spring and early summer months (March to May) exhibited a transitional phase, with more diverse plankton composition in the *C. madrasensis* gut, while a noticeable increase in taxonomic richness was observed from July to November. Notably, the gut content in November and December showed higher proportions of *Fragilaria*, *Skeletonema*, and larval forms such as copepods and mollusks (Fig. 6A).

The PCA analysis further supported these temporal shifts, with Dim1 and Dim2 explaining 24.1 % and 20 % of the variation, respectively (Fig. 6B). The PCA and CVA analyses revealed that the multivariate spaces of most of the months showed partial overlap, indicating varying degrees of similarity in ingested plankton, but with notable seasonal gradients (Fig. 6B-C). The multivariate spaces of February were completely separated from the other months (Fig. 6B) due to the excessive ingestions we noticed for the *Amphidinium* plankton. The ingestion of specific plankton groups also varied seasonally, as revealed by the visualization of CVA density plots (Fig. 7). During winter, ingestion was dominated by Dinophyceae and total phytoplankton, indicating a preference for phytoplankton groups likely driven by higher availability and nutritional content (Fig. 7). Spring showed continued dominance of total phytoplankton, accompanied by a notable presence of Chlorophyceae and Bacillariophyceae. In summer, ingestion is dominated by Coscinodiscophyceae and zooplankton. The rainy season exhibited elevated ingestion of Coscinodiscophyceae. Late autumn displayed an increased intake of Chlorophyceae and Dinophyceae. These seasonal patterns emphasize oysters' dietary plasticity, aligning plankton ingestion with temporal resource availability and physiological requirements (Fig. 7).

A correlation analyses were carried out linking ecological factors with the composition of plankton consumed to evaluate the impact of environmental variables on dietary intake (Fig. 8). Temperature exhibited significant negative correlations with the ingestion of Chlorophyceae ($r = -0.37$, $p < 0.001$) and Dinophyceae ($r = -0.26$, $p < 0.01$). Dissolved oxygen and chlorophyll-a concentrations were inversely correlated with zooplankton intake ($r = -0.26$, $p < 0.01$ and $r = -0.43$, $p < 0.001$, respectively). Additionally, salinity and turbidity negatively influenced the ingestion of Bacillariophyceae ($r = -0.60$, $p < 0.001$) and Chlorophyceae ($r = -0.36$, $p < 0.001$). Conversely, chlorophyll-a concentrations were positively correlated with the ingestion of all phytoplankton groups, reflecting higher feeding activity in response to greater primary productivity. Nutrient levels (NO_3-N, NO_2-N, PO_4-P) also showed positive associations with the ingestion of most phytoplankton groups. However, Fragilariophyceae and Dinophyceae showed negative correlations with nitrate ($r = -0.30$, $p < 0.001$) and nitrite ($r = -0.20$, $p < 0.05$), respectively. Zooplankton consumption was negatively

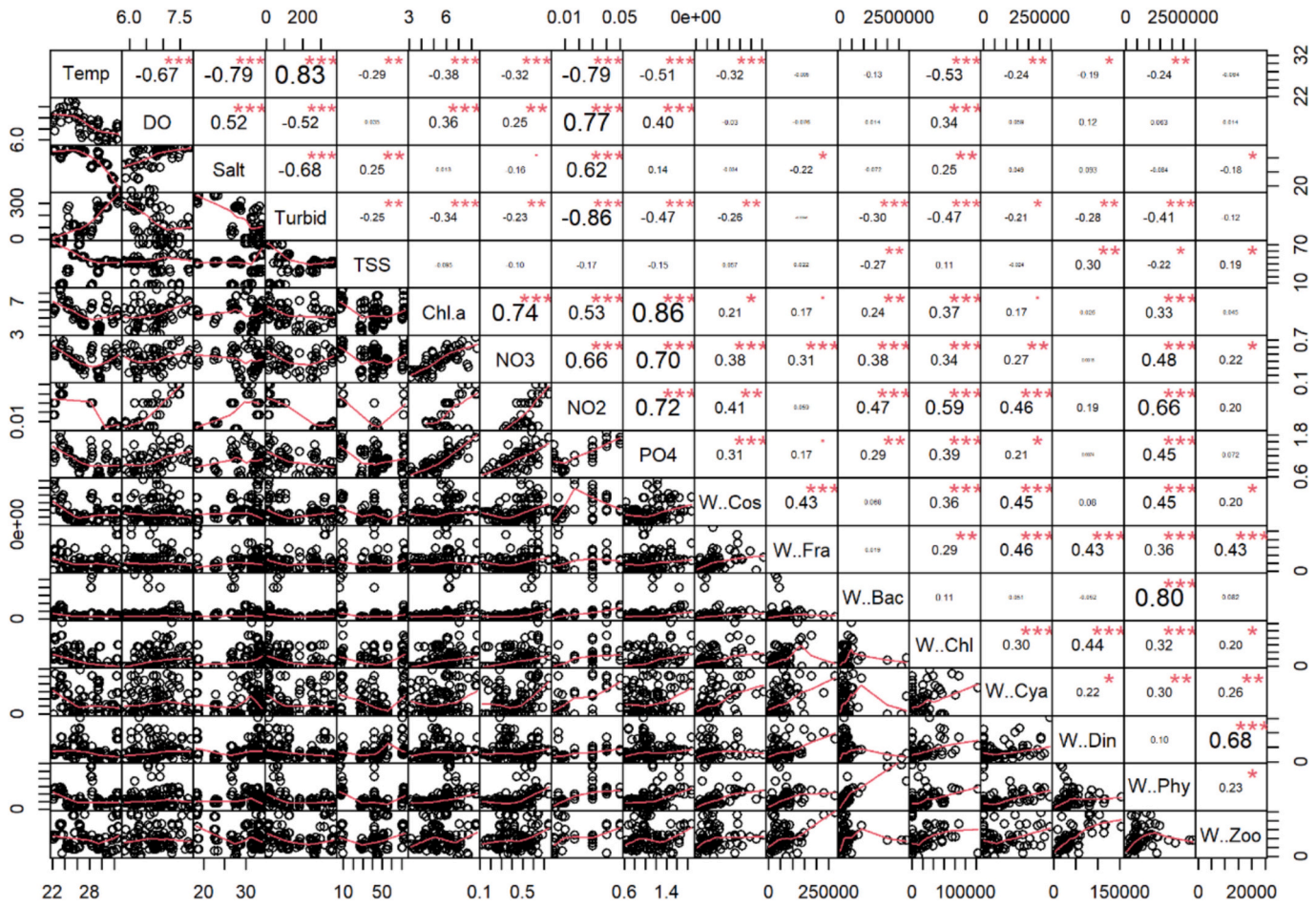

Fig. 4. Relationships between the annual fluctuations in water quality parameters and the monthly dynamics of plankton abundance (cells or individuals/L) found in the water column of *Crassostrea madrasensis* collection sites located across the southeast coast of the Bay of Bengal, Bangladesh. Here, the variables' full names are: Temp- water temperature (°C); DO- dissolved oxygen (ppm); Salt- salinity (ppt), Turbid- turbidity (NTU); TSS- total suspended solids (ppm); Chl.a- chlorophyll *a* (μg/L); NO3- nitrate-nitrogen (ppm); NO2- nitrite-nitrogen (ppm); PO4- phosphate-phosphorus (ppm); W.Cos – Coscinodiscophyceae in water; W.Fra – Fragilariophyceae in water; W.Baci – Bacillariophyceae in water; W.Chlo – Chlorophyceae in water; W.Cya – Cyanophyceae in water; W.Dino – Dinophyceae in water; W.Phyto – total water phytoplankton; W.Zoo – water zooplankton. The scale is log10 of the actual abundance values (cells or individuals/L). The values given around all the axes are the range of each individual parameter's measured unit values. Correlation coefficients (r) are indicated with numeric values, where the font size of r gets bigger as the correlation gets stronger. The significance levels (p) are denoted by asterisks (* < 0.05, ** < 0.01, *** < 0.001).

correlated with all three major nutrients: nitrate ($r = -0.53$, $p < 0.001$), nitrite ($r = -0.27$, $p < 0.01$), and phosphate ($r = -0.35$, $p < 0.001$).

To further examine the interaction between ecological factors, seasonality, and gut plankton composition, a multivariate PCA was performed (Fig. 9). The first two principal components (PC1 and PC2) accounted for 48.2 % of the total variance. PC1 (29.3 %) was positively associated with the ingestion of Coscinodiscophyceae, Chlorophyceae, Cyanophyceae, Dinophyceae, and total phytoplankton, and correlated positively with chlorophyll-a, DO, salinity, TSS, and nutrient levels (NO_3-N, NO_2-N, PO_4-P), while showing negative correlations with temperature and turbidity. PC2 (18.9 %) was primarily driven by Coscinodiscophyceae, Bacillariophyceae, Cyanophyceae, and total phytoplankton. It showed positive correlations with temperature, turbidity, chlorophyll-a, and nutrient concentrations, and negative associations with DO, salinity, and TSS. These results highlight that plankton ingestion by oysters between October and February was distinct from other months, likely reflecting the influence of seasonal ecological conditions on feeding behaviour (Fig. 9).

3.3. Selective ingestion of plankton by the oyster

Analysis of Ivlev's electivity indices revealed clear patterns of selective feeding behaviour by *C. madrasensis*, indicating that oysters did not ingest all available plankton taxa equally (Fig. 10). Out of the 69 plankton genera/groups identified in the surrounding water column, oysters showed positive selection for 17 genera/groups. These included two genera from Coscinodiscophyceae, one from Fragilariophyceae, six from Bacillariophyceae, two from Chlorophyceae, one from Cyanophyceae, one from Dinophyceae, and four zooplankton genera/groups (Fig. 10). Specifically, the oyster displayed positive electivity for *Coscinodiscus* and *Cyclotella* (within Coscinodiscophyceae), *Lioloma* (Fragilariophyceae), *Cylindrotheca*, *Lampriscus*, *Lauderia*, *Navicula*, *Nitzschia*, and *Pleurosigma* (Bacillariophyceae), *Chlorella* and *Pediastrum* (Chlorophyceae), *Anabaena* (Cyanophyceae), and *Amphidinium* (Dinophyceae). Among zooplankton, preferential consumption was observed for *Acetes*, Amphipoda, Copepoda, and mollusc larvae (Fig. 10). Of all groups, Bacillariophyceae emerged as the most selectively consumed group across the study period (Fig. 10B). Notably, the genus *Amphidinium* under the Dinophyceae group exhibited the highest electivity index (EI = 0.8), particularly during the months January and February (Fig. 10C). To assess seasonal trends in feeding selectivity, electivity indices of different groups of plankton were further analyzed by season using a bar graph (Fig. 11). The results indicated that oysters showed seasonal shifts in their plankton preferences. Genera/groups from Coscinodiscophyceae were most actively selected during the autumn months (October–November), while Fragilariophyceae were favoured in

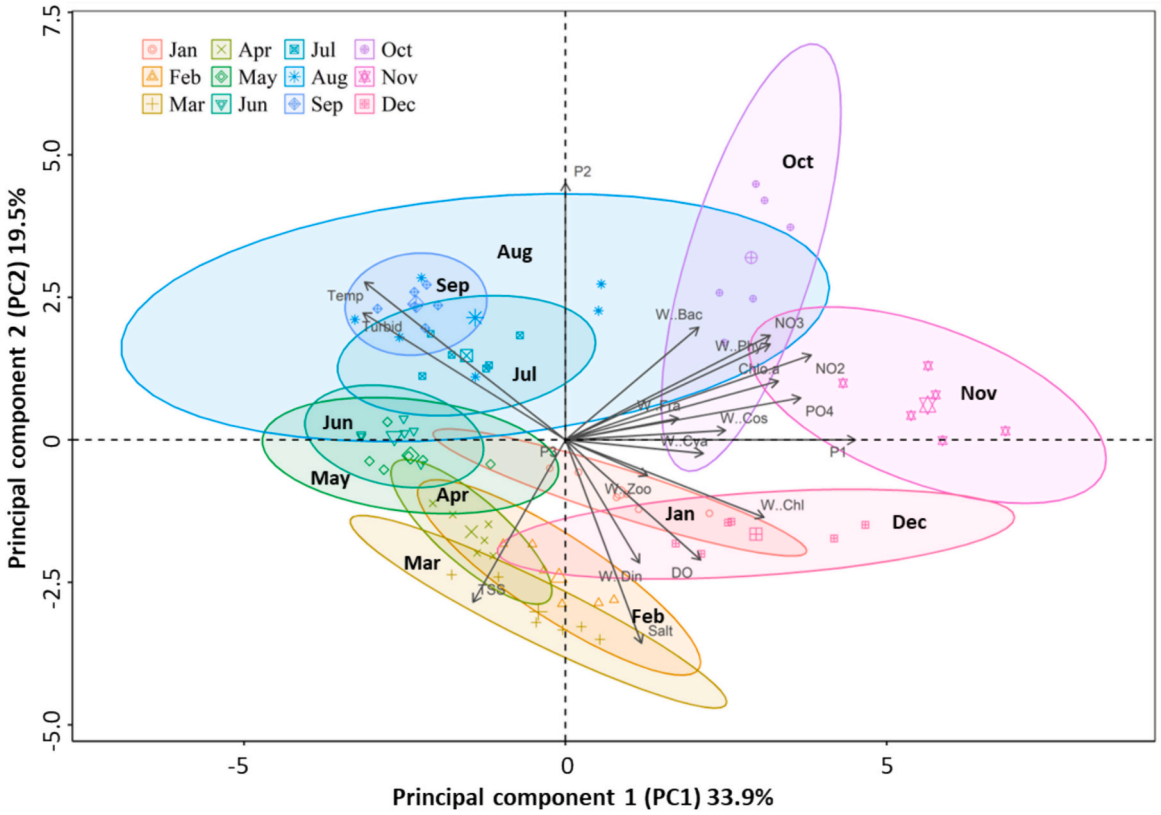

Fig. 5. Biplots of the principal component analysis (PCA) of the monthly variation of water plankton abundance from the oyster collection sites and ecological factors. The analysis consists of 6 observations of water quality parameters for each month (n = 72), 6 observations of water plankton abundance for each month (n = 72). Here, the variables' full names are: Temp- water temperature (°C); DO- dissolved oxygen (ppm); Salt- salinity (ppt), Turbid- turbidity (NTU); TSS- total suspended solids (ppm); Chlo.a- chlorophyll *a* (μg/L); NO3- nitrate-nitrogen (ppm); NO2- nitrite-nitrogen (ppm); PO4- phosphate-phosphorus (ppm); W.Cos – Coscinodiscophyceae in water; W.Fra – Fragilariophyceae in water; W.Baci – Bacillariophyceae in water; W.Chlo – Chlorophyceae in water; W.Cya – Cyanophyceae in water; W.Dino – Dinophyceae in water; W.Phyto – total water phytoplankton; W.Zoo – water zooplankton.

the summer (June). Oysters showed the highest selectivity for Bacillariophyceae during the monsoon season (July–August), and for Chlorophyceae immediately before and after the monsoon period (May and September). Cyanophyceae were preferentially consumed in autumn (October), Dinophyceae during winter (December to February), and zooplankton taxa during the summer months (May–June).

3.4. Plankton ingestion associated with the reproductive cycle

CVA was employed to evaluate the influence of plankton ingestion on the reproductive stages of *C. madrasensis* during pre-monsoon (March–June) and post-monsoon (October–February) gametogenic cycle. The analysis revealed distinct clustering patterns, particularly during the post-monsoon gametogenic cycle, that corresponded to different gonadal stages, indicating a strong relationship between gonadal development and dietary intake. During the pre-monsoon spawning phase (Fig. 12A), CV1 (61.26 %) and CV2 (28.60 %) explained 89.86 % of the total variation. While the multivariate spaces of gonadal stages showed marked overlap, mature and spawning stages formed partially distinct clusters, suggesting stage-specific plankton preferences or ingestion rates. Density plots (Fig. 12C) further supported these patterns, with mature and spawning stages exhibiting broader distributions across CV dimensions, indicative of selective and intensified plankton uptake during gametogenesis. Notably, the early developing stage showed relatively narrow distributions, suggesting lower dietary intake. In contrast, during the post-monsoon season, the first canonical axis (CV1) explained 59.76 % of the total variation, while the second axis (CV2) accounted for 35.54 % (Fig. 12B). The clustering showed clear segregation between spawning, mature, and other gonadal stages, suggesting dietary shifts associated with the post-monsoon gametogenic cycle (Fig. 12B).

The PCA analysis was further employed to investigate the patterns of plankton ingestion across different gonadal development stages of *C. madrasensis* during pre-monsoon (March–June) and post-monsoon (October–February) gametogenic cycle (Fig. 12E-F). In the pre-monsoon season (Fig. 12E), Dim1 and Dim2 accounted for 34.1 % and 27.7 % of the variance, respectively. The distribution of gonadal stages during pre-monsoon was more overlapping compared to the post-monsoon season, though some separation was still evident (Fig. 12E). During the post-monsoon season (Fig. 12F), Dim1 and Dim2 explained 47.5 % and 16.1 % of the total variation, respectively. Clear clustering of gonadal stages was observed in the post-monsoon gametogenic cycle, particularly with spent individuals separating from early developmental stages. Mature and spawning oysters were more closely associated with higher ingestion of overall total zooplankton and phytoplankton. In contrast, early and late developing stages were more associated with the higher ingestion of Cyanophyceae, Chlorophyceae, and Dinophyceae (Fig. 12 F). Overall, both the CVA and PCA analyses suggest that the *C. madrasensis* followed opportunistic schemes on plankton ingestion during the post-monsoon gametogenic cycle.

3.5. Interlinkages among seasonal plankton dynamics, the eco-physiology factor, and feeding behaviour.

A comprehensive PCA was conducted to better understand the complex interactions among feeding patterns, seasonal changes, environmental variables, plankton availability in the water column, and the reproductive phases of *C. madrasensis* (Fig. 13). This approach allowed for the integration and synthesis of insights derived from multiple previously described datasets, providing a holistic view of these

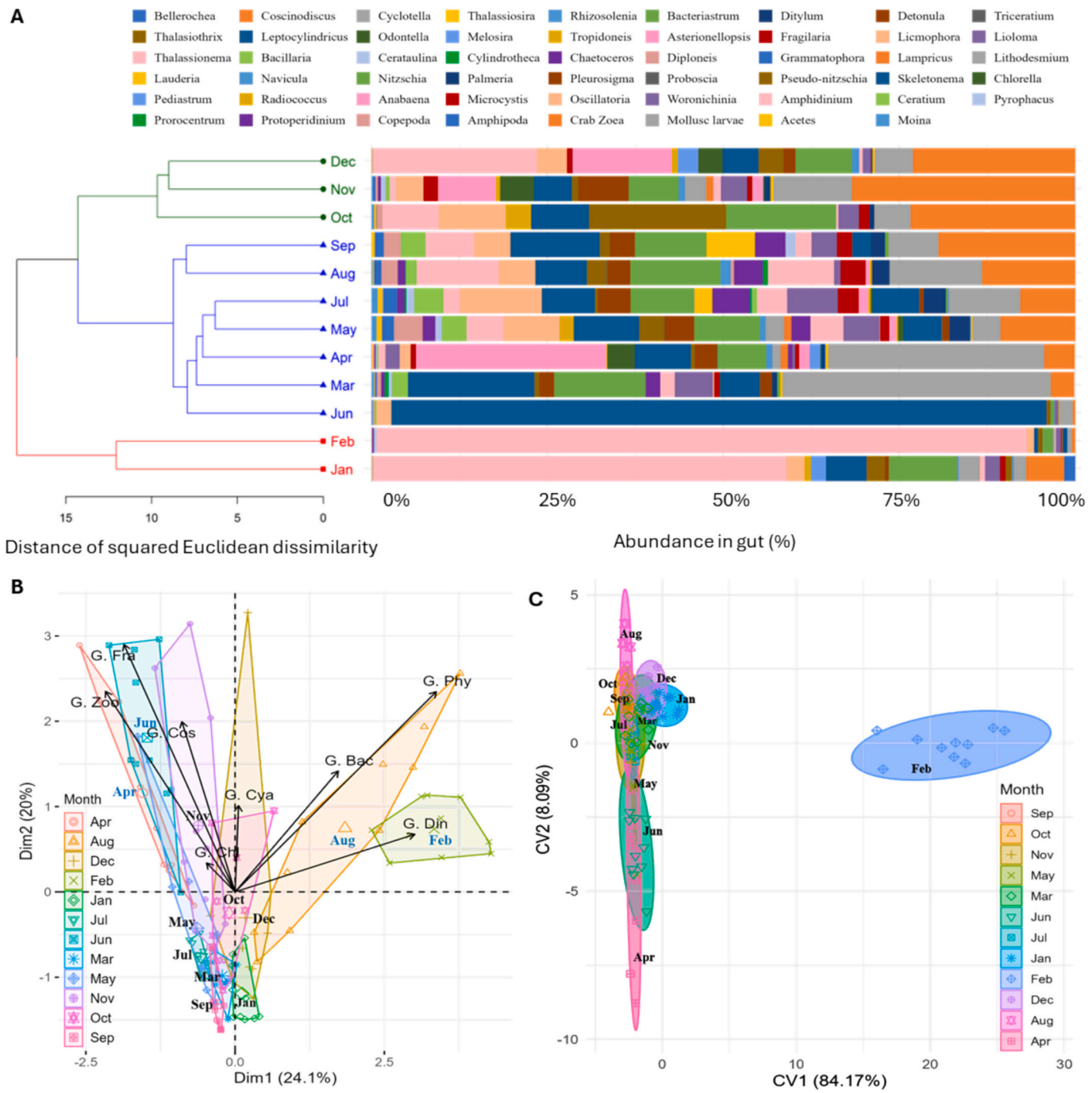

Fig. 6. Cluster and multivariate analyses illustrating the monthly variation in plankton communities (cells or individuals/oyster) within the gastrointestinal tract of *Crassostrea madrasensis*, collected from the southeastern coastal region of the Bay of Bengal, Bangladesh. (A) Dendrogram generated using squared Euclidean distance to reflect dissimilarities in monthly plankton composition (%). The sequential arrangement of groups within each stacked bar precisely mirrors their rank order as presented in the legend. (B) Principal Component Analysis (PCA) biplot depicting the distribution of monthly plankton abundance patterns. (C) Canonical Variate Analysis (CVA) biplot visualizing differentiation in plankton abundance across months. The analysis is based on the 10 replicated measurements of gut plankton data for each month ($n = 120$).

interconnected extrinsic ecological factors and intrinsic physiological processes. The first two principal components explain 36.6 % of the variance, with Dim1 (23.2 %) and Dim2 (13.4 %) distinctly segregating the pre-monsoon (March–June), monsoon (July–September), and post-monsoon (October–January) periods. Pre-monsoon months (March to June) are grouped in the negative space of Dim1 and Dim2, closely associated with higher water temperature and turbidity, aligning with gut contents somewhat enriched in zooplankton and Fragilariophyceae. Although the embedded bar chart of condition index values in Fig. 13 indicates that *C. madrasensis* follows a pre-monsoon gametogenic cycle primarily driven by elevated temperatures, this reproductive activity appears not to depend on the increased availability and ingestion of plankton. In contrast, post-monsoon months (October to January) occupy the positive space of Dim1, closely linked to increased salinity, dissolved oxygen, chlorophyll *a*, and nutrients, which correlate strongly with the elevated abundance of phytoplankton groups such as Coscinodiscophyceae, Cyanophyceae, and Dinophyceae in the water column. These months also exhibit higher concentrations of corresponding gut

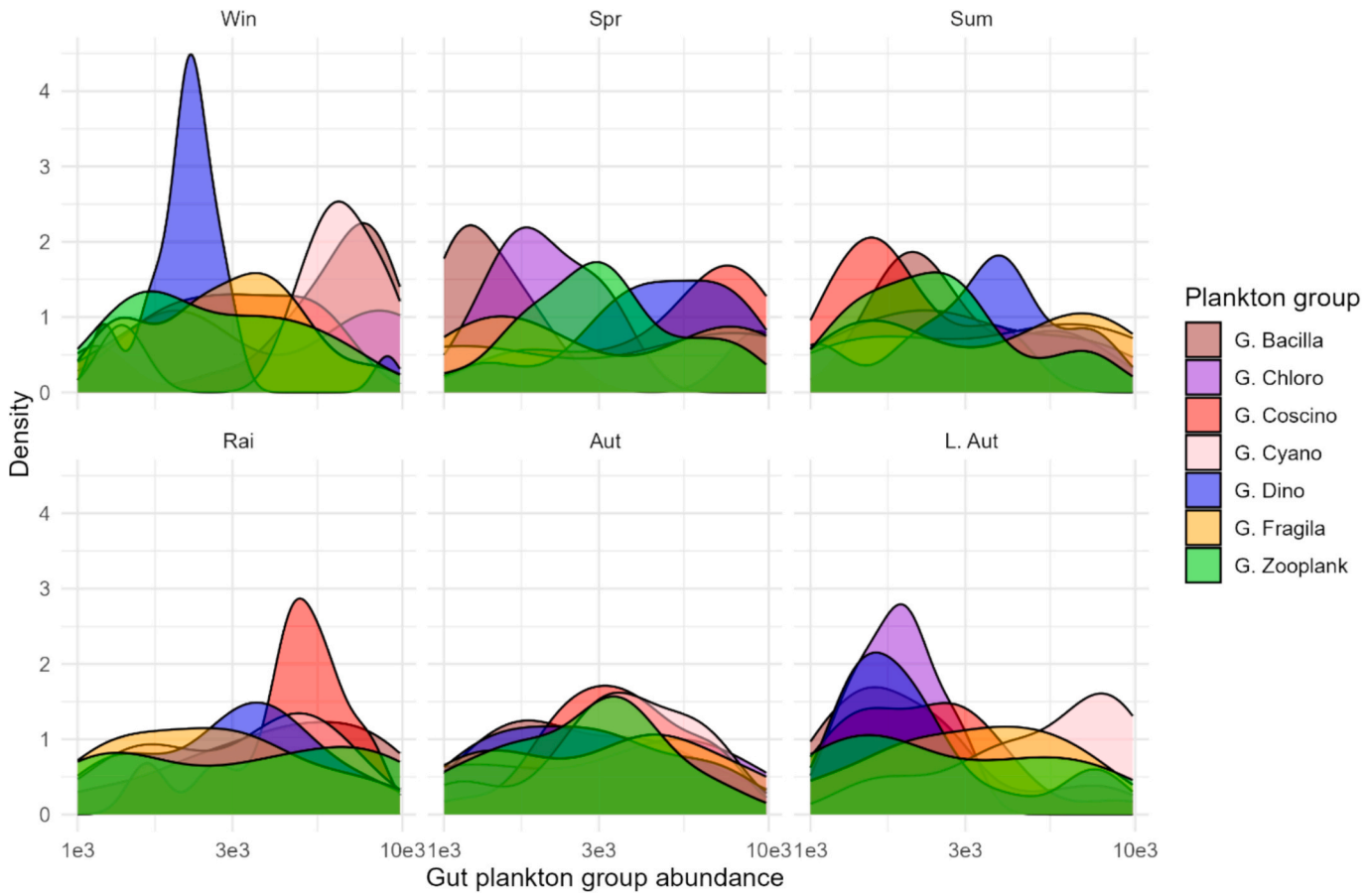

Fig. 7. Density plot of seasonal dynamics of plankton composition found in the gastrointestinal tract of *Crassostrea madrasensis*, sampled from the southeastern Bay of Bengal, Bangladesh. Here, G. Bacilla –Gut Bacillariophyceae, G. Chloro –Gut Chlorophyceae, G. Coscino –Gut Coscinodiscophyceae, G. Cyano –Gut Cyanophyceae, G. Dino –Gut Dinophyceae, G. Fragila –Gut Fragilariophyceae, G. Zooplank –Gut Zooplankton, Win – Winter, Spr – Spring, Sum – Summer, Rai – Rainy, Aut – Autumn, L. Aut – Late Autumn. The scale is log10 of the actual abundance values (cells/L).

contents.

4. Discussion

The present study elucidates the intricate interactions between environmental variability, plankton dynamics, and the feeding behaviour of *Crassostrea madrasensis* along the southeast coast of the Bay of Bengal. Seasonal fluctuations in hydrographic conditions and plankton availability exerted pronounced influences on oyster dietary composition, selective feeding patterns, and trophic adjustments across gametogenic cycles. The following discussion interprets these patterns in relation to environmental modulation, plankton community structure, and reproductive physiology, contextualizing them within broader ecological frameworks and previous studies from similar monsoon-driven coastal systems. However, before interpreting the feeding patterns, it is important to recognize that this study quantified only plankton larger than 20 μm. Smaller cells, which can be abundant in estuarine systems, were not included in the analysis due to methodological limitations. Their potential contribution to oyster feeding cannot be evaluated here, so the patterns reported in this study reflect only the identifiable fraction of the available food.

4.1. Seasonal rhythms and environmental modulations of plankton dynamics

Plankton communities are highly responsive to temporal fluctuations in physicochemical parameters, serving as key indicators of coastal water quality and ecosystem dynamics (Inyang and Wang, 2020; Srichandan et al., 2019; Asaduzzaman et al., 2020). The present study highlights pronounced seasonal shifts in plankton communities and water quality parameters in the southeastern Bay of Bengal, consistent with oceanographic processes in tropical monsoon-driven systems (see Figs. 2–5). Similar to other monsoon-influenced coasts, hydrographic variability and nutrient loading shaped plankton turnover (Manuri et al., 2020; Panigrahi et al., 2009). Freshwater inflow during the southwest monsoon reduced salinity and increased turbidity, suppressing light-dependent taxa (Noor et al., 2021; Khan et al., 2023), while nutrient dilution during peak monsoon months further constrained phytoplankton productivity (Asaduzzaman et al., 2020). In contrast, post-monsoon regeneration of nutrients and clearer waters promoted phytoplankton proliferation (Jewel et al., 2002; Asaduzzaman et al., 2025), producing algal maxima linked to nutrient enrichment as reported in earlier Bangladeshi coastal studies (Gopakumar et al., 2009; Khan et al., 2019; Asaduzzaman et al., 2020).

Seasonal structuring of the plankton community conforms to ecological succession theory, where environmental filters shape taxonomic composition (Gogoi et al., 2021; Vajravelu et al., 2022). The detection of 69 genera/groups (61 phytoplankton, 8 zooplankton) aligns with earlier reports (Asaduzzaman et al., 2019, 2020), though variations in dominance underscore regional specificity (Baho et al., 2020; Vanderploeg et al., 2023). Diversity peaked between March and July, likely due to optimal light and moderate nutrient conditions (Sarmento et al., 2010; D'Silva et al., 2012; Noor et al., 2021). PCA and cluster analyses identified post-monsoon to late autumn (October–December) as distinct, showing resurgence of Bacillariophyceae, Coscinodiscophyceae, and Dinophyceae (see Fig. 2B), groups commonly linked to upwelling or

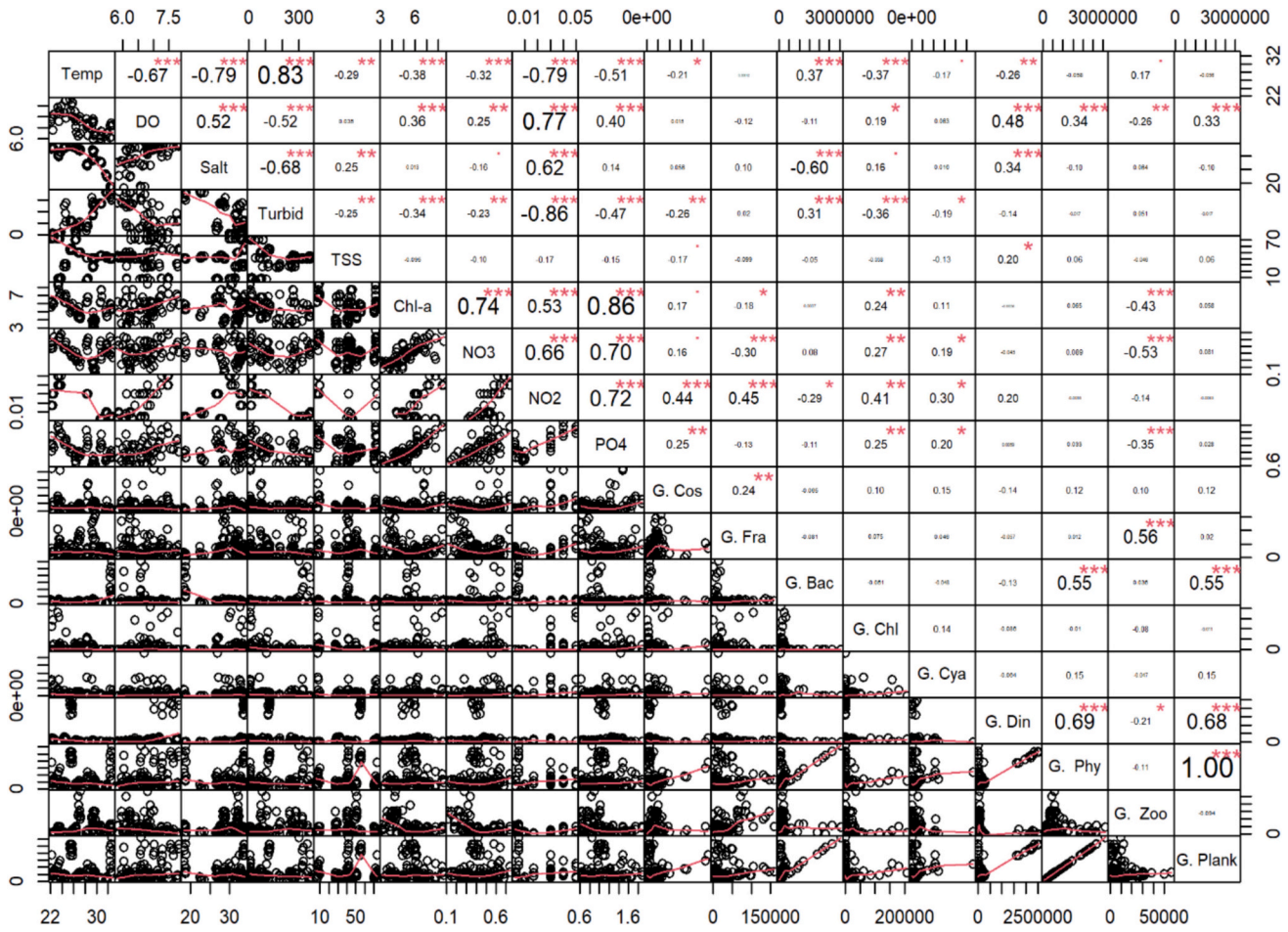

Fig. 8. Relationships between the annual fluctuations in water quality parameters and the monthly dynamics of plankton composition (cells or individuals/oyster) found in the gastrointestinal tract of *Crassostrea madrasensis*, sampled from the southeastern Bay of Bengal, Bangladesh. The variables are denoted as follows: Temp – water temperature (°C); DO – dissolved oxygen (ppm); Salt – salinity (ppt); Turbid – turbidity (NTU); TSS – total suspended solids (mg/L); Chl.a – chlorophyll *a* (μg/L); NO_3 – nitrate-nitrogen (ppm); NO_2 – nitrite-nitrogen (ppm); PO_4 – phosphate-phosphorus (ppm); G.Cos – gut Coscinodiscophyceae; G.Fra – gut Fragilariophyceae; G.Baci – gut Bacillariophyceae; G.Chlo – gut Chlorophyceae; G.Cya – gut Cyanophyceae; G.Dino – gut Dinophyceae; G.Phyto – gut phytoplankton; G.Zoo – gut zooplankton; G.Plank – total gut plankton. The axes display the measurement ranges for each parameter. Correlation coefficients (r) are presented numerically, with font size increasing proportionally to correlation strength. Asterisks indicate statistical significance levels: $p < 0.05$, $\boldsymbol{p} < 0.01$, $\boldsymbol{p} < 0.001$.

vertical mixing during monsoon retreat (Asaduzzaman et al., 2020; Islam et al., 2021). This period likely benefited from nutrient replenishment via monsoonal flushing, supporting the "flushing-and-blooming" model of tropical coasts (Jyothibabu et al., 2015; Patel et al., 2020). Density plots (Fig. 3) further illustrated succession patterns; summer's co-dominance of Chlorophyceae and Dinophyceae alongside elevated zooplankton densities suggests close trophic coupling (Gabaldón et al., 2019; Pershing et al., 2015). Such synchrony indicates strong bottom-up control in Bay of Bengal waters (Shin-ichiro et al., 2018; Susana et al., 2023). The transient Fragilariophyceae peak in August reflects nutrient pulses from monsoonal inflow (Madhu et al., 2007; Cloern and Jassby, 2010), while reduced densities in the rainy season confirm dilution effects and instability (Parakkandi et al., 2021; Patil and Anil, 2015). The spring dominance of Dinophyceae suggests nutrient stratification or local upwelling fostering dinoflagellate blooms (Sathish et al., 2022).

Environmental correlations emphasize abiotic control of plankton dynamics (Fig. 4). Temperature showed negative correlations with most phytoplankton groups, indicating thermal inhibition of cell division or increased metabolic loss (Berges et al., 2002; Low et al., 2018). Turbidity inversely affected abundance, highlighting light limitation during monsoon (Millette et al., 2021). Chlorophyceae alone correlated positively to salinity and DO, reflecting broad tolerance and preference for oxygenated, nutrient-enriched waters (Choi et al., 2010; Masmoudi et al., 2015). Chlorophyll-a, as a proxy for phytoplankton biomass, correlated positively with all groups (El-Shaarawi and Munawar, 1978; Van De Poll et al., 2013). Among nutrients, phosphate, nitrate, and nitrite were principal drivers of plankton growth, matching nutrient-limitation models for monsoon-driven coasts (Kamykowski et al., 2002; Malerba et al., 2012; Gera et al., 2023; Malik et al., 2015).

4.2. Ecological rhythms and feeding responses of C. madrasensis

Seasonal dietary variation in *C. madrasensis* reflects its adaptive response to changing plankton availability. The broad range of ingested taxa (Fig. 6) indicates dietary flexibility typical of suspension feeders inhabiting dynamic estuarine systems (Asaduzzaman et al., 2020; Hasan et al., 2021; Noor et al., 2021). Feeding activity was strongly influenced by environmental variables (Figs. 8–9). Negative correlations between temperature and ingestion of Chlorophyceae and Dinophyceae (Fig. 8) indicate thermal thresholds, particularly those exceeding 30 °C, may suppress feeding, consistent with findings in *C. virginica* and *Saccostrea glomerata* (Anestis et al., 2007; Pernet et al., 2007; Kinsella, 2019; Wang and Li, 2020). This does not necessarily imply reduced overall feeding, since oysters may still consume particles smaller than 20 μm that were not measured here. High turbidity constrained the feeding efficiency of

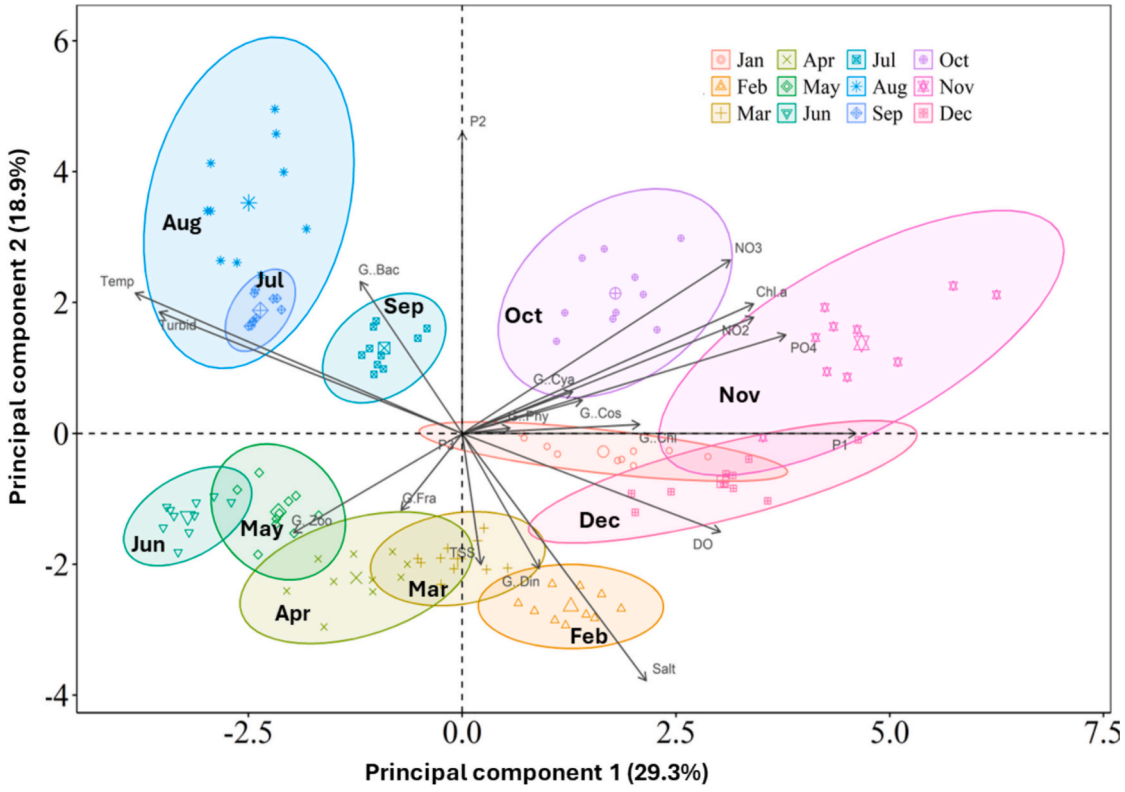

Fig. 9. Biplots of the principal component analysis (PCA) to depict the relationship between ecological factors and the monthly variation of ingested plankton (cells or individuals/oyster) in the gastrointestinal tract by *Crassostrea madrasensis* collected from the southeastern coast of the Bay of Bengal, Bangladesh. The analysis consists of 6 observations of water quality parameters (n = 72) and 10 observations of gut plankton abundance for each month (n = 120). The variables are denoted as follows: Temp – water temperature (°C); DO – dissolved oxygen (ppm); Salt – salinity (ppt); Turbid – turbidity (NTU); TSS – total suspended solids (mg/L); Chl.a – chlorophyll *a* (μg/L); NO_3 – nitrate-nitrogen (ppm); NO_2 – nitrite-nitrogen (ppm); PO_4 – phosphate-phosphorus (ppm); G.Cos – gut Coscinodiscophyceae; G.Fra – gut Fragilariophyceae; G.Baci – gut Bacillariophyceae; G.Chlo – gut Chlorophyceae; G.Cya – gut Cyanophyceae; G.Dino – gut Dinophyceae; G.Phyto – gut phytoplankton; G.Zoo – gut zooplankton; G.Plank – total gut plankton.

most phytoplankton groups in *C. madrasensis*, except Bacillariophyceae, as suspended sediments clog gills and increase sorting costs, whereas the larger, denser diatoms remain more easily retained and available under such conditions (Cranford et al., 2011; Madon et al., 1998; Barillé et al., 1997; Ward and Shumway, 2004). Reduced zooplankton ingestion during high DO and chlorophyll-a periods suggests dietary shifts toward abundant phytoplankton (Boltovskoy et al., 1995; Davenport et al., 2011). Chlorophyll-a correlated positively with nearly all phytoplankton groups ingestions, reinforcing its consistency as a proxy for plankton availability (Hasan et al., 2021; Galimany et al., 2017; Zhang et al., 2024). The observed link between phytoplankton ingestion and elevated concentrations of nitrate, nitrite, and phosphate (Fig. 8) reinforces the idea that nutrient-driven productivity enhances plankton availability, thereby promoting increased ingestion (Weissberger and Glibert, 2021). Inverse nutrient correlations for Fragilariophyceae and Dinophyceae may imply competition or seasonal bloom dynamics (Bode et al., 2005; Hambright and Zohary, 2000).

Multivariate analyses further reveal complex interactions between environmental factors and oyster feeding, particularly between post- and pre-monsoon periods (Figs. 6–7). Plankton composition in oyster guts varied significantly across seasons (Fig. 7), indicating adjustments to prevailing conditions (Villalejo-Fuerte et al., 2005; Yukihira et al., 1999). These shifts likely reflect changing metabolic demands, reproductive cycles, or optimization of energy intake under varying constraints (Hatzonikolakis et al., 2017; Villalejo-Fuerte et al., 2005). Distinct gut plankton assemblages during late autumn and winter, dominated by Dinophyceae and total phytoplankton, mirror patterns reported in temperate and tropical bivalves that favour a diet rich in plankton during cooler, nutrient-rich months (Kang et al., 2006; Lønborg et al., 2021). Salinity above 30 ppt during these periods may have enhanced feeding performance, as optimal filtration rates for *C. madrasensis* occur within this range (Chang et al., 2016; Do Nascimento et al., 2022). Higher DO and lower turbidity during these seasons are likely to promote efficient filtration and particle selection (Gray and Langdon, 2019; Perrino and Ruez Jr., 2019). During summer, increased consumption of zooplankton and Coscinodiscophyceae suggests a shift toward omnivory, possibly due to reduced phytoplankton biomass from stratification and higher metabolic demand in warm waters (Levinton, 2019; Weissberger and Glibert, 2021). The ingestion of copepods and molluscan larvae indicates exploitation of animal particles, compensating for phytoplankton scarcity or reduced quality. Rainy-season peaks in large centric diatoms (Coscinodiscophyceae) reflect nutrient-rich, turbulent conditions following monsoonal runoff (Hernández Almeida et al., 2019; Mukherjee, 2025), providing high-quality food for suspension feeders. Seasonal dominance of Cyanophyceae further suggests opportunistic incorporation despite lower palatability (Avila-Poveda et al., 2014; Poot-Delgado et al., 2018). The high abundance of *Amphidinium* likely reflects its richness in polyunsaturated fatty acids essential for bivalve growth and reproduction (Mendoza-Flores and Sánchez-Saavedra, 2023; Řezanka et al., 2017).

4.3. Selective ingestion strategies of plankton in C. madrasensis

Selective feeding is a crucial ecological trait in suspension-feeding bivalves, allowing them to optimize nutrient intake and maintain physiological homeostasis in environments with diverse and fluctuating food resources (Jónasdóttir, 2019; Lavaud et al., 2021). The electivity patterns (Figs. 10–11) in *C. madrasensis* demonstrate pronounced

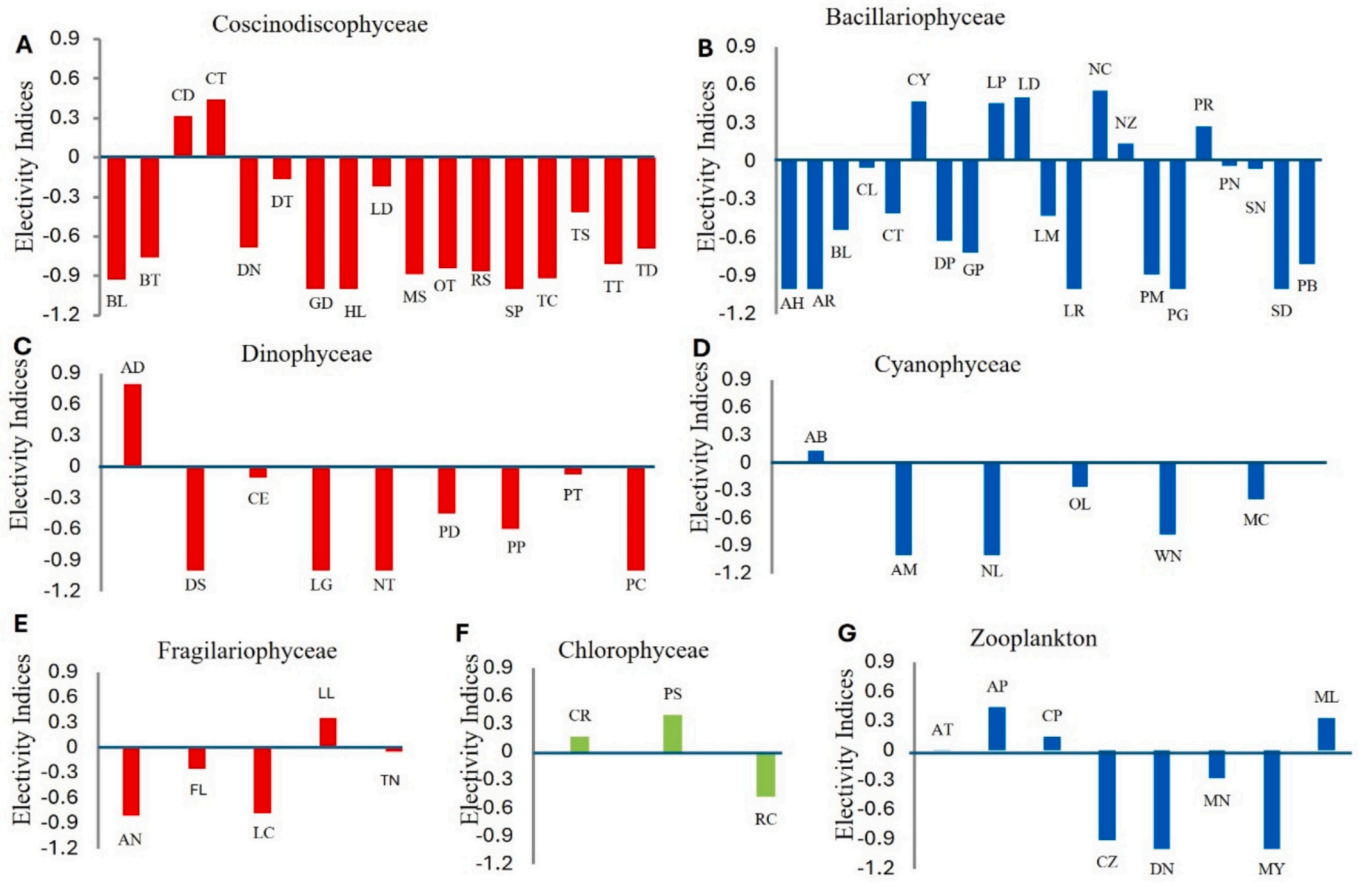

Fig. 10. Electivity indices representing the selective ingestion of various plankton under each group by *Crassostrea madrasensis* from the southeastern Bay of Bengal, Bangladesh. The indices were calculated using gut plankton data from 10 oysters sampled monthly (total n = 120) and water plankton data based on six replicate measurements per month (total n = 72). In Concinodiscophyceae (A): BL, *Bellerochea*; BT, *Bacteriastrum;* CD, *Coscinodiscus*; CT, *Cyclotella*; DN, *Detonula*; DT, *Ditylum*; GD, *Guinardia*; HL, *Hemiaulus*; LD, *Leptocylindricus*; MS, *Melosira*; OT, *Odontella*; RS, *Rhizosolenia*; SP, *Stephanopyxis*; TC, *Triceratium*; TS, *Thalassiosira*; TT, *Thalassiothrix;* TD, *Tropidoneis*. In Bacillariophyceae (B): AH, *Amphora*; AR, *Asteromphalus*; BL, *Bacillaria*; CL, *Cerataulina*; CT, *Cheatoceros*; CY, *Cylindrotheca*; DP, *Diploneis*; GP, *Grammatophora*; LP, *Lampriscus*; LD, *Lauderia*; LM, *Lithodesmium*; LR, *Lyrella*; NC, *Navicula*; NZ, *Nitzschia*; PM, *Palmeria*; PG, *Plagiodiscus*; PR, *Pleurosigma*; PN, *Pseudo-nitzschia*; SN, *Skeletonema*; SD, *Stephanodiscus*; PB, *Proboscia*. In Dinophyceae (C): *AD, Amphidinium;* DS, *Dinophysis*; CE, *Ceratium*; LG, *Ligulodinium*; NT, *Noctiluca*; PD, *Protoperidinium*; PP, *Pyrophacus*; PT, *Prorocentrum*; PC, Pyrocystis. In Cyanophyceae (D): AB, *Anabaena*; AM, *Aphanizomenon*; NL, *Nodularia*; OL, *Oscillatoria*; WN, *Woronichinia*; MC, *Microcystis*. In Fragilariophyceae (E): AN, *Asterionellopsis*; FL, *Fragilaria*; LC, *Licmophora*; LL, *Lioloma*; TN, *Thalassionema*. In Chlorophyceae (F): CR, *Chlorella*; PS, *Pediastrum*; RC, *Radiococcus*. In Zooplankton (G): AT, Acetes; AP, Amphipoda; CP, Copepoda; CZ, Crab zoea; DN, Daphnia; MN, Moina; MY, Mysids; ML, Mollusc larvae.

plankton selectivity, challenging the notion of indiscriminate filter feeding often associated with bivalves (Jørgensen, 1996; Ostroumov, 2005). Feeding behaviour appears to be a regulated process involving particle selection based on size, nutritional content, digestibility, and biochemical cues rather than mere availability (Cosling, 2003; Prasetiya et al., 2017; Rahman et al., 2020). Seasonal variations in Ivlev's electivity index (Fig. 11) reveal that selective feeding is dynamic, adjusting to changes in plankton composition and environmental conditions (Bayne, 1976; Jewel et al., 2002; Weissberger and Glibert, 2021). Such dietary flexibility enables oysters to maximize energy intake and sustain vital processes like growth and gametogenesis, which vary seasonally in bivalves (Lopes-Lima et al., 2014; Soon and Ransangan, 2014; Akélé et al., 2022).

Among phytoplankton groups, a strong preference for diatoms, especially Bacillariophyceae and Coscinodiscophyceae, is notable. Diatoms are highly nutritious, rich in essential fatty acids such as EPA, and their siliceous frustules enhance digestibility (Celi et al., 2022; Ghobara et al., 2024). Their preferential selection by *C. madrasensis* aligns with findings in *C. gigas* and *Ostrea edulis* (Ezgeta-Balić et al., 2020; Stechele et al., 2022). High electivity indices for genera/groups like *Navicula*, *Pleurosigma*, *Nitzschia*, *Coscinodiscus*, and *Cyclotella* suggest that diatoms are not only nutritionally superior but also efficiently retained and digested due to optimal size and morphology (Davenport et al., 2011; Houki et al., 2018). Selective ingestion of Dinophyceae, despite smaller cell size or mobility, may reflect chemical attractants or nutritional benefits observed in other filter feeders (Cheng et al., 2020; Davenport et al., 2011). The exceptionally high electivity of *Amphidinium* during the months January and February may not necessarily indicate a true feeding preference, as it could partly result from methodological and analytical constraints. Specifically, the inflated EI value likely reflects the mathematical sensitivity of Ivlev's index to low water abundances during these periods, the underrepresentation of smaller plankton (<20 μm) in water samples due to mesh-size limitation of the plankton net, and possible differential digestion of other planktons that favors the detection of *Amphidinium* cells high in gut analyses. Moderate ingestion of Chlorophyceae likely reflects their limited nutritional value. These algae, dominated by C16 and C18 fatty acids and lacking long-chain PUFA, are generally less nutritious (Jónasdóttir, 2019; Irmak and Arzu, 2020). Their moderate selection suggests consumption when superior food sources are scarce, indicating feeding preferences depend on both absolute and relative food quality (Ren et al., 2000; Ashour et al., 2025). In contrast, Cyanophyceae were largely avoided, likely due to

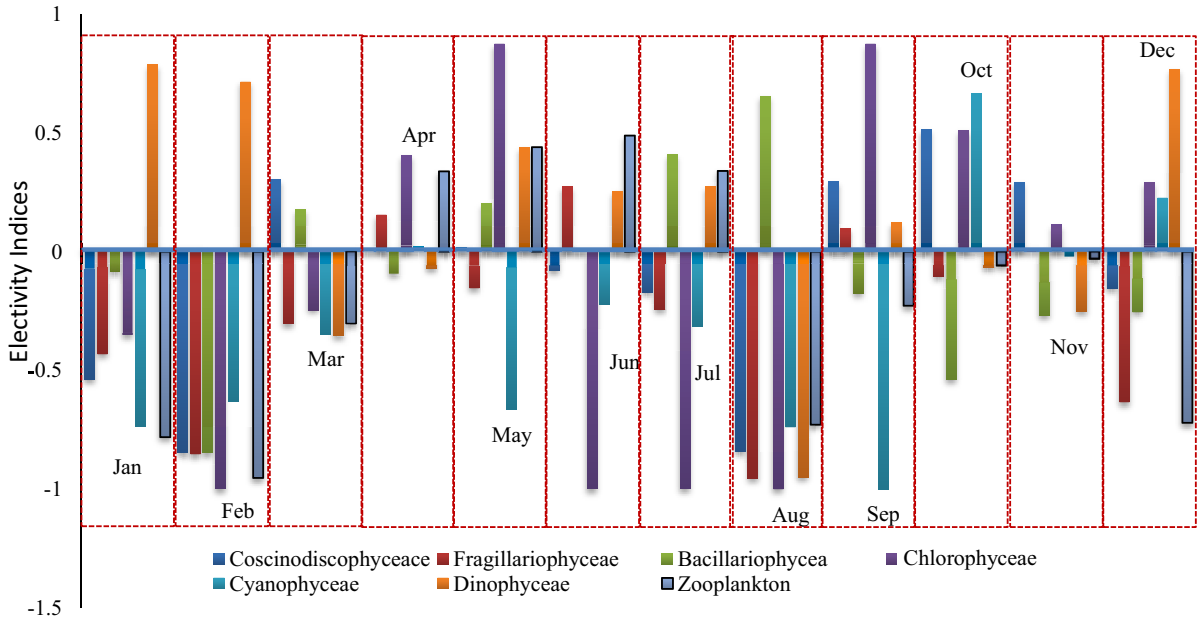

Fig. 11. Monthly variations in Ivlev's electivity indices (EI) for different plankton groups ingested by *Crassostrea madrasensis* collected from the southeastern coast of the Bay of Bengal, Bangladesh. The EI values are derived from gut content analysis of 10*C. madrasensis* per month (n = 120), compared with six replicate water column plankton samples collected monthly (total n = 72).

low nutritional quality and potential toxicity. Cyanobacteria lack essential PUFAs and often produce microcystins harmful to aquatic organisms (Vargas et al., 1998; Jónasdóttir, 2019; Rastogi et al., 2014; Pham and Tran, 2019). This avoidance highlights the oyster's ability to detect and exclude low-quality or toxic food, consistent with earlier reports (Weissberger and Glibert, 2021; Akélé et al., 2022). The selection for zooplankton taxa, particularly copepods, amphipods, and molluscan larvae, is another notable aspect of this study. Though typically herbivorous, oysters can exhibit opportunistic omnivory, particularly during periods of increased nutritional demand (Peharda et al., 2012; Akélé et al., 2022). Zooplankton provides protein- and lipid-rich food, supplementing phytoplankton diets during critical life stages or resource-scarce periods (Ashaari et al., 2024; Khan and Rahman, 2025). Preference for larval forms, such as molluscan larvae, supports previous evidence of larviphagy and demonstrates the oyster's capacity to exploit drifting animal plankton in benthic–pelagic coupling zones (Griffiths et al., 2017; Ronowicz et al., 2024).

4.4. *Strategic modulation of selective feeding across annual gametogenic cycles in C. madrasensis*

The pre-monsoon and post-monsoon reproductive cycle of *C. madrasensis* appears to be intricately and contrastingly linked with variations in plankton ingestion (see Figs. 12, 13), reflecting adaptive shifts in dietary strategies to meet the metabolic demands of gametogenesis. The relatively overlapping multivariate distributions observed (see Fig. 12A) indicate a diffuse pattern of dietary differentiation among gonadal stages, suggesting that feed availability exerted limited influence on the reproductive development of *C. madrasensis* during the pre-monsoon gametogenic cycle. Pre-monsoon gametogenesis in tropical estuaries is often triggered by elevated temperatures, which induce spawning in oysters by accelerating the metabolic and physiological processes involved in gametogenesis and prompting the final release of gametes (Reed et al., 2021; Rodríguez-Jaramillo et al., 2022). The environmental conditions during the pre-monsoon cycle in the southeastern Bay of Bengal are typically characterized by lowered nutrient availability and decreased plankton abundance (Asaduzzaman et al., 2020; Mozumder et al., 2023; Khan et al., 2023). Under such low-food conditions where plankton larger than 20 μm are scarce, *C. madrasensis* may shift toward a conservative energy strategy, reallocating stored reserves, primarily from glycogen and lipids accumulated in somatic tissues, to fuel gonadal development. Similar energy reallocation mechanisms have been documented in other bivalves, including *C. gigas*, under conditions of food scarcity (Bayne, 2002; Purroy et al., 2018). In contrast, during the post-monsoon gametogenic cycle, the strong segregation of gonadal stages in the CVA and PCA multivariate spaces underscores a more defined relationship between reproductive activity and specific dietary intake. The distinct clustering of mature and spawning stages with increased ingestion of plankton (see Fig. 12) supports previous observations that oysters augment their energy reserves through intensified feeding on high-quality food sources during reproductive peaks (Fournier et al., 2012; Ubertini et al., 2017). Pre-monsoon waters exhibited an oligotrophic signal based on the plankton groups quantified in this study, which helps explain the reduced ingestion rates observed during this period. Although smaller planktonic cells were not measured and the full structure of the pre-monsoon food field cannot be completely resolved, the available data still indicate a marked seasonal decline in food availability that corresponds with the observed feeding patterns. The spatial separation of spent individuals from early developing stages in post-monsoon PCA (see Fig. 12F) further indicates a distinct shift in dietary intake post-spawning, possibly reflecting the reduced energetic demands and altered feeding priorities for tissue recovery and maintenance. These observations suggest that *C. madrasensis* adopts an opportunistic trophic strategy during the post-monsoon gametogenic cycle by directly increasing the ingestion of energy-rich plankton to meet the heightened metabolic demands of gamete maturation. This pattern is consistent with findings from other oyster species, where enhanced food availability is closely associated with intensified reproductive effort (Le Moullac et al., 2013; Acarli et al., 2015; Tackett et al., 2024). The increased availability of plankton during the post-monsoon period provides an optimal window for oysters to maximize exogenous energy intake, which likely supports the rapid proliferation of gametes observed during this season. Overall, the contrasting opportunistic and conservative strategies exhibited by *C. madrasensis* across seasons highlight its flexible energy allocation mechanisms for optimizing reproductive

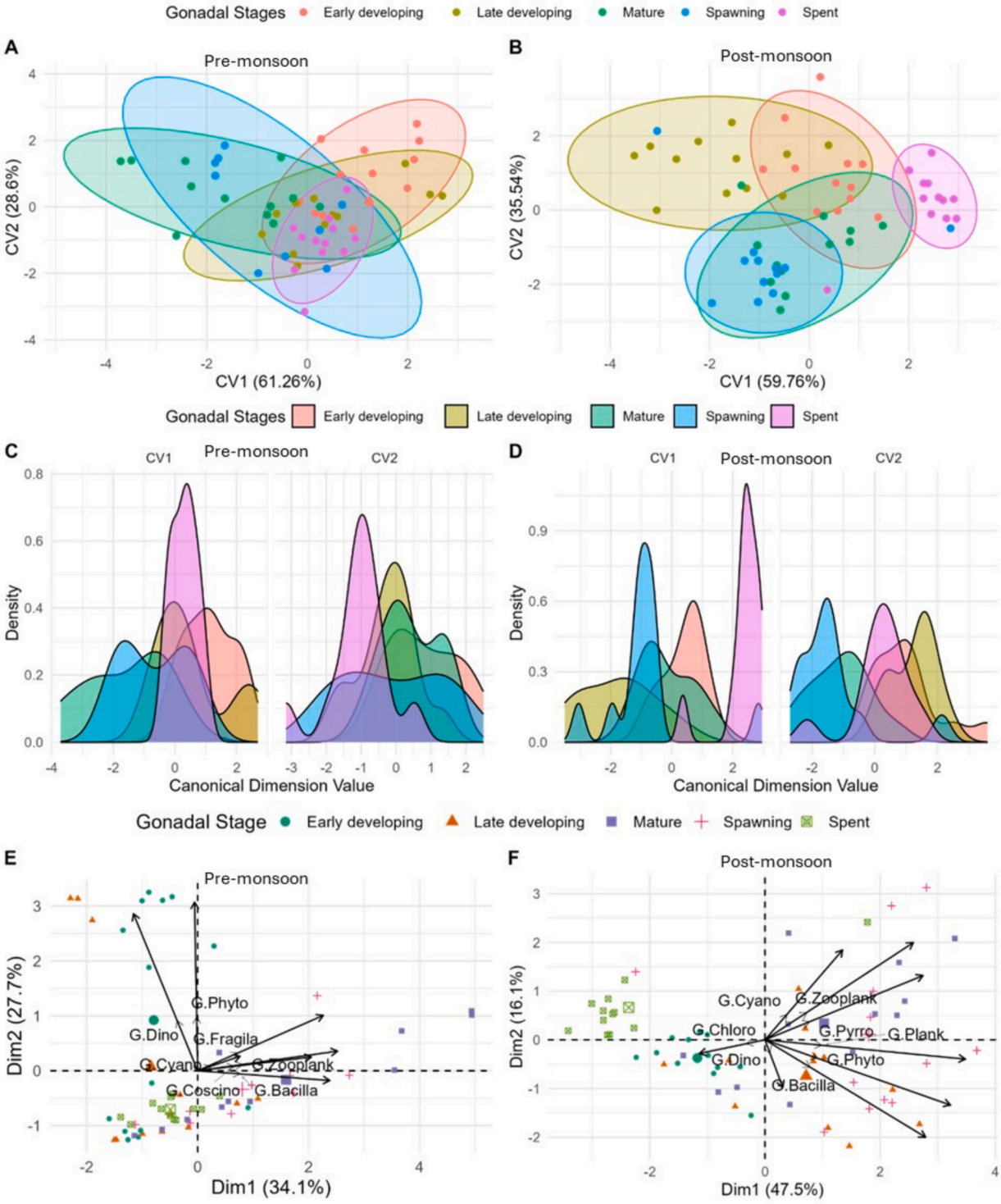

Fig. 12. Principal Component Analysis (PCA) and Canonical Variate Analysis (CVA) were conducted to examine the composition of plankton ingested by *Crassostrea madrasensis* across different stages of gametogenesis, based on samples collected from the southeastern coast of the Bay of Bengal, Bangladesh. Panels A and B present CVA biplots illustrating the variation in gut plankton composition during the pre-monsoon (A) and post-monsoon (B) phases of the gametogenic cycle. Panels C and D depict density plots of the first (CV1) and second (CV2) canonical variates corresponding to gut plankton during the pre-monsoon (C) and post-monsoon (D) periods. Panels E and F show PCA biplots representing the distribution patterns of ingested gut plankton during the pre-monsoon (E) and post-monsoon (F) gametogenic phases.

success under varying environmental conditions. Such dual strategies likely confer an evolutionary advantage in dynamic estuarine ecosystems, allowing *C. madrasensis* to maintain reproductive continuity despite seasonal variability in food availability and environmental conditions.

5. Conclusion

This study demonstrates that the selective feeding behaviour of *Crassostrea madrasensis* is closely modulated by seasonal environmental variations, plankton availability, and reproductive demands along the

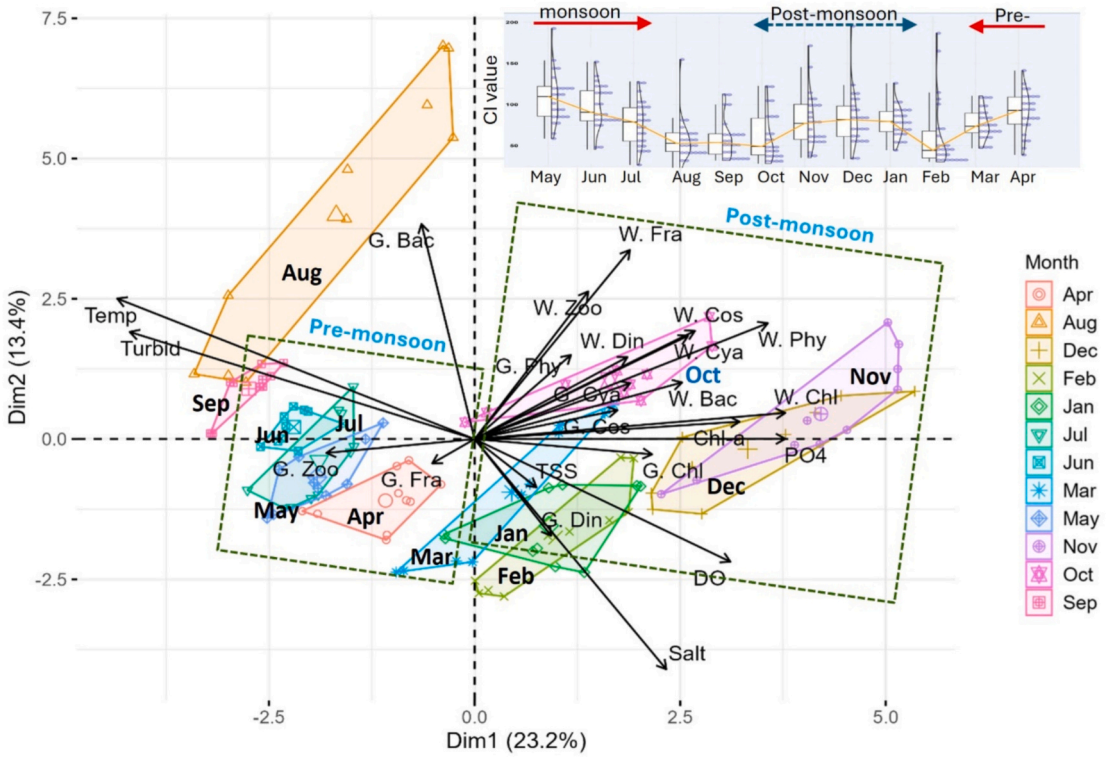

Fig. 13. The principal component analysis (PCA) plot illustrates the relationships among ecological parameters, water plankton abundance (cells or individuals/L), and plankton consumption (cells or individuals/oyster) with seasonal patterns, particularly during the pre-monsoon (March–July) and post-monsoon (October–January) phases of the gametogenic cycle of *Crassostrea madrasensis*, sampled from the southeastern coastline of the Bay of Bengal in Bangladesh. The bar chart within the figure displays the month-to-month fluctuations in the condition index (CI) of *C. madrasensis*. The abbreviations used represent the following variables: Temp – water temperature (°C); Salt – salinity (ppt); Turbid – turbidity (NTU); DO – dissolved oxygen (ppm); TSS – total suspended solids (mg/L); Chl.a – chlorophyll *a* concentration (μg/L); NO3 – nitrate-nitrogen (ppm); PO4 – phosphate-phosphorus (ppm); W.Cos – water Coscinodiscophyceae; W.Fra – water Fragillariophyceae; W.Baci – water Bacillariophyceae; W.Chlo – water Chlorophyceae; W.Cya – water Cyanophyceae; W.Dino –water Dinophyceae; W.Zoo –water Zooplankton; G.Cos – gut Coscinodiscophyceae; G.Fra – gut Fragilariophyceae; G.Baci – gut Bacillariophyceae; G.Chlo – gut Chlorophyceae; G.Cya – gut Cyanophyceae; G.Dino – gut Dinophyceae; G.Zoo – gut Zooplankton.

southeast coast of the Bay of Bengal. Within the size range examined (>20 μm), the species displayed patterns consistent with an opportunistic strategy during the post-monsoon gametogenic cycle, marked by increased ingestion of energy-rich plankton. During the pre-monsoon period, when plankton above 20 μm were less abundant, the observed patterns suggest a possible shift toward greater reliance on stored reserves. These insights advance our understanding of the eco-physiological mechanisms linking feeding plasticity with reproductive dynamics in tropical estuarine oysters. However, several limitations should be acknowledged. The study was spatially restricted to two estuarine sites, which may not capture the full variability of feeding strategies across hydrodynamic gradients. The plankton sampling method targeted the >20 μm fraction, potentially under-representing pico- and nanoplankton that may contribute substantially to oyster diets. Gut content analysis, while informative, cannot account for rapidly digested or morphologically fragile taxa such as cryptophytes and unarmored dinoflagellates, and feeding rate measurements were not directly quantified. Additionally, community-level selectivity indices are constrained by the partial digestibility of some taxa, and plankton abundance data were not reported in absolute terms. Future studies integrating molecular or pigment-based dietary tools (e.g., eDNA metabarcoding, CHEMTAX) and biochemical profiling of gonad and somatic tissues could more precisely elucidate energy allocation and nutrient assimilation pathways. Long-term, spatially broader monitoring under projected climate scenarios will further clarify how environmental variability influences oyster trophic and reproductive resilience. Despite these constraints, this study provides a robust foundation for refining sustainable oyster aquaculture and ecosystem-based management in monsoon-driven tropical estuaries.

Declaration of generative AI in scientific writing

During the preparation of this work, the authors used ChatGPT in the writing process to improve the readability and language of the manuscript. After using this tool/service, the authors reviewed and edited the content as needed and took full responsibility for the content of the published article.

CRediT authorship contribution statement

Khandakar Zakir Hossain: Software, Methodology, Investigation, Data curation, Writing – original draft. **Israt Jahan:** Methodology, Investigation, Data curation, Writing – original draft. **Md Nayeem Hossain:** Software, Formal analysis, Data curation. **Afshana Ferdous:** Methodology, Formal analysis, Writing – review & editing. **Md. Ramzan Ali:** Project administration, Investigation, Writing – review & editing. **Md Moshiur Rahman:** Software, Methodology, Data curation, Writing – review & editing. **Mohammad Sadequr Rahman Khan:** Supervision, Project administration, Writing – review & editing. **Md Asaduzzaman:** Supervision, Software, Project administration, Investigation, Funding acquisition, Data curation, Conceptualization, Writing – original draft.

Declaration of competing interest

The authors declare that they have no known competing financial interests or personal relationships that could have appeared to influence

the work reported in this paper.

Acknowledgements

This work was conducted as a part of the research plan of the Bangladesh Academy of Sciences- United States Department of Agriculture (BAS-USDA) Endowment 5th phase project implemented by Chattogram Veterinary and Animal Sciences University through a collaborative agreement with BAS (F 127). We would like to thank the director and other staff of the BAS-USDA Endowment Program for providing funding for this research work. We also thank the staff of the Oceanography Laboratory, Department of Marine Bioresource Science, Chattogram Veterinary and Animal Sciences University, for helping with oyster sampling and parameter analysis.

Data availability

Data will be made available on request.

References

Acarli, S., Lök, A., Kirtik, A., Acarli, D., Serdar, S., Kucukdermenci, A., Yigitkurt, S., Yildiz, H., Nur, A., 2015. Seasonal variation in reproductive activity and biochemical composition of flat oyster (*Ostrea edulis*) in the Homa Lagoon, Izmir Bay, Turkey. Sci. Mar. 79 (4), 487–495. https://doi.org/10.3989/scimar.04202.16A.

Achary, M.S., Panigrahi, S., Satpathy, K.K., Sahu, G., Mohanty, A.K., Selvanayagam, M., Panigrahy, R.C., 2014. Nutrient dynamics and seasonal variation of phytoplankton assemblages in the coastal waters of southwest bay of Bengal. Environ. Monit. Assess. 186, 5681–5695. https://doi.org/10.1007/s10661-014-3812-8.

Ahmed, N., Thompson, S., 2019. The blue dimensions of aquaculture: A global synthesis. Sci. Total Environ. 652, 851–861. https://doi.org/10.1016/j.scitotenv.2018.10.163.

Akélé, D., Gougbédji, A., Agadjihouédé, H., Lalèyè, P., 2022. Diet of the mangrove oyster *Crassostrea gasar* (Adanson, 1757) and plankton diversity in Lake Nokouré. Int. J. Dev. Res. 12 (5), 56072–56076. https://doi.org/10.37118/ijdr.24480.05.2022.

Al-Kandari, M., Al-Yamani, F.Y., Al-Rifaie, K., 2009. Marine Phytoplankton Atlas of Kuwait's Waters. Kuwait Institute of Scientific Research, Kuwait, p. 351.

Anestis, A., Lazou, A., Pörtner, H.O., Michaelidis, B., 2007. Behavioral, metabolic, and molecular stress responses of marine bivalve *Mytilus galloprovincialis* during long-term acclimation at increasing ambient temperature. Am. J. Phys. Regul. Integr. Comp. Phys. 293, R911–R921. https://doi.org/10.1152/ajpregu.00124.2007.

APHA, 1992. Standard methods for the examination of water and wastewater. In: American Public Health Association (APHA), American Water Works Association (AWWA) and Water Pollution Control Federation (WPCF), Washington DC, 18th ed.

Asaduzzaman, M., Rahi, N.A., Rahman, M.M., Akter, S., Hoque, N.F., Shakil, A., Wahab, M.A., 2019. Reproductive biology and ecology of the green mussel *Perna viridis*: A multidisciplinary approach. Biology 8 (4), 88. https://doi.org/10.3390/biology8040088.

Asaduzzaman, M., Akter, S., Hoque, N.F., Shakil, A., Noor, A.R., Akter, M.N., Rahman, M. M., 2020. Multifaceted linkages among eco-physiological factors, seasonal plankton dynamics and selective feeding behavior of the green mussel (*Perna viridis*) in the south-east coast of the bay of Bengal. J. Sea Res. 160, 101933. https://doi.org/10.1016/j.seares.2020.101933.

Asaduzzaman, M., Nahiduzzaman, M., Chowdhury, M.T.H., Rahman, M.M., Mamun, A. A., Hossain, M.M., 2025. Advancing low-trophic extractive mariculture (LTEM): strategies for a thriving blue economy in Bangladesh. Mar. Policy 173, 106557. https://doi.org/10.1016/j.marpol.2024.106557.

Ashaari, A., Iehata, S., Kim, H.J., Rasdi, N.W., 2024. Recent advancement of zooplankton enriched with nutrients and probiotic isolates from aquaculture systems: a review. J. Appl. Anim. Res. 52 (1). https://doi.org/10.1080/09712119.2024.2417052.

Ashour, M., Ringø, E., El-Haron, E., Goda, A.M.A., 2025. The importance of plankton in marine fish and shellfish larval nutrition. IntechOpen. https://doi.org/10.5772/intechopen.1008788.

Avila-Poveda, O.H., Torres-Ariño, A., Girón-Cruz, D.A., Cuevas-Aguirre, A., 2014. Evidence for accumulation of *Synechococcus elongatus* (Cyanobacteria: Cyanophyceae) in the tissues of the oyster *Crassostrea gigas* (Mollusca: Bivalvia). Tissue Cell 46, 379–387. https://doi.org/10.1016/j.tice.2014.07.001.

Baho, D.L., Drakare, S., Johnson, R.K., Angeler, D.G., 2020. Phytoplankton size- and abundance-based resilience assessments reveal nutrient rather than water level effects. Sci. Total Environ. 746, 141110. https://doi.org/10.1016/j.scitotenv.2020.141110.

Barillé, L., Prou, J., Héral, M., Bougrier, S., 1997. Effect of high natural seston concentration on the feeding, selection, and absorption of the oyster *Crassostrea gigas*. J. Exp. Mar. Biol. Ecol. 212 (2), 149–172. https://doi.org/10.1016/S0022-0981(96)02756-6.

Barr, J.M., Munroe, D., Rose, J.M., 2024. Seasonal feeding behavior of aquaculture eastern oysters (*Crassostrea virginica*) in the mid-Atlantic. Estuar. Coasts 47, 789–804. https://doi.org/10.1007/s12237-023-01293-9.

Bayne, B.L., 1976. Marine Mussels: Their Ecology and Physiology. Cambridge University Press, Cambridge, UK.

Bayne, B., 2002. A physiological comparison between Pacific oysters *Crassostrea gigas* and Sydney rock oysters *Saccostrea glomerata*: food, feeding and growth in a shared estuarine habitat. Mar. Ecol. Prog. Ser. 232, 163–178. https://doi.org/10.3354/meps232163.

Berges, J., Varela, D., Harrison, P., 2002. Effects of temperature on growth rate, cell composition and nitrogen metabolism in the marine diatom *Thalassiosira pseudonana* (Bacillariophyceae). Mar. Ecol. Prog. Ser. 225, 139–146. https://doi.org/10.3354/meps225139.

Berthelin, C., Kellner, K., Mathieu, M., 2000. Storage metabolism in the Pacific oyster (*Crassostrea gigas*) in relation to summer mortalities and reproductive cycle (west coast of France). Comp. Biochem. Physiol. B Biochem. Mol. Biol. 125 (3), 359–369. https://doi.org/10.1016/S0305-0491(99)00187-X.

BMD, 2017. Record Book of Meteorological Data. Bangladesh Meteorological Department, Kutubdia station. https://live6.bmd.gov.bd/.

Bode, A., Álvarez-Ossorio, M.T., González, N., Lorenzo, J., Rodríguez, C., Varela, M., Varela, M.M., 2005. Seasonal variability of plankton blooms in the ria de Ferrol (NW Spain): II. Plankton abundance, composition and biomass. Estuar. Coast. Shelf Sci. 63, 285–300. https://doi.org/10.1016/j.ecss.2004.11.021.

Boltovskoy, D., Izaguirre, I., Correa, N., 1995. Feeding selectivity of *Corbicula fluminea* (Bivalvia) on natural phytoplankton. Hydrobiologia 312, 171–182. https://doi.org/10.1007/BF00015510.

Botes, L., 2001. Phytoplankton Identification Catalogue – Saldanha Bay, South Africa. GloBallast Monograph Series No. 7. IMO, London, p. 88.

Bourlès, Y., Alunno-Bruscia, M., Pouvreau, S., Tollu, G., Leguay, D., Arnaud, C., Goulletquer, P., Kooijman, S.A.L.M., 2009. Modelling growth and reproduction of the Pacific oyster *Crassostrea gigas*: advances in the oyster-DEB model through application to a coastal pond. J. Sea Res. 62, 62–71. https://doi.org/10.1016/j.seares.2009.03.002.

Boyd, C.E., 1979. Water Quality in Warmwater Fish Ponds. Auburn University Press, Auburn, AL.

Cabre, M.L., Hosegood, P., Attrill, M.J., Bridger, D., Sheehan, E.V., 2021. Offshore longline mussel farms: a review of oceanographic and ecological interactions to inform future research needs, policy and management. Rev. Aquac. 13, 1864–1887. https://doi.org/10.1111/raq.12549.

Celi, C., Fino, D., Savorani, F., 2022. *Phaeodactylum tricornutum* as a source of value-added products: a review on recent developments in cultivation and extraction technologies. Bioresour. Technol. Rep. 19, 101122. https://doi.org/10.1016/j.biteb.2022.101122.

Chang, G.O.J.L., Inn, L.V., Hwai, A.T.S., Yasin, Z., 2016. The effects of salinity on the filtration rates of juvenile tropical oyster *Crassostrea iredalei*. Trop. Life Sci. Res. 27, 45–51. https://doi.org/10.21315/tlsr2016.27.3.7.

Cheng, P., Zhou, C., Chu, R., Chang, T., Xu, J., Ruan, R., Chen, P., Yan, X., 2020. Effect of microalgae diet and culture system on the rearing of bivalve mollusks: nutritional properties and potential cost improvements. Algal Res. 51, 102076. https://doi.org/10.1016/j.algal.2020.102076.

Choi, T.S., Kang, E.J., Kim, J.H., Kim, K.Y., 2010. Effect of salinity on growth and nutrient uptake of *Ulva pertusa* (Chlorophyta) from an eelgrass bed. Algae 25, 17–26. https://doi.org/10.4490/algae.2010.25.1.017.

Choudhury, A.K., Pal, R., 2010. Phytoplankton and nutrient dynamics of shallow coastal stations at bay of Bengal, eastern Indian coast. Aquat. Ecol. 44, 55–71. https://doi.org/10.1007/s10452-009-9252-9.

Cloern, J.E., Jassby, A.D., 2010. Patterns and scales of phytoplankton variability in estuarine–coastal ecosystems. Estuar. Coasts 33, 230–241. https://doi.org/10.1007/s12237-009-9195-3.

Cosling, E.M., 2003. Bivalve Molluscs: Biology, Ecology and Culture. Fishing News Books, Malden, Oxford. https://doi.org/10.1002/9780470995532.

Costello, C., Cao, L., Gelcich, S., Cisneros-Mata, M.Á., Free, C.M., Froehlich, H.E., Golden, C.D., Ishimura, G., Maier, J., Macadam-Somer, I., Mangin, T., Melnychuk, M.C., Miyahara, M., De Moor, C.L., Naylor, R., Nøstbakken, L., Ojea, E., O'Reilly, E., Parma, A.M., Plantinga, A.J., Thilsted, S.H., Lubchenco, J., 2020. The future of food from the sea. Nature 588, 95–100. https://doi.org/10.1038/s41586-020-2616-y.

Cranford, P.J., Ward, J.E., Shumway, S.E., 2011. Bivalve filter feeding: variability and limits of the aquaculture biofilter. Shellfish Aquac. Environ. 10, 81–124. https://doi.org/10.1002/9780470960967.ch4.

Cranford, P.J., Strohmeier, T., Filgueira, R., Strand, Ø., 2016. Potential methodological influences on the determination of particle retention efficiency by suspension feeders: *Mytilus edulis* and *Ciona intestinalis*. Aquat. Biol. 25, 61–73. https://doi.org/10.3354/ab00654.

Dag, O., Dolgun, A., Konar, N.M., 2017. One-Way Tests in Independent Groups Designs. R Package Version 1.5. Available from: https://CRAN.R-project.org/package=onewaytests (accessed 04.12.2019).

Das, S., Giri, S., Das, I., Chanda, A., Ghosh, A., Mukhopadhyay, A., Akhand, A., Choudhury, S.B., Dadhwal, V.K., Maity, S., Srinivasa Kumar, T., Lotliker, A.A., Mitra, D., Hazra, S., 2017. Nutrient dynamics of northern bay of Bengal (nBoB)—emphasizing the role of tides. Reg. Stud. Mar. Sci. 10, 116–134. https://doi.org/10.1016/j.rsma.2017.01.006.

Davenport, J., Ezgeta-Balić, D., Peharda, M., Skejić, S., Ninčević-Gladan, Ž., Matijević, S., 2011. Size-differential feeding in *Pinna nobilis* L. (Mollusca: Bivalvia): exploitation of detritus, phytoplankton and zooplankton. Estuar. Coast. Shelf Sci. 92, 246–254. https://doi.org/10.1016/j.ecss.2010.12.033.

Do Nascimento, V.S., Lapa, K.R., De Miranda Gomes, C.H.A., Gray, M., Da Silva, G., Garbossa, L.H.P., Suplicy, F.M., De Melo, C.M.R., 2022. Filtration and biodeposition rates of *Crassostrea* oysters for southern Brazilian waters. Reg. Stud. Mar. Sci. 56, 102677. https://doi.org/10.1016/j.rsma.2022.102677.

D'Silva, M.S., Anil, A.C., Naik, R.K., D'Costa, P.M., 2012. Algal blooms: a perspective from the coast of India. Nat. Hazards 63, 1225–1253. https://doi.org/10.1007/s11069-012-0190-9.

Dupuy, C., Vaquer, A., Höai, T., Rougier, C., Mazouni, N.G., Lautier, J., Collos, Y., Gall, S. L., 2000. Feeding rate of the oyster *Crassostrea gigas* in a natural planktonic community of the Mediterranean Thau lagoon. Mar. Ecol. Prog. Ser. 205, 171–184. https://doi.org/10.3354/meps205171.

El-Shaarawi, A., Munawar, M., 1978. Statistical evaluation of the relationships between phytoplankton biomass, chlorophyll a, and primary production in Lake Superior. J. Great Lakes Res. 4, 443–455. https://doi.org/10.1016/S0380-1330(78)72213-6.

Enríquez-Díaz, M., Pouvreau, S., Chávez-Villalba, J., Le Pennec, M., 2009. Gametogenesis, reproductive investment, and spawning behavior of the Pacific giant oyster *Crassostrea gigas*: evidence of an environment-dependent strategy. Aquac. Int. 17, 491–506. https://doi.org/10.1007/s10499-008-9219-1.

Ezgeta-Balić, D., Šantić, D., Šegvić-Bubić, T., Bojanić, N., Bužančić, M., Vidjak, O., Varezić, D.B., Stagličić, N., Kundid, P., Peharda, M., Žužul, I., Grubišić, L., Briski, E., 2020. Competitive feeding interactions between native *Ostrea edulis* and non-native *Crassostrea gigas* with implications of introducing *C. Gigas* into commercial aquaculture in the eastern Adriatic Sea. Mar. Environ. Res. 160, 105051. https://doi.org/10.1016/j.marenvres.2020.105051.

FAO, 2024. The State of World Fisheries and Aquaculture 2024: Blue Transformation in Action. Food and Agriculture Organization of the United Nations. https://doi.org/10.4060/cd0683en.

Fournier, J., Levesque, E., Pouvreau, S., Pennec, M., Moullac, G., 2012. Influence of plankton concentration on gametogenesis and spawning of the black lip pearl oyster *Pinctada margaritifera* in Ahe atoll lagoon (Tuamotu archipelago, French Polynesia). Mar. Pollut. Bull. 65 (10−12), 463–470. https://doi.org/10.1016/j.marpolbul.2012.03.027.

Fox, J., Weisberg, S., 2019. An R Companion to Applied Regression, third ed. Sage Publications. https://doi.org/10.32614/CRAN.package.car.

Free, C.M., Cabral, R.B., Froehlich, H.E., Battista, W., Ojea, E., O'Reilly, E., Palardy, J.E., García Molinos, J., Siegel, K.J., Arnason, R., Juinio-Meñez, M.A., Fabricius, K., Turley, C., Gaines, S.D., 2022. Expanding Ocean food production under climate change. Nature 605, 490–496. https://doi.org/10.1038/s41586-022-04674-5.

Gabaldón, C., Devetter, M., Hejzlar, J., Šimek, K., Znachor, P., Nedoma, J., Seďa, J., 2019. Seasonal strengths of the abiotic and biotic drivers of a zooplankton community. Freshw. Biol. 64, 1326–1341. https://doi.org/10.1111/fwb.13308.

Galili, T., 2015. Dendextend: an R package for visualizing, modifying, and comparing dendrograms. Bioinform 31 (22), 3718–3720. https://doi.org/10.1093/bioinformatics/btv428.

Galimany, E., Lunt, J., Freeman, C.J., Reed, S., Segura-García, I., Paul, V.J., 2017. Feeding behavior of eastern oysters *Crassostrea virginica* and hard clams *Mercenaria mercenaria* in shallow estuaries. Mar. Ecol. Prog. Ser. 567, 125–137. https://doi.org/10.3354/meps12050.

Geetha, S., Krishnakumar, P.K., Thomas, S., Sampathkumar, G., Nagaraja, D., Bhat, G.S., 2007. Influence of environmental factors on growth rate of *Crassostrea madrasensis* (Preston) in suspended culture. Asian Fish. Sci. 20 (3), 241–255. https://doi.org/10.33997/j.afs.2007.20.3.002.

Gera, A., Gayathri, R., Ezhilarasan, P., Ranga Rao, V., Ramana Murthy, M.V., 2023. Coupled physical-biogeochemical simulations of upwelling, ecological response to fresh water. Ecol. Model. 476, 110246. https://doi.org/10.1016/j.ecolmodel.2022.110246.

Ghobara, M., El-Sheekh, M., Hamed, A.F., Abdelhamid, M.A.A., Pack, S.P., 2024. Diatom nanostructured biosilica. In: Abomohra, A., Ende, S. (Eds.), Value-Added Products from Algae. Springer, Cham, pp. 461–492. https://doi.org/10.1007/978-3-031-42026-9_14.

Gogoi, P., Das, S.K., Das Sarkar, S., Chanu, T.N., Manna, R.K., Sengupta, A., Raman, R.K., Samanta, S., Das, B.K., 2021. Environmental factors driving phytoplankton assemblage pattern and diversity: insights from Sundarban eco-region, India. Ecohydrol. Hydrobiol. 21, 354–367. https://doi.org/10.1016/j.ecohyd.2020.09.005.

Gopakumar, G., Sulochanan, B., Venkatesan, V., 2009. Bloom of *Noctiluca scintillans* (Macartney) in gulf of Mannar, southeast coast India. J. Mar. Biol. Assoc. India 55, 75–80.

Gosling, E., 2003. Bivalve Molluscs: Biology, Ecology and Culture. Fishing News Books, Blackwell Publishing, p. 443. https://doi.org/10.1002/9780470995532.

Gray, M.W., Langdon, C., 2019. Particle processing by Olympia oysters *Ostrea lurida* and Pacific oysters *Crassostrea gigas*. Estuar. Coasts 42, 779–791. https://doi.org/10.1007/s12237-018-0480-x.

Griffiths, J.R., Kadin, M., Nascimento, F.J.A., Tamelander, T., Törnroos, A., Bonaglia, S., Bonsdorff, E., Brüchert, V., Gårdmark, A., Järnström, M., Kotta, J., Lindegren, M., Nordström, M.C., Norkko, A., Olsson, J., Weigel, B., Žydelis, R., Blenckner, T., Niiranen, S., Winder, M., 2017. The importance of benthic–pelagic coupling for marine ecosystem functioning in a changing world. Glob. Chang. Biol. 23, 2179–2196. https://doi.org/10.1111/gcb.13642.

Hambright, K.D., Zohary, T., 2000. Phytoplankton species diversity control through competitive exclusion and physical disturbances. Limnol. Oceanogr. 45, 110–122. https://doi.org/10.4319/lo.2000.45.1.0110.

Hasan, J., Hoque, M.M., Rabbi, A.F., Rahman, S., Zulfikar, M.A., 2021. Investigation on suitable spat collectors and culture sites for edible oyster in the coast of bay of Bengal, Bangladesh. Bangladesh J. Zool. 49 (2), 257–265. https://doi.org/10.3329/bjz.v49i2.56262.

Hassan, M.M., Qin, J.G., Li, X., 2018. Gametogenesis, sex ratio and energy metabolism in *Ostrea angasi*: implications for the reproductive strategy of spermcasting marine bivalves. J. Molluscan Stud. 84, 38–45. https://doi.org/10.1093/mollus/eyx041.

Hatzonikolakis, Y., Tsiaras, K., Theodorou, J., Petihakis, G., Sofianos, S., Triantafyllou, G., 2017. Simulation of mussel *Mytilus galloprovincialis* growth with a dynamic energy budget model in Maliakos and Thermaikos gulfs (eastern Mediterranean). Aquac. Environ. Interact. 9, 371–383. https://doi.org/10.3354/aei00236.

Hawkins, A.J.S., Bayne, B.L., Bougrier, S., Héral, M., Navarro, E., Smith, R.F.M., Urrutia, M.B., 1988. Some general relationships in comparing the feeding physiology of suspension-feeding bivalve mollusks. J. Exp. Mar. Biol. Ecol. 219 (1–2), 87–103. https://doi.org/10.1016/S0022-0981(97)00176-7.

Hernández Almeida, O.U., Estrada-Gutierrez, K.M., Siqueiros-Beltrones, D.A., Inda-Díaz, E.A., 2019. Diatom species composition in the in situ diet of the placer oyster *Crassostrea corteziensis* in an estuarine system. Hidrobiológica 29, 109–127. https://doi.org/10.24275/uam/izt/dcbs/hidro/2020v29n3/Hernandez.

Hothorn, T., Bretz, F., Westfall, P., 2010. Multiple Comparisons Using *R*. CRC Press. https://doi.org/10.32614/CRAN.package.multcomp.

Houki, S., Kawamura, T., Ogawa, N., Watanabe, Y., 2018. Efficient crushing of hard benthic diatoms in the gut of the Manila clam *Ruditapes philippinarum* – experimental and observational evidence. J. Exp. Mar. Biol. Ecol. 505, 35–44. https://doi.org/10.1016/j.jembe.2018.04.007.

Inyang, A.I., Wang, Y.-S., 2020. Phytoplankton diversity and community responses to physicochemical variables in mangrove zones of Guangzhou Province, China. Ecotoxicology 29, 650–668. https://doi.org/10.1007/s10646-020-02209-0.

Irmak, Ş.O., Arzu, A.B., 2020. Determination of the fatty-acid composition of four native microalgae species. GSC Adv. Res. Rev. 4, 001–008. https://doi.org/10.30574/gscarr.2020.4.1.0053.

Islam, M.S., Alam, M.M., Chowdhury, M.S., Hasan, M.K., 2021. Phytoplankton in contrasting ecosystems of the southeastern coast of Bangladesh: composition, abundance, and relationships with environmental variables. Environ. Monit. Assess. 193, 88. https://doi.org/10.1007/s10661-021-08868-9.

Ivlev, V.S., 1961. Experimental Ecology of the Feeding of Fishes. Yale University Press, New Haven, Connecticut.

Jacquet, J., 2017. Seafood in the future: bivalves are better. Solut. J. 8, 27–32.

Jewel, M.A.S., Haque, M.M., Khan, S., 2002. Seasonal dynamics of phytoplankton in relation to environmental factors in the Moheshkhali channel, Cox's Bazar, Bangladesh. Bangladesh J. Fish. Res. 6 (2), 173–181. https://doi.org/10.3329/bjfr.v6i2.1068.

Jónasdóttir, S.H., 2019. Fatty acid profiles and production in marine phytoplankton. Mar. Drugs 17, 151. https://doi.org/10.3390/md17030151.

Jørgensen, C.B., 1996. Bivalve filter feeding revisited. Mar. Ecol. Prog. Ser. 142, 287–302.

Jyothibabu, R., Vinayachandran, P.N., Madhu, N.V., Robin, R.S., Karnan, C., Jagadeesan, L., Anjusha, A., 2015. Phytoplankton size structure in the southern bay of Bengal modified by the summer monsoon current and associated eddies: implications on the vertical biogenic flux. J. Mar. Syst. 143, 98–119. https://doi.org/10.1016/j.jmarsys.2014.10.018.

Kamykowski, D., Zentara, S., Morrison, J.M., Switzer, A.C., 2002. Dynamic global patterns of nitrate, phosphate, silicate, and iron availability and phytoplankton community composition from remote sensing data. Glob. Biogeochem. Cycles 16, 1023. https://doi.org/10.1029/2001GB001640.

Kang, C.K., Park, M., Lee, P.Y., Choi, W.J., Lee, W.C., 2000. Seasonal variations in condition, reproductive activity, and biochemical composition of the Pacific oyster *Crassostrea gigas* (Thunberg), in suspended culture in two coastal bays of Korea. J. Shellfish Res. 19, 771–778. https://www.researchgate.net/publication/279555506.

Kang, C., Lee, Y., Choy, E., Shin, J., Seo, I., Hong, J., 2006. Microphytobenthos seasonality determines growth and reproduction in intertidal bivalves. Mar. Ecol. Prog. Ser. 315, 113–127. https://doi.org/10.3354/meps315113.

Karray, S., Smaoui-Damak, W., Rebai, T., Hamza-Chaffai, A., 2015. The reproductive cycle, condition index, and glycogen reserves of the cockles *Cerastoderma glaucum* from the Gulf of Gabès (Tunisia). Environ. Sci. Pollut. Res. 22, 17317–17329. https://doi.org/10.1007/s11356-015-4337-6.

Khan, N.S., Rahman, M.S., 2025. Zooplankton in aquaculture: A perspective on nutrition and cost-effectiveness. Aquac. Res. 2025 (1), 1–14. https://doi.org/10.1155/are/5347147.

Khan, S., Jahan, R., Rahman, M.A., Haque, M.M., 2019. Eutrophication enhances phytoplankton abundance in the Moheshkhali channel, Bay of Bengal, Bangladesh. Aust. J. Sci. Technol. 3 (3), 141–147.

Khan, A.B.S., Islam, M.A., Ullah, M.R., Akhter, M., Hasan, K.R., Mahmud, Y., 2023. Growth performance and survival of oyster, *Saccostrea cucullata* (born, 1778) and green mussel, *Perna viridis* (Linnaeus, 1758) cultivated in Bangladesh coast. Arch. Agric. Environ. Sci. 8 (1), 62–67. https://doi.org/10.26832/24566632.2023.0801010.

Kinsella, J.D., 2019. Environmental Effects on Cultured Oyster *Crassostrea virginica*: Implications for Filtration Capacity and Production. Ph.D. Thesis. Univ. North Carolina Wilmington, USA, p. 86. https://nerrssciencecollaborative.org/media/resources/Kinsella_FinalThesis_081219.pdf.

Krause, G., Buck, B., Breckwoldt, A., 2019. Socio-Economic Aspects of Marine Bivalve Production. Goods and Services of Marine Bivalves, In, pp. 317–334. https://doi.org/10.1007/978-3-319-96776-9_17.

Kumar, S.P., Madhupratap, M., Kumar, M.D., Muraleedharan, P.M., De Souza, S.N., Gauns, M., Sarma, V.V.S.S., 2001. High biological productivity in the central Arabian Sea during the summer monsoon driven by Ekman pumping and lateral advection. Curr. Sci. 81 (12), 1633–1638.

Lavaud, R., Peyre, M.K., Justic, D., Peyre, J., 2021. Dynamic energy budget modelling to predict eastern oyster growth, reproduction, and mortality under river management

and climate change scenarios. Estuar. Coast. Shelf Sci. 251, 107188. https://doi.org/10.1016/j.ecss.2021.107188.
Le Moullac, G., Soyez, C., Sham-Koua, M., Levy, P., Moriceau, J., Vonau, V., Maihota, M., Cochard, J.C., 2013. Feeding the pearl oyster *Pinctada margaritifera* during reproductive conditioning. Aquac. Res. 44. https://doi.org/10.1111/j.1365-2109.2011.03045.x.
Lê, S., Josse, J., Husson, F., 2008. FactoMineR: an R package for multivariate analysis. J. Stat. Softw. 25 (1), 1–18. https://doi.org/10.18637/jss.v025.i01.
Levinton, J., 2019. Feeding access of eastern oysters to the winter–spring phytoplankton bloom: evidence from Jamaica Bay, New York. J. Shellfish Res. 38 (1), 115. https://doi.org/10.2983/035.038.0111.
Li, Y., Qin, J.G., Li, X., Benkendorff, K., 2009. Spawning-dependent stress response to food deprivation in Pacific oyster *Crassostrea gigas*. Aquaculture 286, 309–317. https://doi.org/10.1016/j.aquaculture.2008.09.035.
Lønborg, C., Müller, M., Butler, E.C.V., Jiang, S., Ooi, S.K., Trinh, D.H., Wong, P.Y., Ali, S. M., Cui, C., Siong, W.B., Yando, E.S., Friess, D.A., Rosentreter, J.A., Eyre, B.D., Martin, P., 2021. Nutrient cycling in tropical and temperate coastal waters: is latitude making a difference? Estuar. Coast. Shelf Sci. 262, 107571. https://doi.org/10.1016/j.ecss.2021.107571.
Lopes-Lima, M., Lima, P., Hinzmann, M., Rocha, A., 2014. Selective feeding by *Anodonta cygnea* (Linnaeus, 1771): the effects of seasonal changes and nutritional demands. Limnologica 44, 18–22. https://doi.org/10.1016/j.limno.2013.07.001.
Low, J.S.Y., Chew, L.L., Ng, C.C., Goh, H.C., Lehette, P., Chong, V.C., 2018. Heat shock response and metabolic stress in the tropical estuarine copepod *Pseudodiaptomus annandalei* converge at its upper thermal optimum. J. Therm. Biol. 74, 14–22. https://doi.org/10.1016/j.jtherbio.2018.02.012.
Madhu, N.V., Jyothibabu, R., Balachandran, K.K., Honey, U.K., Vijay, J.G., Shiyas, C.A., Gupta, G.V.M., Achuthankutty, C.T., 2007. Monsoonal impact on planktonic standing stock and abundance in a tropical estuary (Cochin backwaters – India). Estuar. Coast. Shelf Sci. 73 (1–2), 54–64. https://doi.org/10.1016/j.ecss.2006.12.009.
Madhupratap, M., Gauns, M., Ramaiah, N., Prasanna Kumar, S., Muraleedharan, P.M., De Sousa, S.N., Sardessai, S., Muraleedharan, U., 2003. Biogeochemistry of the Bay of Bengal: Physical, chemical and primary productivity characteristics of the central and western Bay of Bengal during summer monsoon 2001. Deep Sea Res. Part II Top. Stud. Oceanogr. 50 (5), 881–896. https://doi.org/10.1016/S0967-0645(02)00611-2.
Madon, S.P., Schneider, D.W., Stoeckel, J.A., Sparks, R.E., 1998. Effects of inorganic sediment and food concentrations on energetic processes of the zebra mussel, *Dreissena polymorpha*: implications for growth in turbid rivers. Can. J. Fish. Aquat. Sci. 55, 401–413. https://doi.org/10.1139/f97-214.
Malerba, M.E., Connolly, S.R., Heimann, K., 2012. Nitrate–nitrite dynamics and phytoplankton growth: formulation and experimental evaluation of a dynamic model. Limnol. Oceanogr. 57, 1555–1571. https://doi.org/10.4319/lo.2012.57.5.1555.
Malik, A., Fernandes, C.E.G., Gonsalves, M.J.B.D., Subina, N.S., Mamatha, S.S., Krishna, K., Varik, S., Kumari, R., Gauns, M., Cejoice, R.P., Pandey, S.S., 2015. Interactions between trophic levels in upwelling and non-upwelling regions during summer monsoon. J. Sea Res. 95, 56–69. https://doi.org/10.1016/j.seares.2014.10.012.
Manuri, D.B., Chandrasekaran, M., Perumal, M., Mallavarapu, R.V., 2020. Environmental gradients along the tropical coast drive plankton biomass and alter food web interactions. Environ. Sci. Pollut. Res. 27, 36186–36202. https://doi.org/10.1007/s11356-020-09488-4.
Masmoudi, S., Tastard, E., Guermazi, W., Caruso, A., Morant-Manceau, A., Ayadi, H., 2015. Salinity gradient and nutrients as major structuring factors of the phytoplankton communities in salt marshes. Aquat. Ecol. 49, 1–19. https://doi.org/10.1007/s10452-014-9500-5.
Meitei, M.M., Muralidhar, A.P., Syamala, K., Sureesh, S., Biswas, G., Megarajan, S., Munilkumar, S., 2025. Assessment of filtration capacity of different bivalve species suitable for integrated multi-trophic aquaculture (IMTA) systems Vis-à-Vis waste valorization for sustainable environment. Discov. Sustain. 6, 240. https://doi.org/10.1007/s43621-025-01104-0.
Mendo, T., Semmens, J.M., Lyle, J.M., Tracey, S.R., Moltschaniwskyj, N., 2016. Reproductive strategies and energy sources fuelling reproductive growth in a protracted spawner. Mar. Biol. 163, 2. https://doi.org/10.1007/s00227-015-2785-7.
Mendoza-Flores, A., Sánchez-Saavedra, M.D.P., 2023. Light irradiance modifies the fatty acid composition of *Amphidinium carterae* (Dinophyceae). Phycologia 62, 525–531. https://doi.org/10.1080/00318884.2023.2244813.
Millette, N., Da Costa, M., Mora, J., Gast, R., 2021. Temporal and spatial variability of phytoplankton and mixotrophs in a temperate estuary. Mar. Ecol. Prog. Ser. 677, 17–31. https://doi.org/10.3354/meps13850.
Mitra, A., Banerjee, K., Gangopadhyay, A., 2013. Introduction to Marine Plankton. Daya Publ. House, New Delhi, p. 102.
Mozumder, P.K., Biswas, B.C., Mollah, M.A.R., 2023. Plankton seasonality and its relationship with some physicochemical factors in south-eastern coasts of Bay of Bengal, Bangladesh. Dhaka Univ. J. Biol. Sci. 32 (2), 135–148. https://doi.org/10.3329/dujbs.v32i2.67673.
Mukherjee, A., 2025. Light microscopic morphometry of species under two cosmopolitan centric diatom *Coscinodiscus* and *Chaetoceros* from Hooghly-Matla estuarine Waters around Indian Sundarbans. Corpus Int. J. Oceanogr. Aquat. Res. 3, 1–10. https://doi.org/10.54026/CIJOAR/1004.
Mukhopadhyay, S.K., Biswas, H., De, T.K., Jana, T.K., 2006. Fluxes of nutrients from the tropical River Hooghly at the land–ocean boundary of Sundarbans, NE Coast of Bay of Bengal, India. J. Mar. Syst. 62, 9–21. https://doi.org/10.1016/j.jmarsys.2006.03.004.
Noor, A.R., Shakil, A., Hoque, N.F., Rahman, M.M., Akter, S., Talukder, A., Ahmad-Al-Nahid, S., Wahab, M.A., Nahiduzzaman, M., Rahman, M.J., Asaduzzaman, M., 2021. Effect of eco-physiological factors on biometric traits of green mussel *Perna viridis* cultured in the south-east coast of the Bay of Bengal, Bangladesh. Aquac. Rep. 19, 100562. https://doi.org/10.1016/j.aqrep.2020.100562.
Ojea, J., Pazos, A.J., Martínez, D., Novoa, S., Sanchez, J.L., Abad, M., 2004. Seasonal variation in weight and biochemical composition of the tissues of the oyster *Crassostrea gigas* in relation to the gametogenic cycle. Aquaculture 238 (1–4), 451–468. https://doi.org/10.1016/j.aquaculture.2004.05.022.
O'Shea, T., Jones, R., Markham, A., Norell, E., Scott, J., Theuerkauf, S., Waters, T., 2019. Towards a Blue Revolution: Catalyzing Private Investment in Sustainable Aquaculture Production Systems. The Nature Conservancy and Encourage Capital, Arlington, Virginia, p. 159.
Ostroumov, S.A., 2005. Some aspects of water filtering activity of filter-feeders. Hydrobiologia 542 (1), 275–286.
Pales Espinosa, E., Barillé, L., Allam, B., 2007. Use of encapsulated live microalgae to investigate pre-ingestive selection in *Crassostrea gigas*. J. Exp. Mar. Biol. Ecol. 343 (1), 118–126. https://doi.org/10.1016/j.jembe.2006.12.002.
Panigrahi, S., Wikner, J., Panigrahy, R.C., Satapathy, K.K., Acharya, B.C., 2009. Variability of nutrients and phytoplankton biomass in a shallow brackish water ecosystem (Chilika lagoon, India). Limnology 10, 73–85. https://doi.org/10.1007/s10201-009-0262-z.
Parakkandi, J., Saha, A., Sarkar, U.K., Das, B.K., Puthiyottil, M., Muhammadali, S.A., Ramteke, M., Johnson, C., Kumari, S., 2021. Spatial and temporal dynamics of phytoplankton in association with habitat parameters in a tropical reservoir, India. Arab. J. Geosci. 14, 827. https://doi.org/10.1007/s12517-021-07194-0.
Patel, S., Vithalpura, M., Mallick, S.K., Ratheesh, S., 2020. Temporal and spatial variations of monsoonal upwelling along the southwest and east coasts of India. Mar. Geod. 43, 414–432. https://doi.org/10.1080/01490419.2019.1703061.
Patil, J., Anil, A., 2015. Effect of monsoonal perturbations on the occurrence of phytoplankton blooms in a tropical bay. Mar. Ecol. Prog. Ser. 530, 77–92. https://doi.org/10.3354/meps11289.
Pearse, A.G.E., 1985. Histochemistry: Theoretical and Applied, 4th ed. Churchill Livingstone, Edinburgh, London, Melbourne and New York https://www.scirp.org/reference/referencespapers?referenceid=1513327.
Peharda, M., Ezgeta-Balić, D., Davenport, J., Bojanic, N., Vidjak, O., Nincevic-Gladan, Z., 2012. Differential ingestion of zooplankton by four species of bivalves (Mollusca) in the Mali Ston Bay, Croatia. Mar. Biol. 159, 881–895. https://doi.org/10.1007/s00227-011-1866-5.
Pernet, F., Gauthier, C.S., Elise, M., 2007. Change in lipid composition in eastern oyster (*Crassostrea virginica* Gmelin) exposed to constant or fluctuating temperature regimes. Comp. Biochem. Physiol. B Biochem. Mol. Biol. 147 (3), 557–565. https://doi.org/10.1016/j.cbpb.2007.03.009.
Perrino, J.E., Ruez Jr., D.R., 2019. Eastern oyster (*Crassostrea virginica*) filtration efficiency of chlorophyll-a under dynamic conditions in the Hudson-Raritan Estuary at Pier 40, New York City. Open J. Ecol. 9, 238–271. https://doi.org/10.4236/oje.2019.97019.
Pershing, A.J., Mills, K.E., Record, N.R., Stamieszkin, K., Wurtzell, K.V., Byron, C.J., Fitzpatrick, D., Golet, W.J., Koob, E., 2015. Evaluating trophic cascades as drivers of regime shifts in different ocean ecosystems. Philos. Trans. R. Soc. B 370, 20130265. https://doi.org/10.1098/rstb.2013.0265.
Peterson, B., Carl, P., 2024. Performance Analytics: Econometric Tools for Performance and Risk Analysis. R Package Version 2.0.8. https://cran.r-project.org/package=PerformanceAnalytics.
Pham, T.L., Tran, N.D., 2019. Microcystins in freshwater ecosystems: Occurrence, distribution, and current treatment approaches. In: Water and Wastewater Treatment Technologies, pp. 15–36. https://doi.org/10.1007/978-981-13-3259-3_2.
Poot-Delgado, C.A., Okolodkov, Y.B., Aké-Castillo, J.A., Rendón Von Osten, J., 2018. Potentially harmful cyanobacteria in oyster banks of Términos lagoon, southeastern Gulf of Mexico. Acta Biol. Colomb. 23, 51–58. https://doi.org/10.15446/abc.v23n1.65809.
Pouvreau, S., 2000. Gametogenic cycle and reproductive effort of the tropical blacklip pearl oyster, *Pinctada margaritifera* (Bivalvia: Pteriidae), cultivated in Takapoto atoll (French Polynesia). Aquat. Living Resour. 13, 37–48. https://doi.org/10.1016/S0990-7440(00)00135-2.
Prasetiya, F.S., Decottignies, P., Barillé, L., Gastineau, R., Figiel, A., Morançais, M., Mouget, J., Cognie, B., 2017. Cell size-based, passive selection of the blue diatom *Haslea ostrearia* by the oyster *Crassostrea gigas*. J. Molluscan Stud. 83 (2), 145–152. https://doi.org/10.1093/mollus/eyx012.
Purroy, A., Milano, S., Schöne, B.R., Thébault, J., Peharda, M., 2018. Drivers of shell growth of the bivalve, *Callista chione* (L. 1758) – combined environmental and biological factors. Mar. Environ. Res. 134, 138–149. https://doi.org/10.1016/j.marenvres.2018.01.011.
R Core Team, 2024. R: A Language and Environment for Statistical Computing. R Foundation for Statistical Computing, Vienna, Austria. https://www.R-project.org/.
Rahman, M.A., Henderson, S., Miller-Ezzy, P.A., Li, X.X., Qin, J.G., 2020. Analysis of the seasonal impact of three marine bivalves on seston particles in water column. J. Exp. Mar. Biol. Ecol. 522, 151251. https://doi.org/10.1016/j.jembe.2019.151251.
Rastogi, R., Sinha, R., Incharoensakdi, A., 2014. The cyanotoxin-microcystins: current overview. Rev. Environ. Sci. Biotechnol. 13 (2). https://doi.org/10.1007/s11157-014-9334-6.
Reed, A.J., Godbold, J.A., Solan, M., Grange, L.J., 2021. Invariant gametogenic response of dominant infaunal bivalves from the Arctic under ambient and near-future climate change conditions. Front. Mar. Sci. 8, 576746. https://doi.org/10.3389/fmars.2021.576746.

Ren, J.S., Ross, A.H., Schiel, D.R., 2000. Functional descriptions of feeding and energetics of the Pacific oyster *Crassostrea gigas* in New Zealand. Mar. Ecol. Prog. Ser. 208, 119–130. https://doi.org/10.3354/meps208119.

Řezanka, T., Lukavský, J., Nedbalová, L., Sigler, K., 2017. Lipidomic profile in three species of dinoflagellates containing very long chain polyunsaturated fatty acids. Phytochemistry 139, 88–97. https://doi.org/10.1016/j.phytochem.2017.04.012.

Rodríguez-Jaramillo, C., García-Corona, J.L., Zenteno-Savín, T., Palacios, E., 2022. Effects of temperature on gametogenesis and stress in oysters: *Crassostrea gigas* vs. *Crassostrea corteziensis*. Aquaculture 561, 738683. https://doi.org/10.1016/j.aquaculture.2022.738683.

Ronowicz, M., Balazy, P., Chelchowski, M., Kuklinski, P., Patuła, W., Sowa, A., Søreide, J., Weydmann-Zwolicka, A., 2024. Factors shaping pelagic-benthic coupling in Arctic fjord settlement processes. Sci. Rep. 14 (1). https://doi.org/10.1038/s41598-024-74062-8.

Rosa, M., Ward, J.E., Shumway, S.E., 2018. Selective capture and ingestion of particles by suspension-feeding bivalves: A review. J. Shellfish Res. 37 (4), 727–746. https://doi.org/10.2983/035.037.0405.

Sarker, M.J., Tanmoy, M.H., Islam, M.S., Nazrul, K.M.S., Hossen, S., Ali, M.M., 2021. Seasonal variation in phytoplankton and environmental responses in the Naf River, bay of Bengal. Int. J. Aquat. Biol. 9 (5), 309–325. https://doi.org/10.22034/ijab.v9i5.1275.

Sarmento, H., Montoya, J.M., Vázquez-Domínguez, E., Vaqué, D., Gasol, J.M., 2010. Warming effects on microbial food web processes: how far can we go? Philos. Trans. R. Soc. Lond. B Biol. Sci. 365, 2137–2149. https://doi.org/10.1098/rstb.2010.0045.

Sathish, T., Nazrin, A.K., Thomas, L.C., Padmakumar, K.B., 2022. Seasonal dynamics of dinoflagellates with focus on harmful species in a tropical estuary, SW India. J. Oceanogr. 78, 397–408. https://doi.org/10.1007/s10872-022-00648-3.

Saurel, C., Gascoigne, J.C., Palmer, M.R., Kaiser, M.J., 2007. Mussel feeding behavior in situ: regulation by food and tidal conditions. Limnol. Oceanogr. 52, 1919–1929. https://doi.org/10.4319/lo.2007.52.5.1919.

Shin-ichiro, M., Suzuki, K., Kadoya, T., Nakagawa, M., Takamura, N., 2018. Bottom-up links in a shallow, hypereutrophic lake. Ecology 99 (9). https://doi.org/10.1002/ecy.2414.

Siddiqui, K.U., Islam, M.A., Kabir, S.M.H., Ahmad, M., Ahmed, A.T.A., Rahman, A.K.A., Haque, E.U., Ahmed, Z.U., Begum, Z.N.T., Hassan, M.A., Khondker, M., Rahman, M. M., 2007. Encyclopedia of Flora and Fauna of Bangladesh, vol. 17. Molluscs. Asiatic Society of Bangladesh, Dhaka, p. 415.

Singh, A., Kumar, M., 2021. Seasonal and spatial sensitivity of anthropogenic nutrient enrichment in bay of Bengal phytoplankton. Mar. Pollut. Bull. 169, 112554. https://doi.org/10.1016/j.marpolbul.2021.112554.

Singh, D., Tsiang, M., Rajaratnam, B., Diffenbaugh, N.S., 2014. Changes in wet and dry spells during south Asian monsoon. Nat. Clim. Chang. 4, 456–461. https://doi.org/10.1038/nclimate2208.

Smaal, A.C., Ferreira, J.G., Grant, J., Petersen, J.K., Strand, Ø. (Eds.), 2019. Goods and Services of Marine Bivalves. Springer Nature. https://doi.org/10.1007/978-3-319-96776-9.

Soon, T.K., Ransangan, J., 2014. Review on feeding, growth, reproduction, and aquaculture site selection of *Perna viridis*. Adv. Biosci. Biotechnol. 5, 462–469. https://doi.org/10.4236/abb.2014.55056.

Srichandan, S., Baliarsingh, S.K., Prakash, S., Lotliker, A.A., Parida, C., Sahu, K.C., 2019. Seasonal phytoplankton dynamics in contrasting coastal ecosystems. Environ. Sci. Pollut. Res. 26, 12025–12041. https://doi.org/10.1007/s11356-019-04569-5.

Stechele, B., Maar, M., Wijsman, J., Van Der Zande, D., Degraer, S., Bossier, P., Nevejan, N., 2022. Life history and environment tolerance in two oyster species via DEB theory. Conserv. Physiol. 10, coac034. https://doi.org/10.1093/conphys/coac034.

Susana, R.G., Diego, M., Laura, P., Javier, R., 2023. Top-down and bottom-up phytoplankton control in shelf ecosystems. Prog. Oceanogr. 217, 103083. https://doi.org/10.1016/j.pocean.2023.103083.

Tackett, V.M., James, A.S., Rikard, F.S., Andrea, M.T., Ian, A.E.B., 2024. Seasonal effects on reproductive physiology in diploid and tetraploid *Crassostrea virginica*. Aquaculture 593, 741276. https://doi.org/10.1016/j.aquaculture.2024.741276.

Thangavelu, R., 1988. Natural food of *Crassostrea madrasensis* in Pulicat lake, India. Proc. Anim. Sci. 97, 463–470. https://doi.org/10.1007/BF03179954.

Theuerkauf, S.J., Barrett, L.T., Alleway, H.K., Costa-Pierce, B.A., St. Gelais, A., Jones, R. C., 2021. Habitat value of bivalve and seaweed aquaculture. Rev. Aquac. 14 (1), 54–72. https://doi.org/10.1111/raq.12584.

Ubertini, M., Lagarde, F., Mortreux, S., Le Gall, P., Chiantella, C., Fiandrino, A., Bernard, I., Pouvreau, S., Roque d'Orbcastel, E., 2017. Environment-dependent gametogenesis in *Crassostrea gigas* in Thau lagoon. Aquaculture 473, 51–61. https://doi.org/10.1016/j.aquaculture.2017.01.025.

Vajravelu, M., Mariasingarayan, Y., Natarajan, M., Ayyappan, S., 2022. Changes in micro-phytoplankton community structure due to seasonal and inter-annual variation in environmental parameters at Parangipettai coastal water, Bay of Bengal. Thalass. Int. J. Mar. Sci. 38, 957–976. https://doi.org/10.1007/s41208-022-00432-6.

Van De Poll, W.H., Kulk, G., Timmermans, K.R., Brussaard, C.P.D., Van Der Woerd, H.J., Kehoe, M.J., Mojica, K.D.A., Visser, R.J.W., Rozema, P.D., Buma, A.G.J., 2013. Phytoplankton chlorophyll a biomass, composition, and productivity along a temperature and stratification gradient in the Northeast Atlantic Ocean. Biogeosciences 10, 4227–4240. https://doi.org/10.5194/bg-10-4227-2013.

Vanderploeg, H.A., Glyshaw, P.W., Carrick, H.J., Carter, G.S., Dahal, N., Denef, V.J., Fanslow, D.L., Godwin, C.M., 2023. Seasonal interactions between Quagga mussel grazing and phytoplankton in western Lake Erie. Aquat. Ecosyst. Health Manag. 26, 111–119. https://doi.org/10.14321/aehm.026.04.111.

Vargas, M.A., Rodríguez, H., Moreno, J., Olivares, H., Campo, J.A.D., Rivas, J., Guerrero, M.G., 1998. Biochemical composition and fatty acid content of filamentous nitrogen-fixing cyanobacteria. J. Phycol. 34, 812–817. https://doi.org/10.1046/j.1529-8817.1998.340812.x.

Venables, W.N., Ripley, B.D., 2002. Modern Applied Statistics with *S*, 4th ed. Springer, p. 498. https://doi.org/10.1007/978-0-387-21706-2.

Villalejo-Fuerte, M., Muñetón-Gómez, M.D.S., Gárate-Lizárraga, I., García-Domínguez, F., 2005. Gut content, phytoplankton abundance and reproductive season in the black oyster (*Hyotissa hyotis*) at Isla Espiritu Santo, Gulf of California. J. Shellfish Res. 24, 185–190. https://doi.org/10.2983/0730-8000(2005)24[185:GCPAAR]2.0.CO;2.

Wahab, A., Kamarudin, K.A., Toriman, E., Ata, M.M., Juahir, F., Ghazali, H., Anuar, A., 2018. Evaluation of DO, TSS and SSC in Terengganu River, Malaysia. Int. J. Eng. Technol. 7 (3.14), 44–48. https://doi.org/10.14419/ijet.v7i3.14.16860.

Wang, T., Li, Q., 2020. Effects of temperature, salinity and body size on the physiological responses of the Iwagaki oyster *Crassostrea nippona*. Aquac. Res. 51, 728–737. https://doi.org/10.1111/are.14423.

Ward, J.E., Shumway, S.E., 2004. Effects of suspended and benthic particle composition on bivalve feeding behavior. Aquat. Biol. 4, 207–215.

Ward, J.E., Sanford, L.P., Newell, R.I.E., MacDonald, B.A., Thompson, R.J., 1998. A new explanation of particle capture in suspension-feeding bivalves. Limnol. Oceanogr. 43 (5), 741–752. https://doi.org/10.4319/lo.1998.43.5.0741.

Weissberger, E.J., Glibert, P.M., 2021. Diet of *Crassostrea virginica* in a eutrophic tributary of Chesapeake Bay. Aquac. Rep. 20, 100655. https://doi.org/10.1016/j.aqrep.2021.100655.

Wickham, H., 2016. ggplot2: Elegant Graphics for Data Analysis. Springer. https://doi.org/10.1007/978-3-319-24277-4.

Willer, D.F., Nicholls, R.J., Aldridge, D.C., 2021. Opportunities and challenges for global bivalve seafood production. Nat. Food 2, 935–943. https://doi.org/10.1038/s43016-021-00423-5.

Yukihira, H., Klumpp, D., Lucas, J., 1999. Feeding adaptations of *Pinctada margaritifera* and *P. Maxima* to particulate variation. Mar. Ecol. Prog. Ser. 182, 161–173. https://doi.org/10.3354/meps182161.

Zhang, R., Fang, J., Zhang, Y., Qin, X., Zeng, C., Wang, J., 2024. Effects of mussel-phytoplankton interactions on aquatic environment. Aquac. Rep. 37, 102242. https://doi.org/10.1016/j.aqrep.2024.102242.

Aquaculture 614 (2026) 743576

Contents lists available at ScienceDirect

Aquaculture

journal homepage: www.elsevier.com/locate/aquaculture

Integrated insight into somato-gonadal fatty acid dynamics and environmental synchrony: Unravelling post-monsoon gametogenic strategies of oysters *Crassostrea madrasensis* in raft-cultivation systems

Afshana Ferdous [a,b], Israt Jahan [a], Md. Nayeem Hossain [a,c], Sourav Chowdhury [a], Md Moshiur Rahman [d], Md Asaduzzaman [a,*,1]

[a] Department of Marine Bioresource Science, Chattogram Veterinary and Animal Sciences University, Khulshi 4225, Chattogram, Bangladesh
[b] Department of Marine Fisheries and Oceanography, Sher-e-Bangla Agricultural University, Sher-e-Bangla Nagar, Dhaka 1207, Bangladesh
[c] Department of Marine Fisheries and Aquaculture, Faculty of Earth and Ocean Science, Bangladesh Maritime University, Dhaka 1216, Bangladesh
[d] Fish Conservation and Culture Laboratory, Department of Biological and Agricultural Engineering, University of California Davis, 17501 Byron Hwy, Byron, CA 94514, USA

ARTICLE INFO

Keywords:
Indian backwater oyster
Reproductive physiology
Gametogenesis
Fatty acid mobilization
Trophic interactions
Climate change resilience

ABSTRACT

The Indian backwater oyster, *Crassostrea madrasensis,* is a keystone estuarine bivalve of ecological and economic importance. Despite its significance, the links between environmental variability, trophic inputs, and internal fatty acid (FA) dynamics for their reproductive success remain poorly understood. This study investigated the post-monsoon gametogenic strategy of *C. madrasensis* from raft cultivation systems along the southeast coast of the Bay of Bengal using an integrated approach combining histological staging, FA profiling of somatic and gonadal tissues, gut plankton analysis, and environmental monitoring. Histology confirmed five gametogenic stages: early development, late development, mature, spawning, and spent, each exhibiting distinctive FA signatures. Statistical analyses, including ANOVA, PCA, and PLS-DA, revealed significant variation in 21 of the 28 fatty acids. Early development was characterized by the enrichment of eicosatrienoic, myristic, and linolenic acids, reflecting preparatory energy storage, whereas late development was dominated by MUFA, n-6 PUFA, and linoleic acid. Mature gonads accumulated arachidic, erucic, and heptadecanoic acids, whereas spawning displayed a pronounced increase in octanoic acid, eicosenoic acid, behenic acid, and long-chain PUFA, particularly DHA and EPA, highlighting their role in gamete maturation and membrane formation. The spent stage exhibited elevated arachidonic acid but depleted DHA and EPA, indicating transfer into gametes. Somatic tissues displayed complementary but offset patterns, and strong positive correlations between body and gonad pools confirmed active lipid mobilization. Gut content analysis revealed that essential FAs were acquired both directly from ingested plankton, particularly Bacillariophyceae, Dinophyceae, and Zooplankton, and indirectly via somatic reserves. Environmental drivers strongly influenced these dynamics; rising salinity, nutrient enrichment, and high phytoplankton abundance coincided with maturation and spawning, whereas elevated temperature and turbidity corresponded to resting stages. Overall, reproductive output in *C. madrasensis* is governed by a finely tuned synergy between environmental factors, trophic coupling, and somato-gonadal fatty acid mobilizations. This study provides mechanistic insights into estuarine bivalve reproduction, establishes a framework for evaluating climate-linked reproductive shifts, and informs aquaculture strategies for broodstock conditioning under dietary regimes that mimic natural cues.

1. Introduction

The dynamic interaction of organisms with their environments is a vital question in marine ecology, particularly in the context of reproductive physiology (Gosling, 2015; Maneiro et al., 2017). Marine bivalves, specifically species belonging to the genus *Crassostrea*, serve as

* Corresponding author.
E-mail address: a_zamanbau@yahoo.com (M. Asaduzzaman).
[1] Orcid ID: 0000–0002–8211-146

https://doi.org/10.1016/j.aquaculture.2025.743576
Received 27 September 2025; Received in revised form 25 November 2025; Accepted 18 December 2025
Available online 22 December 2025

an excellent model organism due to their ecological and economic importance (Kasmini and Batubara, 2022). Among them, *C. madrasensis* is a significant bivalve that occurs in the estuarine and coastal waters of the Indian subcontinent, as well as in other tropical regions. Ecologically, *C. madrasensis* has a substantial role in maintaining water quality through filtration of an enormous amount of water, nutrient recycling, and assimilating excess anthropogenic nutrients from the aquatic environment (Meitei et al., 2025; Bricker et al., 2020; Asha et al., 2014). Natural and/or aquaculture analogues to oyster reefs have complex structure and provide multiple habitat services, such as (i) increased foraging space for juvenile fish and invertebrates, (ii) better breeding habitats, (iii) refuge from predators, and so forth (O'Shea et al., 2019; Theuerkauf et al., 2022). Moreover, these reefs can act as natural breakwaters that attenuate wave energy and shoreline erosion in intertidal and subtidal areas (van der Schatte Olivier et al., 2020). In addition to its ecological value, *C. madrasensis* is a commercially important aquaculture species with a rapid growth rate and high market demand, contributing economically toward the livelihood support of many coastal communities (Yosuva et al., 2019; Sanjeevaraj, 2008). Its ecological and economic significance underscores the importance of understanding its reproductive physiology in relation to environmental drivers.

The timing and extent of bivalve reproduction in marine environments are vital for population dynamics, survival rates, health, and the resilience of aquatic ecosystems (Carson et al., 2010; Asaduzzaman et al., 2019). Generally, gametogenesis is a coordinated sequence of sequential and synchronized changes in gonadal development, ending with the release of mature gametes into the environment for fertilization. The gametogenic phenology of *C. madrasensis* is a physiological process influenced by various external factors (such as environmental conditions, seasonality, and food availability) and internal stimuli (including physiological state, energy reserves, and nutritional quality) (Gosling, 2003; Kim et al., 2010; Uddin et al., 2013). The reproductive cycle of *C. madrasensis* has been examined histologically across different regions of the Indian subcontinent (Park and Choi, 2004; Uddin et al., 2013; Uddin et al., 2024). Previous research indicated a prolonged periodic single spawning for *C. madrasensis* (Pakhmode et al., 2022; Ezgeta-Balić et al., 2020), yet this species also shows two distinct spawning seasons (Toyokawa et al., 2023; Uddin et al., 2024), depending on habitat type, physiological condition, and environmental stimuli.

Gametogenesis in marine bivalves is an energy-demanding process, requiring the mobilization of energy stores, particularly lipids and fatty acids from various tissues, to support physiological functions and reproduction (Fernández-Reiriz et al., 2007; Bridier et al., 2023). Stored triglycerides in the hepatopancreas and other tissues serve as key energy reserves (Wenne and Polak, 1989), which are accumulated during the pre-spawning period in response to favorable environmental conditions. These reserves are later mobilized to support gamete development, with timing often synchronized to seasonal changes and periods of abundant food, allowing oysters to replenish energy stores post-spawning (Camacho et al., 2003; Su et al., 2006; Joaquim et al., 2011; Nguyen et al., 2024). The transfer of nutrients from somatic to gonadal tissues is essential for sustaining gamete quality and reproductive success in *C. madrasensis*. Depending on environmental conditions, this species may employ either an opportunistic strategy, relying on energy from external food sources (Garrido and Barber, 2001; Enríquez-Díaz et al., 2009), or a conservative strategy, drawing on previously stored somatic energy reserves (Hassan et al., 2018; Pouvreau, 2000; Kang et al., 2000; Lopes-Lima et al., 2014; Asaduzzaman et al., 2019). Understanding whether *C. madrasensis* predominantly uses stored reserves, externally acquired energy, or a combination during gametogenesis, which remains limited.

Fatty acids, the primary components of lipids, are crucial in the reproductive biology of marine bivalves, functioning as essential elements of cellular membranes, energy reserves, and signalling molecules, and are vital for gamete development and maturation (Ventrella et al., 2008; Liu and Kong, 2013). Alterations in fatty acid composition directly influence gamete quality, fertilization success, and overall reproductive output in oysters, underscoring the significance of dietary fatty acids during critical reproductive phases (Cho et al., 2023). Saturated fatty acids (SFAs) are predominantly oxidized to produce ATP, the cellular energy currency, facilitating the energy-demanding processes of gametogenesis and spawning. Although oysters cannot often synthesize polyunsaturated fatty acids (PUFAs), some saturated fatty acids (SFAs) may act as precursors in the biosynthesis of long-chain unsaturated fatty acids (Renaud et al., 2002). Polyunsaturated fatty acids (PUFAs), especially omega-3 and omega-6 fatty acids, are essential for preserving cellular membrane integrity and fluidity, which is critical for fertilization and the initial stages of embryonic or larval development (De Moreno et al., 1980; Asaduzzaman et al., 2019). Furthermore, polyunsaturated fatty acids (PUFAs) serve as precursors for eicosanoids, including prostaglandins and leukotrienes, which modulate reproductive processes such as gamete maturation, spawning timing, and fertilization, thereby synchronizing gamete release in response to environmental stimuli to enhance reproductive success (Whyte et al., 1992; Caers et al., 2003).

Fatty acid composition in bivalves reflects both their feeding regimen and surrounding environmental conditions, serving as a key indicator of physiological status and reproductive potential (Freites et al., 2002; Gatenby et al., 2003; Kim et al., 2019). Similar to other marine bivalves, *C. madrasensis* is a filter feeder that depends on phytoplankton and particulate organic matter (POC) as primary sources of nutrition and energy during gametogenesis (Meitei et al., 2025; Thangavelu, 1988). Seasonal fluctuations and environmental variability strongly influence plankton abundance in the Bay of Bengal and other coastal regions of the Indian subcontinent (Asaduzzaman et al., 2020; Noor et al., 2021). Furthermore, *C. madrasensis* exhibits selective feeding behaviour, adjusting its ingestion patterns according to both reproductive stage and environmental conditions (Hossain et al., 2025; Soon and Ransangan, 2014; Navarro and Iglesias, 1995). Therefore, a comprehensive analysis of fatty acid mobilization, trophic relationships, and environmental variability is essential for elucidating the reproductive strategies and ecological resilience of *C. madrasensis*.

Although numerous studies have investigated fatty acid composition throughout the gametogenic stages in oysters (Cho et al., 2023; Dridi and Romdhane, 2017; Vahirua-Lechat et al., 2008), substantial knowledge gaps persist concerning the mechanisms by which *C. madrasensis* and other marine bivalves transfer fatty acids between somatic and gonadal tissues during various stages of gonadal maturation. Here, we hypothesize that reproductive output in *C. madrasensis* is governed by a synergistic interaction among environmental cues, dietary inputs, and somato-gonadal fatty acid reallocation. We analyzed fatty acid profiles at various stages of gonadal maturity and investigated their transfer between somatic and gonadal tissues throughout the reproductive cycle. Furthermore, we investigated the impact of ambient environmental conditions and consumed plankton on fatty acid mobilization to clarify energy allocation mechanisms during gametogenesis. Comprehending these mechanisms is essential for enhancing knowledge of reproductive biology and for guiding conservation and management strategies, especially regarding climate change, which can interfere with life cycles and jeopardize the reproductive health of *C. madrasensis* populations.

2. Materials and methods

2.1. Study area and sampling strategies

The Indian backwater oysters (*C. madrasensis*) were collected from the raft cultivation systems in Moheshkhali Channel on the west coast of Moheshkhali, Cox's Bazar, Bangladesh (Fig. 1). This channel connects directly to the Bay of Bengal and represents a dynamic estuarine habitat on the southeast coast of Bangladesh. From September to February

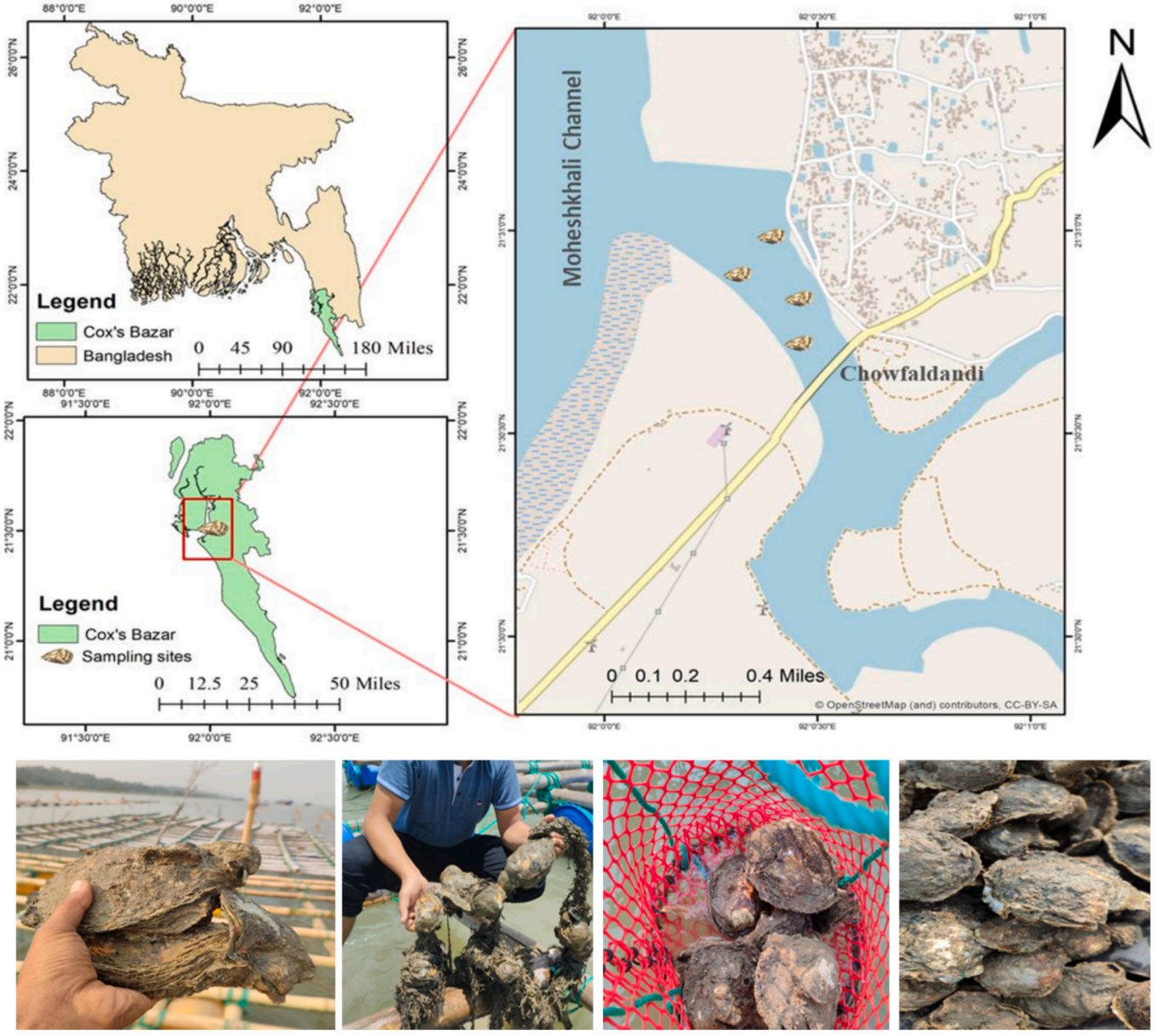

Fig. 1. Map showing the sampling sites of the oysters (*Crassostrea madrasensis*) from the southeastern coastal water of the Bay of Bengal, Bangladesh. The oysters were collected from the attached ropes or cages in the raft cultivation systems.

2023–2024, 25–30 mature oysters (shell length > 80 mm) were sampled fortnightly from the hanging ropes or cages (Fig. 1) in floating raft systems to ensure adequate representation of all gonadal maturity stages during the post-monsoon gametogenic cycle. To ensure adequate representation of all gonadal maturity stages at each sampling event, 25–30 oysters were collected per sampling date, which aligns with established sample sizes commonly used for reproductive histology and fatty acid studies in bivalves (Kripa and Mohamed, 2008; Lango-Reynoso et al., 2000). Collected specimens were transported live in ambient seawater to the Oceanography Laboratory at Chattogram Veterinary and Animal Sciences University. In the laboratory, shells were brushed clean to remove fouling organisms, sediments, and debris, followed by rinsing with clean water. Biometric traits, including shell length, width, and height, were measured using vernier callipers (±0.01 mm), while whole-body weight was recorded on an electronic balance (PS 1200.R2, Radwag, Poland) to the nearest 0.1 g after draining intervalval fluids. During dissection, individuals exhibiting visible gonadal development (excluding resting/undifferentiated stages) were assigned unique identification codes for fatty acid (FA) and gut plankton analyses. Subsamples of gonadal tissue were preserved in fixatives for histological confirmation of sex and maturity stage. Remaining gonadal and somatic tissues were stored in pre-labeled vials at −20 °C for FA profiling. Each coded oyster was also processed for gut plankton analysis. Based on histological confirmation of gonadal maturity, 30 individuals in the early developmental stage, 24 in the late developmental stage, 30 in the mature stage, 25 in the spawning stage, and 25 in the spent stage were obtained for FA profiling. Subsequently, body and gonad tissues from the above individuals were selected to form three independent replicates, while maintaining a balanced male: female ratio (1:1) at each developmental stage for FA profiling. Following the exclusion of unused samples, gut plankton data from the same individuals per maturity stage were analyzed in this study.

2.2. Histological analyses of the gonad tissues

Histological examinations of *C. madrasensis* gonads were conducted

following the protocol of Hamli et al. (2015). Gonadal tissues were carefully separated from the mantle and immediately fixed in Bouin's solution for 24 h. After fixation, tissues were dehydrated through a graded ethanol series (80–100 %) and cleared with xylene before being embedded in paraplast blocks. Transverse sections (7 μm) were prepared using a rotary microtome and mounted on glass slides. Slides were further dehydrated through ascending ethanol concentrations and stained with haematoxylin and eosin, following Pearse (1985), to differentiate cellular structures. Microscopic observations were performed under a digital microscope (Optika B-190 TB, Ponteranica, Italy) using 10 × −40× magnification objectives, enabling sex determination and staging of gonadal development. Gonadal condition was classified into different categories according to Uddin et al. (2024): resting, early development (ED), late development (LD), mature (Mat), spawning (Spn), and spent (Spt). Sex was identified based on the presence of oocytes in females and spermatogenic cells in males. Multiple sections from each individual were examined to ensure diagnostic accuracy, and representative micrographs were captured for documentation and further analysis.

2.3. Measurement of water quality parameters

Sampling was conducted monthly throughout the study period. Because the oysters were cultivated on floating raft systems suspended within the surface–subsurface layer (0–30 cm), water sampling was designed to capture the physicochemical conditions directly experienced by the cultured individuals. Although the study site is an estuarine channel, the Moheshkhali Channel is tidally energetic and vertically well-mixed during the post-monsoon period, resulting in minimal stratification; thus, surface–subsurface water reliably represents the water column across the culture depth. In situ measurements of surface water temperature, dissolved oxygen (DO), pH, and salinity were obtained using a multifunctional water quality probe (YSI, Loveland, USA), while current velocity was recorded with a digital flow meter (Flow Probe FP311, Global Water, USA). Turbidity was measured using a portable turbidity meter (Turb 430 IR, WTW, Germany). During each sampling event, composite surface water samples were collected using a depth-integrated Kemmerer sampler (1200-E, USA). Physical parameters were measured immediately on board to minimize handling errors. Approximately 800 mL of water was then transported to the laboratory under controlled conditions for further analysis. Before chemical and biological assessments, samples were filtered through Whatman GF/C glass microfiber filters using a vacuum pump. Nutrient concentrations (NO_2, NO_3, PO_4) were quantified spectrophotometrically with a Photo-Flex STD (WTW, Germany), following APHA (1992) standard protocols. Chlorophyll a content was determined spectrophotometrically at 664, 647, 630, and 750 nm (Optizen Pop 2102, Korea) according to Boyd (1979).

2.4. Fatty acid analysis

Gonadal and somatic tissues (see Section 2.1) were first homogenized and freeze-dried with a FreeZone 4.5 unit (LABCONCO, Kansas City, MO, USA) until a constant dry weight was reached. Lipids were isolated from the dried material using a Soxhlet extractor with diethyl ether maintained at 60 °C as the solvent. The recovered lipid fraction served as the substrate for fatty acid methyl ester (FAME) preparation. For transesterification, 1.5 mL of methanolic NaOH was added to the lipid extract, and the mixture was heated in an ultrasonic bath at 80 °C for 5 min. After cooling, 2 mL of methanolic boron trifluoride was introduced and incubated for 30 min at the same temperature. The reaction was terminated by adding 1 mL of isooctane, followed by 5 mL of saturated NaCl solution to facilitate phase separation. The organic layer was carefully withdrawn and transferred into 1 mL GC vials for analysis. FAMEs were analyzed using gas chromatography–mass spectrometry (GC–MS; GCMS-QP2020, Shimadzu, Japan) for compound identification, and gas chromatography with flame ionization detection (GC-FID; Hewlett Packard 6890 Series) for quantification. Separations were achieved on an Omegawax 250 capillary column (30 m × 0.25 mm i.d., 0.25 μm film thickness), with helium as the carrier gas at a flow rate of 1 mL/min. The oven temperature program was initiated at 150 °C, increased to 250 °C at 4 °C/min, and held isothermally at 250 °C. Fatty acids were identified by comparison with retention times from a certified standard mixture (Supelco 37 Component FAME Mix). The quantification was performed by peak area integration relative to an internal standard, and results were expressed as percentages of total identified fatty acids.

2.5. Gut plankton analyses

The encoded specimens of *C. madrasensis* were examined to evaluate the qualitative composition and quantitative abundance of gut plankton. Since the oysters were collected directly from their natural habitats, it was not possible to obtain pseudofeces samples for a detailed assessment of feeding behaviour. Consequently, we circumvented this possibility and employed a conventional technique for transferring the maximum volume of gut contents utilizing a disposable Pasteur pipette. The collected gut was diluted in 30 mL of filtered, autoclaved seawater within a glass Petri dish. To quantify gut plankton (cells/individual) in a specimen, a Sedgewick–Rafter (S–R) counting chamber, including 1000 squares with a volume of 1 mm^3, was employed as delineated by Asaduzzaman et al. (2025). Following thorough agitation, a 1-mL subsample was transferred into the chamber, and planktonic cells in 10 randomly selected grids were enumerated using a binocular microscope (Optika B-190 TB; Ponteranica, Italy). The estimated number of gut plankton is calculated as $N = (P \times C \times 100)$, where N denotes the estimated number of plankton cells per gut, P signifies the number of cells counted in 10 S–R chamber fields, and C indicates the total volume (ml) of the diluted material. The taxonomic identification was conducted at the genus level, after which the plankton was categorized into major taxonomic groups according to established guidelines from prior studies (Asaduzzaman et al., 2020). Non-planktonic particles and detrital organic materials were excluded from the analysis.

2.6. Statistical analysis

The dataset consisted of 28 fatty acids and their aggregated classes within tissues and reproductive stages. The data were log-transformed (natural-log) and auto-scaled to remove analytical noise as well as artefacts. Normality was tested with the Shapiro–Wilk test, and variance homogeneity by Levene's test, both performed using R version 4.4.2 with the car package (Fox and Weisberg, 2019; R Core Team, 2024). Comparison of fatty acid composition among tissues and maturity stages was first analyzed by ANOVA, and then pairwise comparisons were carried out by independent-sample *t*-tests to compare gonadal and somatic tissues within each stage. To account for potential Type I errors associated with multiple comparisons, *p*-values have been adjusted with the false discovery rate (FDR) correction procedure (Benjamini and Hochberg, 1995). Volcano plots were obtained for visualization purposes and used to indicate statistically significant differences according to FDR-adjusted p-values and fold change ±1. The structure of the data and its stage-specific variability were also examined by PCA. The discrimination of fatty acid profiles among the gonadal maturity stages was conducted using partial least squares discriminant analysis (PLS-DA) with R^2, Q^2, and permutation tests performed for model validation. Variables with a VIP score > 1 were considered to be important contributors. Tissue- and stage-specific fatty acid distributions were depicted with clustered heatmaps (Euclidean distance, Ward's linkage). For analysis of trophic linkages, Spearman rank correlation was performed with fatty acid concentrations (in gonad or body) and relative abundance of gut plankton group (correlation matrices visualized by the ggcorrplot package in R) (Kassambara, 2023). In the end, an integrative

PCA was performed on the merged dataset made of water quality parameters, fatty acid profiles, and gut plankton abundance (variables scaled) with the FactoMineR package (Lê et al., 2008). Further methodological information and supporting results can be found in the supplementary information files.

3. Results

3.1. Microscopic confirmation of gonad development stages

Based on oogenic and spermatogenic traits, five main gonadal phases were found in *C. madrasensis* (Fig. 2). Storage cells were present during the resting phase (Fig. 2A). Males displayed spermatogenic cell aggregations along the basal follicular wall during the early developmental stage (Fig. 2B), whereas females displayed small early (EO) and growing oocytes (GO) attached to the follicle wall (Fig. 2C). Male follicles showed centripetally arranged spermatocytes, spermatids, and spermatozoa with few spermatogonia during the late developmental stage (Fig. 2D). Female follicles had a central nucleus and vitelline membrane, and about half of the oocytes were attached to the wall (Fig. 2E). These follicles also contained EO and GO. Gamete-filled, fully enlarged follicles were a feature of the mature phase. Females had free mature ova with prominent central nuclei (Fig. 2G), while males had spermatozoa that were densely packed and orientated concentrically (Fig. 2F). The spawning stage was characterized by partially emptied follicles; females had ruptured germinal vesicles and partially released ova (ES) (Fig. 2I), while males displayed spiral-arranged spermatozoa and vacant spaces (Fig. 2H). In the spent stage, females showed fragmented follicle walls with scattered, unreleased oocytes (Fig. 2K–L), while males retained few residual spermatozoa in degenerative follicles (Fig. 2J).

3.2. Influence of gonadal stages and tissues on fatty acid profile in C. madrasensis

There was a significant effect of the gonadal maturity stage, tissue type, and their interaction on the fatty acid profile of *C. madrasensis*, as examined by a two-way ANOVA (Fig. 3). Across reproductive stages, nearly all fatty acids, including arachidic, arachidonic, behenic, decanoic, docosahexaenoic (DHA), eicosapentaenoic (EPA), eicosatrienoic, eicosenoic, heneicosanoic, lauric, linoleic, linolenic, myristic, nervonic, oleic, palmitic, palmitoleic, stearic, and tridecanoic acids, along with grouped fractions such as MUFA, PUFA, n-3 PUFA, n-6 PUFA, and SAFA, were found to be highly significant across reproductive stages (FDR $<$ 0.001). The tissue types of effects were also robust. Arachidic, DHA,

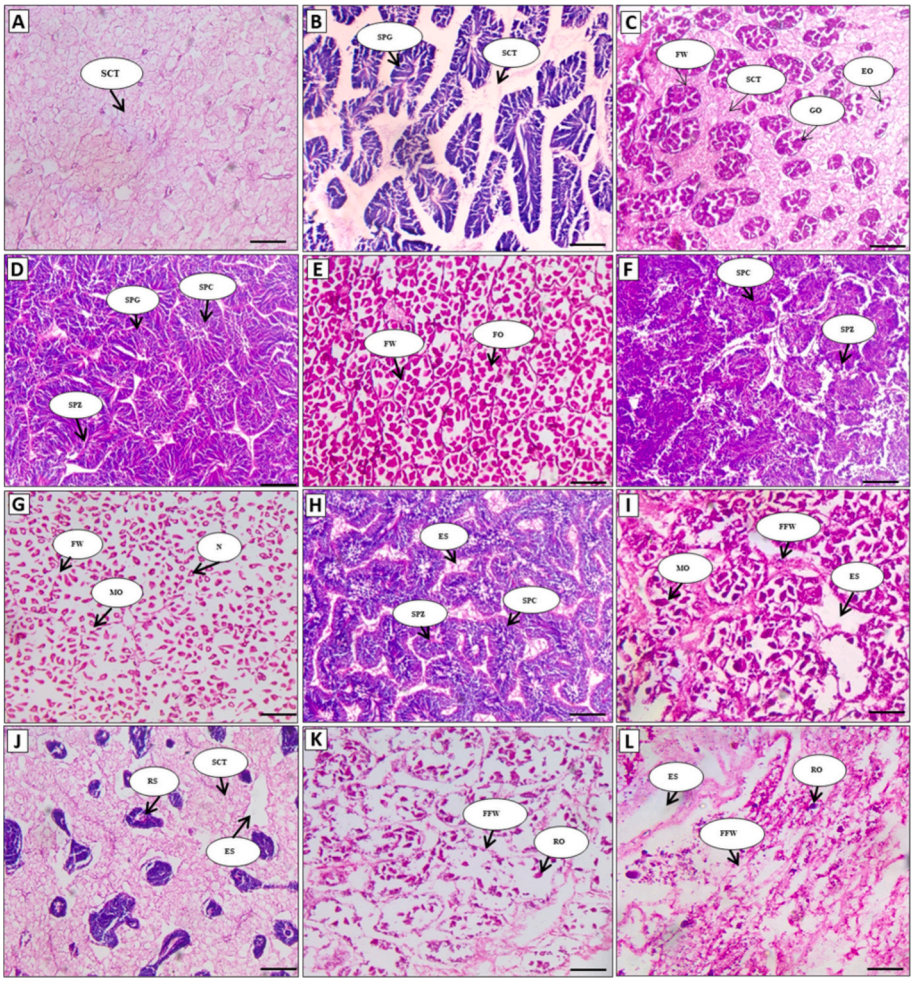

Fig. 2. Photomicrograph depicting the developmental stage of gonads during the post-monsoon gametogenesis cycle (September to February) of the oyster (*Crassostrea madrasensis*) sourced from the southeastern shore of the Bay of Bengal, Bangladesh. The photomicrograph depicted (A) Resting state, (B–C) Early developmental stage (B: male, C: female), (D-E) Late developmental stage (D: male, E: female), (F-G) Mature stage (F: male, G: female), (H–I) Spawning phase (H: male, I: female), (J-L) Spent stage (J: male; K, L: female). In this context, FW denotes follicular wall; SCT refers to storage connective tissue; SPG signifies spermatogonia; SPC indicates spermatocyte; SPZ represents spermatozoa; EO stands for early oocyte; GO denotes growing oocyte; FO refers to free oocyte inside the lumen; MO signifies mature oocyte; N represents nucleus; FFW indicates fragmented follicle wall; ES denotes empty space; RS refers to residual spermatozoa and RO refers to residual oocyte. The scale bar represents 100 μm.

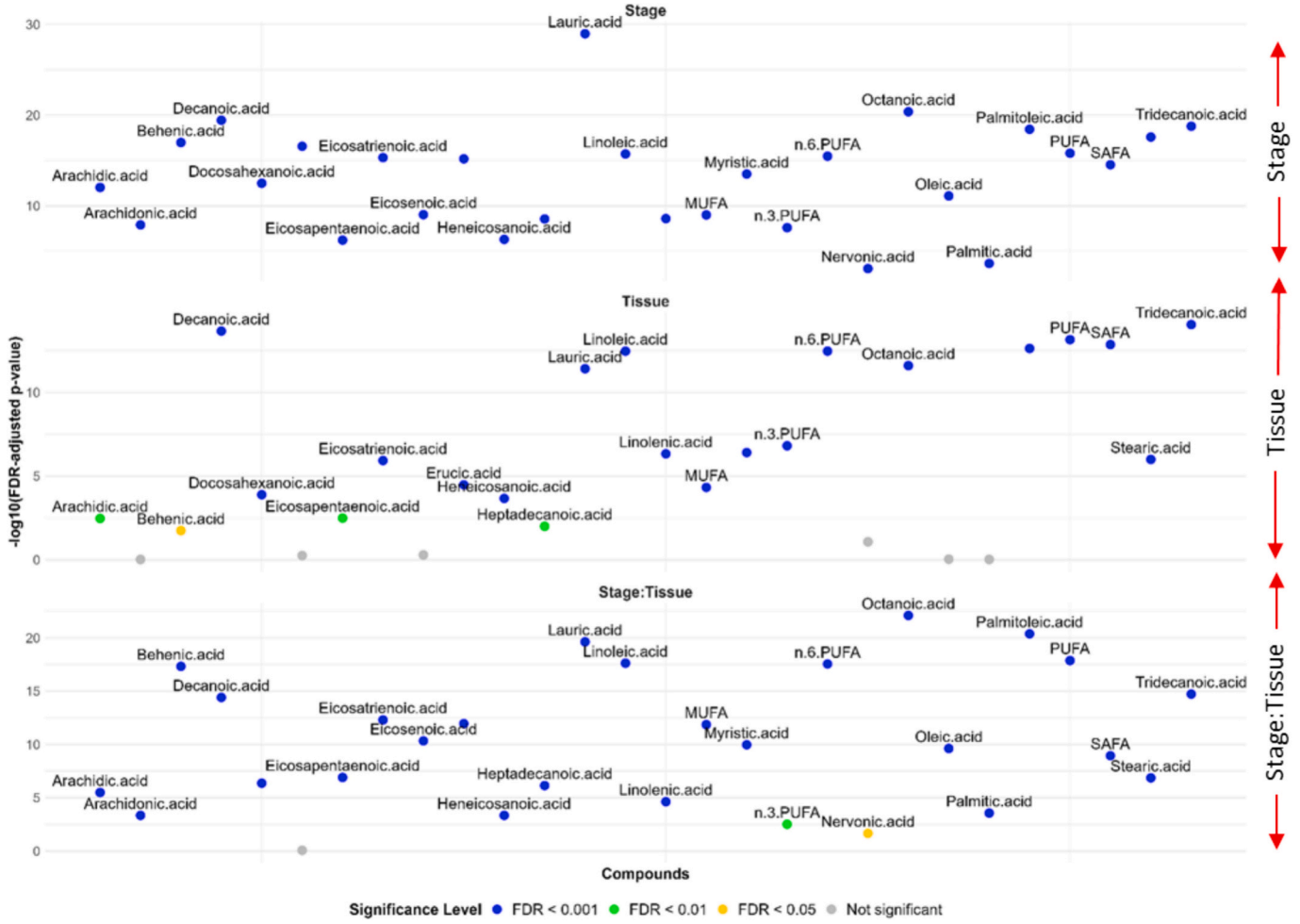

Fig. 3. Two-way ANOVA (Stage × Tissue) results for fatty acid composition in *Crassostrea madrasensis*. The plot shows the significance levels of individual fatty acids and fatty acid groups under three model terms: stage, tissue, and their interaction (stage × tissue). Each point represents a fatty acid or group, with the y-axis indicating statistical significance as –log10 (FDR-adjusted *p*-value). Colors denote the false discovery rate thresholds: blue for highly significant differences (FDR < 0.001), green for significant differences (FDR < 0.01), yellow for moderate significance (FDR < 0.05), and grey for nonsignificant effects. (For interpretation of the references to colour in this figure legend, the reader is referred to the web version of this article.)

EPA, eicosatrienoic, erucic, heneicosanoic, heptadecanoic, lauric, linolenic, palmitoleic, and stearic acids and the composite group (MUFA, PUFA, n-3 PUFA, n-6 PUFA, SAFA) were significantly different between gonadal and somatic tissues at FDR < 0.001. Additional significant tissue effects were observed for arachidic, EPA, and heptadecanoic acids (FDR < 0.01), with only a few fatty acids being nonsignificant. The gametogenic stage-tissue type interaction further emphasized the complexity of fatty acid dynamics, where almost all compounds exhibited highly significant differences (FDR < 0.001). These findings validate that reproductive stage and tissue-specific processes function coordinately in the regulation of fatty acid mobilization in *C. madrasensis*.

3.3. Fatty acid dynamics within gonad tissues across different gametogenic stages

The heatmap (Fig. 4A) demonstrated that fatty acid profiles from the more advanced gametogenic stages (late development, mature, and spawning) were distinctly clustered apart from those of the early development and spent stages. The heatmap and PCA (Fig. 4A-B) consistently indicated that the early development stage was marked by increased concentrations of eicosatrienoic acid, myristic acid, and linolenic acid, whereas the late development stage was linked to heightened levels of docosapentaenoic acid, linoleic acid, MUFA, PUFA, and n-6 PUFA. The mature stage was characterized by elevated levels of lauric acid, decanoic acid, arachidic acid, erucic acid, and heptadecanoic acid, whereas the spawning stage exhibited increased concentrations of eicosapentaenoic acid, docosahexaenoic acid, octanoic acid, eicosenoic acid, behenic acid, and nervonic acid. The spent stage was predominantly characterized by the presence of arachidonic acid, accompanied by relatively diminished levels of DHA and EPA. PCA differentiated the five stages according to fatty acid composition, with PC1 accounting for 31 % and PC2 for 25.6 % of the variation, underscoring unique correlations of fatty acids with each gametogenic phase. The PLS-DA and variable importance in projection (VIP) analysis (Fig. 4C) found 14 fatty acids with VIP values over 1.0 as significant discriminators of gametogenic phases. Docosahexaenoic acid, behenic acid, and MUFA demonstrated the greatest VIP ratings (VIP > 1.5), with heneicosanoic acid, eicosatrienoic acid, palmitic acid, oleic acid, arachidonic acid, erucic acid, n-3 PUFA, n-6 PUFA, linoleic acid, and PUFA as further contributors. The heatmap associated with the VIP analysis validated these stage-specific distributions: the two (docosahexaenoic acid and behenic acid) highest-ranking fatty acids (VIP > 1.5) were predominantly concentrated in spent and spawning tissues, while being least abundant in early and late development tissues. Among other discriminating fatty acids (VIP > 1.0), eicosatrienoic acid was predominantly concentrated in the early development stage; heneicosanoic acid, oleic acid, n-6 PUFA, PUFA; and linoleic acid in the late

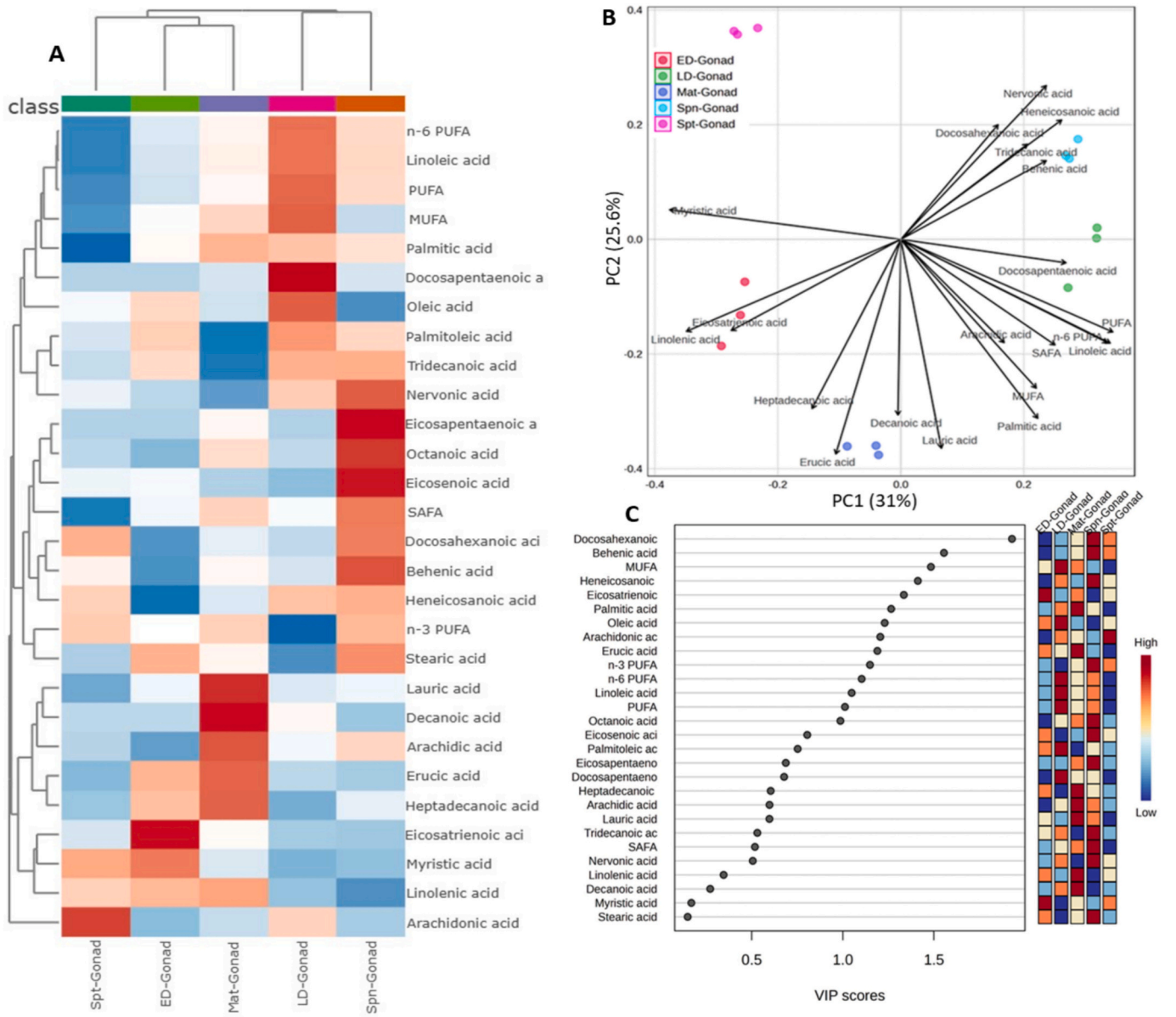

Fig. 4. Dynamics of fatty acids in gonadal tissues related to the post-monsoon gametogenesis cycle of oysters (*Crassostrea madrasensis*). (A) The heatmap depicts the fatty acid composition throughout five distinct stages of gonadal development. The map was created using clustering data derived from the fatty acid profiles of gonadal tissues at five developmental stages. The heatmap displays the twenty-eight fatty acids and their respective groups found using *t*-test analysis (FDR-adjusted $p < 0.05$). Distance is quantified by Pearson correlation, while grouping is established via the Ward algorithm. Each colored cell in the heat map represents a concentration of fatty acids or their respective groups on the right side. In the colored cells, red signifies a high concentration, while blue denotes a low concentration. (B) Principal component analysis (PCA) biplots depicting five distinct stages of gonad development with fatty acids as explanatory variables. (C) The Variable Importance in Projection (VIP) figure illustrates the variations in fatty acid profiles linked to several stages of gametogenesis in gonadal tissues, as determined by Partial Least Squares Discriminant Analysis (PLS-DA). The colourful boxes on the right represent the relative concentrations of the relevant fatty acids during five phases of gametogenesis in gonadal tissues.VIP is a weighted summation of the squares of the PLS-DA loadings, considering the proportion of the explained Y-variable in each dimension. ED denotes early development stage; LD signifies late development stage; Mat represents mature stage; Spn indicates spawning stage; and spt refers to spent stages. (For interpretation of the references to colour in this figure legend, the reader is referred to the web version of this article.)

development stage, erucic acid and palmitic acid in the mature stages.

3.4. Fatty acid dynamics within somatic tissues across different gametogenic stages

The heatmap (Fig. 5A) demonstrated that fatty acid profiles in somatic tissues throughout late developmental and mature stages of the gonad were differently grouped from those of early developmental, spawning, and spent stages. During the initial developmental phase, both the heatmap and PCA (Fig. 5B) consistently indicated elevated concentrations of eicosenoic acid, eicosatrienoic acid, myristic acid, stearic acid, heptadecanoic acid, and erucic acid in somatic tissues, while the later developmental phase correlated with increased levels of docosapentaenoic acid, eicosapentaenoic acid, arachidonic acid, and octanoic acid. The mature stage was marked by elevated levels of arachidic acid, linolenic acid, lauric acid, decanoic acid, n-6 PUFA, PUFA, linoleic acid, and n-3 PUFA, whereas the spawning stage was defined by heightened concentrations of MUFA, SAFA, palmitoleic acid, and nervonic acid. Conversely, the spent stage was characterized by elevated concentrations of behenic acid, heneicosanoic acid,

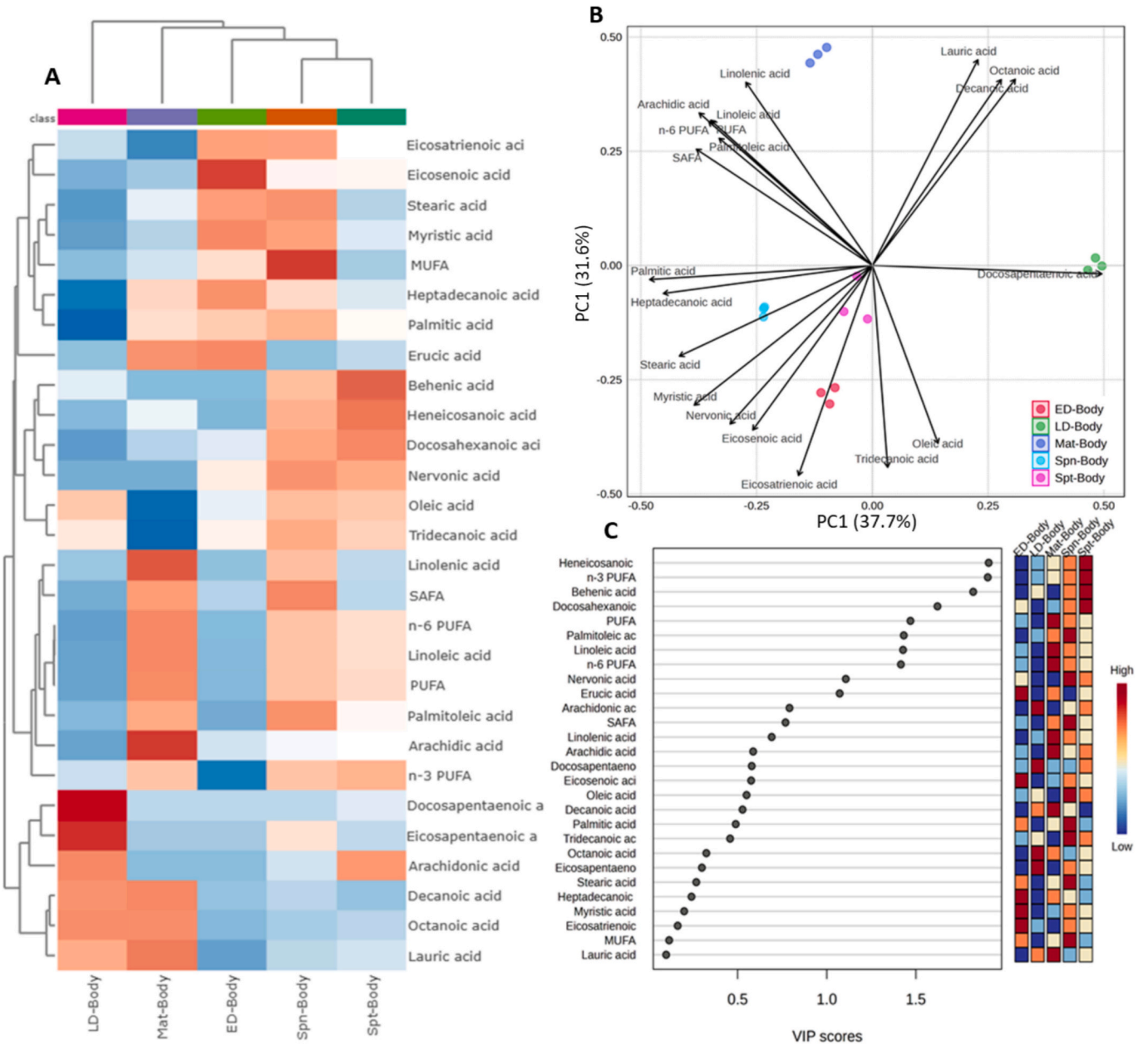

Fig. 5. The dynamics of fatty acids in body tissues correlate with the post-monsoon gametogenesis cycle of oysters (*Crassostrea madrasensis*). (A) The heatmap depicts the fatty acid profile of bodily tissues linked to five distinct stages of gametogenic development. The map was created using clustering outcomes derived from fatty acid profiles. The heatmap displays the twenty-eight fatty acids and their respective groups found using t-test analysis (FDR-adjusted $p < 0.05$). Distance is quantified by Pearson correlation, while grouping is established via the Ward algorithm. Each colored cell in the heat map represents a concentration of fatty acids or their groupings, indicated on the right side. In the colored cells, red signifies a high concentration, while blue denotes a low concentration. (B) Principal component analysis (PCA) biplots of fatty acid profiles from bodily tissues linked to five stages of gonadal development and their explanatory variables. (C) The Variable Importance in Projection (VIP) figure illustrates the variations in the fatty acid profiles of bodily tissues linked to five recognized gametogenesis stages, as determined by partial least squares discriminant analysis (PLS-DA). The colourful boxes on the right represent the relative concentrations of the relevant fatty acids during five phases of gametogenesis in gonadal tissues. VIP is a weighted summation of the squares of the PLS-DA loadings, taking into account the proportion of the explained Y-variable in each dimension. ED denotes early development stage; LD signifies late development stage; Mat represents mature stage; Spn indicates spawning stage; and spt refers to spent stages. (For interpretation of the references to colour in this figure legend, the reader is referred to the web version of this article.)

docosahexaenoic acid, and arachidonic acid. PCA significantly delineated the five stages of somatic tissues, with PC1 (37.7 %) and PC2 (31.6 %) collectively accounting for 69.3 % of the variance, underscoring unique correlations of fatty acid content with each gametogenic phase. PLS-DA and VIP score analysis (Fig. 5C) found ten fatty acids with VIP scores exceeding 1.0 as principal discriminators of somatic tissue profiles across stages. Heneicosanoic acid, n-3 PUFA, behenic acid, and docosahexaenoic acid exhibited the greatest VIP ratings (VIP > 1.5), but PUFA, palmitoleic acid, linoleic acid, n-6 PUFA, nervonic acid, and erucic acid were also significant (VIP > 1.0). The heatmap associated with the VIP analysis validated these stage-specific distributions: the four highest-ranking fatty acids (VIP > 1.5) were predominantly concentrated in spent and spawning tissues, while being least abundant in early development tissues. Other discriminating fatty acids (VIP > 1.0) were predominantly concentrated in mature and spawning tissues, exhibiting relatively diminished amounts in the early and late developmental phases.

3.5. Discriminant analysis of fatty acids between somatic and gonadal tissues

The variations in fatty acid profiles among the five gametogenic stages of *C. madrasensis* were illustrated by paired comparisons of body and gonad tissues utilizing VIP score plots (Fig. 6) and volcano plots (Fig. 7). In the ED gametogenic stage, 25 fatty acids/groups were identified, with 14 fatty acids demonstrating a significant increase (FDR-adjusted $p < 0.05$), 3 fatty acids showing a significant decrease (FDR < 0.05), and 8 fatty acids exhibiting no significant change (FDR-adjusted p < 0.05) in gonad tissue relative to body tissue (Fig. 7A). The volcano and VIP score plots demonstrated that palmitoleic acid, oleic acid, n-6 PUFA, PUFA, linoleic acid, and saturated fatty acids (SAFA) were markedly increased in gonadal tissue, whereas erucic acid and eicosenoic acid were significantly diminished, elucidating the disparities between gonadal and somatic tissues during the ED phase of the gametogenic cycle. During the LD gametogenic stage, the gonad tissue had considerably elevated (FDR-adjusted p < 0.05) levels of 14 fatty acids/groups and significantly reduced (FDR-adjusted p < 0.05) levels of 3 fatty acids/groups in comparison to body tissue, while 11 fatty acids/groups revealed no significant difference (Fig. 7B). During this stage, there was a large rise in MUFA, PUFA, linoleic acid, n-6 PUFA, and oleic acid in gonad tissue compared to body tissue. In contrast, octanoic acid, decanoic acid, eicosapentaenoic acid, and lauric acid were considerably decreased.

During the Mat gametogenic phase, 26 fatty acids were identified in both gonadal and somatic tissues. Among these, 22 fatty acids/groups had significantly elevated levels, whereas 3 fatty acids were decreased in gonad tissue relative to body tissue, with 3 fatty acids demonstrating no significant variance. At this time, behenic acid, oleic acid, and tridecanoic acid were markedly increased, whereas palmitoleic acid, decanoic acid, and octanoic acid were dramatically diminished in gonad tissue, underscoring the disparities between the two tissues at the Mat stage. The Spn gametogenic stage revealed a total of 28 fatty acids detected in both tissues. The gonad tissue exhibited considerably elevated levels of 15 fatty acids/groups and diminished levels of 6 fatty acids/groups, but 7 fatty acids showed no significant difference between the tissues. Both volcano and VIP score plots indicate that octanoic acid, heneicosanoic acid, saturated fatty acids (SAFA), behenic acid, n-3 polyunsaturated fatty acids (PUFA), and stearic acid were significantly elevated in gonadal tissue, whereas oleic acid, myristic acid, and monounsaturated fatty acids (MUFA) were significantly diminished, elucidating the disparities between gonadal and somatic tissues during the Spn stage. Ultimately, in the Spt gametogenic phase, 27 fatty acids were detected in the gonadal and somatic tissues. Gonad tissue demonstrated markedly elevated quantities of 3 fatty acids/groups and diminished levels of 8 fatty acids, whereas 16 fatty acids displayed no significant variation. In the Spt stage, myristic acid, palmitoleic acid, and linolenic acid were markedly elevated in gonadal tissue, while palmitic acid, lauric acid, tridecanoic acid, linoleic acid, and polyunsaturated fatty acids (PUFAs) were significantly diminished, elucidating the disparities between gonadal and somatic tissues during this phase of the gametogenic cycle.

3.6. Correlation analysis of somato-gonadal lipid dynamics

A correlation heatmap plot was generated to examine the relationships between individual fatty acids (FAs) and their groups in gonadal and body tissues during the energy-demanding gametogenesis cycle of *C. madrasensis* (Fig. 8). The heatmap revealed a total of 15 fatty acids, or FA groups, that exhibited statistically significant positive correlations between gonadal and body tissues, as indicated by the "+" sign. These included n-3 PUFA, eicosatrienoic acid, decanoic acid, stearic acid, tridecanoic acid, SAFA, nervonic acid, myristic acid, linolenic acid, lauric acid, heneicosanoic acid, docosapentaenoic acid, arachidonic acid, arachidic acid, and erucic acid. These positive correlations reflect consistent patterns in the relative abundance of these fatty acids across both tissue types. In addition, five fatty acids displayed significant negative correlations between gonadal and body tissues, denoted by the "−" sign. These included PUFA, palmitoleic acid, linoleic acid, octanoic acid, and monounsaturated fatty acids (MUFAs).

3.7. Fatty acid dynamics associated with trophic coupling

To evaluate the dietary origin and physiological allocation of fatty acids during the gametogenic cycle of *C. madrasensis*, a correlation matrix (Fig. 9) was constructed between dominant ingested plankton groups and key FA or FA groups in gonadal and body tissues. The plot revealed both positive and negative associations. Eight fatty acids, or FA groups, exhibited significant positive correlations (solid rectangular boxes) with plankton, supporting the hypothesis that these fatty acids are directly derived from dietary intake. Notably, strong positive associations were observed between Bacillariophyceae (diatoms) and gonadal n-3 PUFA, SAFA, and stearic acid, indicating that diatoms are a major trophic source of essential polyunsaturated fatty acids critical for gametogenesis. Likewise, Dinophyceae were positively associated with gonadal n-3 PUFA, further emphasizing the role of diverse phytoplankton taxa in supporting reproductive lipid pools. Additionally, zooplankton ingestion positively correlated with body tridecanoic acid, heneicosanic acid, and n-3 PUFA. In contrast, five FAs or FA groups showed significant negative correlations with gonadal tissues but positive correlations with body tissues (dotted rectangular boxes). This pattern, most evident in MUFA, linoleic acid, palmitoleic acid, and PUFA, suggests a physiological trade-off wherein these FAs, although initially accumulated in somatic tissues through dietary assimilation, are selectively mobilized or depleted in gonadal tissues. Such a negative correlation with gonads despite a positive correlation with diet indicates a translocation mechanism, whereby body lipids are redirected to support gamete synthesis, particularly during the late development and maturation stages. The absence of direct positive correlations between certain plankton groups and gonadal fatty acids (despite positive body correlations) may also reflect stage-specific metabolic partitioning or selective lipid remodeling before reproductive assimilation. Overall, the data suggest that essential fatty acids in gonadal tissues originate either directly from ingested plankton or via somatic reserves.

3.8. Multifaceted linkages among environmental synchrony, trophic linkage and fatty acid dynamics

The principal component analysis (PCA) revealed clear associations between environmental variables, ingested plankton, and FA composition in both body (Fig. 10A) and gonad tissues (Fig. 10B) of *C. madrasensis* across different gonadal stages. In body tissues (Fig. 10A), the first two principal components explained 55.2 % of the total variation (PC1: 32.5 %, PC2: 22.7 %). Early development and spent stages were positioned in the positive region of PC2 and associated with temperature, turbidity, and total suspended solids. Late development was grouped separately along the negative axis of PC2 with limited overlap, showing weaker associations with the major fatty acid vectors. The mature stage clustered strongly along PC1 and was positively related to PUFA, linoleic acid, n-3 PUFA, and linolenic acid, whereas the spawning stage is characterized by MUFA, tridecanoic acid, Bacillariophyceae, phytoplankton, and zooplankton, as well as salinity as an environmental inducer. In gonad tissues (Fig. 10B), PC1 and PC2 together accounted for 51.1 % of the total variation (PC1: 28.4 %, PC2: 22.7 %). Early development and spent stages were aligned with turbidity, TSS, and eicosatrienoic acid along the negative axis of PC1. The mature stage clustered positively with salinity, Bacillariophyceae, phytoplankton, zooplankton, n-3 PUFA, and decanoic acid, whereas the spawning stage showed a strong association with SAFA, octanoic acid, stearic acid, and pH. Late development was positioned along PC2 and grouped with PUFA, MUFA, palmitoleic acid, and linoleic acid.

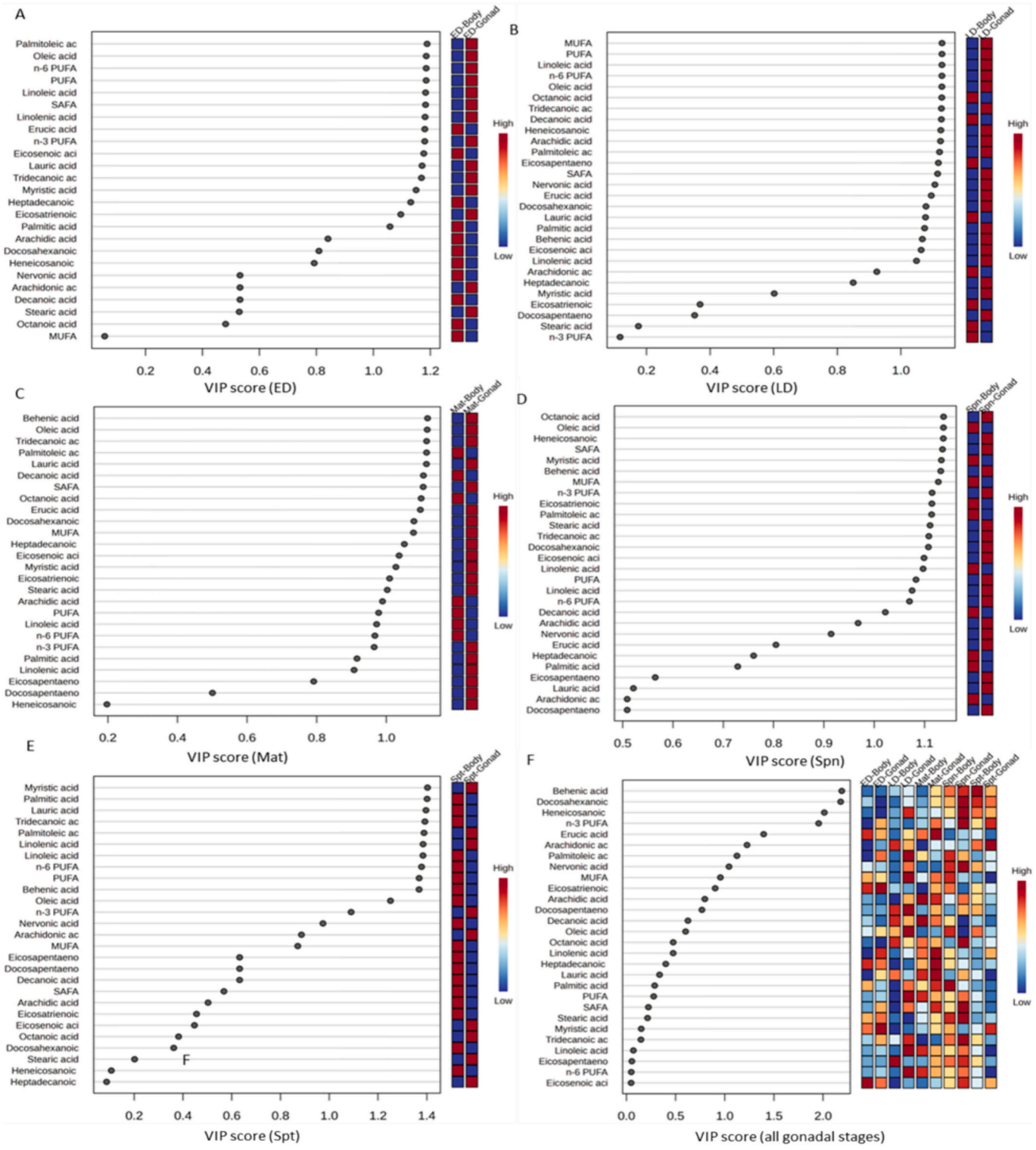

Fig. 6. The ranking of various fatty acids and their classifications determined by partial least squares discriminant analysis (PLS-DA) based on the VIP score on the x-axis, contrasting body tissues and gonad tissues across five stages of gonadal development linked to the post-monsoon gametogenesis cycle of oysters (*Crassostrea madrasensis*). The disparities in fatty acid profiles between somatic tissues and gonadal tissues are illustrated during the early development (ED) stage (A), late development (LD) stage (B), mature (Mat) stage (C), spawning (Spn) stage (D), spent (Spt) stage (E), and over all five phases (F). The colourful boxes on the right represent the relative concentrations of the relevant fatty acids during five phases of gametogenesis in gonadal tissues. VIP is a weighted summation of the squares of the PLS-DA loadings, considering the proportion of the explained Y-variable in each dimension.

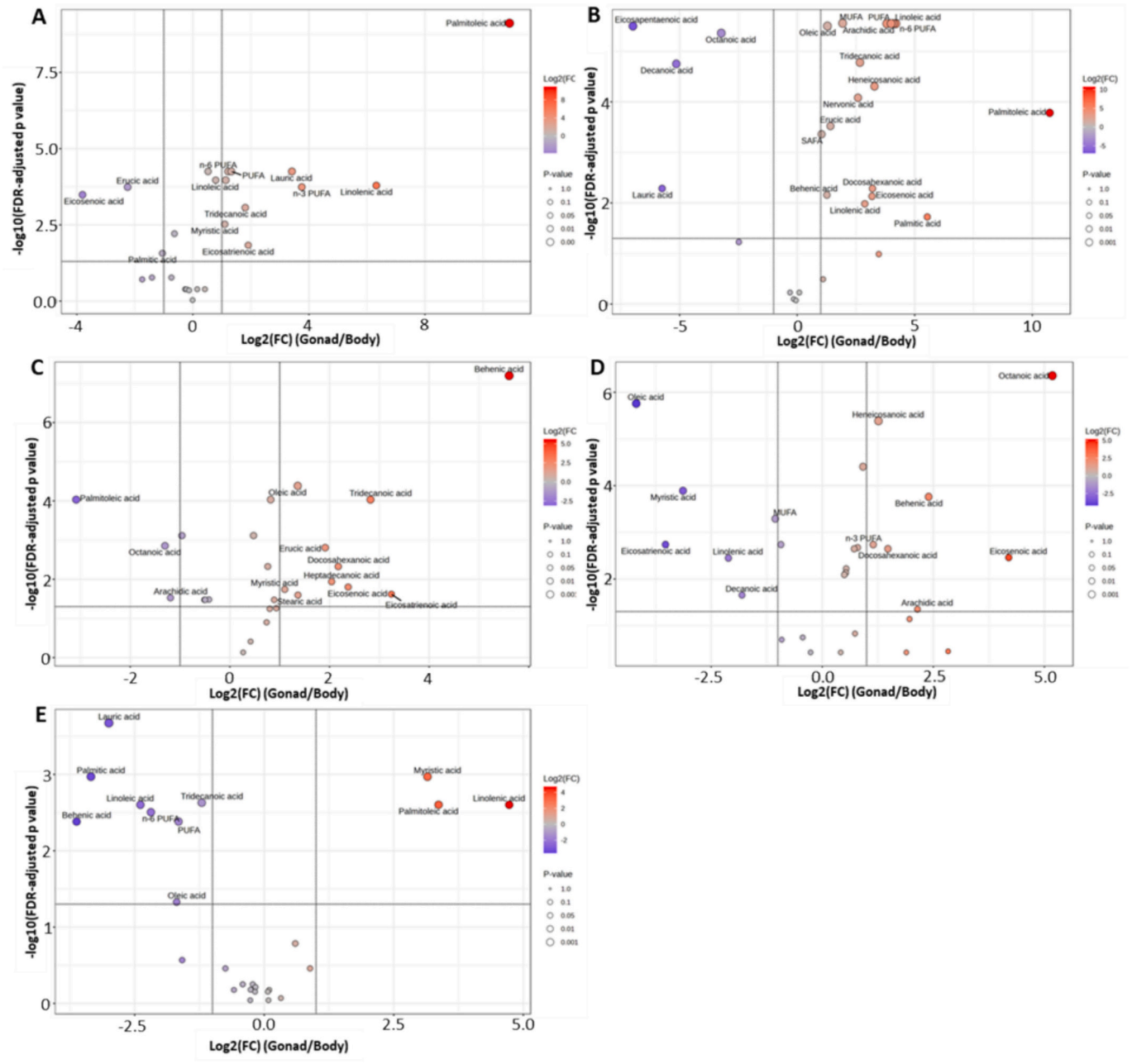

Fig. 7. Volcano plots illustrated alterations in fatty acid profiles between body tissues and gonadal tissues across five stages of gonadal development linked to the post-monsoon gametogenesis cycle of oysters (*Crassostrea madrasensis*). The volcano plots illustrated variations in fatty acid profiles between body tissues and gonadal tissues during the early development (ED) stage (A); late development (LD) stage (B); mature (Mat) stage (C); spawning (spn) stage (D); and spent (spt) stages (E). In the volcano plots (A-E), the X-axis denotes the fold change of the fatty acids and their respective groups (log2 scale), while the Y-axis indicates the *p*-values on a − log10 scale. The horizontal line within the plot denotes a threshold for statistical significance (FDR-adjusted $p < 0.05$). Two vertical lines within the plot indicated the thresholds of log2 fold-change ≥ 1 and ≤ -1.

4. Discussion

The post-monsoon period in tropical estuaries serves as a significant physiological catalyst, representing a biological occurrence subsequent to the relative calm of the monsoon. Our study of the gametogenic cycle of the Indian backwater oyster, *C. madrasensis*, uncovers a coordinated interaction among environmental rejuvenation, trophic linkages, and internal fatty acid reconfiguration. The interaction reveals strategic resource allocation, with fatty acids serving as the foundation for reproductive success. This analysis transcends mere cataloging of stages and fatty acid dynamics and clarifies a fundamental synergy in which the oyster's internal physiological processes are directly influenced by the exterior environmental stimuli. The post-monsoon bloom, defined by distinct plankton communities, supplies the essential nutrients that the oyster assimilates, conveys, and modifies to meet the specific energetic and structural requirements of gametogenesis, all regulated by abiotic factors such as salinity and temperature.

4.1. Somato-gonadal fatty acid reallocation across the gametogenic cycle

The reproductive cycle of *C. madrasensis* emerges from a finely tuned interplay between histological development, environmental seasonality, and fatty acid biochemistry. Histological validation of the five gametogenic phases provides the anatomical framework upon which these

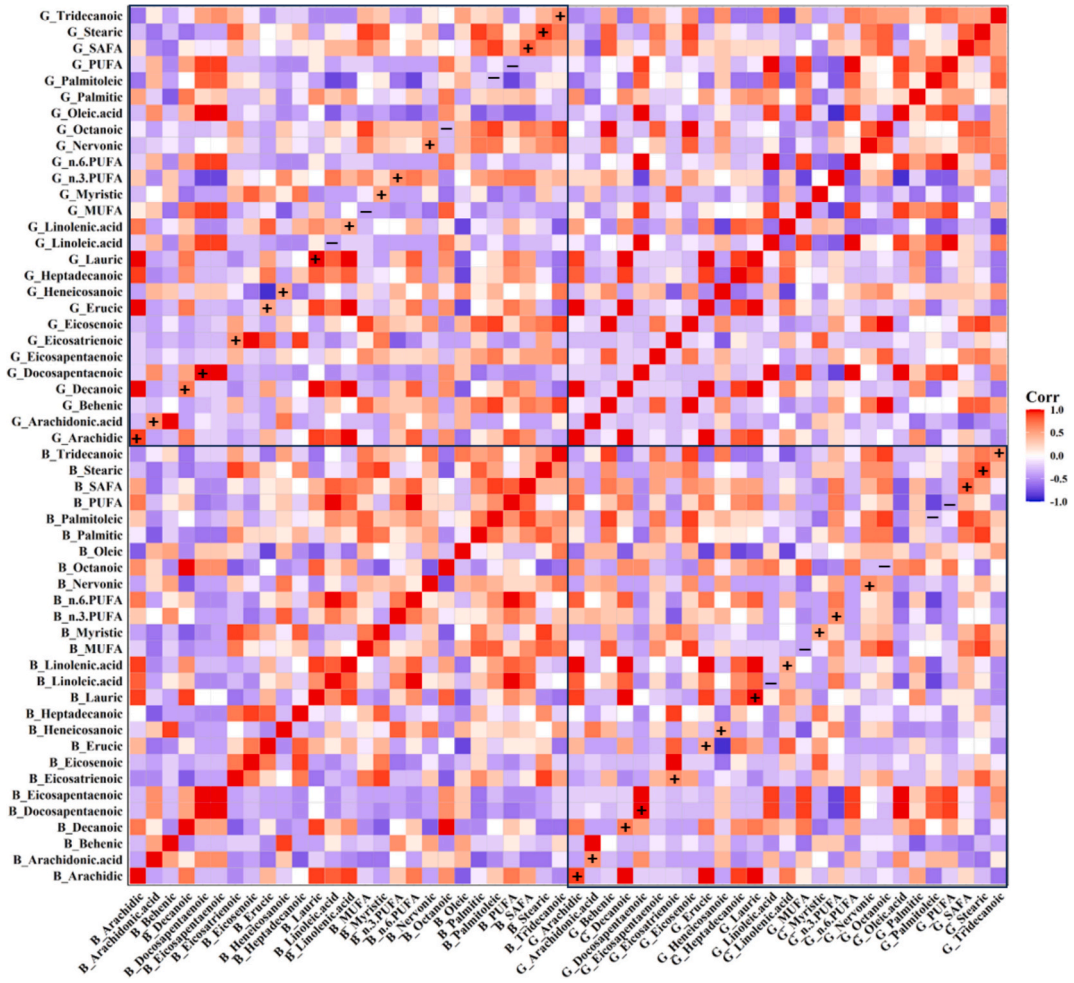

Fig. 8. Spearman corrplot illustrating the correlation of fatty acids and their classifications between body tissues and gonadal tissues related to the gametogenesis cycle of *Crassostrea madrasensis*. The intensity of the glyph's colour (red signifies positive and blue signifies negative) is proportionate to the correlation coefficients. The + symbol denotes a statistically significant ($p < 0.05$) positive connection of a fatty acid/group between body and gonadal tissues. The − sign denotes a statistically significant ($p < 0.05$) negative connection of a fatty acid/group between body and gonadal tissues. (For interpretation of the references to colour in this figure legend, the reader is referred to the web version of this article.)

processes unfold. The sequence from early development through maturation, spawning, and the spent phase mirrors the reproductive patterns reported across diverse oyster and bivalve species (Dinamani, 1987; Barber et al., 1991; Paixão et al., 2013; Aranda et al., 2014; Asaduzzaman et al., 2019; Osada and Matsumoto, 2021; Hossain et al., 2023). Crucially, this cycle is governed by an intricate reorganization of fatty acid metabolism, in which both somatic and gonadal tissues participate in a tightly coordinated exchange pattern. Therefore, the patterns observed reflect a metabolic strategy optimized for life in monsoon-driven estuaries, where resources fluctuate dramatically over short temporal scales. During early development, oysters accumulated myristic, ecosenoic acid, and eicosatrienoic acids predominantly in somatic tissues, indicating a preparatory phase of energy storage prior to gonadal investment. These fatty acids are among the most readily mobilized for β-oxidation and serve as substrates for long-chain PUFA (LC-PUFA) biosynthesis, suggesting that somatic tissues function as strategic reservoirs that support subsequent reproductive development (Renaud et al., 2002; Fernández-Reiriz et al., 2007). Similar somatic preloading has been documented in *C. gigas*, *Mytilus galloprovincialis*, and *Ruditapes philippinarum* (Carboni et al., 2013; Zárate et al., 2016) and is often interpreted as an adaptive response to seasonally pulsed environments.

As the gonads progressed from early to late development, a rapid and selective enrichment of LC-PUFAs, particularly DHA, EPA, ARA, and DPA, became evident. These fatty acids are essential components of reproductive tissues, contributing to membrane fluidity, oocyte stability, and eicosanoid-mediated physiological regulation (Soudant et al., 1999; Alava et al., 2007; Da Costa et al., 2015). Their marked increase in mature and spawning stages underscores their central role in optimizing gamete viability. The high discriminatory power of DHA and nervonic acid in the multivariate models emphasizes their importance in reproductive tissue remodeling (Zhu et al., 2024; Soudant et al., 1999). Comparable LC-PUFA-driven maturation has been reported across diverse bivalves, including scallops, mussels, and pearl oysters (Caers et al., 2002; Fournier et al., 2012; Gao et al., 2019), and is widely considered a hallmark of successful gametogenesis. In our study, the post-spawning depletion of LC-PUFAs, coupled with increased proportions of SAFAs such as linolenic and myristic acids, indicates the exhaustion of metabolic reserves following spawning. This shift resembles post-reproductive metabolic depression documented in *Mytilus edulis* and *Crassostrea gigas* (Berthelin et al., 2000; Liu et al., 2020), where oysters enter a recovery phase supported largely by catabolic maintenance metabolism.

Cross-tissue correlations in our dataset further highlight the integrative nature of lipid management. Strong positive associations between somatic and gonadal pools for key fatty acids, including DPA, ARA, stearic acid, and heneicosanoic acid, demonstrate that lipid allocation is not simply a one-time transfer but rather a dynamic feedback

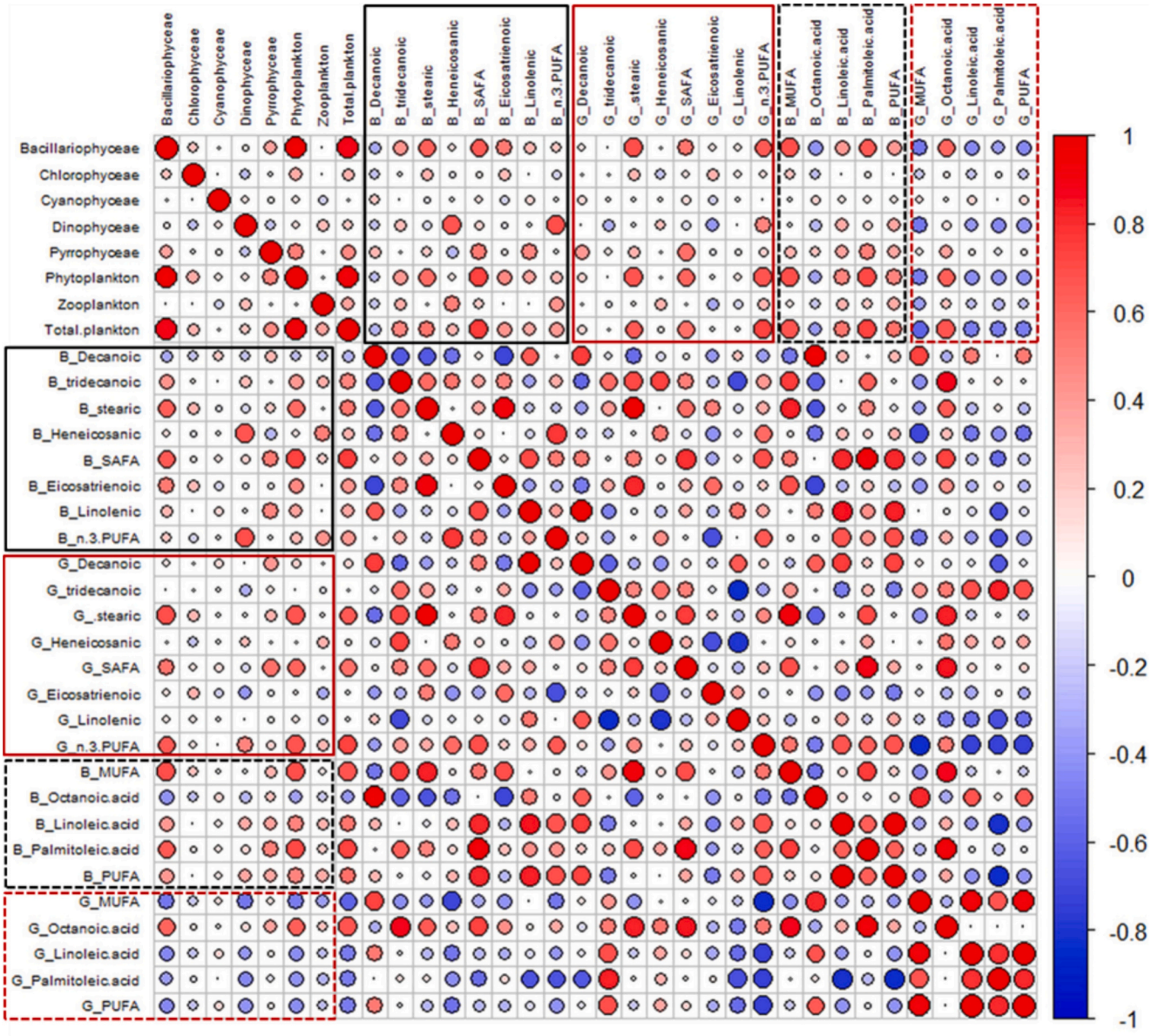

Fig. 9. Spearman corrplot illustrates the correlation between various categories of ingested plankton (number of plankton in gut content) and the principal gonadal and body fatty acids/groups linked to the gametogenesis cycle of *Crassostrea madrasensis*. The circular areas within the squares denote the absolute values of the respective correlation coefficients. The intensity of the glyph's colour (red signifies positive and blue signifies negative) is proportionate to the correlation coefficients. The eight fatty acids and their groups that are considerably positively connected ($p < 0.05$) are displayed in the solid rectangular box, whereas the five fatty acids and their groups that are significantly negatively correlated are shown in dotted boxes. (For interpretation of the references to colour in this figure legend, the reader is referred to the web version of this article.)

system. Such metabolic coupling has been observed in *C. virginica* and *R. philippinarum*, where somatic stores are mobilized in response to gonadal demands (Camacho et al., 2003; Döring and Ekau, 2017). Collectively, these findings suggest that *C. madrasensis* adopts a mixed reproductive strategy that blends conservative and opportunistic resource use. By first accumulating fats somatically and later reallocating them to the gonads, oysters can buffer against short-term environmental variability while still capitalizing on seasonal peaks in food availability. This combination of opportunistic and conservative traits, common in species inhabiting unpredictable environments (Enríquez-Díaz et al., 2009; Maneiro et al., 2017), appears finely tuned to the hydrological rhythm of the Bay of Bengal.

4.2. Fatty acid dynamics governed by trophic coupling and dietary assimilation

The strong correspondence between FA signatures and the composition of the gut plankton community confirms that dietary sources play a decisive role in shaping reproductive fatty acid profiles. The post-monsoon period in the Bay of Bengal, characterized by high phytoplankton productivity, especially diatoms and dinoflagellates, creates a trophic window during which oysters can rapidly acquire essential fatty acids. Diatoms provided substantial contributions of EPA and ALA, while dinoflagellates offered DHA-rich biochemical resources, consistent with global plankton FA profiles (Peltomaa et al., 2019; Chakraborty et al., 2016). The positive associations between these plankton groups and gonadal LC-PUFAs indicate that the availability of high-quality dietary lipids may serve as a proximal cue for the initiation

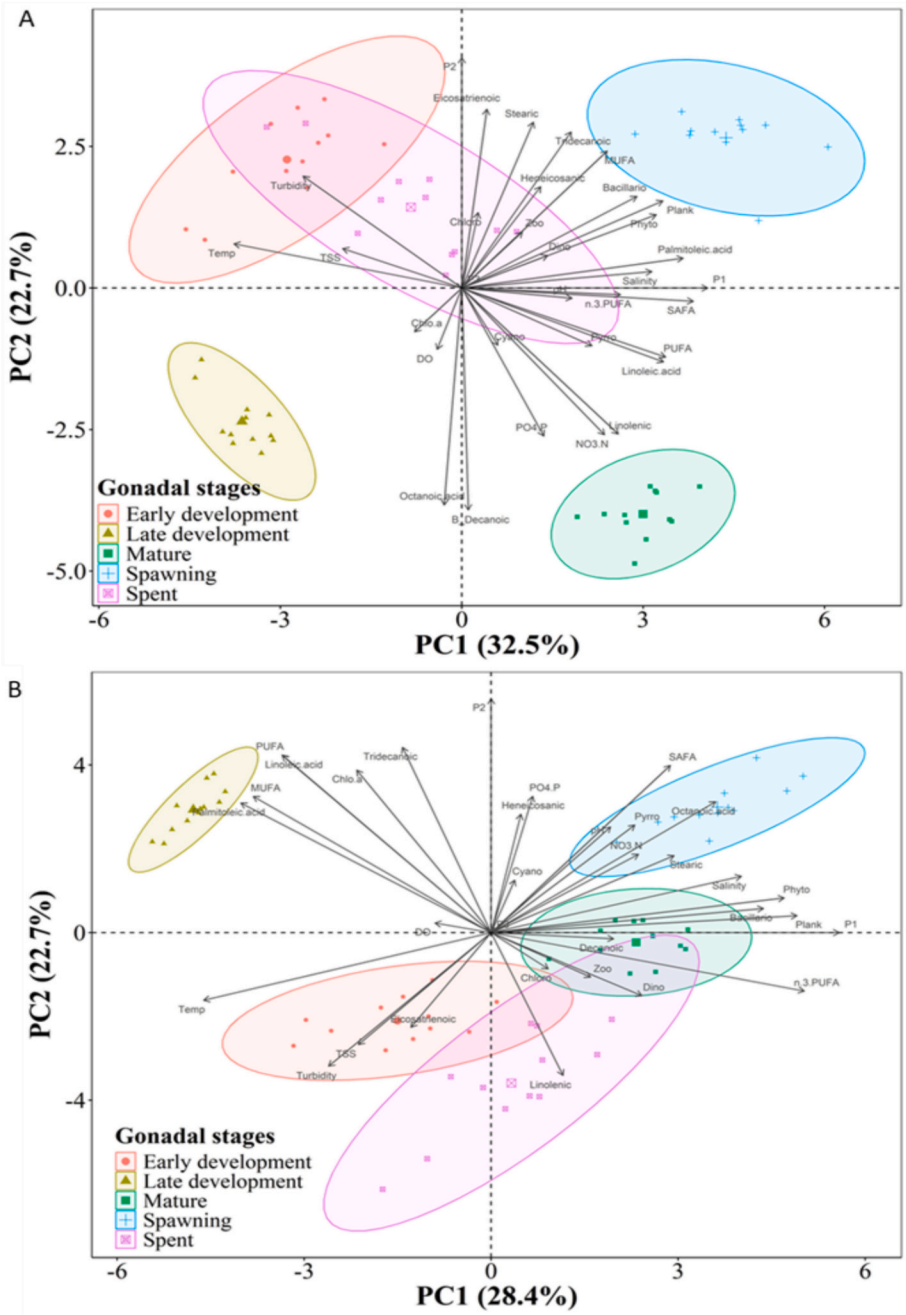

Fig. 10. Biplot of principal component analysis (PCA) illustrating the interrelations among ambient conditions, ingested intestinal plankton, and the fatty acid composition of body tissues (A) and gonads (B) linked to the gametogenesis cycle of *Crassostrea madrasensis*.

and progression of gametogenesis (Pernet et al., 2012). Comparable diet–lipid linkages have been demonstrated in *Pinctada margaritifera*, *Argopecten purpuratus*, and *C. virginica*, where reproductive performance strongly depends on the abundance and FA composition of planktonic prey (Fournier et al., 2012; Caers et al., 2003; Da Costa et al., 2016).

Interestingly, several fatty acids, including MUFA, PUFA, palmitoleic acid, and linoleic acid, exhibited positive correlations with somatic tissues but negative correlations with gonads. This pattern suggests a sequential trophic–somatic–gonadal lipid allocation pathway. In this model, oysters first assimilate dietary lipids into somatic reserves, which are then selectively mobilized toward reproductive tissues in response to internal biochemical signals. Such two-step lipid routing has been proposed for scallops and mussels (Freites et al., 2002; Freites et al., 2010) and may provide metabolic flexibility under fluctuating food conditions. Our results indicate that *C. madrasensis* employs this strategy to integrate dietary pulses into longer-term reproductive investment.

The FA signatures associated with zooplankton, particularly odd-chain and branched-chain fatty acids, suggest that heterotrophic microfauna also contributes to dietary lipid intake. This dietary breadth likely enhances resilience during periods of phytoplankton scarcity, enabling oysters to maintain fatty acid acquisition despite variable primary productivity (Mathieu et al., 2025). Similar trophic flexibility has been observed in estuarine bivalves exposed to fluctuating turbidity and nutrient regimes (Hofmann et al., 1992; Jardine et al., 2020). The presence of zooplankton-derived fatty acids further underscores the complexity of energy pathways supporting reproduction in tropical estuarine environments.

Overall, the clear trophic–biochemical coupling revealed by our

dataset positions FA profiling as an effective tracer of energy flow from plankton to oyster tissues. In monsoon–influenced ecosystems, where stable isotope baselines shift rapidly due to monsoonal freshwater inputs, FA biomarkers may provide more sensitive and temporally resolved insights into trophic interactions (Galloway and Winder, 2015; Lee et al., 2021). In the context of aquaculture, understanding these diet–fatty acid linkages are essential for designing broodstock conditioning regimes that mimic natural feeding periodicity, ensuring sufficient LC-PUFA supply for optimal reproductive output.

4.3. Environmental modulation of fatty acid dynamics and adaptive responses to estuarine variability

Environmental conditions exerted pronounced effects on FA composition and reproductive stage clustering, revealing a tightly integrated eco-physiological system. Salinity emerged as the dominant environmental driver structuring FA profiles, with mature and spawning oysters closely associated with higher salinity, elevated plankton abundance, and greater LC-PUFA and MUFA concentrations. Increasing post-monsoon salinity likely enhances filtration efficiency, digestive enzyme activity, and lipid assimilation capacity, thereby promoting rapid reproductive advancement (Soudant et al., 1996; Delaporte et al., 2005). Salinity also serves as a key phenological cue for spawning in many estuarine bivalves (Davis, 1958; Asaduzzaman et al., 2019; Drescher et al., 2019), helping synchronize gamete release with periods of favorable hydrodynamic and trophic conditions. The coupling of salinity-driven physiological changes with plankton-driven nutritional inputs thereby creates a predictable environmental window that maximizes reproductive success.

Temperature and turbidity played equally important roles but acted in contrasting directions. Higher temperatures were associated with early gametogenesis, reflecting increased metabolic rates and accelerated tissue turnover typical of tropical bivalves (Suárez et al., 2005; Aranda et al., 2014). In contrast, high turbidity and TSS were linked with early developmental and spent stages, likely due to reduced filtration efficiency under suspended load, which limits energy acquisition during critical recovery periods. These findings align with work showing that elevated particulate matter reduces feeding efficiency in filter feeders, thereby influencing reproductive timing and metabolic investment (Clements et al., 2021). The combined effects of salinity, temperature, and turbidity thus create a complex environmental matrix that shapes lipid utilization patterns throughout the reproductive cycle.

The integration of environmental cues, trophic availability, and internal lipid dynamics suggests that *C. madrasensis* operates within a narrow phenological window optimized for post-monsoon conditions. However, the stability of this window is increasingly uncertain. Climate-driven alterations in monsoon timing, freshwater discharge, and estuarine salinity dynamics pose significant risks to the synchrony between environmental cues and reproductive processes (IPCC, 2021). Even slight mismatches between phytoplankton blooms and the metabolic demands of gametogenesis may reduce larval production and recruitment, as observed in other marine broadcast spawners (Carson et al., 2010; Padilla-Gamiño et al., 2022). Given its rapid reproductive turnover and reliance on condensed productive seasons, *C. madrasensis* may be particularly vulnerable to these disruptions.

From an applied perspective, our findings provide important insights into broodstock conditioning, site selection, and adaptive aquaculture under changing environmental conditions. Conditioning protocols designed to mimic natural post-monsoon salinity increases and temperature ranges may enhance lipid assimilation and reproductive success. Likewise, supplying broodstock with diatom- and dinoflagellate-rich diets can better support LC-PUFA deposition, improving gamete quality and larval performance (Caers et al., 2002; Da Costa et al., 2016). On a broader management scale, protecting estuarine water quality and nutrient dynamics to sustain natural plankton cycles could help maintain reproductive resilience in wild populations.

5. Conclusion

The results of this study reveal that the reproductive output of *C. madrasensis* is driven synergistically by environmental drivers, dietary inputs, and internal metabolic allocation. Post-monsoon environmental restoration, characterized by changes in salinity, temperature, and plankton blooms, initiates a series of gametogenic events mediated by the mobilization of polyunsaturated fatty acids from somatic to gonadal tissues. The preferential accumulation of long-chain polyunsaturated fatty acids, in particular DHA, EPA, and ARA, during maturation and spawning reflects their structural and regulatory role for the development of gametes, fertilization, and viability of eggs/larvae. Similarly, positive correlations with Bacillariophyceae and Dinophyceae also indicate the importance of phytoplankton-origin lipids for reproductive allocation, and stage-specific metabolic changes may reflect an adaptive opportunistic–conservative pattern to energy allocation. Together, these results provide a mechanistic basis for the association of somato-gonadal fatty acid dynamics with environmental synchrony in monsoon-influenced estuaries. Beyond advancing fundamental ecological understanding, the results carry applied significance in mariculture, particularly conditioning broodstock under salinity and dietary regimes that mimic natural cues can optimize spawning and larval performance. Furthermore, the sensitivity of reproductive events to changes in monsoonal patterns indicates that *C. madrasensis* is highly sensitive to climate-mediated alterations and needs urgent integrated action for its management and conservation along with the estuarine ecosystem. While associations with plankton groups are clear evidence of trophic transfer, the actual assimilation pathways and potential selective rejections are yet unknown. Future work should continue to develop this conceptual framework by conducting analyses on diets that vary both in spatial (among sites) and time (across seasons), with the use of stable isotope and compound-specific results to provide a more precise means of estimating dietary lipid assimilation.

Declaration of generative AI in scientific writing

The authors used ChatGPT to enhance the readability and language of the manuscript during its preparation. Following the use of this tool/service, the authors carefully reviewed and revised the content as necessary and took full responsibility for the final published article.

CRediT authorship contribution statement

Afshana Ferdous: Writing – original draft, Visualization, Software, Methodology, Investigation, Formal analysis, Data curation. **Israt Jahan:** Writing – review & editing, Methodology, Investigation, Data curation. **Md. Nayeem Hossain:** Visualization, Software, Formal analysis, Data curation. **Sourav Chowdhury:** Writing – review & editing, Methodology, Data curation. **Md Moshiur Rahman:** Visualization, Software, Formal analysis, Data curation. **Md Asaduzzaman:** Writing – original draft, Supervision, Software, Resources, Project administration, Funding acquisition, Formal analysis, Conceptualization.

Declaration of competing interest

The authors declare that they have no known competing financial interests or personal relationships that could have appeared to influence the work reported in this paper.

Acknowledgements

This work was conducted as a part of the research plan of the Bangladesh Academy of Sciences- United States Department of Agriculture (BAS-USDA) Endowment 5th phase project implemented by Chattogram Veterinary and Animal Sciences University through a collaborative agreement with BAS (F 127). We would like to thank the

director and other staff of the BAS-USDA Endowment Program for providing funding for this research work. We also thank the staff of the Oceanography Laboratory, Department of Marine Bioresource Science, Chattogram Veterinary and Animal Sciences University, for helping with oyster sampling and parameter analysis.

Appendix A. Supplementary data

Supplementary data to this article can be found online at https://doi.org/10.1016/j.aquaculture.2025.743576.

Data availability

Data will be made available on request.

References

Alava, V.R., Quinitio, E.T., De Pedro, J.B., Priolo, F.M.P., Orozco, Z.G.A., Wille, M., 2007. Lipids and fatty acids in wild and pond-reared mud crab *Scylla serrata* (Forsskål) during ovarian maturation and spawning. Aquacult. Res. 38 (14), 1468–1477. https://doi.org/10.1111/j.1365-2109.2007.01793.x.

APHA, 1992. Standard Methods for the Examination of Water and Wastewater, 18th ed. American Public Health Association (APHA), American Water Works Association (AWWA) and Water Pollution Control Federation (WPCF), Washington DC.

Aranda, D.A., Díaz, M.E., Reynoso, F.L., Brulé, T., Montero, J., Cárdenas, E.B., 2014. Reproductive strategies of the eastern oyster *Crassostrea virginica* (Gmelin 1791) in tropical lagoons of the Mexican Gulf of Mexico. J. Shellfish. Res. 33 (1), 145–152. https://doi.org/10.2983/035.033.0114.

Asaduzzaman, M., Rahi Noor, A., Rahman, M.M., Akter, S., Hoque, N.F., Shakil, A., Wahab, M.A., 2019. Reproductive biology and ecology of the green mussel *Perna viridis*: a multidisciplinary approach. Biology 8 (4), 88. https://doi.org/10.3390/biology8040088.

Asaduzzaman, M., Akter, S., Hoque, N.F., Shakil, A., Noor, A.R., Akter, M.N., Rahman, M. M., 2020. Multifaceted linkages among eco-physiological factors, seasonal plankton dynamics and selective feeding behavior of the green mussel (*Perna viridis*) in the south-east coast of the bay of Bengal. J. Sea Res. 160, 101933. https://doi.org/10.1016/j.seares.2020.101933.

Asaduzzaman, M., Nahiduzzaman, M., Chowdhury, M.T.H., Rahman, M.M., Mamun, A. A., Hossain, M.M., 2025. Advancing low-trophic extractive mariculture (LTEM): strategies for a thriving blue economy in Bangladesh. Mar. Policy 173, 106557. https://doi.org/10.1016/j.marpol.2024.106557.

Asha, K.K., Anandan, R., Mathew, S., Lakshmanan, P.T., 2014. Biochemical profile of oyster *Crassostrea madrasensis* and its nutritional attributes. Egypt. J. Aquat. Res. 40 (1), 35–41. https://doi.org/10.1016/j.ejar.2014.02.001.

Barber, B.J., Ford, S.E., Wargo, R.N., 1991. Genetic variation in the timing of gonadal maturation and spawning of the eastern oyster *Crassostrea virginica* (Gmelin). Biol. Bull. 181 (2), 216–221. https://doi.org/10.2307/1542092.

Benjamini, Y., Hochberg, Y., 1995. Controlling the false discovery rate: a practical and powerful approach to multiple testing. J. R. Stat. Soc. Ser. B Methodol. 57, 289–300. https://doi.org/10.1111/j.2517-6161.1995.tb02031.x.

Berthelin, C., Kellner, K., Mathieu, M., 2000. Storage metabolism in the Pacific oyster (*Crassostrea gigas*) in relation to summer mortalities and reproductive cycle (west coast of France). Comp. Biochem. Physiol. B Biochem. Mol. Biol. 125 (3), 359–369. https://doi.org/10.1016/S0305-0491(99)00187-X.

Boyd, C.E., 1979. Water Quality in Warmwater Fish Ponds. Auburn University Press, Auburn, AL.

Bricker, S.B., Grizzle, R.E., Trowbridge, P., Rose, J.M., Ferreira, J.G., Wellman, K., Zhu, C., Galimany, E., Wikfors, G.H., Saurel, C., Landeck, M.R., Wands, J., Rheault, R., Steinberg, J., Jacob, A.P., Davenport, E.D., Ayvazian, S., Chintala, M., Tedesco, M.A., 2020. Bioextractive removal of nitrogen by oysters in Great Bay Piscataqua River estuary, New Hampshire, USA. Estuar. Coasts 43 (1), 23–38. https://doi.org/10.1007/s12237-019-00661-8.

Bridier, G., Olivier, F., Grall, J., Chauvaud, L., Sejr, M.K., Tremblay, R., 2023. Seasonal lipid dynamics of four Arctic bivalves: implications for their physiological capacities to cope with future changes in coastal ecosystems. Ecol. Evol. 13 (11), e10691. https://doi.org/10.1002/ece3.10691.

Caers, M., Utting, S., Coutteau, P., Millican, P., Sorgeloos, P., 2002. Impact of the supplementation of a docosahexaenoic acid–rich emulsion on the reproductive output of oyster broodstock, *Crassostrea gigas*. Mar. Biol. 140 (6), 1157–1166. https://doi.org/10.1007/s00227-002-0798-5.

Caers, M., Coutteau, P., Sorgeloos, P., Gajardo, G., 2003. Impact of algal diets and emulsions on the fatty acid composition and content of selected tissues of adult broodstock of the Chilean scallop *Argopecten purpuratus* (Lamarck, 1819). Aquaculture 217, 437–452. https://doi.org/10.1016/S0044-8486(02)00144-8.

Camacho, A.P., Delgado, M., Fernández-Reiriz, M.J., Labarta, U., 2003. Energy balance, gonad development and biochemical composition in the clam *Ruditapes decussatus*. Mar. Ecol. Prog. Ser. 258, 133–145. https://doi.org/10.3354/meps258133.

Carboni, S., Hughes, A.D., Atack, T., Tocher, D.R., Migaud, H., 2013. Fatty acid profiles during gametogenesis in sea urchin (*Paracentrotus lividus*): effects of dietary inputs on gonad, egg and embryo profiles. Comp. Biochem. Physiol. A Mol. Integr. Physiol. 164 (2), 376–382. https://doi.org/10.1016/j.cbpa.2012.11.010.

Carson, H.S., López-Duarte, P.C., Rasmussen, L., Wang, D., Levin, L.A., 2010. Reproductive timing alters population connectivity in marine metapopulations. Curr. Biol. 20 (21), 1926–1931. https://doi.org/10.1016/j.cub.2010.09.057.

Chakraborty, K., Chakkalakal, S.J., Joseph, D., Joy, M., 2016. Nutritional composition of edible oysters (*Crassostrea madrasensis* L.) from the southwest coast of India. J. Aquat. Food Prod. Technol. 25 (8), 1172–1189. https://doi.org/10.1080/10498850.2015.1039682.

Cho, I.K., Seo, B.S., Hwang, S.Y., Lee, Y.I., Moon, J.S., Park, S.J., Choi, Y.H., 2023. The annual reproductive cycle, proximate composition, fatty acid and amino acid content of Pacific oyster, *Crassostrea gigas* (*Magallana gigas*), in Gadeok-do, Korea. Dev. Reprod. 27 (3), 101. https://doi.org/10.12717/dr.2023.27.3.101.

Clements, J.C., Carver, C.E., Mallet, M.A., Comeau, L.A., Mallet, A.L., 2021. CO_2-induced low pH in an eastern oyster (*Crassostrea virginica*) hatchery positively affects reproductive development and larval survival but negatively affects larval shape and size, with no intergenerational linkages. ICES J. Mar. Sci. 78 (1), 349–359. https://doi.org/10.1093/icesjms/fsaa089.

Da Costa, F., Robert, R., Quéré, C., Wikfors, G.H., Soudant, P., 2015. Essential fatty acid assimilation and synthesis in larvae of the bivalve *Crassostrea gigas*. Lipids 50 (5), 503–511. https://doi.org/10.1007/s11745-015-4006-z.

Da Costa, F., Petton, B., Mingant, C., Bougaran, G., Rouxel, C., Quere, C., Robert, R., 2016. Influence of one selected *Tisochrysis lutea* strain rich in lipids on *Crassostrea gigas* larval development and biochemical composition. Aquacult. Nutr. 22 (4), 813–836. https://doi.org/10.1111/anu.12301.

Davis, H.C., 1958. Survival and growth of clam and oyster larvae at different salinities. Biol. Bull. 114 (3), 296–307. https://doi.org/10.2307/1538986.

De Moreno, J.E.A., Pollero, R.J., Moreno, V.J., Brenner, R.R., 1980. Lipids and fatty acids of the mussel (*Mytilus platensis* d'Orbigny) from South Atlantic waters. J. Exp. Mar. Biol. Ecol. 48, 263–276. https://doi.org/10.1016/0022-0981(80)90081-7.

Delaporte, M., Soudant, P., Moal, J., Kraffe, E., Marty, Y., Samain, J.F., 2005. Incorporation and modification of dietary fatty acids in gill polar lipids by two bivalve species *Crassostrea gigas* and *Ruditapes philippinarum*. Comp. Biochem. Physiol. A Mol. Integr. Physiol. 140 (4), 460–470. https://doi.org/10.1016/j.cbpb.2005.02.009.

Dinamani, P., 1987. Gametogenic patterns in populations of Pacific oyster, *Crassostrea gigas*, in Northland, New Zealand. Aquaculture 64 (1), 65–76. https://doi.org/10.1016/0044-8486(87)90206-7.

Döring, J., Ekau, W., 2017. Using oocyte essential fatty acid composition to assess spawner reproductive potential under hypersaline conditions. Mar. Ecol. Prog. Ser. 584, 199–212. https://doi.org/10.3354/meps12366.

Drescher, B.D., Brown-Peterson, N.J., Walker, J.M., 2019. A reproductive histological analysis of *Rangia cuneata* (Venerida: Mactridae): effects of abiotic factors. Am. Malacol. Bull. 37 (1), 12–20. https://doi.org/10.4003/006.037.0102.

Dridi, S., Romdhane, M.S., 2017. Nutritional quality in terms of lipid content and fatty acid composition of neutral and polar lipids in the adductor muscle of the oyster *Crassostrea gigas* (Thunberg, 1794) farmed in the Bizert lagoon (Tunisia) in relation with sexual cycle and environmental settings. Egypt. J. Aquat. Res. 43 (4), 329–336.

Enríquez-Díaz, M., Pouvreau, S., Chávez-Villalba, J., Le Pennec, M., 2009. Gametogenesis, reproductive investment, and spawning behavior of the Pacific giant oyster *Crassostrea gigas*: evidence of an environment-dependent strategy. Aquac. Int. 17 (5), 491–506. https://doi.org/10.1007/s10499-008-9219-1.

Ezgeta-Balić, D., Radonić, I., Bojanić Varezić, D., Zorica, B., Arapov, J., Stagličić, N., Jozić, S., Peharda, M., Briski, E., Lin, Y., Šegvić-Bubić, T., 2020. Reproductive cycle of the non-native Pacific oyster, *Crassostrea gigas*, in the Adriatic Sea. Mediterr. Mar. Sci. 21 (1), 49–61. https://doi.org/10.12681/mms.21304.

Fernández-Reiriz, M.J., Pérez-Camacho, A., Delgado, M., Labarta, U., 2007. Dynamics of biochemical components, lipid classes and energy values on gonadal development of *Ruditapes philippinarum* associated with the temperature and ingestion rate. Comp. Biochem. Physiol. A Mol. Integr. Physiol. 147 (4), 1053–1059. https://doi.org/10.1016/j.cbpa.2007.03.018.

Fournier, J., Levesque, E., Pouvreau, S., Le Pennec, M., Le Moullac, G., 2012. Influence of plankton concentration on gametogenesis and spawning of the black lip pearl oyster *Pinctada margaritifera* in Ahe atoll lagoon (Tuamotu archipelago, French Polynesia). Mar. Pollut. Bull. 65 (10−12), 463–470. https://doi.org/10.1016/j.marpolbul.2012.03.027.

Fox, J., Weisberg, S., 2019. An R Companion to Applied Regression, 3rd ed. Sage, Thousand Oaks.

Freites, L., Labarta, U., Fernández, M.J., 2002. Evolution of fatty acid profiles of subtidal and rocky shore mussel seed (*Mytilus galloprovincialis*, Lmk.): influence of environmental parameters. J. Exp. Mar. Biol. Ecol. 268, 185–204. https://doi.org/10.1016/S0022-0981(01)00377-X.

Freites, L., García, N., Troccoli, L., Maeda-Martínez, A.N., Fernández-Reiriz, M.J., 2010. Influence of environmental variables and reproduction on the gonadal fatty acid profile of tropical scallop *Nodipecten nodosus*. Comp. Biochem. Physiol. B Biochem. Mol. Biol. 157 (4), 408–414. https://doi.org/10.1016/j.cbpb.2010.09.001.

Galloway, A.W., Winder, M., 2015. Partitioning the relative importance of phylogeny and environmental Soudant conditions on phytoplankton fatty acids. PloS One 10 (6), e0130053. https://doi.org/10.1371/journal.pone.0130053.

Gao, X.Q., Fei, F., Liu, Z.F., Guan, C.T., Huang, B., Liu, B.L., Hong, L., 2019. Lipid content and fatty acid composition in female American shad, *Alosa sapidissima*, at different stages of ovarian development under reared conditions. Aquacult. Res. 50 (2), 439–448. https://doi.org/10.1111/are.13905.

Garrido, C.L., Barber, B.J., 2001. Effects of temperature and food ration on gonad growth and oogenesis of the green sea urchin *Strongylocentrotus droebachiensis*. Mar. Biol. 138, 447–456. https://doi.org/10.1007/s002270000473.

Gatenby, C.M., Orcutt, D.M., Kreeger, D.A., Parker, B.C., Jones, V.A., Neves, R.J., 2003. Biochemical composition of three algal species proposed as food for captive

freshwater mussels. J. Appl. Phycol. 15, 1–11. https://doi.org/10.1023/A:1022929423011.
Gosling, E., 2003. Bivalve Molluscs: Biology, Ecology and Culture. Fishing News Books, Blackwell Publishing, Oxford, 443 pp.
Gosling, E., 2015. Reproduction, settlement and recruitment. In: Marine Bivalve Molluscs, 2nd ed. John Wiley & Sons, Ltd., pp. 157–202. https://doi.org/10.1002/9781119045212.ch5
Hamli, H., Idris, M.H., Rajaee, A.H., Kamal, A.H.M., 2015. Reproductive cycle of hard clam, *Meretrix lyrata* Sowerby, 1851 (Bivalvia: Veneridae) from Sarawak, Malaysia. Trop. Life Sci. Res. 26 (2), 59.
Hassan, M.M., Qin, J.G., Li, X., 2018. Gametogenesis, sex ratio and energy metabolism in *Ostrea angasi*: implications for the reproductive strategy of spermcasting marine bivalves. J. Moll. Stud. 84, 38–45. https://doi.org/10.1093/mollus/eyx041.
Hofmann, E.E., Powell, E.N., Klinck, J.M., Wilson, E.A., 1992. Modeling oyster populations III. Critical feeding periods, growth and reproduction. J. Shellfish. Res. 11, 399–416.
Hossain, M.Y., Uddin, M., Rahman, M.A., Haque, M.K., Kormoker, T., Samad, M.A., Tsang, Y.F., 2023. Species identification, reproductive biology, and nutritional value of marine shellfish (*Meretrix lyrata*) in the Bay of Bengal. Mar. Environ. Res. 192, 106222. https://doi.org/10.1016/j.marenvres.2023.106222.
Hossain, K.Z., Jahan, I., Hossain, M.N., Ferdous, A., Ali, M.R., Rahman, M.M., Khan, M.S.R., Asaduzzaman, M., 2025. Feeding selectivity and gametogenic cycle of Crassostrea madrasensis in relation to seasonal plankton and environmental variability in the southeast coast of the Bay of Bengal. Bangladesh. J. Sea Res. 208, 102646. https://doi.org/10.1016/j.seares.2025.102646.
IPCC, 2021. Climate Change 2021: The Physical Science Basis. Contribution of Working Group I to the Sixth Assessment Report of the Intergovernmental Panel on Climate Change. Cambridge University Press, Cambridge, United Kingdom and New York, NY, USA. https://doi.org/10.1017/9781009157896. In press.
Jardine, T.D., Galloway, A.W., Kainz, M.J., 2020. Unlocking the power of fatty acids as dietary tracers and metabolic signals in fishes and aquatic invertebrates. Philos. Trans. R. Soc. B 375 (1804), 20190639. https://doi.org/10.1098/rstb.2019.0639.
Joaquim, S., Matias, D., Matias, A.M., Moura, P., Arnold, W.S., Chícharo, L., Baptista Gaspar, M., 2011. Reproductive activity and biochemical composition of the pullet carpet shell *Venerupis senegalensis* (Gmelin, 1791) (Mollusca: Bivalvia) from ria de Aveiro (northwestern coast of Portugal). Sci. Mar. 75, 217–226. https://doi.org/10.3989/scimar.2011.75n2217.
Kang, C.K., Park, M., Lee, P.Y., Choi, W.J., Lee, W.C., 2000. Seasonal variations in condition, reproductive activity, and biochemical composition of the Pacific oyster *Crassostrea gigas* (Thunberg), in suspended culture in two coastal bays of Korea. J. Shellfish. Res. 19, 771–778.
Kasmini, L., Batubara, A.S., 2022. Biology and ecological function of genus *Crassostrea* (Bivalvia: Ostreidae): a review. Depik 11 (1), 75–84. https://doi.org/10.13170/depik.11.1.23444.
Kassambara, A., 2023. ggcorrplot: Visualization of a Correlation Matrix using 'ggplot2'. R package version 0.1.4.1. https://CRAN.R-project.org/package=ggcorrplot.
Kim, B., Kang, D., Ko, D., Yang, H., Kim, D., Kang, C., Choi, K., 2010. Annual reproductive cycle of the oyster *Saccostrea kegaki* (Torigoe & Inaba, 1981) on the southern coast of Jeju Island, Korea. Invert. Reprod. Dev. 54 (1), 19–26. https://doi.org/10.1080/07924259.2010.9652312.
Kim, J.S., Won Seo, W., Baek, D., 2019. Seasonally varying effects of environmental factors on phytoplankton abundance in the regulated rivers. Sci. Rep. 9, 9266. https://doi.org/10.1038/s41598-019-45621-1.
Kripa, V., Mohamed, K.S., 2008. Green mussel (Perna viridis) farming in India, technology diffusion process and socioeconomic impacts. J. World Aquac. Soc. 9, 612–613. https://doi.org/10.1111/j.1749-7345.2008.00191.x.
Lango-Reynoso, F., Chavez-Villalba, J., Cochard, J.C., Le Pennec, M., 2000. Oocyte size, a means to evaluate the gametogenic development of the Pacific oyster, *Crassostrea gigas* (Thunberg). Aquaculture 190 (1–2), 183–199.
Lê, S., Josse, J., Husson, F., 2008. FactoMineR: an R package for multivariate analysis. J. Stat. Softw. 25, 1–18. https://doi.org/10.18637/jss.v025.i01.
Lee, I.O., Noh, J., Lee, J., Kim, B., Hwang, K., Kwon, B.O., et al., 2021. Stable isotope signatures reveal the significant contributions of microphytobenthos and saltmarsh-driven nutrition in the intertidal benthic food webs. Sci. Total Environ. 756, 144068. https://doi.org/10.1016/j.scitotenv.2020.144068.
Liu, W., Kong, L., 2013. Reproductive cycle and seasonal variations in lipid content and fatty acid composition in gonad of the cockle *Fulvia mutica* in relation to temperature and food. J. Ocean Univ. China 12, 427–433. https://doi.org/10.1007/s11802-013-1979-1.
Liu, Z., Zhang, Y., Zhou, Z., Zong, Y., Zheng, Y., Liu, C., Song, L., 2020. Metabolomic and transcriptomic profiling reveals the alteration of energy metabolism in oyster larvae during initial shell formation and under experimental ocean acidification. Sci. Rep. 10, 6111. https://doi.org/10.1038/s41598-020-62963-3.
Lopes-Lima, M., Lima, P., Hinzmann, M., Rocha, A., 2014. Selective feeding by *Anodonta cygnea* (Linnaeus, 1771): the effects of seasonal changes and nutritional demands. Limnologica 44, 18–22. https://doi.org/10.1016/j.limno.2013.07.001.
Maneiro, V., Silva, A., Pazos, A.J., Sánchez, J.L., Pérez-Parallé, M.L., 2017. Effects of temperature and photoperiod on the conditioning of the flat oyster (*Ostrea edulis* L.) in autumn. Aquacult. Res. 48 (8), 4554–4562. https://doi.org/10.1111/are.13280.
Mathieu, F., Rautio, M., Marshall, J., Woods, R., Kainz, M.J., 2025. Diet predicts fatty acids of zooplankton more than environmental or geographical variables: evidence from subarctic to subtropical aquatic ecosystems. Inland Waters 15 (1), 2511112. https://doi.org/10.1080/20442041.2025.2511112.
Meitei, M.M., Muralidhar, A.P., Syamala, K., Sureesh, S., Biswas, G., Megarajan, S., Munilkumar, S., 2025. Assessment of filtration capacity of different bivalve species suitable for integrated multi-trophic aquaculture (IMTA) systems Vis-à-Vis waste valorization for sustainable environment. Discov. Sustain. 6 (1), 1–16. https://doi.org/10.1007/s43621-025-01104-0.
Navarro, E., Iglesias, J.I.P., 1995. Energetics of reproduction related to environmental variability in bivalve molluscs. Haliotis 24, 43–55.
Nguyen, M.V., Kakooza, D., Tran, A.P., Tran, V.T.T., 2024. Variation in the lipid profile of Pacific oyster (*Crassostrea gigas*) cultured in Khanh Hoa coast, Vietnam, based on location and harvest period. Pol. J. Food Nutr. Sci. 74 (1). https://doi.org/10.31883/pjfns/178395.
Noor, A.R., Shakil, A., Hoque, N.F., Rahman, M.M., Akter, S., Talukder, A., Ahmad-Al-Nahid, S., Wahab, M.A., Nahiduzzaman, M., Rahman, M.J., Asaduzzaman, M., 2021. Effect of eco-physiological factors on biometric traits of green mussel *Perna viridis* cultured in the south-east coast of the Bay of Bengal. Bangladesh. Aquac. Rep. 19, 100562. https://doi.org/10.1016/j.aqrep.2020.100562.
Osada, M., Matsumoto, T., 2021. Endocrine control of gametogenesis and spawning in bivalves. In: Physiology of Molluscs. Apple Academic Press, pp. 179–219. https://doi.org/10.1201/9781315207117-6.
O'Shea, T., Jones, R., Markham, A., Norell, E., Scott, J., Theuerkauf, S., Waters, T., 2019. Towards a Blue Revolution: Catalyzing Private Investment in Sustainable Aquaculture Production Systems. The Nature Conservancy and Encourage Capital, Arlington, Virginia, 159 pp.
Padilla-Gamiño, J.L., Alma, L., Spencer, L.H., Venkataraman, Y.R., Wessler, L., 2022. Ocean acidification does not overlook sex: review of understudied effects and implications of low pH on marine invertebrate sexual reproduction. Front. Mar. Sci. 9, 977754. https://doi.org/10.3389/fmars.2022.977754.
Paixão, L., Ferreira, M.A., Nunes, Z., Fonseca-Sizo, F., Rocha, R., 2013. Effects of salinity and rainfall on the reproductive biology of the mangrove oyster (*Crassostrea gasar*): implications for the collection of broodstock oysters. Aquaculture 380, 6–12. https://doi.org/10.1016/j.aquaculture.2012.11.019.
Pakhmode, P.K., Mohite, S.A., Takar, S., Gurjar, U.R., 2022. Reproductive biology of rock oyster, *Saccostrea cucullata* (Born, 1778) along Aare-ware rocky shore of Ratnagiri, Maharashtra, India. Indian J. Geo-Mar. Sci. 50 (10), 802–809. https://doi.org/10.56042/ijms.v50i10.38085.
Park, K.I., Choi, K.S., 2004. Application of enzyme-linked immunosorbent assay for studying of reproduction in the Manila clam *Ruditapes philippinarum* (Mollusca: Bivalvia): I. Quantifying eggs. Aquaculture 241 (1–4), 667–687.
Pearse, A.G.E., 1985. Histochemistry: Theoretical and Applied, 4th ed. Churchill Livingstone, Edinburgh, London, Melbourne, New York https://www.scirp.org/reference/referencespapers?referenceid=1513327.
Peltomaa, E., Hällfors, H., Taipale, S.J., 2019. Comparison of diatoms and dinoflagellates from different habitats as sources of PUFAs. Mar. Drugs 17 (4), 233. https://doi.org/10.3390/md17040233.
Pernet, F., Malet, N., Pastoreaud, A., Vaquer, A., Quéré, C., Dubroca, L., 2012. Marine diatoms sustain growth of bivalves in a Mediterranean lagoon. J. Sea Res. 68, 20–32. https://doi.org/10.1016/j.seares.2011.11.004.
Pouvreau, S., 2000. Gametogenic cycle and reproductive effort of the tropical black-lip pearl oyster, Pinctada margaritifera (Bivalvia: Pteriidae), cultivated in Takapoto atoll (French Polynesia). Aquat. Living Resour. 13, 37–48. https://doi.org/10.1016/S0990-7440(00)00135-2.
R Core Team, 2024. R: A Language and Environment for Statistical Computing. R Foundation for Statistical Computing, Vienna. https://doi.org/10.32614/r.manuals.
Renaud, S.M., Thinh, L.V., Lambrinidis, G., Parry, D.L., 2002. Effect of temperature on growth, chemical composition and fatty acid composition of tropical Australian microalgae grown in batch cultures. Aquaculture 211 (1–4), 195–214. https://doi.org/10.1016/S0044-8486(01)00875-4.
Sanjeevaraj, P.J., 2008. Oysters in a new classification of keystone species. Resonance 13, 648–654. https://doi.org/10.1007/s12045-008-0071-4.
Soon, T.K., Ransangan, J., 2014. A review of feeding behavior, growth, reproduction and aquaculture site selection for green-lipped mussel, *Perna viridis*. J. adv. biol. biotechnol. 5 (5), 462–469. https://doi.org/10.4236/abb.2014.55056.
Soudant, P., Marty, Y., Moal, J., Robert, R., Quéré, C., Le Coz, J.R., Samain, J.F., 1996. Effect of food fatty acid and sterol quality on Pecten maximus gonad composition and reproduction process. Aquaculture 143 (3–4), 361–378. https://doi.org/10.1016/0044-8486(96)01276-8.
Soudant, P., Van Ryckeghem, K., Marty, Y., Moal, J., Samain, J.F., Sorgeloos, P., 1999. Comparison of the lipid class and fatty acid composition between a reproductive cycle in nature and a standard hatchery conditioning of the Pacific oyster *Crassostrea gigas*. Comp. Biochem. Physiol. B Biochem. Mol. Biol. 123 (2), 209–222. https://doi.org/10.1016/S0305-0491(99)00063-2.
Su, X.Q., Antonas, K., Li, D., Nichols, P., 2006. Seasonal variations of total lipid and fatty acid contents in the muscle of two Australian farmed abalone species. J. Food Lipids 13 (4), 411–423. https://doi.org/10.1111/j.1745-4522.2006.00063.x.
Suárez, M.P., Alvarez, C., Molist, P., San Juan, F., 2005. Particular aspects of gonadal cycle and seasonal distribution of gametogenic stages of *Mytilus galloprovincialis* cultured in the estuary of Vigo. J. Shellfish. Res. 24 (2), 531–540. https://doi.org/10.2983/0730-8000(2005)24[531:PAOGCA]2.0.CO;2.
Thangavelu, R., 1988. Natural food of *Crassostrea madrasensis* in Pulicat Lake, India. Proc. Anim. Sci. 97, 463–470. https://doi.org/10.1007/BF03179954.
Theuerkauf, S.J., Barrett, L.T., Alleway, H.K., Costa-Pierce, B.A., Gelais, A., Jones, R.C., 2022. Habitat value of bivalve shellfish and seaweed aquaculture for fish and invertebrates: pathways, synthesis and next steps. Rev. Aquac. 14 (1), 54–72. https://doi.org/10.1111/raq.12584.
Toyokawa, M., Saito, H., Yurimoto, T., 2023. Reproductive cycle of the edible oyster *Crassostrea belcheri* in the Myeik coastal area of southern Myanmar. Jpn. Agric. Res. Q. 57 (3), 241–249. https://doi.org/10.6090/jarq.57.241.
Uddin, M.J., Jeung, H.D., Yang, H.S., Kim, B.K., Ju, S.J., Choi, K.S., 2013. Quantitative assessment of reproductive effort of the Manila clam *Ruditapes philippinarum* in a

lagoon on Jeju Island (Korea) using enzyme-linked immunosorbent assay. Invert. Reprod. Dev. 57 (4), 316–324. https://doi.org/10.1080/07924259.2013.793219.

Uddin, M.J., Rahman, M.S., Sonia, S.S., Kubra, S.K., Mia, M.S., Yeasmine, S., 2024. Annual gametogenic phenology of oyster *Magallana bilineata* (Röding, 1798) collected from the west coast of Moheshkhali Island, Cox's Bazar, Bangladesh. Heliyon 10 (7). https://doi.org/10.1016/j.heliyon.2024.e28753.

Vahirua-Lechat, I., Laure, F., Le Coz, J.R., Bianchini, J.P., Bellais, M., Le Moullac, G., 2008. Changes in fatty acid and sterol composition during oogenesis in the pearl oyster *Pinctada margaritifera*. Aquacult. Res. 39 (16), 1739–1746. https://doi.org/10.1111/j.1365-2109.2008.02050.x.

van der Schatte Olivier, A., Jones, L., Vay, L.L., Christie, M., Wilson, J., Malham, S.K., 2020. A global review of the ecosystem services provided by bivalve aquaculture. Rev. Aquacult. 12, 3–25. https://doi.org/10.1111/raq.12301.

Ventrella, V., Pirini, M., Pagliarani, A., Trombetti, F., Manuzzi, M.P., 2008. Effect of temporal and geographical factors on fatty acid composition of *Mytilus galloprovincialis* from the Adriatic Sea. Comp. Biochem. Physiol. B Biochem. Mol. Biol. 149, 241–250. https://doi.org/10.1016/j.cbpb.2007.09.012.

Wenne, R., Polak, L., 1989. Lipid composition and storage in the tissues of the bivalve Macoma balthica. Biochem. Syst. Ecol. 17 (7–8), 583–587. https://doi.org/10.1016/0305-1978(89)90103-8.

Whyte, J.N.C., Bourne, N., Ginther, N.G., Hodgson, C.A., 1992. Compositional changes in the larva to juvenile development of the scallop *Patinopecten yessoensis* (jay). J. Exp. Mar. Biol. Ecol. 149, 67–79.

Yosuva, M., Jeyapragash, D., Saravanan, S., 2019. Impact of environmental parameters on the growth rate of *Crassostrea madrasensis* (Preston) spatfall at Vellar estuary, India. Indian J. Geo-Mar. Sci. 48 (1), 120–125.

Zárate, E.V., de Vivar, M.E.D., Avaro, M.G., Epherra, L., Sewell, M.A., 2016. Sex and reproductive cycle affect lipid and fatty acid profiles of gonads of *Arbacia dufresnii* (Echinodermata: Echinoidea). Mar. Ecol. Prog. Ser. 551, 185–199. https://doi.org/10.3354/meps11737.

Zhu, Y., Liao, K., Huang, H., Liu, Y., Zhang, Y., Chen, D., et al., 2024. Effects of dietary docosahexaenoic acid (DHA) levels on growth performance, fatty acid profile, and NF-κB/Nrf2 pathway-related gene expression of razor clam Sinonovacula constricta. Aquacult. Nutr. 2024 (1), 9107191.

Regional Studies in Marine Science 81 (2025) 103981

Contents lists available at ScienceDirect

Regional Studies in Marine Science

journal homepage: www.elsevier.com/locate/rsma

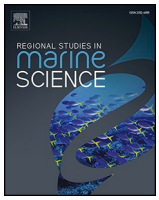

Ecology intersects with mariculture: How cultivation depth and site-specific environmental factors shape growth and nutritional profile of green mussels (*Perna viridis*)

Md Asaduzzaman [a,1,*], Md Mohiuddin [a], Md Moshiur Rahman [b], Ilias Ebne Kabir [c], Md Nahiduzzaman [c]

[a] *Department of Marine Bioresource Science, Faculty of Fisheries, Chattogram Veterinary and Animal Sciences University, Khulshi, Chattogram 4225, Bangladesh*
[b] *Fish Conservation and Culture Laboratory, Department of Biological and Agricultural Engineering, University of California Davis, 17501 Byron Hwy, Byron, CA 94514, USA*
[c] *WorldFish Bangladesh and South Asia, Dhaka, Bangladesh*

ARTICLE INFO

Keywords:
Bivalves
Coastal mariculture
Extractive shellfish
Growth metrics
Amino acid contents
Fatty acid profile

ABSTRACT

Understanding the interlinkages between ecological conditions and mariculture practices are vital for enhancing growth performance and nutritional profiling of marine bivalves. However, highly productive mariculture practices under different local ecological conditions have not been comprehensively documented to achieve sustainable outcomes. This study investigates how depth (0.5 m, 1 m, and 1.5 m) and site-specific ecological factors of three farming sites (Moheshkhali, Khurushkul, and Choufaldandi) influence the growth performance and nutritional profile of green mussels (*Perna viridis*) in floating raft mariculture systems in the southeast coast of the Bay of Bengal, Bangladesh. For this purpose, 20 uniform green mussel spats (2.9 ± 0.08 g) were inoculated across three cultivation depths in ten replicated mussel net socks, which were suspended vertically in the water column from horizontal floating rafts and cultured for six months (October-March) at the above-mentioned three farming sites. Among environmental factors, the two-way ANOVA model displayed both depth- and site-specific significant variation of ecological parameters (DO, salinity, turbidity, NO_3-N, PO_4-P, Chlorophyll-a) and food availability (Coscinodiscophyceae, Bacillariophyceae, Chlorophyceae, and Dinophyceae) in the studied areas. Our findings based on the two-way ANOVA model also revealed that both the depth and site-specific ecological settings significantly impact ($p < 0.05$) growth performance, shell morphometry and nutritional profiles of green mussels. Various univariate and multivariate analyses further revealed that the above ecological factors are closely interlinked with the observed differences in growth performance and nutritional profiles of mussels. By integrating these ecological and environmental variables, our study provides actionable insights for optimizing green mussel farming practices, potentially leading to improved yield and nutritional quality in floating raft systems.

1. Introduction

The *Perna viridis*, also known as the green mussel, is a notably valuable filter-feeding bivalve species that is native to the tropical and subtropical regions of the Indo-Pacific, encompassing China, Singapore, Thailand, India, and the Philippines (Sivalingam, 1977; Rajagopal et al., 2006). Additional distributions of this species include Japan, Malaysia, Papua New Guinea, the South Pacific Islands, and the Persian Gulf (Sivalingam, 1977; Rajagopal et al., 2006). Specifically, the Cox's Bazar coast of the Bay of Bengal in Bangladesh is rich in green mussels, with notable concentrations found in locations including St. Martin Island, Shahporir Dwip, Naf River, and the Moheshkhali Channel (Shahabuddin et al., 2010). *P. viridis* is regarded as a valuable food source for human consumption because of its abundant protein content and well-balanced nutritional makeup (España et al., 2007; Chakraborty et al., 2014; Saritha et al., 2015; Chakraborty et al., 2016). Owing to its exceptional nutritional content, green mussels have become a vital element of worldwide aquaculture, making significant contributions to both food

* Corresponding author.
E-mail address: a_zamanbau@yahoo.com (M. Asaduzzaman).
[1] Orcid ID: 0000-0002-8211-1462

https://doi.org/10.1016/j.rsma.2024.103981
Received 1 October 2024; Received in revised form 9 December 2024; Accepted 13 December 2024
Available online 15 December 2024

security and economic progress (Duarte et al., 2020; FAO, 2022; Huang et al., 2021). The adaptability of *P. viridis* to different climatic circumstances renders it a desirable species for aquaculture, especially in localities susceptible to climate change, where conventional fishing activities may be diminishing (Rajagopal, 1997; Rajagopal et al., 1998; Tang et al., 2011). As these species do not need extra feed, reach harvestable size in around six months, and do not require the removal of mangroves for site preparation, mussel farming has a smaller carbon impact (Tang et al., 2011; Waldbusser et al., 2013; Filgueira et al., 2015; Rejeki et al., 2021). Its cultivation is devoid of complex methods, expertise, or equipment, rendering it especially well-suited for small-scale artisanal environments (Bin Sallih and Þórðarson, 2005; Rejeki et al., 2021). *P. viridis*, being a significant bivalve, plays a crucial role in marine ecology by its ability to filter water and provide habitat and nutritious resources for a wide range of aquatic species (Hawkins et al., 1998). Green mussel mariculture presents a nature-oriented method for managing coastal resources, which involves controlling services such as carbon sequestration, nutrient remediation, and coastal defence. This practice also offers economic prospects and ecological advantages for coastal communities (Shumway et al., 2003; Lindahl et al., 2005; Herbert et al., 2012; Seitz et al., 2014; Rejeki et al., 2021).

Various cultivation methods for green mussels, such as bottom and off-bottom, have been developed in response to the growing demand for sustainable seafood. These techniques provide distinct benefits that are adapted to local environmental conditions and management objectives (Aypa S, M, 1990; Forrest and Creese, 2006; Dubois et al., 2007; Rejeki et al., 2021). The bottom cultivation system, which involves growing mussels directly on the seabed in the intertidal zone, is a cost-effective method that enables natural feeding. However, it is more prone to increased mortality caused by sedimentation and competition with other benthic inhabitants (Aypa S, M, 1990; Forrest and Creese, 2006). Furthermore, off-bottom techniques such as floating rafts and suspended long lines are applicable in both intertidal and deepwater regions (Sivalingam, 1977; Aypa S, M, 1990; Rejeki et al., 2021). The floating raft cultivation approach is well recognized for its effectiveness in optimizing space and promoting water flow around the mussels, resulting in higher growth rates and superior health (Rivonker et al., 1993; Noor et al., 2019; Rejeki et al., 2021). To achieve maximum exposure to nutrients and phytoplankton in the water column, mussels are affixed to ropes or nets suspended from a floating raft (Rivonker et al., 1993; Noor et al., 2019; Rejeki et al., 2021). In coastal regions characterized by powerful currents and abundant nutrients, the floating raft technique is often used due to its capacity to enhance growth and reduce the likelihood of sedimentation, therefore safeguarding the overall health of mussels (Cheney et al., 2010; Noor et al., 2019). The efficacy of floating raft techniques in certain areas has underscored the potential of green mussel aquaculture as a reliable approach to tackle protein insufficiencies in emerging nations (Rivonker et al., 1993; Noor et al., 2019; Rejeki et al., 2021). Nevertheless, the achievement of maximum yield and biochemical profile in green mussels necessitates meticulous management and the selection of the most suitable site (Tan and Ransangan, 2016; Hoque et al., 2021). Therefore, it is essential to comprehend the impact of these factors on the development and nutritional characteristics of green mussels to fully optimize mariculture techniques (Tan and Ransangan, 2014).

Cultivation depth plays a crucial role in determining the production and nutritional quality of green mussels in floating raft systems (Fuentes et al., 2000; Dobretsov and Miron, 2001). Although coastal waters often have enhanced light availability for phytoplankton proliferation, they are also susceptible to sedimentation and nutrient runoff, which can lead to the burial of mussels and negatively impact their health (Huisman et al., 1999). In contrast, offshore deep seas offer a more consistent setting characterized by reduced variations in temperature and salinity. This can greatly enhance the health, growth, and general welfare of mussels by reducing fouling and predation, as well as facilitating water exchange (Cheney et al., 2010). A growing interest in offshore deepwater mussel farming has been fuelled by the claimed benefits of cultivating mussels in deeper water (Cheney et al., 2010). In agreement, research from various regions supports the notion that more profound water cultivation often provides superior conditions for shellfish species (Langan and Horton, 2003; Buck, 2007; Yu et al., 2010). However, conducting cultivation in deeper water may provide difficulties, such as decreased light penetration and modified nutrient dynamics, which can affect the growth and nutritional quality of mussels (Huisman et al., 1999). The intricate interaction between the depth of culture and the biology of mussels emphasizes the need for meticulous selection of sites and depth to enhance production efficiency and nutritional quality (Ogilvie et al., 2004). Nevertheless, the precise influence of depth on the growth and nutritional composition of green mussels in floating raft systems has not been well investigated. A comprehensive understanding of these relationships is essential for optimizing mussel production and ensuring product quality.

Successful culture of green mussels is dependent on many site-specific environmental conditions, which have a direct impact on their feeding, respiration, and reproduction (Loesch and Evans, 1994; Alvarado and Castilla, 1996; Iglesias et al., 1996; Noor et al., 2021). Prior studies have investigated the ecological requirement, survival, and growth performance of *P. viridis* in both natural environments and human-controlled laboratory settings (Parulekar et al., 1982; Chatterji et al., 1984; Chaitanawisuti and Menasveta, 1987; Rivonker et al., 1993; Rajagopal et al., 1998; Wang et al., 2011; Taib et al., 2016; Rejeki et al., 2021). The ideal ecological parameters for the growth of green mussels are moderate temperatures ranging from 25 to 30°C (Hickman, 1979), and consistent salinity levels ranging from 20 to 35 ppt (Aypa S, M, 1990). Adequate nutrient availability, namely nitrogen and phosphorus, is essential for sustaining phytoplankton abundance, which is the main source of food for green mussels. Hence, the choice of farming locations is frequently dictated by the presence of elevated chlorophyll-a levels (Rajagopal et al., 1998; Xu et al., 2010; Hoque et al., 2021), which serve as an indicator of phytoplankton abundance. Prior research indicates that the chlorophyll-a distribution in mussel farming varies between 0.7 mg/m^3 and 17 mg/m^3 (Rajagopal et al., 1998; Tan and Ransangan, 2017; Hoque et al., 2021). Plankton is the main food consumed by *P. viridis* and serves as a vital source of nutrients and energy for gametogenesis (Tan and Ransangan, 2017; Asaduzzaman et al., 2019; Asaduzzaman et al., 2021). Elevated phytoplankton biomass is correlated with accelerated mussel growth (Kamal and Khan, 1998; Ren and Ross, 2005; Noor et al., 2021). The abundance of plankton in the water and its uptake by green mussels from the water column is markedly influenced by seasonality and environmental circumstances (Tan and Ransangan, 2017; Asaduzzaman et al., 2020). Furthermore, the nutritional quality of green mussels is greatly influenced by ecological factors, which affect numerous aspects such as food availability, growth, and biochemical makeup (Asaduzzaman et al., 2020). However, the multifaceted linkages among the ecological factors, growth performance, and nutritional quality of green mussels are not comprehensively documented within the context of the floating raft cultivation system.

The coastline of Bangladesh spans 710 km and has 8500 km^2 of shallow coastal and nearshore waters, which are less than 5 m deep (Tasnim et al., 2024). Featuring a wide range of coastal habitats such as mangroves, salt marsh, sea grass, corals, and stony reefs, this vast shallow region sustains a diversified bivalve population (Shahabuddin et al., 2010). Considering the increasing seafood demand in the country and the vulnerability of coastal communities, the establishment of small-scale commercial green mussel farming offers a favourable prospect for economic rejuvenation. Hence, the objective of this work is to examine the growth efficiency and nutritional parameters of green mussels (*P. viridis*) grown in raft systems, specifically analysing the influence of culture depths and site-specific ecological variables. Our hypothesis posits that varying cultivation depths will lead to unique growth rates and nutritional components for mussels, which are impacted by the surrounding ecological circumstances of the cultivation

sites. Furthermore, the study investigated the intricate relationships among environmental variables, seasonality, food availability, and mussel growth performances. By elucidating these relationships, this research seeks to optimize mussel farming practices, promote sustainable mariculture, and enhance the economic viability of mussel production in the floating raft system.

2. Materials and Methods

2.1. Study area

The cultivation study of *P. viridis* was conducted from October 2022 to March 2023 at three locations: Moheshkhali (21°31'58"N, 91°58'52"E), Khurushkul (21°30'40"N, 91°59'53"E), and Choufaldandi (21°30'42"N, 92°0'56"E) in the Moheshkhali Channel, Cox's Bazar, Bangladesh (Fig. 1). This channel is bordered on the east and west by the Bay of Bengal and is located on the southeast coast of Bangladesh. The selected locations are ideal for cultivating green mussels due to their natural abundance and favourable water quality parameters (Shahabuddin et al., 2010; Asaduzzaman et al., 2020).

2.2. Installation of cultivation system and spat inoculation

Using bamboo and plastic drums, floating bamboo raft systems with an area of 36 m^2 each were built for this study (Fig. 2D) and installed at three distinct sites in the Moheshkhali Channel (Moheshkhali, Khurushkul, and Choufaldandi) (Fig. 1). These culture systems have been deployed in near-shore shallow water areas with a maximum water level of 2.0 m at low tide to prevent navigational conflicts and possible interference from fishing activities. For this study, three water depths (0.5 m, 1 m, and 1.5 m) were considered from the surface layer (Fig. 2B–C). The mussels' net socks (1.5 m long and 15 cm wide) were prepared by manual swing using a black nylon fishing net (mesh size 0.8 cm) and hung vertically from the floating raft (Fig. 2B–C). The green mussel spats (2.9 ± 0.08 g) were collected from the rope substrate of existing nearby green mussel culture activities in the same Moheshkhali Channel using a spatula and scissors to cut through the byssus threads (Fig. 2A). After collecting the spats, their biometric traits were measured and 20 of them with uniform size were inoculated to each of the three different depths (0.5 m, 1 m, and 1.5 m) in each of the mussel socks (Fig. 2B–C). In each of the cultivation areas, ten mussel socks (as

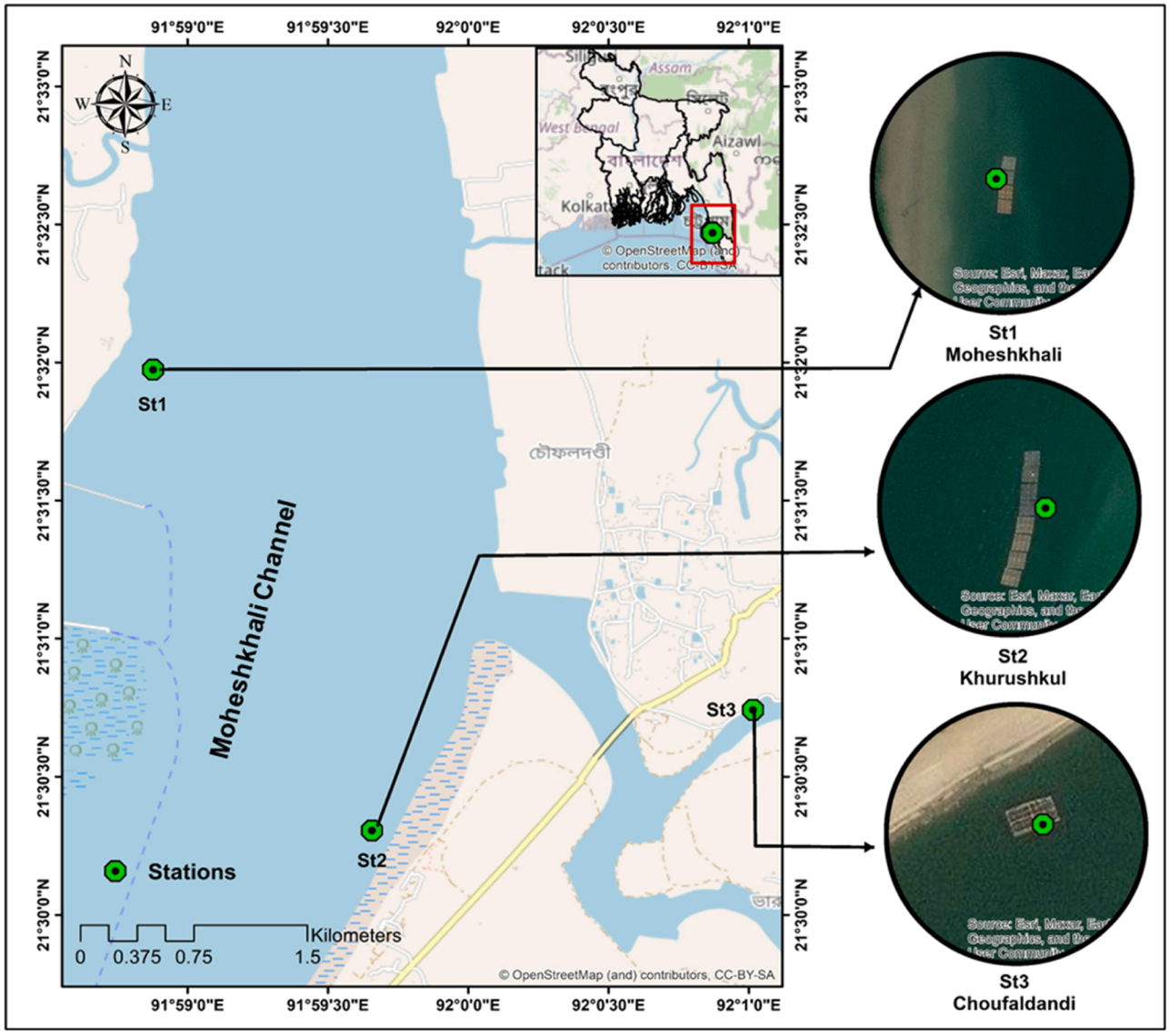

Fig. 1. Satellite view of the study areas (Source: Esri) illustrating the floating raft system of the green mussel (*Perna viridis*) along the Moheshkhali Channel in Cox's Bazar, Bangladesh. The experiment was conducted at three locations: Moheshkhali (21°31'58"N, 91°58'52"E), Khurushkul (21°30'40"N, 91°59'53"E), and Choufaldandi (21°30'42"N, 92°0'56"E). The map was prepared using ArcGIS.

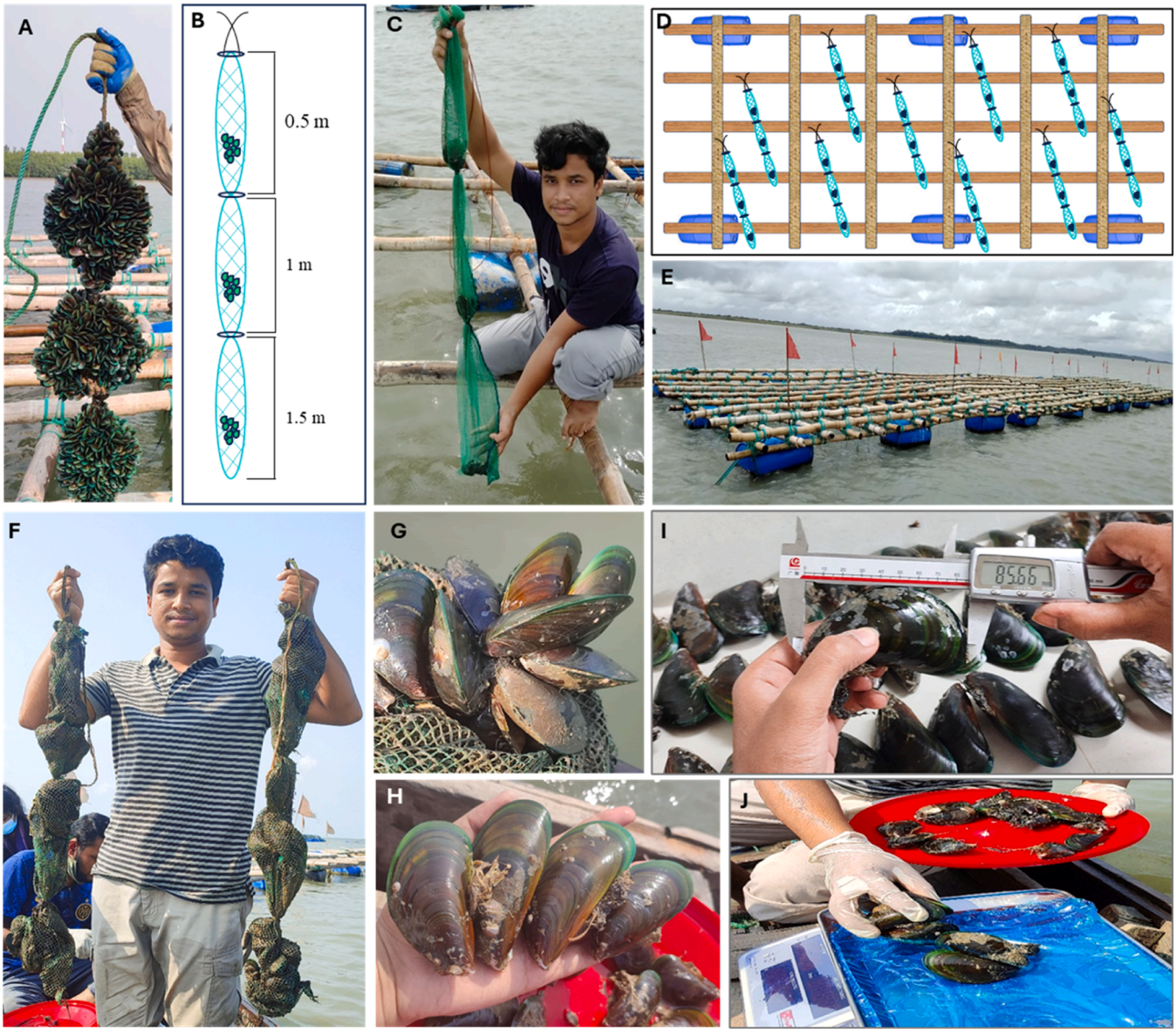

Fig. 2. Photographic overview of the experimental design and biometric measurements of harvested green mussels (*Perna viridis*) cultivated for six months at three depths (0.5 m, 1.0 m, and 1.5 m) across three sites (Khurushkul, Maheshkhali, and Choufaldandi) in the Maheshkhali Channel of the Bay of Bengal, Bangladesh. (A) Spats of green mussels (2.9 ± 0.08 g) collected from the rope substrate of existing cultivation activities for use in this study; (B-C) Design and actual views of each mussel sock, each containing 20 spats, at the three water depths (0.5 m, 1 m, and 1.5 m; (D) Ten mussel socks (replicated units) hung vertically from a floating raft using nylon rope at each location (Khurushkul, Maheshkhali, and Choufaldandi; (E) Actual photographs of the installed floating raft system used in this study at each location; (F) Photographs of each mussel sock at the end of the six months cultivation periods (October 2022 to March 2023; (G-H) Photographs of harvested green mussels; and (I-J) Photographs of the biometric measurements of the harvested green mussels.

replicated units) were hung from the raft by attaching a separate nylon rope so that whole socks (1.5 m) remained suspended vertically in the water (Fig. 2D). Thus, this study had a factorial design with three depths (0.5 m, 1 m, and 1.5 m) as the first factor and three locations (Khurushkul, Moheshkhali, and Choufaldandi) as the second factor.

2.3. Measurement of water quality parameters

Physical parameters (temperature, pH, dissolved oxygen, salinity, and turbidity) were measured monthly in triplicate at low-tide conditions for each cultivation depth (0.5 m, 1 m, and 1.5 m) at three sites (Moheshkhali, Khurushkul, and Choufaldandi). A Celsius thermometer was used to measure water temperature, a digital pH meter (EcoSense pH10A by YSI) was used to determine pH, a digital DO meter (PDO-519 by Lutron) was used to measure dissolved oxygen (DO), a digital refractometer (Bellingham and Stanley E-Line by Xylem) was used to assess salinity, and a digital turbidity meter (Turb 430 IR, WTW, Weilheim, Germany) was used to measure turbidity. Among these factors, dissolved oxygen was directly detected by submerging the sensors to appropriate depths. To assess other physical parameters, a horizontal water sampler (1120–1180 Horizontal Alpha™ Bottles, WildCo, FL, USA) was used to collect composite water samples from each cultivation depth. The collected water was then put directly in a bucket placed on the boat and other water quality parameters were measured directly and freshly by using specific equipment as mentioned above. Following the measurement of physical characteristics, composite water samples (about 800 ml) from each cultivation depth and site were transported to the lab under ice storage conditions for chemical water quality analysis. To investigate nutrients and chlorophyll-a, water samples were filtered through microfiber glass filter paper (Whatman GF/C) using a vacuum

pressure air pump. Concentrations of NO_2-N, NO_3-N, NH_3-N, and PO_4-P were measured spectrophotometrically (PhotoFlex STD, WTW, Weilheim, Germany) in triplicates (APHA, 1992). Chlorophyll-a concentrations were measured at 664, 647, and 630 nm using an Optizen Pop 2102 (Daejeon, Republic of Korea), following Boyd's (1979) method.

2.4. Qualitative and quantitative estimation of water plankton abundance

Throughout the study period, the qualitative and quantitative abundance of water plankton was measured monthly in triplicate at each depth and sampling location. Initially, 20 L of composite water samples were obtained from each cultivation depth using a horizontal water sampler (1120–1180 Horizontal Alpha™ Bottles, WildCo, FL, USA). The obtained pooled water samples (20 L) were filtered through a 25-μm mesh plankton net. The concentrated samples were then stored in small plastic bottles containing 5 % buffered formalin. The plankton (cells L^{-1}) was quantitatively measured using a Sedgewick-Rafter (S-R) cell composed of 1000 1-mm^3 cells (Asaduzzaman et al., 2008). A 1-ml sample was placed into the S–R cell, and the plankton in 10 cells chosen at random were enumerated using a binocular microscope (Optika B-190 TB, Ponteranica, Italy). The calculation of plankton abundance was performed using the formula $N = (P \times C \times 100)/L$. Here, N represents the number of plankton cells or units per litre of water, P represents the number of plankton included in 10 fields, C represents the volume of the final concentrate of the sample (ml), and L represents the volume of the water sample used. Utilizing keys developed by Botes (Botes, 2003; Mitra et al., 2013; McGaraghan, 2018), plankton were taxonomically identified up to the genus level and categorized into distinct groups according to the approach of Al-Kandari et al. (Al-Kandari et al., 2009).

2.5. Growth monitoring, harvesting and biometric measurements of green mussels

During the cultivation period, the weight gain of green mussels was recorded monthly by measuring the live weight of 10 individuals for each depth and from each location. Green mussels typically require six months to reach a harvestable size. Accordingly, the experiment was conducted over six months, from October 2022 to March 2023. Following harvest, the collected mussels were thoroughly cleaned to remove encrusting critters and their byssus threads (Fig. 2G–H). The total gross weight from each cultivation depth and the survival (in terms of % alive) were recorded on site (Fig. 2J). Subsequently, samples from different depths were immediately transported to the laboratory for biometric measurements and growth parameter analysis. Mussels from each depth and location were measured for their shell length, width, and height using vernier callipers with a 0.01 mm accuracy (Fig. 2I). The weight of each mussel was then determined by an electronic balance, to the nearest 0.1 g (PS 1200.R2, Radwag, Poland), after draining fluids from the intervalvar area. The meat section was then separated from the shell, and the soft tissue and shell weights were recorded individually. The specific growth rate for *P. viridis* was computed independently for each depth and each location. Specific Growth Rate (SGR % day^{-1}) for green mussels was calculated as follows: $SGR = \{(\ln Wt - \ln W0)/ t\} \times 100$ %; Where W0 = Initial weight (g); Wt = Final weight (g); t = Length of cultivation (day).

2.6. Sample preparation for biochemical analysis

After cleaning and washing with distilled water, the meat portion of 20 randomly selected samples from each cultivation site for each depth (i.e., 60 individuals for each replicated sample from three sites for each depth of 0.5 m, 1.0 m, and 1.5 m) was pooled together and chopped carefully for different biochemical analyses. For each cultivation depth, a portion of the pooled raw samples from each replicate was freeze-dried and ground in powder form for fatty acid analysis. The remaining pooled raw samples were dried at 60°C in a hot air oven until they attained a constant weight. The dried samples were then pulverized into a fine powder using a blender (Kiam, BL-100, 750 watts, Bangladesh). Powdered samples of green mussels from each cultivation depth were subsequently used for proximate composition and amino acid analyses. All biochemical analyses were conducted in triplicate for each cultivation depth.

2.7. Proximate composition

The analysis of proximate composition, including protein, fat, and ash, was conducted at the laboratory of the Poultry Research and Training Centre (PRTC) at Chattogram Veterinary and Animal Sciences University. The Kjeldahl experimental setup was employed to quantify the concentration of crude protein (Guebel et al., 1991). From the nitrogen concentration, the crude protein content was determined using a conversion ratio of 6.25 (AOAC, 2000). Quantification of total lipid content was carried out using the Soxhlet equipment (AOAC, 2005). Ash content was quantified using the incineration technique outlined by AOAC (AOAC, 2000).

2.8. Amino acid analysis

The AccQ-Tag Amino Acid Analysis approach was used to quantify the amino acid composition of *P. viridis* at three distinct depths of cultivation. To perform acid hydrolysis, 2 g of the green mussel sample were immersed in 20 millilitres of 6 N hydrochloric acid in a hermetically sealed test tube. The mixture was then stirred for 20 minutes and then placed in an oven set at 105 °C for 24 hours. After the hydrolysis process, 20 ml of deionised water was introduced to each sample solution. The filtrate was then passed through Whatman No. 1 filter paper and then through a nylon acetate (cellulose) membrane filter with a pore size of 0.2 μm and a diameter of 47 mm. The samples underwent neutralisation using a 0.1 N $NaOH/NH_3$-OH solution after hydrolysis. Tryptophan was subjected to alkaline hydrolysis by employing 20 ml of 4.3 N LiOH continuously heated in an oven at 160 °C for 16 hours. For a total volume of 100 ml, deionised water and 9 ml of a 6 N hydrochloric acid solution were added. After adjusting the pH of the solution to 4.5 with HCl, it was filtered once again using Whatman No. 1 filter paper and nylon cellulose acetate membrane. Following hydrolysis, the samples were subjected to derivatisation using a reagent kit (AccQ-Fluor Reagent, WAT052875, Waters). A column temperature of 37 °C was established for acid hydrolysates, whereas the temperature for alkaline hydrolysates was maintained at room temperature. 10 μl of the derivatised samples were injected into a high-performance liquid chromatography (HPLC) system (e2695, Waters) at a flow rate of 1 ml per minute. The HPLC system was equipped with a C18RP column (3.9 × 150 mm) and a fluorescence detector (2475, Waters), with a chromatographic run time of 60 min. Peak detection was aided by the UV detector operating at a wavelength of 248 nm, while the fluorescence detector was configured with an excitation wavelength of 250 nm and an emission wavelength of 395 nm. The detection and quantification of amino acids were achieved by comparing the retention periods and peak regions of standards (WAT088122, Waters). A total of 15 amino acids were both discovered and measured in mg g^{-1} of mussel, based on their dry weight.

2.9. Fatty acids analysis

In order to determine the fatty acids, the procedure outlined by Prato et al. (2017) was followed. The first step was to use a Soxhlet equipment to extract lipids from 2 g of dried green mussels. The solvent used for lipid extraction was diethyl ether, with the final phase of extraction conducted at a maintained temperature of 60 °C. Following lipid extraction, fatty acid methyl esters (FAMEs) were evaluated from the extracted lipid sample. The analysis of FAMEs was conducted using gas chromatography-mass spectrometry (GC-MS) with a GCMS-QP2020 (Shimadzu, Japan) equipped with a flame ionization detector.

Separation of the FAMEs was achieved using a capillary column measuring 30 m in length, 0.25 mm in inner diameter, 0.15 m in film thickness, and 250 phase ratios. Helium was utilized as the carrier gas, flowing at a rate of 1.42 ml/min. A temperature ramp of 5 °C per minute was used to get the column temperature from 180 °C to 280 °C, and then it was maintained at 280 °C. FAMEs were identified by comparing their retention times with a standard (FAME mix C8-C24; Sigma-Aldrich, Germany). Measurements were recorded in parts per million (ppm) and subsequently converted to percentages of total fatty acids.

2.10. Statistical analysis

All statistical analyses were conducted using R, version 4.2.2 (R Development Core Team, 2022). To confirm the normal distribution

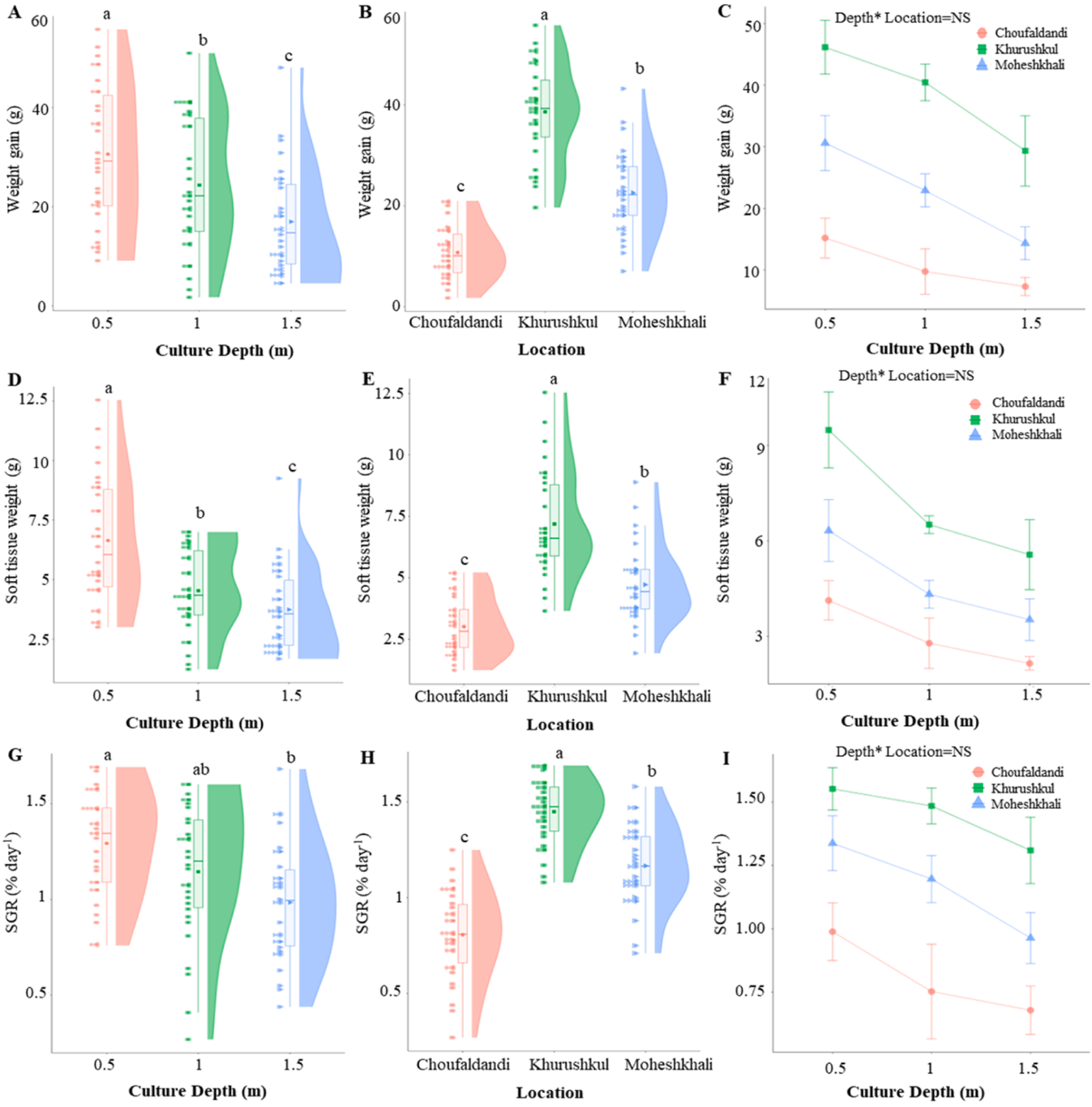

Fig. 3. Growth performance of green mussels (*Perna viridis*) after six months of cultivation at three depths (0.5 m, 1.0 m, and 1.5 m) across three sites (Khurushkul, Maheshkhali, and Choufaldandi) in the Maheshkhali Channel of the Bay of Bengal, Bangladesh. (A-C) Weight gain (g) of green mussels at different depths (A), across the three cultivation sites (B), and their interaction (C) based on two-way ANOVA. (D-F) Soft tissue weight (g) of green mussels at various depths (D), across three cultivation sites (E), and their interaction (F) based on two-way ANOVA. (G-I) Specific growth rate (SGR, %/day) of green mussels at different depths (G), across the three cultivation sites (H), and their interaction (I) based on two-way ANOVA. Significant differences ($p < 0.05$) are indicated with superscript letters. Raincloud plots (A, B, D, E, G, H) illustrate data distribution (the "cloud") with jittered sample data (the "rain"), showcasing the variation in growth performance of green mussels across the three depths and locations through a combination of density distribution and boxplots. The boxplots indicate median values (represented by horizontal lines) and the upper and lower quartiles, with each dot representing an individual sample. Error bars on these plots show the maximum and minimum values. NS indicates not significant ($p > 0.05$).

assumptions for all datasets, the Shapiro-Wilk test and Levene's test were employed using the 'oneway tests' package (Dag et al., 2018). An analysis of variance (ANOVA) was conducted using the 'car' package developed by Fox and Weisberg (Fox and Weisberg, 2019). The data of the growth performance, survival, and shell morphometric parameters were analysed by two-way ANOVA, considering cultivation depth as the first factor and farming sites as the second factor. Additionally, Tukey multiple comparison tests were performed for each parameter at various culture depths and locations using the'multcomp' program developed by Hothorn et al. (Hothorn et al., 2008). PerformanceAnalytics programs were utilised to examine and illustrate the correlations among the variables (Peterson and Carl, 2020). A principal component analysis (PCA) was conducted on all datasets using the 'FactoMineR' software (Sebastien et al., 2008). We only considered the first and second principal components (PCs) in all cases, because they accounted for most of the variations. All graphics were generated using the 'ggplot2' program (Wickham, 2016). The analysis of amino acids and fatty acids data was conducted using MetaboAnalyst 6.0 (Pang et al., 2024). A total of 28 fatty acids/groups and 17 amino acids/groups underwent natural logarithmic transformation and auto-scaling to eliminate noise and artefacts. An ANOVA model was conducted to examine variations in amino acid and fatty acid concentrations across different depths. T-tests were used to compare the two depth groups, with the false discovery rate (FDR) adjusted to consider multiple comparisons. To emphasise notable disparities, the results were graphically represented using volcano and other data visualisations. Comparative analysis using partial least squares discriminant analysis (PLS-DA) was performed to discover variations in metabolic profiles among the treatment groups and to identify important metabolites. Significant contributors in the PLS-DA models were identified as amino acids and fatty acids with a Variable Importance in Projection (VIP) score above 1. To provide a thorough picture of the variations in amino acids and fatty acids levels across the various groups, clustered heatmaps were produced to depict the relative concentrations of amino acids and fatty acids.

3. Results

3.1. Growth performance of Perna viridis in different depths and locations

The differences in individual weight gain, soft tissue weight, and specific growth rate (SGR) of green mussels across three cultivation depths and locations are presented in Fig. 3. At a culture depth of 0.5 m, the mean individual weight gain (g), soft tissue weight gain (g), and SGR (% day-1) of *P. viridis* were substantially higher ($p < 0.001$) compared to the subsequent depths (Fig. 3). More precisely, the specific weight gain of mussels collected at a depth of 0.5 m was 25 % and 80 % higher ($p < 0.001$) compared to mussels collected from depths of 1 m and 1.5 m, respectively (Fig. 3A). Furthermore, the weight of individual soft tissue in samples obtained from depths of 0.5 m was found to be 46 % and 77 % greater ($p < 0.001$) compared to samples collected from depths of 1 m and 1.5 m, respectively (Fig. 3D). Mussels grown at a depth of 0.5 m showed a 31 % increased SGR ($p < 0.001$) in comparison to those grown at a depth of 1.5 m (Fig. 3G). Location-wise, mussels harvested from the Khurushkul site showed 71 % and 259 % higher individual weight gain ($p < 0.001$) compared to samples harvested from the Moheshkhali and Choufaldandi sites, respectively (Fig. 3B). Similarly, the individual soft tissue weight of samples from the Khurushkul site was 52 % higher than that from the Moheshkhali site and 138 % higher ($p < 0.001$) than that from the Choufaldandi site (Fig. 3E). Compared to the Moheshkhali and Choufaldandi locations, the average SGR at the Khurushkul site was 24 % and 79 % higher ($p < 0.001$) correspondingly (Fig. 3H). The interaction effects between cultivation depth and sites were found to be non-significant ($p > 0.05$) (additive effects) for individual weight gain (Fig. 3C), soft tissue weight (Fig. 3F) and SGR (Fig. 3I).

The influence of cultivation depth and sites on the survival of green mussels is presented in Fig. 4. The survival of green mussels at 0.5 m depth (89 %) was significantly higher ($p < 0.001$), intermediate at 1.0 m depth (82.2 %), and the lowest at 1.5 m depth (76 %) (Fig. 4A). For location-specific variation, a significantly higher ($p < 0.001$) survival (88.33 %) of green mussels was recorded at Khurushkul site, intermediate at Moheshkhali site (84 %), and lower at the Choufaldandi site (74.83 %) (Fig. 4B). However, a significant interaction effect ($p < 0.05$) between cultivation depth and sites was observed for the survival of green mussels (Fig. 4C).

The variations of shell morphometric parameters (length, width and height) of green mussels across three cultivation depths and locations are presented in Fig. 5. The individual shell length, shell width, and shell height of green mussels were significantly greater ($p < 0.001$) at 0.5 m depth, intermediate at 1 m depth, and lowest at 1.5 m depth (Fig. 5A,D, G). Specifically, the individual shell length of mussels harvested from 0.5 m depth was 11.9 % and 22.3 % higher ($p < 0.001$) than that of mussels from 1 m and 1.5 m depths, respectively (Fig. 5A). Likewise, the individual shell width of samples collected from 0.5 m depth was 9.02 % and 17.2 % higher ($p < 0.001$) than that of samples harvested from 1 m and 1.5 m depths, respectively (Fig. 5D). Furthermore, the individual shell height of mussels cultivated at 0.5 m depth was 5.2 % and 17.06 % higher ($p < 0.001$) than that of those at 1.0 m and 1.5 m depths, respectively (Fig. 3G). For site-specific variation, individual shell length, shell width and shell height of green mussels were significantly higher ($p < 0.001$) in the Khurushkul site, intermediate in the Moheshkhali site, and significantly lowest ($p < 0.001$) in the Choufaldandi site (Fig. 5B,E,H). Explicitly, the individual shell length of mussels harvested from the Khurushkul site was 19.4 % and 60.4 % higher ($p < 0.001$) than the samples from Moheshkhali and Choufaldandi sites, respectively (Fig. 5B). Similarly, individual shell width of mussels collected from Khurushkul site was 15.3 % and 39.8 % higher ($p < 0.001$) than the sample harvested from Moheshkhali and Choufaldandi sites, respectively (Fig. 5E). In addition, individual shell height of mussels cultivated at Khurushkul site was 15.4 % and 41.1 % higher ($p < 0.001$) than those harvested from Moheshkhali and Choufaldandi sites, respectively (Fig. 3H). The statistical analysis revealed that there were no significant interaction effects for individual shell length (Fig. 5C), individual shell width (Fig. 5F) and individual shell height (Fig. 5I).

3.2. Ecological parameters and growth performance of P. viridis

Variations in water quality parameters among different cultivation depths and locations based on two-way ANOVA are presented in Table 1. Among the ten water quality parameters analyzed in this study, the ANOVA model displayed that cultivation depth significantly influenced DO ($p < 0.01$), NO_3-N ($p < 0.01$), PO_4-P ($p < 0.001$) and Chlorophyll-a ($p < 0.001$) concentration (Table 1). Among the site-specific ecological parameters, DO ($p < 0.001$), salinity ($p < 0.001$), turbidity ($p < 0.001$), NO_3-N ($p < 0.01$), PO_4-P ($p < 0.01$) and chlorophyll-a ($p < 0.001$) showed significant variation among the three cultivation locations (Table 1). Except for NO_3-N ($p < 0.05$), a non-significant interaction effect ($p > 0.05$) between cultivation depth and sites was observed for all other water quality parameters (Table 1).

An intensive correlation study was conducted to investigate the association between the monthly fluctuations in environmental parameters and the individual increase in body weight of mussels (Fig. 6). The correlation test indicated that there was no statistically significant link ($p > 0.05$; $r = 0.12$) between the temperature and the individual body weight gain of green mussels. Significant positive correlations were observed between pH ($p < 0.01$; $r = 0.24$), dissolved oxygen ($p < 0.05$; $r = 0.16$), salinity ($p < 0.001$; $r = 0.42$), chlorophyll a ($p < 0.001$; $r = 0.39$), and the individual body weight gain of the green mussels. Notably, some nutrients such as NO_3-N ($p < 0.001$; $r = 0.42$), NH_3-N ($p < 0.001$; $r = 0.26$), and PO_4-P ($p < 0.001$; $r = 0.33$) also exhibited a substantial positive association with the individual increase in body weight of mussels. Notably, there was a strong negative connection

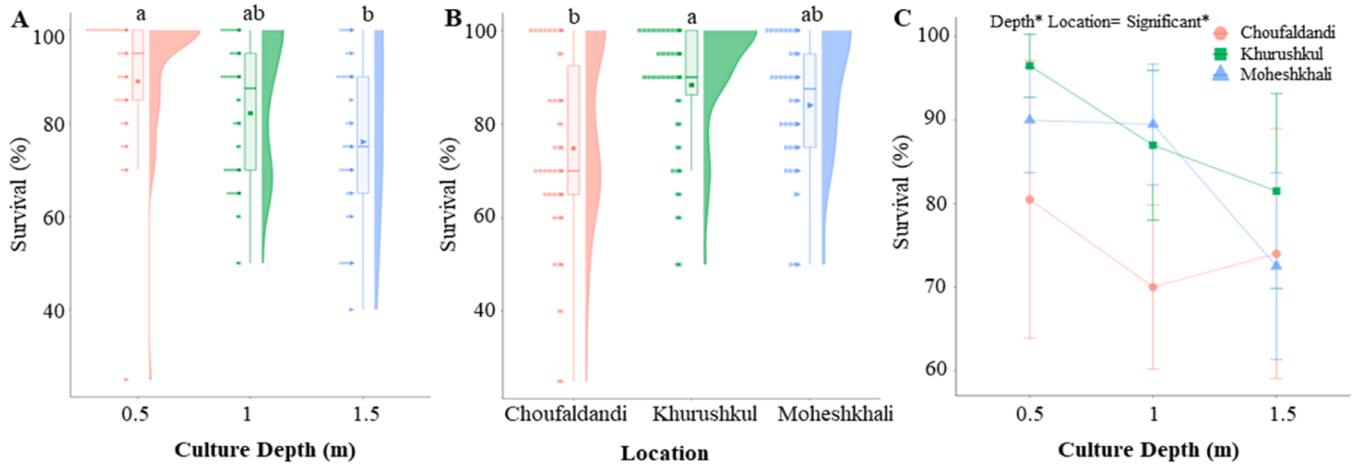

Fig. 4. Survival (%) of green mussels (*Perna viridis*) after six months of cultivation at three depths (0.5 m, 1.0 m, and 1.5 m) across three sites (Khurushkul, Maheshkhali, and Choufaldandi) in the Maheshkhali Channel of the Bay of Bengal, Bangladesh. (A) Survival (%) of green mussels at the three different depths; (B) survival (%) at the three cultivation sites; and (C) survival (%) of green mussels under the interaction effects of depth and cultivation site based on two-way ANOVA. Significant differences ($p < 0.05$) are indicated with superscript letters. Raincloud plots (A and B) illustrate data distribution (the "cloud") with jittered sample data (the "rain"), highlighting the variation in survival rates of green mussels across the three depths and locations through a combination of density distribution and boxplots. The boxplots show median values (represented by horizontal lines) and the upper and lower quartiles, with each dot representing an individual sample. Error bars on these plots indicate the maximum and minimum values.

between turbidity ($p < 0.001$; $r = -0.67$) and NO_2-N ($p < 0.001$; $r = -0.39$) and the individual body weight growth of *P. viridis* (Fig. 6).

3.3. Plankton abundance and growth performance of P. viridis

The cultivation depths and site-specific variation of qualitative and quantitative abundance of different plankton groups based on the two-way ANOVA are presented in Table 2. An estimated 80 % of the total plankton population consisted of phytoplankton. Within the examined geographical area, Bacillariophyceae, Coscinodiscophyceae, and zooplankton emerged as the prominent plankton groups (Table 2). Throughout the duration of the investigation, an overall number of 69 planktonic genera have been found, consisting of 55 phytoplankton and 14 zooplankton. These included groups such as Coscinodiscophyceae (18), Bacillariophyceae (12), Dinophyceae (11), Chlorophyceae (4), Fragillariophyceae (4) and Cyanophyceae (6) along with 14 zooplankton species, across three depths and three cultivation sites of green mussels (data not shown). Out of the 69 planktonic genera, *Coscinodiscus*, *Skeletonema*, *Thalassiothrix*, *Ditylum*, *Rhizosolenia*, *Navicula*, *Protoperidinium*, *Pleurosigma*, *Pseudonitzschia*, Copepod, fish eggs and Rotifera were the primary contributors to the planktonic composition in the water during the study periods (data not shown).

Among the six different groups of phytoplankton, a quantitative abundance of two groups of phytoplankton (Fragilariophyceae and Cyanoophyceae) was not statistically different ($p > 0.05$) across three cultivation depths (Table 2). The other four groups of phytoplankton, Coscinodiscophyceae ($p < 0.01$), Bacillariophyceae ($p < 0.001$), Chlorophyceae ($p < 0.05$), and Dinophyceae ($p < 0.05$), were significantly highest at 0.5 m water depth, while the lowest abundance was recorded at 1.5 m cultivation depth (Table 2). Although the quantitative abundance of zooplankton was not significantly different ($p > 0.05$), total phytoplankton ($p < 0.001$) and total plankton ($p < 0.01$) were considerably higher at 0.5 m compared to the 1.5 m cultivation depth (Table 2). For site-specific variation, except two groups of phytoplankton (Fracillariphyceae and Chlorophyceae), other four groups, namely Coscinodiscophyceae ($p < 0.05$), Bacillariophyceae ($p < 0.01$), Cyanophyceae ($p < 0.05$), and Dinophyceae ($p < 0.05$) were significantly highest at Khurushkul site, while the lowest abundance was recorded at Choufaldandi site. The quantitative abundance of zooplankton showed statistically non-significant variation for three cultivation sites. However, the abundance of total phytoplankton ($p < 0.01$) and total plankton ($p < 0.05$) were significantly higher at the Khurushkul site, intermediate at Moheshkhali site, and the lowest at the Choulfaldandi sites. The interaction effects between cultivation depth and sites were found to be statistically non-significant ($p > 0.05$) for all of the different plankton groups analyzed in this study.

Besides two-way ANOVA model, a comprehensive correlation analysis was conducted to explore the association between the monthly changes in quantitative abundance of distinct categories of plankton and the individual body weight gain of mussels (Fig. 7). The individual body weight gain of *P.viridis* was positively correlated with the quantitative abundance of Coscinodiscophyceae ($p < 0.001$; $r = 0.59$), Bacillariophyceae ($p < 0.001$; $r = 0.35$), Chlorophyceae ($p < 0.001$; $r = 0.40$), Dinophyceae ($p < 0.001$; $r = 0.36$), Fragillariophyceae ($p < 0.01$; $r = 0.21$), Cyanophyceae ($p < 0.05$; $r = 0.20$), zooplankton ($p < 0.001$; ($r = 0.48$), total phytoplankton ($p < 0.001$; $r = 0.35$), and total plankton ($p < 0.001$; $r = 0.42$).

3.4. Interrelationship among ecological factors and growth performance of P. viridis

A multivariate PCA was performed to understand better the multifaceted linkage among water quality parameters, plankton abundance, and the body weight gain of green mussels during the culture period from October to March (Fig. 8). The PCA revealed that the PC1 and PC2 accounted for 52.6 % of the variability in the data (Fig. 8). PC1 (explaining 35.7 % of the variance) was linked to individual body weight gain and was positively correlated with salinity, dissolved oxygen (DO), pH, nitrate (NO_3-N), ammonia (NH_3-N), chlorophyll-a, and plankton abundance, while negatively correlated with nitrite (NO_2-N) and turbidity. The PCA findings further indicated that high levels of nutrients (NO_3-N, NH_3-N), salinity, DO, chlorophyll-a, and plankton abundance positively affected body weight gain from December to March. Conversely, increased turbidity during October and November had a negative impact on the body weight gain of green mussels.

3.5. Proximate composition of P. viridis

Table 3 presents the variations in the proximate composition (% dry matter basis) of the body soft tissues of green mussels across three

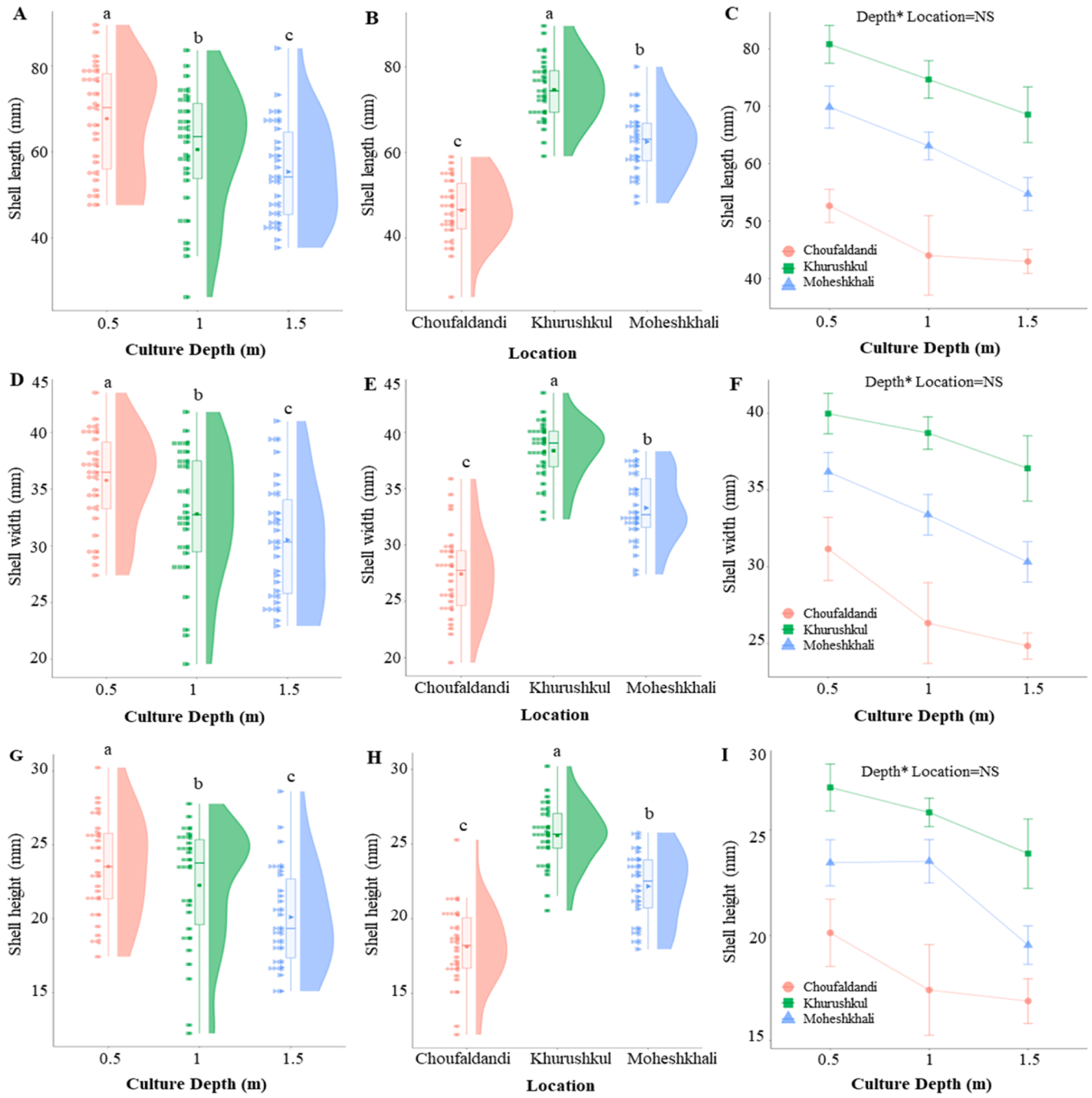

Fig. 5. Shell morphometry of green mussels (*Perna viridis*) after six months of cultivation at different depths (0.5 m, 1.0 m, and 1.5 m) across three sites (Khurushkul, Maheshkhali, and Choufaldandi) in the Maheshkhali Channel of the Bay of Bengal, Bangladesh. (A-C) Shell length (mm) of green mussels at three different depths (A), across the three cultivation sites (B), and their interaction (C) based on two-way ANOVA. (D-F) Shell width (mm) of green mussels at three different depths (D), across the three cultivation sites (E), and their interaction (F) based on two-way ANOVA. (G-I) Shell height (mm) of green mussels at three different depths (G), across the three cultivation sites (H), and their interaction (I) based on two-way ANOVA. Significant differences ($p < 0.05$) are indicated with superscript letters. Raincloud plots (A, B, D, E, G, H) illustrate data distribution (the "cloud") with jittered sample data (the "rain"), highlighting the variation in shell morphometry of green mussels across the three depths and locations through a combination of density distribution and boxplots. The boxplots display median values (represented by horizontal lines) and the upper and lower quartiles, with each dot symbolizing an individual sample. Error bars on these plots indicate the maximum and minimum values. NS indicates not significant ($p > 0.05$).

cultivation depths, as analyzed by one-way ANOVA. The protein content displayed that mussels harvested from the 1.5 m depth having significantly lower protein levels than those from the 1.0 m depths. Likewise, lipid content varied significantly ($p < 0.05$) among the depths. Mussels from the 0.5 m depth had a significantly higher lipid content, while lipid levels at the 1.0 m and 1.5 m depths were similar. No significant difference in ash content ($p > 0.05$) was found across the three cultivation depths.

3.6. Fatty acid profiles

Univariate and multivariate statistical methods were employed to evaluate the impact of various cultivation depths on the fatty acid composition (% of total fatty acids) in the body soft tissues of green

Table 1
Variations in water quality parameters among different depths and locations based on two-way ANOVA.

Variables	Means (Tukey test)						Sig. (p-value)		
	Depth (D)			Location (L)			D	L	D×L
	0.5 m	1 m	1.5 m	Khurushkul	Moheshkhali	Choufaldandi			
Temp (℃)	28.34 ± 1.78^{a}	28.12 ± 1.58^{a}	28.04 ± 1.42^{a}	28.24 ± 1.33^{a}	27.74 ± 1.41^{a}	29.10 ± 1.16^{a}	NS	NS	NS
pH	7.78 ± 0.82^{a}	7.71 ± 0.92^{a}	7.52 ± 0.68^{a}	7.48 ± 0.82^{a}	7.79 ± 0.81^{a}	7.64 ± 0.58^{a}	NS	NS	NS
DO (mg/L)	5.93 ± 0.28^{a}	5.73 ± 0.32^{ab}	5.23 ± 0.22^{b}	5.98 ± 0.12^{a}	5.92 ± 0.12^{a}	5.28 ± 0.12^{b}	**	***	NS
Salinity (ppt)	24.24 ± 1.04^{a}	24.44 ± 1.08^{a}	24.65 ± 1.28^{a}	26.09 ± 0.72^{a}	26.66 ± 0.58^{a}	20.57 ± 1.22^{b}	NS	***	NS
Turb (NTU)	12.35 ± 1.16^{a}	12.46 ± 1.18^{a}	12.06 ± 1.04^{a}	9.86 ± 0.69^{b}	9.57 ± 0.64^{b}	17.6 ± 1.40^{a}	NS	***	NS
PO_4-P (mg/L)	1.55 ± 0.22^{a}	1.11 ± 0.12^{b}	1.09 ± 0.22^{b}	1.49 ± 0.12^{a}	1.23 ± 0.32^{ab}	1.06 ± 0.28^{b}	***	**	NS
NO_2-N (mg/L)	0.19 ± 0.01^{a}	0.15 ± 0.01^{a}	0.16 ± 0.02^{a}	0.14 ± 0.02^{a}	0.18 ± 0.01^{a}	0.18 ± 0.01^{a}	NS	NS	NS
NO_3-N (mg/L)	1.11 ± 0.11^{a}	0.84 ± 0.09^{b}	0.75 ± 0.16^{b}	1.35 ± 0.19^{a}	0.99 ± 0.16^{ab}	0.65 ± 0.09^{b}	**	**	*
NH_3-N (mg/L)	0.17 ± 0.05^{a}	0.23 ± 0.04^{a}	0.18 ± 0.02^{a}	0.22 ± 0.04^{a}	0.17 ± 0.02^{a}	0.19 ± 0.03^{a}	NS	NS	NS
Chlorophyll-a (μg/L)	5.67 ± 0.26^{a}	4.75 ± 0.20^{b}	4.27 ± 0.19^{b}	5.02 ± 0.15^{b}	5.70 ± 0.22^{a}	4.06 ± 0.18^{c}	***	***	NS

The significance levels (p) are denoted by asterisks (*<0.05, **<0.01, ***<0.001, NS= Not significant). Significant variations among various depths and locations are shown by several superscripts in the same row at $p < 0.05$ level.

mussels. The ANOVA model displayed that 21 out of 28 fatty acids/groups varied considerably ($p < 0.05$) among the three cultivation depths (Fig. 9A). Of these, six fatty acids/groups with highly significant differences were highlighted in the box plots around the ANOVA plot (Fig. 9A). Every category of fatty acids, namely saturated fatty acids (SAFA), monounsaturated fatty acids (MUFA), and polyunsaturated fatty acids (PUFA), showed statistically significant variations ($p < 0.05$) across three cultivation depths (Fig. 9B). SAFA content ranged from 43.61 % to 57.74 % of the total fatty acids (Fig. 9B). Notably, the SAFA content was highest in *P. viridis* samples collected from a depth of 1.5 m compared to those from 0.5 m and 1 m depths. Palmitic acid (C16:0), heptadecanoic acid (C17:0), stearic acid (C18:0), and arachidic acid (C20:0), were the predominant SAFA across all depths. MUFA content ranged between 19.98 % and 37.48 % of the total fatty acids (Fig. 9B), with samples from 1 m depth showing higher MUFA levels compared to those from 0.5 m and 1.5 m depths ($p < 0.05$). PUFA comprised about 22 % of the total fatty acids, with n6-PUFA accounting for roughly 90 %. Eicosatrienoic acid (C20:3n-6) and linoleic acid (C18:2n-6) were the major n6-PUFA contributors (Fig. 9B). The n6-PUFA and n3-PUFA contents were considerably higher ($p < 0.05$) in samples from 0.5 m depth compared to those from 1 m and 1.5 m depths. A heatmap was assembled by cluster analysis of the fatty acid profiles of *P. viridis* harvested from different cultivation depths (Fig. 9B). The clustering results revealed that the fatty acid profiles of mussels from 0.5 m depth were more similar to those from 1.5 m depth than to those from 1.0 m depth.

Additionally, the discrimination in the fatty acid profiles of the body soft tissues of *P. viridis* were visualized for pair-wise comparisons of cultivation depths (0.5 m vs 1.0 m, 1.0 m vs 1.5 m, 0.5 m vs 1.5 m) using volcano plots (Fig. 10A–C). The plots revealed that, compared to mussels from the 1.0 m depth, those from the 0.5 m depth had considerably lower ($p < 0.05$) levels of 5 fatty acids/groups (C13:0, C20:0, C20:1, C22:1, and MUFA) and higher ($p < 0.05$) levels of 15 fatty acids/groups (C8:0, C12:0, C14:0, C16:0, C17:0, C22:0, C16:1, C18:1, C18:3n-3, C22:5n-3, C22:6n-3, C20:3n-6, n-3PUFA, n-6PUFA, and PUFA), with 8 fatty acids/groups showing no significant difference ($p > 0.05$) (Fig. 10A). Similarly, mussels from the 1.5 m depth had significantly lower ($p < 0.05$) levels of 16 fatty acids/groups (C14:0, C12:0, C16:1, C22:6n-3, C18:0, C17:0, C8:0, SAFA, C18:1, C20:0, n-3PUFA, C18:3n-3, C20:3n-6, PUFA, n-6PUFA, and C22:0) and considerably higher ($p < 0.05$) levels of 4 fatty acids/group (C13:0, C20:1, C22:1, MUFA) compared to 1.0 m depth, with 8 fatty acids/groups showing no significant ($p > 0.05$) difference (Fig. 10B). Likewise, mussels from the 0.5 m depth exhibited considerably higher ($p < 0.05$) levels of 14 fatty acids/groups (C8:0, C16:0, C16:1, C12:0, C13:0, MUFA, n-3PUFA, PUFA, n-6PUFA, C18:3n-3, C20:3n-6, C14:0, C20:1, C18:1) and significantly lower ($p < 0.05$) levels of 3 fatty acids/groups (C20:0, C18:0, and SAFA) compared to those from the 1.5 m depth, with 11 fatty acids/groups displayed no significant ($p > 0.05$) difference (Fig. 10C). The identified fatty acids were then analyzed using VIP scores (Fig. 10D). The VIP value measures the importance of each fatty acid in the separation between different cultivation depths, with higher VIP values indicating greater importance. Out of the 28 fatty acids/groups analyzed in this study, 13 fatty acids were highlighted with values of VIP scores > 1.0. Moreover, among these 13 fatty acids, C20:0, C18:0 and SAFA exhibited the significantly highest ($p < 0.05$) VIP scores (VIP>1.5, a typical cutoff point that is frequently used in many studies), indicating that these three fatty acids had the highest importance in explaining the differences among the three cultivation depth conditions.

3.7. Amino acid content

In the present study, Arginine (ARG), leucine (LEU), lysine (LYS), methionine (MET), threonine (THR), valine (VAL), isoleucine (ILE), and phenylalanine (PHE) are eight essential amino acids (EAA) and alanine (ALA), aspartic acid (ASP), tyrosine (TYR), glutamine (GLU), serine (SER), cysteine (CYS), and proline (PRO) are seven non-essential amino acids (non-EAA) found in the body soft tissues of green mussels under three cultivation depth conditions. The ANOVA model showed that 13 out of 17 amino acids/groups varied significantly ($p < 0.05$) among the three cultivation depths, with the most highly significant 6 amino acids/group (MET, ILE, GLU, CYS, non-EAA, and THR) are displayed in box plots around ANOVA plot (Fig. 11A). Depending on the cultivation depths, the EAA content of *P. viridis* ranged from 184 to 196 mg g^{-1} of dry weight (Fig. 11B). The most abundant EAA in *P. viridis* across three depths were methionine (69.13–75.3 mg g^{-1}), arginine (66.32–69.44 mg g^{-1}), phenylalanine (24.23–31.12 mg g^{-1}), and lysine (15.02–53.48 mg g^{-1}). Although the total EAA was not significantly different ($p > 0.05$), ARG ($p < 0.01$), LEU ($p < 0.01$), LYS ($p < 0.05$), VAL ($p < 0.05$), and ILE ($p < 0.001$) varied considerably across three cultivation depths (Fig. 11B). The non-EAA content of *P. viridis* ranged from 126.7 to 169.7 mg g^{-1} of dry weight. The total non-EAA content was considerably higher ($p < 0.001$) in the mussels harvested from 0.5 m depth compared to those from 1.0 and 1.5 m cultivation depths. The most dominant non-EAA in *P. viridis* was aspartic acid (56.86–66.38 mg g^{-1}), followed by glutamine (30.37–52.73 mg g^{-1}), proline (22.98–27.81 mg g^{-1}), serine (7.17–7.92 mg g^{-1}), and cysteine (4.97–5.4 mg g^{-1}). Among the non-EAA, ALA ($p < 0.01$), GLU ($p < 0.001$), SER ($p < 0.001$), CYS ($p < 0.001$), PRO ($p < 0.05$) varied among the three cultivation depths (Fig. 11B). Moreover, heatmap-based cluster analysis showed that amino acids profiles of the body soft tissues of *P. viridis* from 0.5 m depth more closely clustered with those from 1.0 m compared to the 1.5 m cultivation depth.

A VIP plot created from the PLS-DA models prioritised specific amino acids for their potency to determine which amino acids caused the most changes across different cultivation depths (Fig. 11C). Of the 17 amino acids/groups analyzed in this study, 14 were identified with VIP scores

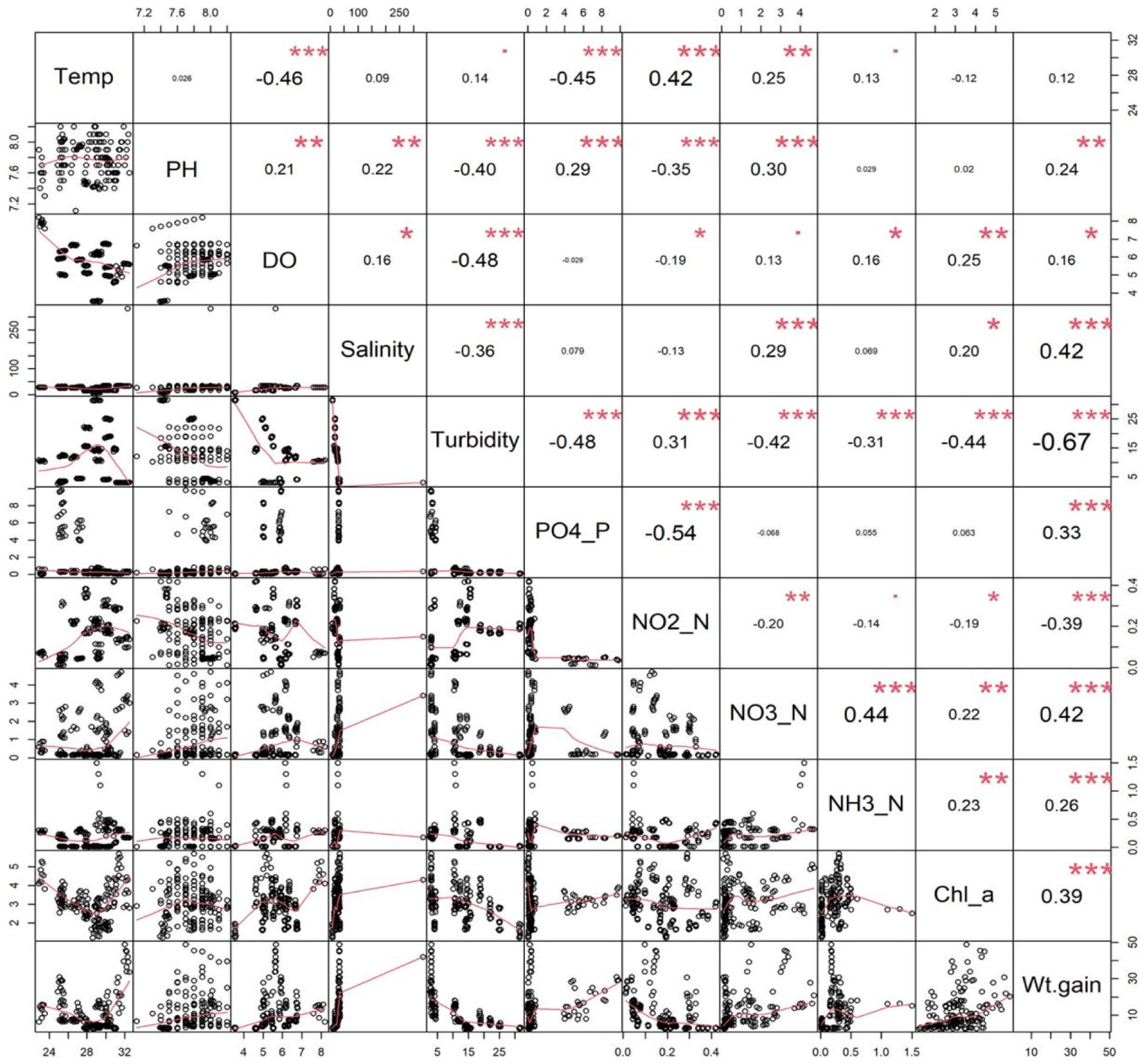

Fig. 6. Interrelationship among ecological factors and body weight gain of green mussels (*Perna viridis*) cultivated at different depths (0.5 m, 1.0 m, and 1.5 m) for six months across three sites (Khurushkul, Maheshkhali, and Choufaldandi) in the Maheshkhali Channel of the Bay of Bengal, Bangladesh. The variables are defined as follows: Temp - water temperature (°C); DO - dissolved oxygen (ppm); Salinity - salinity (ppt); Turbidity - turbidity (NTU); PO4_P - phosphate phosphorus (mg/l); NO2_N - nitrite nitrogen (mg/l); NO3_N - nitrate nitrogen (mg/l); NH3_N - ammonia nitrogen (mg/l); Chl_a - chlorophyll a (µg/L); Wt. gain - individual body weight gain (g). The values indicated around each axis represent the range of measured values for each parameter. Numeric values represent correlation coefficients (r), with larger font sizes indicating stronger correlations. Asterisks denote significance levels (p) as follows: * <0.05, * * < 0.01, * ** <0.001.Top of Form.

greater than 1.0. Among these 14 amino acids, MET and CYS had notably > 1.5 VIP scores ($p < 0.05$), indicating their significant role in determining the major differences among three cultivation depth conditions. As like fatty acid profiles, volcano plots were also generated using amino acid profile data to visualize the pair-wise discrimination of culture depths (0.5 m vs 1.0 m, 1.0 m vs 1.5 m, and 0.5 m vs 1.5 m). The volcano plots displayed that mussels harvested from 0.5 m depth had considerably lower ($p < 0.05$) levels of 5 amino acids (ALA, LYS, TYR, LEU, THR, CYS and ARG) and higher ($p < 0.05$) levels of 7 amino acids/groups (GLU, PHE, PRO, ASP, MET, EAA, and non-EAA) compared to the 1.0 m depth, with 3 amino acids showing no significant ($p > 0.05$) difference ($p > 0.05$) (Fig. 11D). Compared to the 1.5 m cultivation depths, mussels from 1.0 m depth displayed considerably higher ($p < 0.05$) levels of 6 amino acids (MET, ILE, SER, PRO, ALA and PRO) and lower ($p < 0.05$) levels of 3 fatty acids (CYS, VAL, and THR), with 8 amino acids/groups showing no significant ($p > 0.05$) difference (Fig. 10E). Likewise, compared to the 1.5 m cultivation depths, mussels from 5.0 m depth displayed considerably lower ($p < 0.05$) levels of 5 fatty acids/groups (CYS, THR, LYS, VAL and LEU), and higher ($p < 0.05$) levels of 7 amino acids/group (GLU, MET, non-EAA, SER, ILE, ARG, and PRO), with remaining 5 amino acids/group showing no significant ($p > 0.05$) difference (Fig. 10F).

Table 2
Variations of different plankton group ($\times 10^3$ cells L^{-1}) abundance in water among different depths and green mussel cultivation sites based on two-way ANOVA.

Variables	Means (Tukey test)						Sig. (p-value)		
	Depth (D)			Location (L)			D	L	D×L
	0.5 m	1 m	1.5 m	Khurushkul	Moheshkhali	Choufaldandi			
Coscinodiscophyceae	134.6 ± 8.0^{a}	114.6 ± 7.3^{ab}	101.7 ± 6.6^{b}	128.92 ± 7.1^{a}	118.7 ± 7.1^{ab}	103.22 ± 8.0^{b}	**	*	NS
Fragilariophyceae	20.28 ± 3.4^{a}	17.72 ± 2.9^{a}	15.91 ± 2.7^{a}	20.57 ± 3.5^{a}	17.88 ± 2.6^{a}	15.45 ± 2.8^{a}	NS	NS	NS
Bacillariophyceae	139.6 ± 6.2^{a}	119.3 ± 6.1^{b}	105.6 ± 5.4^{b}	135.5 ± 5.3^{a}	124.5 ± 5.9^{ab}	104.5 ± 6.6^{b}	***	**	NS
Chlorophyceae	38.12 ± 2.4^{a}	32.9 ± 2.3^{ab}	29.12 ± 2.1^{b}	36.09 ± 2.1^{a}	34.29 ± 2.4^{a}	29.72 ± 2.5^{a}	*	NS	NS
Cyanophyceae	26.45 ± 2.5^{a}	22.7 ± 2.2^{a}	20.23 ± 1.9^{a}	27.16 ± 2.4^{a}	23.53 ± 2.2^{ab}	18.69 ± 1.9^{b}	NS	*	NS
Dinophyceae	63.55 ± 3.9^{a}	54.9 ± 3.8^{ab}	49.16 ± 3.3^{b}	62.85 ± 3.4^{a}	57.35 ± 3.8^{ab}	47.35 ± 3.6^{b}	*	*	NS
Total Phytoplankton	422.5 ± 18.0^{a}	362.1 ± 18.3^{b}	321.4 ± 16.6^{b}	410.8 ± 15.0^{a}	376.3 ± 17.1^{ab}	318.9 ± 20.8^{b}	***	**	NS
Total zooplankton	103.3 ± 11.7^{a}	92.10 ± 10.7^{a}	82.36 ± 9.6^{a}	98.66 ± 10.7^{a}	94.85 ± 11.2^{a}	84.22 ± 10.2^{a}	NS	NS	NS
Total Plankton	525.8 ± 27.8^{a}	454.2 ± 27.9^{ab}	403.7 ± 25.2^{b}	509.5 ± 23.8^{a}	471.2 ± 27.4^{ab}	403.1 ± 30.1^{b}	**	*	NS

The significance levels (p) are denoted by asterisks (*<0.05, **<0.01, ***<0.001, NS= Not significant). Significant variations among various depths and locations are shown by different superscripts in the same row at $p < 0.05$ level.

4. Discussion

4.1. Depth-specific ecological variation influence growth and nutritional profile of P. viridis

This study examines how the depth-specific ecological factors may significantly influence growth performance, shell morphometry and nutritional content of the mussels by affecting food availability and the physiological responses (Orban et al., 2002; Dridi et al., 2007; Silva et al., 2021). The observed significant difference in individual weight gain, soft tissue weight, SGR, survival, and shell morphometric parameters highlights the critical role of cultivation depth in optimizing the mariculture conditions of green mussels (see Figs. 3–5). Previous research has indicated that cultivation depth significantly influences mussel growth, with faster growth observed in areas nearer to the surface waters (Fuentes et al., 2000; Dobretsov and Miron, 2001). The study conducted by Kautsky (Kautsky, 1982) revealed that mussels farmed in the Baltic Sea at a depth of 4 m showed markedly superior growth in comparison to those cultivated at a depth of 15 m. Mueller (Mueller, 1996) reported that the mussel *M. trossulus* had a notably greater growth rate at depths of 1 and 3 m in Northern Puget Sound, WA, USA, as opposed to 5 m. Furthermore, Gallardi et al. (2017) noted that green mussels in shallower water had a greater overall weight compared to those in deeper areas. This suggests that shallower depths often facilitate more favourable development conditions. Corroborating these investigations, a cultivation depth of 0.5 m yielded notably better growth performance and shell morphometric parameters (length, width, and height) compared to the other depths (refer to Figs. 3–4). This suggests that this depth offers ideal conditions for supporting superior growth metrics of *P. viridis*.

The enhanced growth and nutritional profile of mussels primarily depends on greater availability of food sources, improved feeding conditions, and more favourable hydrographic conditions during the cultivation period (Rivonker et al., 1993; Orban et al., 2002; Tan and Ransangan, 2014; Tan and Ransangan, 2016; Noor et al., 2021). In this study, the ANOVA model displayed a significantly higher level of DO, NO_3-N, PO_4-P, and Chlorophyll-a concentration at 0.5 m depth (see Table 1). Differences in these environmental circumstances are likely responsible for the increased growth and nutritional content seen in green mussels at 0.5 m depth. (Martínez-Pita et al., 2012; Matias et al., 2013). Shallower depths, particularly around 0.5 meters, often provide better oxygen and nutrient concentrations because they are more influenced by surface water mixing, which can enhance the availability of phytoplankton and other food sources (Slavin et al., 2022; Paul et al., 2024). DO is a fundamental environmental parameter that significantly impacts the food consumption and assimilation efficiency, energy allocation for growth rate, byssus production, and shell morphometry of bivalves (Yu et al., 2010; Long et al., 2014; Song et al., 2024). Higher DO levels support better growth, shell morphometry, and nutritional profiles of bivalves by facilitating efficient metabolic processes, enhancing physiological health, and optimal shell development by supporting the biomineralization processes necessary for robust shell formation (Li et al., 2019; Xie et al., 2021; Song et al., 2024). Elevated levels of NO_3-N at 0.5 m depth may promote the growth of different groups of phytoplankton by supplying necessary nitrogen for protein synthesis and cellular metabolism (Howarth and Marino, 2006; Altman and Paerl, 2012). Similarly, PO_4-P is crucial for phytoplankton growth as it is a critical component of nucleic acids and ATP for cellular energy and replication (Reed et al., 2017; Marzetz et al., 2020). Therefore, the observed high availability of these nutrients at 0.5 m depth may support robust primary productivity, leading to enhanced feeding opportunities for bivalves, which in turn results in better growth rates and nutritional profiles (Tan and Ransangan, 2016; Hoque et al., 2021; Noor et al., 2021). Chlorophyll-a serves as an indicator of phytoplankton biomass and primary productivity. Higher chlorophyll-a concentrations at 0.5 meters suggest that this depth supports more robust phytoplankton communities, which directly benefit *P. viridis* by providing ample food resources (Tan and Ransangan, 2016; Hoque et al., 2021; Noor et al., 2021). Although not investigated in this work, variables such as light penetration, current velocity, and water column stability may also affect the growth performance (Aypa, 1990; Tan and Ransangan, 2016; Marzetz et al., 2020; Noor et al., 2021) and nutritional quality of mussels by affecting the availability and composition of plankton (Huisman et al., 1999; O'Brien et al., 2003; Huisman et al., 2006). However, future studies should consider exploring other potential factors influencing *P. viridis* growth with more precise measurements of light availability, water movements, and the possible impacts of different macro and micronutrients.

Following the example of other suspension-feeding bivalves, *P. viridis* consumes a diverse range of plankton with varying shapes and sizes as its primary dietary component (Lopes-Lima et al., 2014; Tan and Ransangan, 2017; Asaduzzaman et al., 2020). Sustaining a varied and harmonious plankton population is crucial for facilitating the growth (Lopes-Lima et al., 2014; Tan and Ransangan, 2017; Hoque et al., 2021; Asaduzzaman et al., 2020; Noor et al., 2021) and nutritional profiles (Abad et al., 1995; Alkanani et al., 2007; Ventrella et al., 2008; Prato et al., 2010; Irisarri et al., 2014) of mussels. Poor growth and condition index of mussels have been documented in lower levels of plankton abundance (Ren and Ross, 2005; Noor et al., 2021). Consistently, we observed a positive correlation between the monthly abundance of different groups of plankton and individual weight gain of green mussels (see Fig. 7). Nutritional composition of various plankton groups exhibits significant variation, which might impact the growth and nutritional value of mussels (Napiorkowska-Krzebietke, 2017). Our study demonstrated a strong connection between water depth, the quantity of major phytoplankton groups, and the nutritional quality of green mussels. At a depth of 0.5 m, the abundance of the phytoplankton groups (Coscinodiscophyceae, Bacillariophyceae, Chlorophyceae, and Dinophyceae)

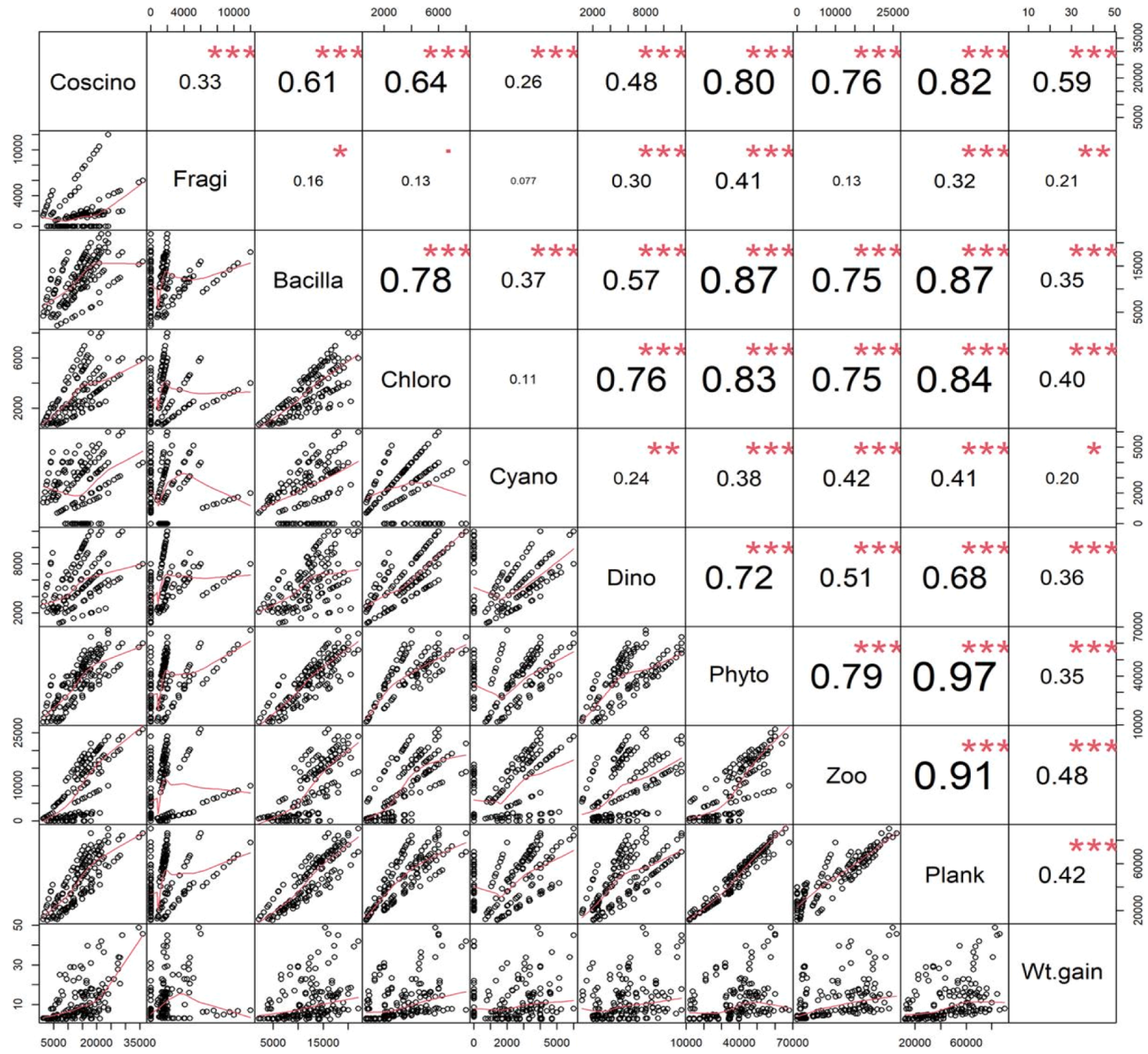

Fig. 7. Interrelationship among the quantitative abundance of different groups of plankton (cells/L) in water and individual body weight gain of the green mussels (*Perna viridis*) cultivated at different depths (0.5 m, 1.0 m, and 1.5 m) for six months across three sites (Khurushkul, Maheshkhali, and Choufaldandi) in the Maheshkhali Channel of the Bay of Bengal, Bangladesh. Here, the variables' full names are Coscino- Coscinodiscophyceae; Fragi- Fragilariophyceae; Bacilla- Bacillariophyceae; Chloro- Chlorophyceae; Cyano- Cyanophyceae; Dino- Dinophyceae; Phyto- Total phytoplankton; Zoo- Total Zooplankton and Plank- Total plankton; Wt. gain- Individual body weight gain (g). The values indicated around each axis represent the range of measured values for each parameter. Numeric values represent correlation coefficients (r), with larger font sizes indicating stronger correlations. Asterisks denote significance levels (p) as follows: * <0.05, * * < 0.01, * ** <0.001.

was notably higher than at a depth of 1.5 m (refer to Table 2). These phytoplankton are crucial food sources and may improve the growth performance, shell morphometric characteristics, and nutritional profiles of green mussels (Tan and Ransangan, 2017; Asaduzzaman et al., 2020; Noor et al., 2021). Previous studies indicated that Coscinodiscophyceae, Bacillariophyceae, Dinophyceae, and Chlorophyceae are critical for marine bivalves due to their high nutritional value, which supports energy needs for physiological processes such as reproduction and growth (Pirini et al., 2007; Khozin-Goldberg and Cohen, 2011; Lopes-Lima et al., 2014; Tan and Ransangan, 2017; Jónasdóttir, 2019). Many of these planktonic species can synthesise long-chain polyunsaturated fatty acids (PUFAs) from the omega-3 family, such as EPA and DHA, which are essential for physiological processes because they act as components of cell membranes (Pirini et al., 2007; Khozin-Goldberg and Cohen, 2011; Jónasdóttir, 2019). Therefore, the observed higher quantities of healthy polyunsaturated fatty acids in shallower depth mussels might be linked with the increased abundance of these plankton groups. Conversely, the fatty acid profiles of Cyanophyceae and Fragillariophyceae are often simpler, largely comprised of saturated fatty acids (C16 and C18) and monounsaturated fatty acids, with a paucity of long-chain PUFAs (Jónasdóttir, 2019). Therefore, mussels from the deeper depths may have different nutrient profiles, including increased monounsaturated and saturated fatty acids due to higher abundance of these two plankton groups. Overall, the depth-specific variation of plankton abundance plays a key role in defining growth and nutritional content of green mussels.

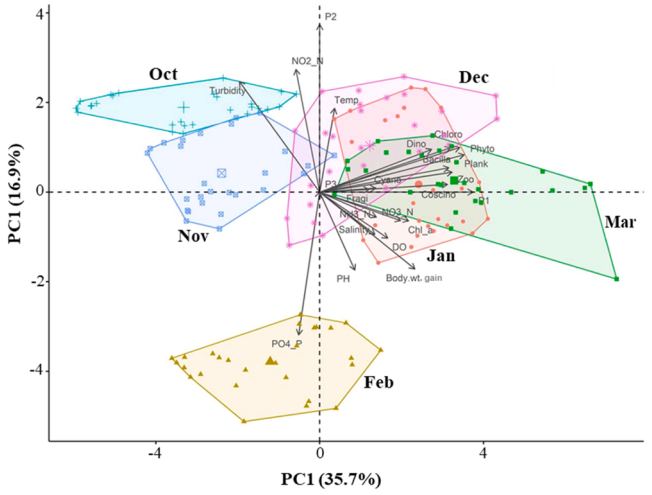

Fig. 8. Biplots of the principal component analysis (PCA) of the variation of ecological factors, water plankton abundance, and individual body weight gain of the green mussels (*Perna viridis*) cultivated at different depths (0.5 m, 1.0 m, and 1.5 m) for six months across three sites (Khurushkul, Maheshkhali, and Choufaldandi) in the Maheshkhali Channel of the Bay of Bengal, Bangladesh. Here, the variables' full names are Temp- water temperature (∘C); DO- dissolved oxygen (ppm); Salinity (ppt), Turbidity (NTU); NO_3·N- nitrate-nitrogen (mg/l); NO_2·N-nitrite-nitrogen (mg/l); PO_4·P-phosphate-phosphorus (mg/l); NH_3·N- ammonia (mg/l); Chl.a- chlorophyll a (µg/L); Coscino- water Coscinodiscophyceae; Fragi- water Fragilariophyceae; Bacilla- water Bacillariophyceae; Chloro- water Chlorophyceae; Cyano- water Cyanophyceae; Dino- water Dinophyceae; Phyto- water phytoplankton; Zoo- water Zooplankton; Plank- total water plankton; Body wt. gain- individual body weight gain (g).

Table 3
Proximate composition (% dry weight) of green mussels (Perna viridis) cultivated in different depths in the Maheshkhali Channel of the Bay of Bengal, Bangladesh.

Proximate composition	Culture Depth (meter)			F-value	p-value
	0.5 m	**1 m**	**1.5 m**		
Protein	70.27 ± 0.76^{ab}	70.72 ± 0.37^{a}	69.28 ± 0.39^{b}	5.608	0.042 *
Lipid	5.85 ± 0.23^{a}	5.19 ± 0.46^{b}	5.05 ± 0.42^{b}	66.426	0.000 * **
Ash	17.11 ± 0.31^{a}	15.47 ± 1.13^{a}	15.53 ± 1.18^{a}	2.787	0.139NS
Moisture	74.45 ± 0.33^{a}	74.43 ± 0.51^{a}	74.32 ± 0.58^{a}	0.055	0.947NS

The significance levels (p) are denoted by asterisks (*<0.05, ***<0.001, NS= Not significant). Different superscripts in the same row denote significant differences among different depths at $p < 0.05$ level.

Understanding these depth-related impacts is critical for optimizing aquaculture techniques, attaining desired nutritional results, and boosting the overall quality of mussel output.

4.2. Growth performances of P. viridis in different locations

The study's findings reveal a significant difference in the growth performance of green mussels harvested from various cultivation sites, highlighting the importance of site-specific environmental conditions in shaping bivalve growth (Loesch and Evans, 1994; Alvarado and Castilla, 1996; Iglesias et al., 1996; Noor et al., 2021). In this study, mussels from the Khurushkul site gained 71 % more individual weight than those from Moheshkhali, and 259 % more than mussels from Choufaldandi (see Fig. 3). This significant difference in growth rates indicates that the environmental conditions at Khurushkul are especially favourable for mussel development (Tan and Ransangan, 2017; Noor et al., 2021). The Khurushkul and Moheshkhali sites are located in the more dynamic Moheshkhali channel, whereas the Choufaldandi site, is located in the closed upstream branches. Hence the Choufaldandi site experiences significant salinity fluctuations due to extensive freshwater surface runoff from the surrounding upstream lands, resulting in lower and more variable salinity levels (see Fig. 1). This site also suffers from high turbidity and low nutrient levels, which are exacerbated by stagnant conditions with minimal water movement (0.04–0.12 m s^{-1}), resulting in the accumulation and settlement of various fouling organisms such as barnacles and small molluscs on cultivation substrates (Hoque et al., 2021). These fouling creatures fiercely compete with green mussels for space and food supplies. Furthermore, the lower water circulation at Choufaldandi limits the mussels' capacity to filter feed efficiently, exacerbating the hurdles to their growth and development (Aypa, 1990; Hoque et al., 2021). The interplay of frequent salinity fluctuations, high turbidity, low nutrient levels, stagnant water conditions, and heavy fouling organism settlement creates an environment less conducive to green mussel growth. As a result, growth rates at Choufaldandi are slower compared to the more dynamic and nutrient-rich conditions at the Khurushkul and Moheshkhali sites (Rajagopal et al., 1998; Apukuttan et al., 2003; Hoque et al., 2021; Noor et al., 2021).

Effective green mussel cultivation depends on a diverse range of site-specific ecological factors that directly influence their feeding, respiration, and reproduction (Loesch and Evans, 1994; Alvarado and Castilla, 1996; Iglesias et al., 1996; Noor et al., 2021). Previous studies have identified a number of critical factors, including water temperature, salinity, wave exposure, food availability, mussel density, reproductive cycle stage, and genetic variations which are essential for shaping growth performances, meat content, and shell development (Alunno-Bruscia et al., 2001; Orban et al., 2002; Penney et al., 2007; Asaduzzaman et al., 2019). More specifically, temperatures between 25 and 35°C (Rajagopal et al., 1998; Hoque et al., 2021), stable high salinity from 21 to 33 ppt (Rajagopal et al., 1998; Apukuttan et al., 2003; Noor et al., 2021), primary production with chlorophyll-a of 0.7–17 µg L^{1} (Rajagopal et al., 1998; Saxby, 2002; Tan and Ransangan, 2014; Hoque et al., 2021), current speeds within the range of 0.1–0.3 m s^{-1} (Aypa, 1990; Tan and Ransangan, 2014; Hoque et al., 2021), and at least 1.5 m water depth (Aypa, 1990; Hoque et al., 2021), have demonstrated key factors for the commercial success of green mussel farming. While DO levels may not directly influence the culture potential of green mussels, their energy-intensive selective feeding behaviour require a high level of oxygen (Bayne, 1998; Long et al., 2014; Song et al., 2024). Therefore, the higher DO levels observed at the Khurushkul site indicate a more oxygen-rich environment (see Table 1), which likely supports enhanced metabolic processes and overall health of the mussels, contributing to superior growth (Li et al., 2019; Xie et al., 2021; Song et al., 2024). Additionally, the salinity at Khurushkul, falling within the optimum ranges (26–35 ppt), further supports ideal growth conditions (Aypa, 1990; Rajagopal et al., 2006; Tan and Ransangan, 2014; Hoque et al., 2021). Turbidity, a measure of the cloudiness or haziness of a fluid caused by suspended particles, can influence the feeding efficiency of filter-feeders' green mussels (Tan and Ransangan, 2014; Tuttle-Raycraft et al., 2017; Buczek et al., 2018). High turbidity can restrict light penetration, negatively affecting photosynthesis and phytoplankton growth, which serve as the primary food source for green mussels (Marinho-Soriano et al., 2009; Hoque et al., 2021).

4.3. Interrelations among growth performance, ecological factors and cultivation months

The growth of marine bivalves is primarily influenced by seasonality, environmental conditions, food availability, reproductive strategies, and various physiological parameters (Alluno-Bruscia et al., 2001; Orban et al., 2002; Penney et al., 2007; Asaduzzaman et al., 2019). While the individual or combined effects of environmental conditions,

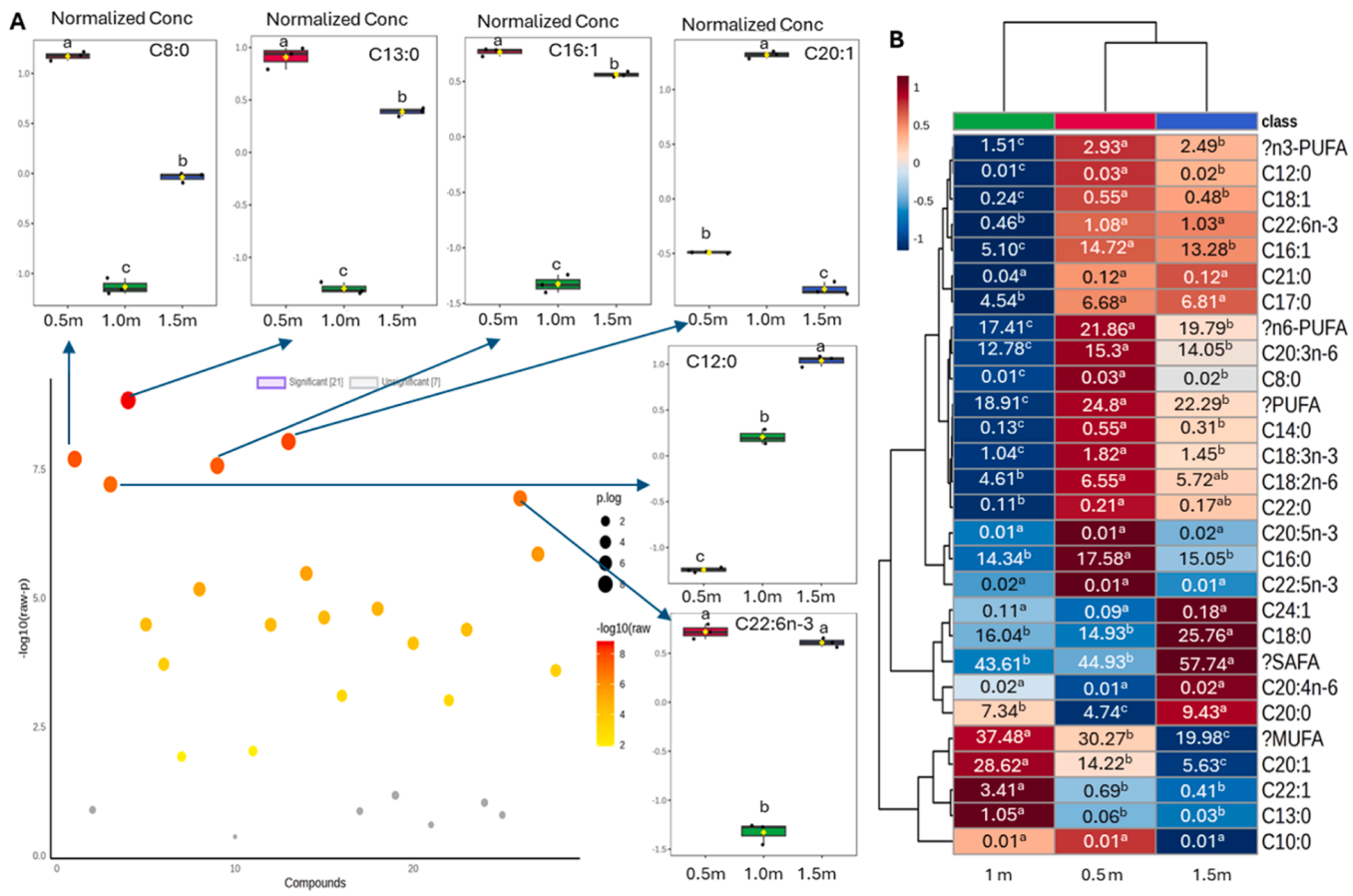

Fig. 9. Variation of fatty acid profiles (% of total fatty acids) of the green mussels (*Perna viridis*) cultivated at different depths (0.5 m, 1.0 m, and 1.5 m) in the Maheshkhali Channel of the Bay of Bengal, Bangladesh. (A), One-way Analysis of Variance (ANOVA) plot shows significantly ($p < 0.05$) detected fatty acids/their groups (21 out of 28) among three depth groups. The box plots around the ANOVA plot show the most significantly differed six fatty acids among three cultivation depths. (B), The heatmap of the fatty acid profile of green mussels cultivated in three depth conditions based on clustering results. Each colored cell in the heat map corresponds to a concentration of fatty acids/their groups on the right side. In the colored cells, red indicates a high concentration, and blue indicates a low concentration. The values inside each colored cell inside the heatmap indicated the mean value of fatty acids/their groups (% of total fatty acids). Significant differences ($p < 0.05$) are indicated with superscript letters based on the one-way ANOVA results.

food availability, and growth performance have been extensively documented, a comprehensive study integrating all these factors to enhance understanding of growth performance remains sparse in *P. viridis* as well as in other marine bivalve species (Noor et al., 2021). PCA in the present study indicated that elevated levels of nutrients (NO_3-N, NH_3-N, PO_4-P), salinity, DO, chlorophyll-a, and plankton abundance positively impacted the growth performance of green mussels from December to March (see Fig. 8). This finding underscores the complex interaction between environmental and nutritional factors affecting green mussel growth in the Maheshkhali channel. The ecological parameters and nutrient availability of the coastal regions of the Bay of Bengal (BoB) are subject to fluctuations due to seasonal upwelling and substantial riverine discharge, which promotes a high abundance of plankton (D'Silva et al., 2012). The vertical transport of nutrient-rich waters from the deeper layers to the surface is impeded by a powerfully stratified surface layer that characterises the southeast coast of the BoB and its associated channels from July to September (Kumar et al., 2002; Banik et al., 2023). Although the coastal regions of the BoB received substantial nutrient inputs (NO_3-N, NO_2-N, NH_3-N, and PO_4-P) during the same period, concentrations did not reach their maximum due to dilution effects from extensive freshwater discharge and intense rainfall (Asaduzzaman et al., 2019; Khan et al., 2019; Chamily et al., 2025). Plankton abundance appears to be stimulated by conditions such as increased radiation, reduced cloud cover, and estuarine processes following this period (Gomes et al., 2000; Jyothibabu et al., 2018; Khan et al., 2019). In line with our findings, the post-monsoon season (October to December) has also been characterised by high plankton abundances in coastal regions of the Bay of Bengal (BoB), such as Tamil Nadu, the Gulf of Mannar, Orissa, Goa, and Mangalore. These results are attributed to the accumulation of nutrients during the monsoon season (Gopakumar et al., 2009; Sanilkumar et al., 2009; Anantharaman et al., 2010). The multivariate analyses demonstrate that plankton biomass is significantly influenced by ecological factors, as indicated by direct plankton counts. Elevated nutrient levels likely enhance primary productivity, as evidenced by increased chlorophyll-a and plankton abundance, thereby providing a richer food source for the mussels. From December to March, the environment is more conducive to the robust growth of green mussels due to the interaction of elevated nutrient levels, increased chlorophyll-a, and abundant plankton, as opposed to other seasons (Asaduzzaman et al., 2019; Noor et al., 2021).

5. Conclusion

This study examined the growth performance and nutritional profiles of green mussels (*P. viridis*) cultivated in a floating raft system, with a focus on the influence of cultivation depth and site-specific ecological factors. Mussels cultivated at a depth of 0.5 m demonstrated superior growth rates and higher levels of essential nutrients compared to those at deeper depths. These results suggest that successful mariculture

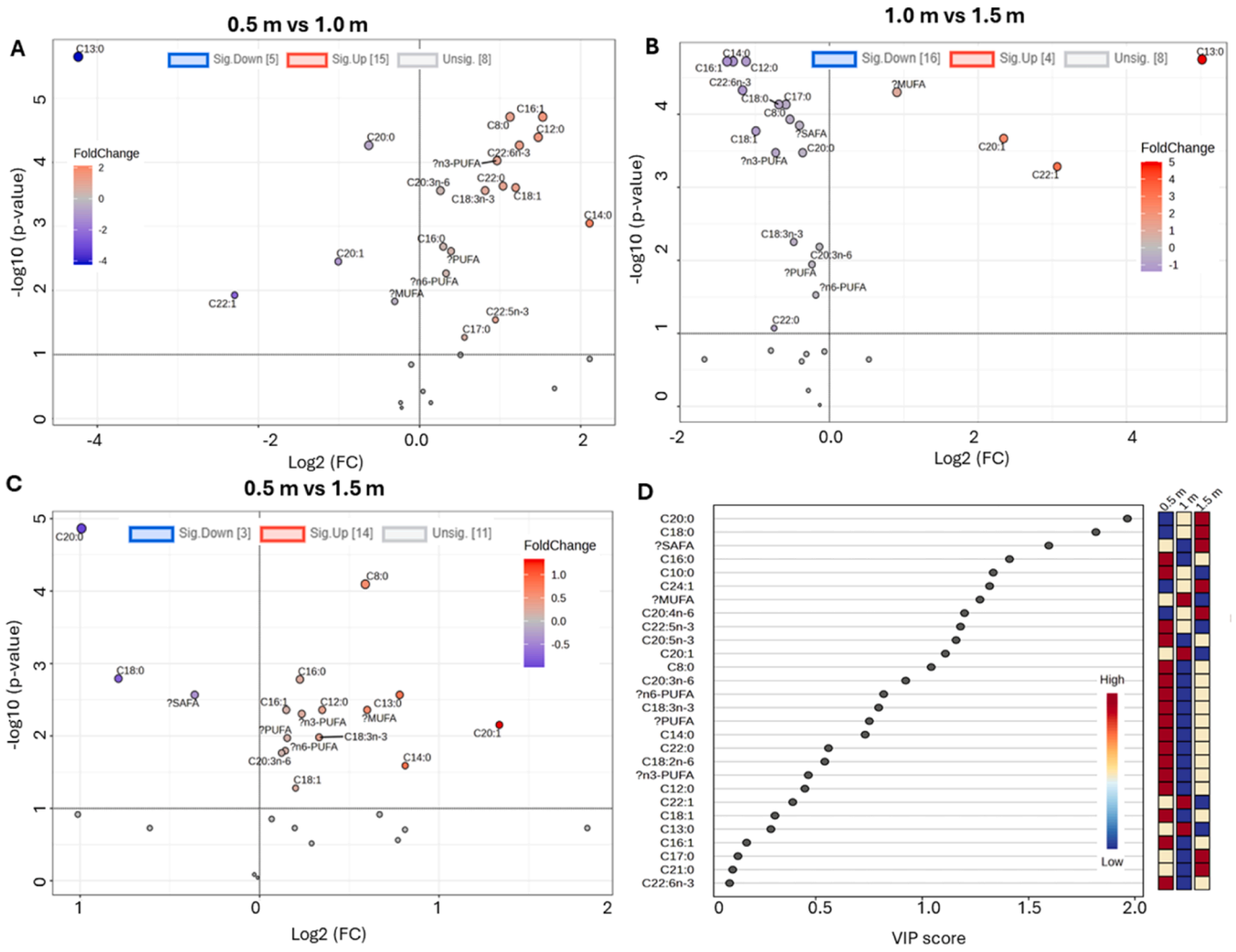

Fig. 10. Volcano and variable importance in projection (VIP) plots illustrating the differences in fatty acid profiles of green mussels (*Perna viridis*) at various depths (0.5 m, 1.0 m, and 1.5 m) in the Maheshkhali Channel of the Bay of Bengal, Bangladesh. The volcano plots showing the results of the paired t-tests highlight the changes in fatty acid profiles between the different cultivation depths: 0.5 m vs. 1.0 m (A), 1.0 m vs. 1.5 m (B), and 0.5 m vs. 1.5 m (C). In these plots, the X-axis represents the fold change of the fatty acids and their groups (log2 scale), while the Y-axis indicates the p-values on a −log10 scale. A horizontal line within the plot marks the statistical significance threshold (adjusted p-values ≤ 0.05), and two vertical lines define the thresholds for log2 fold-change ≥ 1 and ≤ -1. Each colored circle corresponds to a specific fatty acid or group, with its position determined by both the p-value and fold change values. Plot (D) displays the VIP results, highlighting differences in fatty acid profiles among the three cultivation depths as identified by partial least squares discriminant analysis (PLS-DA). The colored boxes on the right indicate the relative concentrations of the corresponding fatty acids. VIP represents a weighted sum of squares of the PLS-DA loadings, considering the amount of explained Y-variable in each dimension.

should be tailored to specific environmental contexts to maximize production outcomes. Future research should investigate additional factors affecting *P. viridis* growth, including more precise measurements of light availability, water movement, sedimentation rates, and the impacts of various macro- and micronutrients. Future research is also needed to investigate the negative effects of harmful algal blooms and climate change impacts on the growth, survival, and safety of green mussels in mariculture systems. Furthermore, examining the economic and logistical implications of implementing depth-specific cultivation strategies can help develop practical guidelines for the bivalve aquaculture industry. Moreover, future research should address the challenges associated with the weak value chain of green mussel aquaculture. This includes exploring breeding programs to ensure a consistent and reliable supply of spat, which is crucial for sustaining production. Additionally, there is a need to develop and implement depuration protocols and regular monitoring of hazardous contaminants to ensure the quality and safety of green mussel products, which will help build consumer trust and expand market opportunities. Strengthening these aspects of the value chain will not only enhance the overall sustainability and profitability of green mussel farming but also support the growth of the bivalve aquaculture industry, particularly in regions where it is still in its early stages.

CRediT authorship contribution statement

Md Nahiduzzaman: Writing – review & editing, Project administration, Investigation, Funding acquisition. **Ilias Ebne Kabir:** Writing – review & editing, Investigation, Data curation. **Md Moshiur Rahman:** Writing – review & editing, Software, Formal analysis, Data curation. **Md Mohiuddin:** Writing – original draft, Methodology, Investigation, Formal analysis, Data curation. **Md Asaduzzaman:** Writing – original draft, Supervision, Project administration, Investigation, Funding acquisition, Formal analysis, Data curation, Conceptualization.

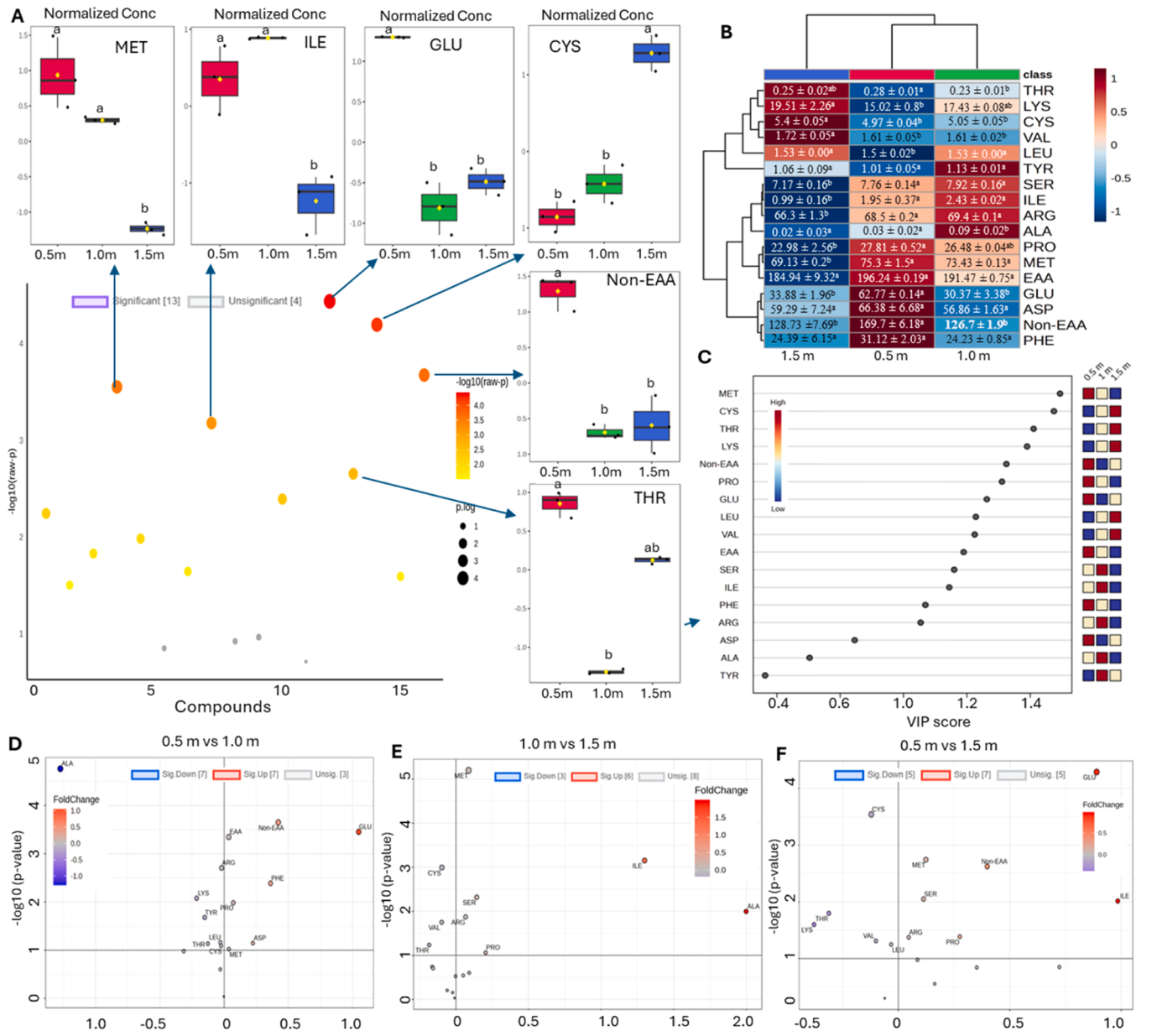

Fig. 11. Variation of amino acid profiles (mg/g of dry weight) of the green mussels (*Perna viridis*) cultivated at different depths (0.5 m, 1 m, and 1.5 m) in the Maheshkhali Channel of the Bay of Bengal, Bangladesh. (A), One-way Analysis of Variance (ANOVA) plot shows significantly ($p < 0.05$) detected amino acids/their groups (13 out of 17) among three depth groups. The box plots around the ANOVA plot show the most significantly differed six amino acids/their groups among three cultivation depths. (B), The heatmap of the fatty acid profile of green mussels cultivated in three depth conditions based on clustering results. Each colored cell in the heat map corresponds to a concentration of amino acids/their groups on the right side. In the colored cells, red indicates a high concentration, and blue indicates a low concentration. The values inside each colored cell inside the heatmap indicated the mean±SD. Plot (C) displays the VIP results, highlighting differences in amino acid profiles among the three cultivation depths as identified by partial least squares discriminant analysis (PLS-DA). The colored boxes on the right indicate the relative concentrations of the corresponding amino acids. VIP represents a weighted sum of squares of the PLS-DA loadings, considering the amount of explained Y-variable in each dimension. The volcano plots highlight the changes in amino acid profiles between the different cultivation depths: 0.5 m vs. 1.0 m (D), 1.0 m vs. 1.5 m (E), and 0.5 m vs. 1.5 m (F). In these plots (D-F), the X-axis represents the fold change of the amino acids and their groups (log2 scale), while the Y-axis indicates the p-values on a −log10 scale. A horizontal line within the plot marks the statistical significance threshold (adjusted p-values ≤ 0.05), and two vertical lines define the thresholds for log2 fold-change ≥ 1 and ≤ −1. Each colored circle corresponds to a specific fatty acid or group, with its position determined by both the p-value and fold change values.

Declaration of Competing Interest

The authors declare that they have no known competing financial interests or personal relationships that could have appeared to influence the work reported in this paper.

Acknowledgements

The fieldwork was done as part of a sub-project of the USAID-funded Enhanced Coastal Fisheries in Bangladesh II (ECOFISH II) activity, which was carried out in collaboration with WorldFish Bangladesh and Chattogram Veterinary and Animal Science University (CVASU) with a grant number PLA13123. This work was also partially financed by the Bangladesh Academy of Science's BAS-USDA endowment fund under

grant number (F 127), specifically for the expenditures connected with various biochemical studies. We are grateful to the ECOFISH II and BAS-USDA project's research associates and research assistants, as well as field workers, for their assistance in data collection and field research for this study.

Data availability

Data will be made available on request.

References

Abad, M., Ruiz, C., Martinez, D., Mosquera, G., Sánchez, J., 1995. Seasonal variations of lipid classes and fatty acids in flat oyster, Ostrea edulis, from San Cibran (Galicia, Spain). Comp. Biochem. Physiol. C Pharmacol. Toxicol. Endocrinol. 110 (2), 109–118.

Alkanani, T., Parrish, C.C., Thompson, R.J., McKenzie, C.H., 2007. Role of fatty acids in cultured mussels, *Mytilus edulis*, grown in Notre Dame Bay, Newfoundland. J. Exp. Mar. Bio. Ecol. 348 (1-2), 33–45.

Al-Kandari, M., Al-Yamani, F., Al-Rifaie, K., 2009. Marine phyto-plankton atlas of Kuwait's Waters. Kuwait Inst. Sci. Res 351. ISBN 99906-41-24-2.

Altman, J.C., Paerl, H.W., 2012. Composition of inorganic and organic nutrient sources influences phytoplankton community structure in the New River Estuary, North Carolina. Aquat. Ecol. 42, 269–282.

Alunno-Bruscia, M., Bourget, E., Fréchette, M., 2001. Shell allometry and length-mass-density relationship for *Mytilus edulis* in an experimental food-regulated situation. Mar. Ecol. Prog. Ser. 219, 177–188.

Alvarado, J.L., Castilla, J.C., 1996. Tridimensional matrices of mussels *Perumytilus purpuratus* on intertidal platforms with varying wave forces in central Chile. Ecol. Prog. Ser. 133, 135–141.

Anantharaman, P., Thirumaran, G., Arumugam, R., Kanna, R.R., Hemaltha, A., Kannathasan, A., et al., 2010. Monitoring of Noctiluca bloom in Mandapam and Keelakarai coastal waters, South-East coast of India. Recent Res. Sci. Technol. 2, 51–58.

AOAC, 2000. Official Methods of Analysis of the Association of Official Analytical Chemist, 17th ed. Washington, D.C.

AOAC, 2005. Official methods of analysis of the association of official analytical chemist. Benyamin Franklin Station. Wash. D. C.

Appukuttan, K.K., Asokan, P.K., Mohamed, S.K., Subramanian, S., Joseph, K.G., 2003. Manual on Mussel Farming. Technical Bulletin No. 3, ICAR (Indian Council of Agricultural Research) research complex for Goa, Old-Goa, India. Tech. Bullet. 28.

Asaduzzaman, M., Akter, S., Hoque, N.F., Shakil, A., Noor, A.R., Akter, M.N., Rahman, M. M., 2020. Multifaceted linkages among eco-physiological factors, seasonal plankton dynamics and selective feeding behavior of the green mussel (*Perna viridis*) in the south-east coast of the Bay of Bengal. J. Sea Res. 164, 101933.

Asaduzzaman, M., Noor, A.R., Rahman, M.M., Akter, S., Hoque, N.F., Shakil, A., Wahab, M.A., 2019. Reproductive biology and ecology of the green mussel *Perna viridis*: a multidisciplinary approach. Biology 8, 88.

Asaduzzaman, M., Wahab, M.A., Verdegem, M.C.J., Azim, M.E., Haque, S., Salam, M.A., 2008. C/N ratio control and substrate addition for periphyton development jointly enhance freshwater prawn *Macrobrachium rosenbergii* production in ponds. Aquaculture 280, 117–12.

Aypa S, M, 1990. Mussel cUlture in Regional Sea Farming Development and Demonstration Project. National Inland Fisheries Institute, Kasetsart University Campus Bangkhen, 38 Bangkok Selected Papers on Mollusc Culture9FAO185.

Banik, U., Mohiuddin, M., Wahab, M.A., Rahman, M.M., Nahiduzzaman, M., Sarker, S., Wong, L., Asaduzzaman, M., 2023. Comparative performances of different farming systems and associated influence of ecological factors on *Gracilaria* sp. seaweed at the south-east coast of the Bay of Bengal, Bangladesh. Aquaculture 574, 739675.

Bayne, B.L., 1998. The physiology of suspension feeding by bivalve molluscs: an introduction to the Plymouth "TROPHEE" workshop. J. Exp. Mar. Biol. Ecol. 219 (1-2), 1–19.

Bin Sallih, K., Þórðarson, J., 2005. Mussel Farming in the State of Sarawak. Malaysia: A feasibility study. Fisheries Training Programme Report, p. 44.

Botes, L., 2003. Phytoplankton identification catalogue ñ Saldanha Bay, South Africa, April 2001. Glob. Monogr. Ser. No. 7. IMO Lond.

Buck, B.H., 2007. Experimental trials on the feasibility of offshore seed production of the mussel *Mytilus edulis* in the German Bight: installation, technical requirements and environmental conditions. Helgol. Mar. Res. 61, 87–101.

Buczek, S.B., Cope, W.G., McLaughlin, R.A., Kwak, T.J., 2018. Effects of turbidity, sediment, and polyacrylamide on native freshwater mussels. J. Am. Water Resour. Assoc. 54 (3), 631–643.

Chaitanawisuti, N., Menasveta, P., 1987. Experimental suspended culture of green mussel, *Perna viridis* (Linn.), using spat transplanted from a distant settlement ground in Thailand. Aquaculture 66 (2), 97–107.

Chakraborty, K., Chakkalakal, S.J., Joseph, D., 2014. Effect of natural additives on the fatty acid signatures of green mussel *Perna viridis* in a time-dependent accelerated shelf-life study. J. Food Qual. 37 (6), 415–428.

Chakraborty, K., Chakkalakal, S.J., Joseph, D., Asokan, P.K., Vijayan, K.K., 2016. Nutritional and antioxidative attributes of green mussel, *Perna viridis* (L.) from the southwestern coast of India. J. Aquat. Food Prod. 25 (7), 968–985.

Chamily, F.A., Mohiuddin, M., Mostakim, M.S., Rahman, M.M., Sourhayda, S.M., Nahiduzzaman, M., Khan, M.S.R., Asaduzzaman, M., 2025. Production performance and biochemical profile of sea lettuce (*Ulva lactuca*): Influence of site-specific ecological factors and culture strategies. Aquaculture 594, 741436.

Chatterji, A., Ansari, Z.A., Ingole, B.S., Parulekar, A.H., 1984. Growth of the green mussel, *Perna viridis* L., in a sea water circulating system. Aquaculture 40 (1), 47–55.

Cheney, D., Langan, R., Heasman, K., Friedman, B., Davis, J., 2010. Shellfish culture in the open ocean: lessons learned for offshore expansion. Mar. Technol. Soc. J. 44 (3), 55–67.

Dag, O., Dolgun, A., Konar, N.M., 2018. Onewaytests: an R package for one-way tests in independent groups designs. R. J. 10.

Dobretsov, S.V., Miron, G., 2001. Larval and post-larval vertical distribution of the mussel *Mytilus edulis* in the White Sea. Mar. Ecol. Prog. Ser. 218, 179–187.

Dridi, S., Romdhane, M.S., Elcafsi, M.H., 2007. Seasonal variation in weight and biochemical composition of the Pacific oyster, *Crassostrea gigas* in relation to the gametogenic cycle and environmental conditions of the Bizert lagoon, Tunisia. Aquaculture 263 (1–4), 238–248.

D'Silva, M.S., Anil, A.C., Naik, R.K., D'Costa, P.M., 2012. Algal Bloom. A Perspect. Coasts India Nat. Hazard. 63, 1225–1253.

Duarte, C.M., Rodriguez-Navarro, A.B., Delgado-Huertas, A., Krause-Jensen, D., 2020. Dense Mytilus beds along freshwater-influenced Greenland shores: resistance to corrosive waters under high food supply. Estuaries Coasts 43, 387–395.

Dubois, S., Marin-Léal, J.C., Ropert, M., Lefebvre, S., 2007. Effects of oyster farming on macrofaunal assemblages associated with *Lanice conchilega* tubeworm populations: a trophic analysis using natural stable isotopes. Aquaculture 271 (1-4), 336–349.

España, M.A., Rodríguez, E.R., Romero, C.D., 2007. Comparison of mineral and trace element concentrations in two molluscs from the Strait of Magellan (Chile). J. Food Compost. Anal. 20 (3-4), 273–279.

FAO, R., 2022. The state of world fisheries and aquaculture 2022. Towards blue transformation. State World Fish. Aquac. (SOFIA) 266.

Filgueira, R., Byron, C.J., Comeau, L.A., Costa-Pierce, B., Cranford, P.J., Ferreira, J.G., Strohmeier, T., 2015. An integrated ecosystem approach for assessing the potential role of cultivated bivalve shells as part of the carbon trading system. Mar. Ecol. Prog. Ser. 518, 281–287.

Forrest, B.M., Creese, R.G., 2006. Benthic impacts of intertidal oyster culture, with consideration of taxonomic sufficiency. Environ. Monit. *Assess.* 112, 159–176.

Fox, J., Weisberg, S., 2019. An R Companion to Applied Regression, 3rd ed. Sage Publication.

Fuentes, J., Gregorio, V., Giráldez, R., Molares, J., 2000. Within-raft variability of the growth rate of mussels, *Mytilus galloprovincialis*, cultivated in the Rıa de Arousa (NW Spain). Aquaculture 189 (1-2), 39–52.

Gallardi, D., Mills, T., Donnet, S., Parrish, C.C., Murray, H.M., 2017. Condition and biochemical profile of blue mussels (*Mytilus edulis* L.) cultured at different depths in a cold-water coastal environment. J. Sea Res. 126, 37–45.

Gomes, H.R., Goes, I.J., Siano, T., 2000. Influence of physical processes and freshwater discharge on the seasonality of phytoplankton regime in the Bay of Bengal. Cont. Shelf Res. 20, 313–330.

Gopakumar, G., Sulochanan, B., Venkatesan, V., 2009. Bloom of *Noctiluca scintillans* (Maccartney) in Gulf of Mannar. Southeast Coast India J. Mar. Biol. Assoc. India 55, 75–80.

Guebel, D.V., Nudel, B.C., Giulietti, A.M., 1991. A simple and rapid micro-Kjeldahl method for total nitrogen analysis. Biotechnol. Tech. 5 (6), 427–430.

Hawkins, A.J.S., Smith, R.F.M., Tan, S.H., Yasin, Z.B., 1998. Suspension-feeding behavior in tropical bivalve molluscs: *Perna viridis*, *Crassostrea belcheri*, *Crassostrea iradelei*, *Saccostrea cucculata* and *Pinctada margarifera*. Mar. Ecol. Prog. Ser. 166, 173–185.

Herbert, R.J.H., Roberts, C., Humphreys, J., Fletcher, S., 2012. The Pacific oyster (*Crassostrea gigas*) in the UK: economic, legal and environmental issues associated with its cultivation, wild establishment and exploitation. Rep. Shellfish Assoc. Gt. Br. 12012, 66.

Hickman, R.W., 1979. Allometry and growth of the green-lipped mussel *Perna canaliculus* in New Zealand. Mar. Biol. 51, 311–327.

Hoque, N.F., Shakil, A., Sultana, F., Wahab, M.A., Rahman, M.J., Nahiduzzaman, M., Akter, S., Asaduzzaman, M., 2021. Feasibility study of green mussel *Perna viridis* farming in the southeast coast of the Bay of Bengal of Bangladesh. Indian J. Agric. Res 39 (2), 195–205.

Hothorn, T., Bretz, F., Westfall, P., 2008. Simultaneous inference in general parametric models. Biometr. J. 50 (3), 346–363.

Howarth, R.W., Marino, R., 2006. Nitrogen as the limiting nutrient for eutrophication in coastal marine ecosystems: evolving views over three decades. Limnol. Oceanogr. 51, 364–376.

Huang, W., Wang, X., Chen, D., Xu, E.G., Luo, X., Zeng, J., Huan, T., Li, L., Wang, Y., 2021. Toxicity mechanisms of polystyrene microplastics in marine mussels revealed by high-coverage quantitative metabolomics using chemical isotope labeling liquid chromatography mass spectrometry. J. Hazard. Mater. 417, 126003.

Huisman, J.E.F., van Oostveen, P., Weissing, F.J., 1999. Critical depth and critical turbulence: two different mechanisms for the development of phytoplankton blooms. Limnol. Oceanogr. 44 (7), 1781–1787.

Huisman, J., Pham Thi, N.N., Karl, D.M., Sommeijer, B., 2006. Reduced mixing generates oscillations and chaos in the oceanic deep chlorophyll maximum. Nature 439 (7074), 322–325.

Iglesias, J.I.P., Pérez-Camacho, A., Navarro, E., Labarta, U., Beiras, R., Hawkins, A.J.S., Widdows, J., 1996. Microgeographic variability in feeding: absorption, and condition of mussels (*Mytilus galloprovincialis* LMK.): a transplant experiment. J. Shellfish Res. 15 (3), 673–680.

Irisarri, J., Fernández-Reiriz, M.J., De Troch, M., Labarta, U., 2014. Fatty acids as tracers of trophic interactions between seston, mussels and biodeposits in a coastal

embayment of mussel rafts in the proximity of fish cages. Comp. Biochem. Physiol. B Biochem. Mol. Biol. 172, 105–115.
Jónasdóttir, S.H., 2019. Fatty acid profiles and production in marine phytoplankton. Mar. Drugs 17, 151.
Jyothibabu, R., Arunpandi, N., Jagadeesan, L., Karnan, C., Lallu, K.R., Vinayachandran, P.N., 2018. Response of phytoplankton to heavy cloud cover and turbidity in the northern Bay of Bengal. Sci. Rep. 8, 11282.
Kamal, D., Khan, Y.S.A., 1998. Growth of the green mussel, *Perna viridis* (Linn. 1758), from Moheshkhali Channel of the Bay of Bengal, Bangladesh. Pak. J. Mar. Sci. 7 (1), 45–55.
Kautsky, N., 1982. Quantitave studies on gonad cycle, fecundity, reproductive output and recruitment in a Baltic *Mytilus edulis* population. Mar. Biol. 68, 143–160.
Khan, S., Jahan, R., Rahman, M.A., Haque, M.M., 2019. Eutrophication enhances phytoplankton abundance in the Maheshkhali channel, Bay of Bengal, Bangladesh. Aust. J. Sci. Technol. 3 (3), 141–147.
Khozin-Goldberg, I., Cohen, Z., 2011. Unraveling algal lipid metabolism: recent advances in gene identification. Biochimie 93, 91–100.
Kumar, S.P., Murleedharan, P.M., Prasad, T.G., Gauns, M., Ramaiah, N., de Souza, S.N., et al., 2002. Why is the Bay of Bengal less productivity during summer monsoon compared to the Arabian sea? Geophys. Res. Lett. 29, 2235.
Langan, R., Horton, C.F., 2003. Design, operation and economics of submerged longline mussel culture in the open Ocean. Bull. Aquac. Assoc. Can. 103-3, 11–20.
Li, Q., Sun, S., Zhang, F., et al., 2019. Effects of hypoxia on survival, behaviour, metabolism and cellular damage of Manila clam (*Ruditapes philippinarum*). PLoS One 14 (4), e0215158.
Lindahl, O., Hart, R., Hernroth, B., Kollberg, S., Loo, L.O., Olrog, L., Syversen, U., 2005. Improving marine water quality by mussel farming: a profitable solution for Swedish society. Ambio: J. Hum. Environ. 34 (2), 131–138.
Loesch, J.G., Evans, D.A., 1994. Quantifying seasonal-variation in somatic tissue-surf clam spisula-solidissima (Dillwyn, 1817)-A Case-Study. J. Shellfish Res. 13 (2), 425.
Long, W.C., Seitz, R.D., Brylawski, B.J., et al., 2014. Individual, population, and ecosystem effects of hypoxia on a dominant benthic bivalve in Chesapeake Bay. Ecol. Monogr. 84, 303–327.
Lopes-Lima, M., Teixeira, A., Froufe, E., Lopes, A., Varandas, S., Sousa, R., 2014. Biology and Conservation of Freshwater Bivalves: Past, Present and Future Perspectives. Hydrobiologia, 735, 1-13.
Marinho-Soriano, E., Nunes, S.O., Carneiro, M.A.A., Pereira, D.C., 2009. Nutrients' removal from aquaculture wastewater using the macroalgae *Gracilaria birdiae*. Biomass Bioenergy 33 (2), 327–331.
Martínez-Pita, I., Sánchez-Lazo, C., Ruíz-Jarabo, I., Herrera, M., Mancera, J.M., 2012. Biochemical composition, lipid classes, fatty acids and sexual hormones in the mussel *Mytilus galloprovincialis* from cultivated populations in south Spain. Aquaculture 358, 274–283.
Marzetz, V., Spijkerman, E., Striebel, M., Wacker, A., 2020. Phytoplankton community responses to interactions between light intensity, light variations, and phosphorus supply. Front. Environ. Sci. 8, 539733.
Matias, D., Joaquim, S., Matias, A.M., Moura, P., de Sousa, J.T., Sobral, P., Leitão, A., 2013. The reproductive cycle of the European clam *Ruditapes decussatus* (L., 1758) in two Portuguese populations: implications for management and aquaculture programs. Aquaculture 406, 52–61.
McGaraghan, A., 2018. Tiny Drifters-a Guide to the Phytoplankton along the California Coast. Kudela Biological and Satellite Oceanography. Laboratory. University of California, Santa Cruz.
Mitra, A., Banerjee, K., Gangopadhyay, A., 2013. Introduction to Marine Plankton. Daya Publishing House, New Delhi.
Mueller, K.W., 1996. A preliminary study of the spatial variation in growth of raft-cultured blue mussels *Mytilus trossulus* in northern Puget Sound, Washington. J. World Aquac. Soc. 27, 240–246.
Napiorkowska-Krzebietke, A., 2017. Phytoplankton response to fish-induced environmental changes in a temperate shallow pond-type lake. Arch. Pol. Fish. 25, 211–264.
Noor, N.M., Nursyam, H., Widodo, M.S., Risjani, Y., 2019. Biological aspects of green mussels *Perna viridis* cultivated on raft culture in Pasaran coastal waters. Indones. AACL Bioflux 12 (2), 448–456.
Noor, A.R., Shakil, A., Hoque, N.F., Rahman, M.M., Akter, S., Talukder, A., Ahmad-Al-Nahid, S., Wahab, M.A., Nahiduzzaman, M., Rahman, M.J., Asaduzzaman, M., 2021. Effect of eco-physiological factors on biometric traits of green mussel *Perna viridis* cultured in the south-east coast of the Bay of Bengal. Bangladesh Aquac. Rep. 19, 100562.
O'brien, K.R., Ivey, G.N., Hamilton, D.P., Waite, A.M., Visser, P.M., 2003. Simple mixing criteria for the growth of negatively buoyant phytoplankton. Limnol. Oceanogr. 48, 1326–1337.
Ogilvie, S.C., Fox, S.P., Ross, A.H., James, M.R., Schiel, D.R., 2004. Growth of cultured mussels (*Perna canaliculus* Gmelin 1791) at a deep-water chlorophyll maximum layer. Aquac. Res. 35 (13), 1253–1260.
Orban, E., Di Lena, G., Nevigato, T., Casini, I., Marzetti, A., Caproni, R., 2002. Seasonal changes in meat content, condition index and chemical composition of mussels (*Mytilus galloprovincialis*) cultured in two different Italian sites. Food Chem. 77 (1), 57–65.
Pang, Z., Lu, Y., Zhou, G., Hui, F., Xu, L., Viau, C., Spigelman, A.F., MacDonald, P.E., Wishart, D.S., Li, S., Xia, J., 2024. MetaboAnalyst 6.0: towards a unified platform for metabolomics data processing, analysis and interpretation. Nucleic Acids Res. 52, W398–W406.
Parulekar, A.H., Dalal, S.G., Ansari, Z.A., Harkantra, S.N., 1982. Environmental physiology of raft-grown mussels in Goa, India. Aquaculture 29 (1-2), 83–93.
Paul, M., Sanyal, P., Mukherjee, R., Gupta, V.K., Bakshi, S., Acharya, A., Bhattacharya, T., Chakraborty, K., Mukhopadhyay, S.K., 2024. Distribution and biogeochemical perspectives of nutrients in the Eastern Equatorial Indian Ocean. Oceanologia 66, 381–393.
Penney, R.W., Hart, M.J., Templeman, N.D., 2007. Shell strength and appearance in cultured blue mussels *Mytilus edulis*, *M. trossulus*, and *M. edulis*× *M. trossulus* hybrids. N. Am. J. Aquac. 69 (3), 281–295.
Peterson, B.G., Carl, P., 2020. PerformanceAnalytics: econometric tools for performance and risk analysis. R. Package Version 2. 0. 4.
Pirini, M., Manuzzi, M.P., Pagliarani, A., Trombetti, F., Borgatti, A.R., Ventrella, V., 2007. Changes in fatty acid composition of Mytilus galloprovincialis (Lmk) fed on microalgal and wheat germ diets. Comp. Biochem. Physiol. B Biochem. Mol. Biol. 4, 616–626.
Prato, E., Danieli, A., Maffia, M., Biandolino, F., 2010. Lipid and fatty acid compositions of *Mytilus galloprovincialis* cultured in the Mar Grande of Taranto (Southern Italy): feeding strategies and trophic relationships. Zool. Stud. 49 (2), 211–219.
Prato, E., Parlapiano, I., Addis, P., Biandolino, F., 2017. Mediterranean Seafood: Functional Food Properties. The Mediterranean Diet: Perspectives, Food Components and Health Effects. Nova Publisher, New York, pp. 171–187.
R Development Core Team, 2022. R: A Language and Environment for Statistical Computing, Version 4.3.2. R Foundation for Statistical Computing. Vienna, Austria. Available online: https://www.r-project.org/ (accessed 10 November 2023).
Rajagopal, S., 1997. The ecology of tropical marine mussels and their control in industrial cooling water systems. Ph.D. Thesis, Univ. Nijmegen, Neth.1184.
Rajagopal, S., Venugopalan, V.P., Nair, K.V.K., Van der Velde, G., Jenner, H.A., 1998. Settlement and growth of the green mussel Perna viridis (L.) in coastal waters: influence of water velocity. Aquat. Ecol. 32, 313–322.
Rajagopal, S., Venugopalan, V.P., Van der Velde, G., Jenner, H.A., 2006. Mussel colonization of a high flow artificial benthic habitat: byssogenesis holds the key. Mar. Environ. Res 62 (2), 98–115.
Reed, M.L., Pinckney, L.J., Keppler, C.J., Brock, L.M., Hogan, S.B., Greenfield, D.I., 2017. The influence of nitrogen and phosphorus on phytoplankton growth and assemblage composition in four coastal, southeastern USA systems. Estuar. Coast. Shelf Sci. 177 (5), 71–82.
Rejeki, S., Debrot, A.O., van Den Brink, A.M., Ariyati, R.W., Lakshmi Widowati, L., 2021. Increased production of green mussels (*Perna viridis*) using longline culture and an economic comparison with stake culture on the north coast of Java, Indonesia. Aquac. Res. 52 (1), 373–380.
Ren, J.S., Ross, A.H., 2005. Environmental influence on mussel growth: a dynamic energy budget model and its application to the green shell mussel *Perna canaliculus*. Ecol. Model. 189 (3-4), 347–362.
Rivonker, C.U., Ansari, Z.A., Parulekar, A.H., 1993. Cultivation of green mussel, *Perna viridis* L., on a floating raft in an estuary along the west coast of India. Aquaculture 112 (1), 47–56.
Sanilkumar, M.G., Thomas, A.M., Philip, A.A., Hatha, M., Sanjeevan, V.N., Saramma, A. V., 2009. First report of Protoperidinium bloom from Indian waters. Harmful Algal N. 39, 15.
Saritha, K., Mary, D., Patterson, J., 2015. Nutritional status of green mussel *Perna viridis* at Tamil Nadu, Southwest Coast of India. J. Nutr. Sci.
Saxby, S.A., 2002. A review of food availability, sea water characteristics and bivalve growthperformance at coastal culture sites in temperateand warm temperate regions of the world. Fish. Res. 132, 1–44.
Sebastien, L., Josse, J., Husson, F., 2008. FactoMineR: An R Package for Multivariate Analysis. J. Stat. Softw. 25, 1–18.
Seitz, R.D., Wennhage, H., Bergström, U., Lipcius, R.N., Ysebaert, T., 2014. Ecological value of coastal habitats for commercially and ecologically important species. ICES J. Mar. Sci. 71 (3), 648–665.
Shahabuddin, A.M., Wahab, M.A., Miah, M.I., Salam, M.A., 2010. Abundance, distribution and culture potentials of three commercially important mollusks species along the coast of the Bay. Bengal J. Agric. Biol. Sci. 6 (6), 754–762.
Shumway, S.E., Davis, C., Downey, R., Karney, R., Kraeuter, J., Parsons, J., et al., 2003. Shellfish aquaculture–in praise of sustainable economies and environments. World Aquac. 34 (4), 8–10.
Silva, C.C.D., Neto, M.J., Nunes, C., Golcalves, F.J.M., Coimbra, A.M., Marques, J.C., Golclaves, A.M.M., 2021. Assessment of seasonal and spatial variations in the nutritional content of six edible marine bivalve species by the response of a set of integrated biomarkers. Ecol. Indic. 124, 107378.
Sivalingam, P.M., 1977. Aquaculture of the green mussel, *Mytilus viridis* Linnaeus, in Malaysia. Aquaculture 11 (4), 297–312.
Slavin, E.I., Wain, D.J., Bryant, L.D., Amani, M., Perkins, R.G., Blenkinsopp, C., et al., 2022. The effects of surface mixers on stratification, dissolved oxygen and cyanobacteria in a shallow eutrophic reservoir. Water Resour. Res. 58.
Song, J., Farhadi, A., Tan, K., Lim, L., Tan, K., 2024. Impact of anthropogenic global hypoxia on the physiological response of bivalves. Sci. Total Environ. 926, 172056.
Taib, A.M., Madin, J., Ransangan, J., 2016. Density, recruitment and growth performance of Asian green mussel (Perna viridis) in Marudu Bay, Northeast Malaysian Borneo, three years after a massive mortality event. Songklanakarin J. Sci. Technol. 38 (6), 631–639.
Tan, K.S., Ransangan, J., 2014. A review of feeding behavior, growth, reproduction and aquaculture site selection for green-lipped mussel, *Perna viridis*. Adv. Biosci. Biotechnol. 5, 462–469.
Tan, K.S., Ransangan, J., 2016. Feasibility of Green Mussel, *Perna viridis* Farming in Marudu Bay, Malaysia. Aquac. Rep. 4, 130–135.
Tan, K.S., Ransangan, J., 2017. Feeding behavior of green mussels, *Perna viridis* farmed in Marudu Bay, Malaysia. Aquac. Res. 48 (3), 1216–1231.

Tang, Q., Zhang, J., Fang, J., 2011. Shellfish and seaweed mariculture increase atmospheric CO_2 absorption by coastal ecosystems. Mar. Ecol. Prog. Ser. 424, 97–104.

Tasnim, R., Sarker, S., Chamily, F.A., Mohiuddin, M., Ferdous, A., Haque, A.M., Nahiduzzaman, M., Wahab, M.A., Rahman, M.M., Asaduzzaman, M., 2024. Site suitability mapping for different seaweed cultivation systems along the coastal and marine waters of Bangladesh: A Generalized Additive Modelling approach for prediction. Algal Res., 103404

Tuttle-Raycraft, S., Morris, T.J., Ackerman, J.D., 2017. Suspended solid concentration reduces feeding in freshwater mussels. Sci. Total Environ. 598, 1160–1168.

Ventrella, V., Pirini, M., Pagliarani, A., Trombetti, F., Manuzzi, M.P., Borgatti, A.R., 2008. Effect of temporal and geographical factors on fatty acid composition of *M. galloprovincialis* from the Adriatic Sea. Comp. Biochem. Physiol. B Biochem. Mol. Biol 149 (2), 241–250.

Waldbusser, G.G., Powell, E.N., Mann, R., 2013. Ecosystem effects of shell aggregations and cycling in coastal waters: an example of Chesapeake Bay oyster reefs. Ecology 94 (4), 895–903.

Wang, Y., Hu, M., Wong, W.H., Shin, P.K., Cheung, S.G., 2011. The combined effects of oxygen availability and salinity on physiological responses and scope for growth in the green-lipped mussel *Perna viridis*. Mar. Pollut. Bull. 63 (5-12), 255–261.

Wickham, H., 2016. ggplot2: Elegant Graphics for Data Analysis. Springer-Verlag, New York.

Xie, Z., Wei, S., Dong, H., et al., 2021. Hemocyte responses of the oyster *Crassostrea hongkongensis* exposed to diel-cycling hypoxia and salinity change. Front. Mar. Sci. 8, 749623.

Xu, H., Paerl, H.W., Qin, B., Zhu, G., Gaoa, G., 2010. Nitrogen and phosphorus inputs control phytoplankton growth in eutrophic Lake Taihu, China. Limnol. Oceanogr. 55 (1), 420–432.

Yu, J., Choi, M., Park, K., et al., 2010. Effects of anoxia on immune functions in the surf clam *Mactra veneriformis*. Zool. Stud. 49, 94–101.

Journal of Sea Research 210 (2026) 102677

Contents lists available at ScienceDirect

Journal of Sea Research

journal homepage: www.elsevier.com/locate/seares

Linking estuarine ecology with reproductive phenology in the Indian backwater oyster *Crassostrea madrasensis*: A multivariate framework perspective

Afshana Ferdous [a,b], Israt Jahan [a], Sourav Chowdhury [a], Md Ramzan Ali [a], Md Nayeem Hossain [a,c], Md Moshiur Rahman [d], Mohammad Sadequr Rahman Khan [a], Md Asaduzzaman [a,*]

[a] Department of Marine Bioresource Science, Faculty of Fisheries, Chattogram Veterinary and Animal Sciences University, Khulshi- 4225, Chittagong, Bangladesh
[b] Department of Marine Fisheries and Oceanography, Faculty of Fisheries and Marine Science, Sher-e-Bangla Agricultural University, Dhaka 1207, Bangladesh
[c] Department of Marine Fisheries and Aquaculture, Faculty of Earth and Ocean Science, Bangladesh Maritime University, Dhaka 1216, Bangladesh
[d] Fisheries and Marine Resource Technology Discipline, Khulna University, Khulna 9208, Bangladesh

ARTICLE INFO

Keywords:
Crassostrea madrasensis
Reproductive phenology
Gametogenesis
Growth dynamics
Ecological drivers
Conservation strategies

ABSTRACT

A nuanced understanding of the reproductive dynamics, growth trajectories, and environmental interactions of the Indian backwater oyster (*Crassostrea madrasensis*) is indispensable for advancing knowledge for ensuring population sustainability, tropical mariculture, and guiding conservation strategies in monsoon-driven tropical ecosystems. Therefore, this study undertook an integrated, year-long (May 2023–April 2024) investigation of reproductive biology, biometric growth patterns, and trophic relationships of *C. madrasensis* from the Moheshkhali Channel, a dynamic marine-influenced habitat along the southeast coast of the Bay of Bengal, Bangladesh, employing a multivariate analytical framework. Biometric assessments revealed consistent negative allometric growth, indicating preferential energetic allocation to shell accretion over somatic tissue development, thereby reflecting adaptive morphological plasticity in response to local environmental pressures. Histological analyses identified two distinct spawning peaks during the pre-monsoon (April–June) and post-monsoon (October–December) periods, corroborated by elevated condition indices (CI) and presumptive gonadosomatic indices (P. GSI). Seasonal fluctuations in sex ratios demonstrated a flexible reproductive strategy, characterized by female predominance during periods of heightened primary productivity and the occurrence of transient hermaphroditism during transitional months. Multivariate analyses (PCA and CVA) revealed strong seasonal coupling among reproductive stages, plankton ingestion patterns, and key environmental drivers, including temperature, salinity, dissolved oxygen, and nutrient availability. Planktonic diet composition exhibited pronounced seasonal shifts aligned with reproductive cycles, underscoring adaptive nutritional adjustments that support gametogenesis. The pre-monsoon reproductive phase appeared to rely primarily on endogenous energy reserves, whereas post-monsoon spawning was closely synchronized with peaks in phytoplankton abundance and nutrient influx, suggesting opportunistic utilization of exogenous energy inputs. Collectively, these findings advance ecological understanding of wild populations of *C. madrasensis*, offering vital baseline knowledge to guide conservation and sustainable utilization for maintaining natural oyster stocks and adaptive mariculture strategies in monsoon-influenced tropical estuarine environments.

1. Introduction

Among the oysters, *Crassostrea madrasensis* (Indian backwater oyster) holds considerable ecological and economic significance across tropical coastal areas of South and Southeast Asia, notably in India, Sri Lanka, and Bangladesh (Gosling, 2015; Asaduzzaman et al., 2025). Its exceptional nutritional profile, characterized by abundant protein, omega-3 fatty acids, and essential micronutrients (zinc, iron, and

* Corresponding author at: Department of Marine Bioresource Science, Faculty of Fisheries, Chattogram Veterinary and Animal Sciences University, Khulshi 4225, Chattogram, Bangladesh.
E-mail address: a_zamanbau@yahoo.com (M. Asaduzzaman).

https://doi.org/10.1016/j.seares.2026.102677
Received 9 September 2025; Received in revised form 9 January 2026; Accepted 27 January 2026
Available online 28 January 2026

vitamins A and B12), underscores its value as a food resource (Waite et al., 2014; Willett et al., 2019; Willer and Aldridge, 2019). In Bangladesh, *C. madrasensis* naturally thrives along the southeastern shores, particularly within the Moheshkhali Channel, which offers ideal environmental conditions like optimal temperature, salinity, sufficient food availability, and comparatively stable hydrographic conditions, that underpin both natural population sustainability and emerging mariculture potential. This resilient bivalve thrives in tropical habitats, including backwaters, lagoons, and rocky shorelines, where it plays a pivotal ecological role by enhancing water quality through biofiltration, stabilizing sediments, and promoting estuarine biodiversity. It functions as a habitat-forming species, offering shelter and food to associated organisms, and serves as an effective agent for biodiversity restoration in estuarine ecosystems. Economically, *C. madrasensis* contributes significantly to coastal livelihoods through small-scale aquaculture and is considered a promising candidate for mariculture due to its rapid growth and abundant spat production (Sanjeeva Raj, 2008). Despite its ecological and economic value, oyster farming in Bangladesh remains underdeveloped (Asaduzzaman et al., 2025), largely owing to limited scientific knowledge of its reproductive biology, inadequate long-term monitoring, and the complex interactions between reproduction and environmental factors. Therefore, elucidating the reproductive dynamics of *C. madrasensis* is essential to optimize hatchery production, ensure sustainable stock management, and support the expansion of oyster mariculture in tropical regions.

The reproductive timing and efficiency of marine bivalves are pivotal determinants of population structure, shaping individual fitness, survival rates, and overall ecosystem resilience. These reproductive processes are modulated by an intricate interplay between intrinsic (genetic and evolutionary) and extrinsic (environmental conditions such as water temperature, salinity, pH, food availability, and various physicochemical stimuli) factors (Gosling, 2003; Kim et al., 2010; Uddin et al., 2013). In addition, a suite of quantitative factors, including biometric relationships, sex ratio (the ratio of females to males), condition index (CI), and gonadosomatic index (GSI), is essential for elucidating the reproductive biology and population dynamics of marine bivalves. Length–weight relationships are widely employed to assess oyster growth performances and physiological condition (Jha and Mohan, 2014; Octavina et al., 2015; Liang et al., 2016; Le Pabic et al., 2016; Vasconcelos et al., 2018). These analyses often reveal divergent allometric growth patterns: for instance, *Magallana gigas* typically exhibits negative allometry (Octavina and Afriana, 2024), whereas positive allometry has been reported in *C. madrasensis* and *C. gryphoides* (Nagi et al., 2011), reflecting differences in meat yield potential and ecological adaptability. Furthermore, examining temporal and spatial variations in sex ratios offers critical insight into reproductive potential, population health, and hatchery management (Lenz, 2008). Notably, oyster populations frequently display shifts in sex ratios in response to environmental stress, age, or nutritional conditions. Many species, including *C. madrasensis*, are also capable of hermaphroditism or sequential sex reversal under specific ecological circumstances (Chávez-Villalba et al., 2007). Moreover, species-specific traits, such as organ development stage, genetic background, and environmental drivers, strongly influence the progression of the gametogenic cycle (Gosling, 2003; Lenz, 2008).

A comprehensive understanding of the reproductive cycle of *C. madrasensis* and its relationship with key environmental drivers is vital for improving mariculture practices and shaping evidence-based strategies for sustainable fisheries management. In marine bivalves, reproductive cycles are commonly assessed either through macroscopic inspection of gonadal features (e.g., size, shape, coloration) or via detailed histological examination of gonadal tissues (Arjarasirikoon et al., 2004; Delgado and Pérez-Camacho, 2005; Etchian et al., 2004). Because *Crassostrea* species lack conspicuous macroscopic sexual dimorphism, gonadal histology has become the most reliable technique for sex identification and reproductive assessment (Solon, 1984; Steele and Mulcahy, 1999; Lango-Reynoso et al., 2000; Fabioux, 2004; Dridi et al., 2006; Ferreira et al., 2006; Normand et al., 2008; Lenz and Boehs, 2011). Nevertheless, histological interpretation can sometimes be subjective; therefore, coupling this qualitative approach with quantitative measures such as CI and GSI offers a more robust framework for characterizing reproductive traits (Gosling, 2008; Gomes et al., 2014). Measuring GSI in oysters, however, is complicated by the diffuse distribution of gonadal tissues within the mantle (Frías-Espericueta et al., 1997, 1999). By contrast, CI is widely employed as a proxy for physiological condition and nutritional status, serving as a reliable indicator of reproductive development and gametogenic activity (Delgado and Pérez-Camacho, 2007). The integration of CI with detailed gonadal histology thus provides a powerful methodological basis for precise staging of reproductive phases and accurate identification of spawning events. Previous studies have reported geographically variable spawning patterns in *C. madrasensis*, including biannual spawning associated with monsoonal fluctuations in southern Indian waters (Alagarswami and Chellam, 1976; Narasimham, 1980). However, baseline information from the mariculture sites in the northern Bay of Bengal, particularly along the southeast coast of Bangladesh, remains scarce. Moreover, the linkages among reproduction, feeding ecology, and environmental variables such as plankton availability and water physicochemistry are still poorly understood in this region (Asaduzzaman et al., 2019; Uddin et al., 2024).

In Bangladesh, despite increasing interest in coastal aquaculture, comprehensive research on *C. madrasensis*' reproductive ecology and its environmental linkages remains limited. In particular, baseline data on reproductive phenology, condition indices, and their relationships with environmental variables along the southeast coast of Bangladesh, a region strongly influenced by monsoonal variability, are scarce, constraining efforts to manage natural broodstocks and promote sustainable oyster mariculture. Prior studies primarily focused on growth performance or isolated aspects of gonadal morphology, neglecting the integrated relationship among reproduction, feeding ecology, and environmental drivers (Asaduzzaman et al., 2019; Uddin et al., 2024; Hossain et al., 2025). Given Bangladesh's recent initiatives promoting sustainable aquaculture within its blue economy framework, addressing these knowledge gaps through targeted scientific research is both timely and crucial. Therefore, the present study provides an integrated, year-long assessment of the reproductive biology, biometric traits, and trophic relationships of *C. madrasensis* from a tropical estuarine system using a multivariate analytical framework. Specifically, the research sought to determine: (1) allometric growth and biometric to characterize growth patterns; (2) reproductive cycles through histological staging, sex ratios, CI, and presumptive gonadosomatic indices (P.GSI); and (3) seasonal linkages among reproductive stages, plankton ingestion patterns, and key environmental drivers. By elucidating the reproductive strategies and environmental synchrony of *C. madrasensis* in a monsoon-driven estuarine ecosystem, this study establishes critical ecological baselines to support the sustainable development of oyster mariculture, inform fisheries management, and guide conservation planning in Bangladesh and comparable tropical coastal systems.

2. Materials and methods

2.1. Sampling strategies of C. madrasensis

The specimens of *C. madrasensis* were collected monthly between May 2023 and April 2024 from the two sites (Khurushkul and Moheshkhali) of the Maheshkhali Channel, Cox's Bazar, Bangladesh (21°30′20″ N, 91°59′19″ E) (Fig. 1). This channel is located along the southeast coast of Bangladesh, maintains a direct hydrological connection to the Bay of Bengal and represent a dynamic marine-influenced habitat. Each month, 50 live oysters were randomly collected by hand-picking methods and transported immediately to the Oceanography Laboratory of Chattogram Veterinary and Animal Sciences

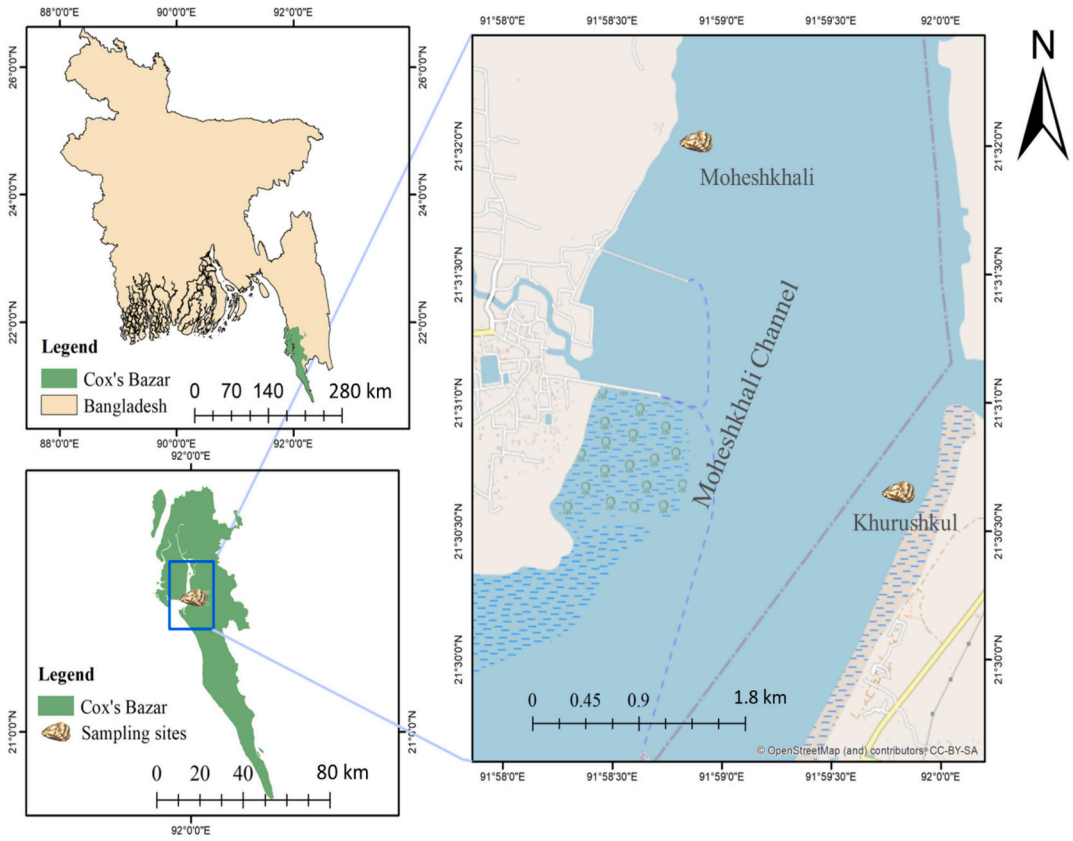

Fig. 1. Map of the two collection sites (Khurushkul and Moheshkhali) of the Indian backwater oyster, *Crassostrea madrasensis* in the Moheshkhali Channel along the southeast coast of the Bay of Bengal, Bangladesh.

University (CVASU). Transportation was conducted in insulated containers filled with ambient seawater collected from the sampling site to minimize handling stress and maintain physiological integrity. From the monthly collection, approximately 20 oysters were randomly selected for sex identification and gonadal histological assessment. An additional set of 20 oysters was utilized for gut plankton analysis to investigate temporal variation in dietary intake. For these individuals, the tentative stage of gonadal development was macroscopically evaluated based on gonadal tissue appearance and relative developmental mass. This allowed for categorization of individuals into developmental stages and enabled comparative analysis of gut plankton content in relation to reproductive status.

2.2. Calculation of biometric traits and gonadosomatic index

To evaluate biometric traits and reproductive development, all of the collected 50 specimens of *C. madrasensis* individuals were analyzed monthly across the annual reproductive cycle. Morphometric traits were assessed by measuring shell length (greatest dimension along the anterior–posterior axis), shell height (maximum span along the dorsal–ventral axis), and shell width (thickest point across the two valves) using a Vernier caliper with ±0.01 mm precision. Before weighing, intervalval water was removed, and the whole-body mass of each oyster was then determined with an electronic balance (PS 1200, R2, Radwag, Poland) accurate to 0.1 g. Subsequently, oysters were dissected, and gonadal tissues were excised with care to avoid damage. In *C. madrasensis*, gonadal tissues are diffusely distributed and embedded within the upper layers of the digestive gland and mantle, making precise extraction and isolation difficult without disrupting surrounding tissues. To account for this limitation, a presumptive GSI (P.GSI) was estimated. After dissection, visible gonadal tissue, distinguishable from surrounding somatic tissue based on colour and consistency, was excised as completely as possible and weighed using a high-precision analytical balance (AS 220.R2, Radwag, Poland) with 0.01 mg sensitivity. The P. GSI was subsequently determined using the formula described by Gaughan and Mitchell (2000):

$$\text{Presumtive gonado} - \text{somatic Index (P.GSI)} = \frac{\text{Weight of presumptive gonad}}{\text{Total weight of oyster}} \times 100$$

2.3. Condition index

In the present study, CI was measured monthly using approximately 25 specimens of *C. madrasensis*. After biometric measurements, oysters were randomly selected for CI measurement and were carefully dissected to separate the soft tissues from the shell. The soft tissue was blotted to remove excess moisture and placed in a preheated oven at 105 °C for 12 h, then cooled in a desiccator to prevent moisture absorption. The desiccated tissues were subsequently weighed using a precision analytical balance (AS 220.R2, Radwag, Poland) to get dry tissue weight. Shell cavity volume was estimated using a water displacement method. After tissue removal, shells were rinsed with freshwater and sun-dried until constant weight prior to weighing. Cleaned and dried shells were immersed in a vertical glass column filled with distilled water. The displaced water, representing the internal shell volume, was collected and measured in a measuring cylinder.

The CI was then calculated using the formula proposed by Yap et al. (2002):

$$\text{CI} = \left[\text{total dry tissue weight (g)}/\text{shell volume (cm}^3\text{)}\right]^{*} 1000$$

2.4. Histology of gonad

For histological analysis of the gonads, tissue sections were carefully excised from the mantle lobes, fixed in Bouin's solution for 24 h, and subsequently dehydrated through a graded ethanol (80–100%) and xylene series. Following dehydration, the tissues were embedded in paraplast, cut into transverse sections of 7 μm thickness, and mounted on glass slides. The mounted preparations were further dehydrated through ascending alcohol concentrations and stained with Harris's hematoxylin and eosin following standard histological protocols (Pearse, 1985). Prepared slides were examined under a digital microscope (Optika B-190 TB, Ponteranica, Italy) at objective magnifications ranging from 10× to 40×, and images were captured with a digital camera (Fein Optic F10; Model- SN 532981, USA) equipped with the microscope for documentation. Based on microscopic features, gonadal development was categorized into five major stages: resting, developing, subdivided into Developing A (early gametogenesis) and Developing B (advanced gametogenesis), mature, spawning subdivided into Spawning A (early spawning) and Spawning B (late spawning), and spent, according to follicle development, germ cell maturity, and degree of gamete discharge following Asaduzzaman et al. (2019).

2.5. Gut plankton analysis

The feeding ecology of *C. madrasensis* was assessed by analyzing the gut contents of 240 individuals (20 per month) over the course of one year to evaluate the contribution of ingested plankton to nutrient and energy requirements during gametogenesis. Upon collection, the gonadal development stage of each specimen was provisionally identified by visually examining the gonad mass. The digestive tract was then dissected, and gut material was withdrawn through a small incision beneath the crystalline style using a glass Pasteur pipette. The contents were diluted with a measured volume of distilled water, from which 1 mL subsamples were transferred to a Sedgewick–Rafter counting cell (S–R cell). Plankton were identified to the genus level and enumerated under a binocular microscope (Optika B-190 TB) at 10× objective magnification, using counts from 10 randomly selected fields. Each gut content sample was analyzed in triplicate to ensure accuracy. Taxonomic classification followed Botes (2001), with grouping into major plankton categories according to Al-Kandari et al. (2009). The abundance of plankton in the gastrointestinal tract was quantified using the equation: $N = (P \times C \times 100)$, where N denotes the total number of plankton units, P represents the average count from 10 microscopic fields, and C is the final concentrate volume (mL).

2.6. Water quality assessments

Water samples were collected from the same collection sites where *C. madrasensis* specimens were obtained in order to evaluate the relationship between environmental conditions and seasonal patterns of reproduction and gametogenesis. In situ measurements of temperature (°C), salinity (ppt), pH, and dissolved oxygen (mg L^{-1}) were taken using a multiparameter sensor (YSI, Loveland, CO, USA), while water current velocity (m/s) was determined with a digital flow meter (Flow Probe FP311, Global Water, College Station, TX, USA) positioned 0.5 m below the surface. For nutrient and chlorophyll-a analysis, samples were obtained with a vertical water sampler (1200-E Kemmerar, Science First/WildCo, Yulee, FL, USA) and filtered through Whatman GF/C microfiber glass filters using a vacuum pump. Triplicate water samples (500 mL) were collected in plastic bottles for nutrient determination (NO_3-N, NO_2-N, NH_3-N, and PO_4-P) and transported to the laboratory under chilled conditions. Subsamples of 10 mL were analyzed for NO_2-N, NH_3-N, and PO_4-P, while 1 mL aliquots were used for NO_3-N determination, all conducted by spectrophotometry (PhotoFlex STD, WTW, Weilheim, Germany) following APHA (1992) protocols. Chlorophyll-a concentration was quantified spectrophotometrically at wavelengths of 664, 647, and 630 nm (Optizen Pop 2102, Daejeon, Republic of Korea) to correct for pigment overlap and ensure accurate estimation in natural waters using standard procedures outlined by Boyd (1979).

2.7. Qualitative and quantitative estimation of water plankton

Monthly assessments of both the qualitative and quantitative composition of plankton were carried out at the oyster collection sites. For each sampling event, 20 L of pooled seawater obtained with a vertical water sampler (1200-E Kemmerar, Science First/WildCo, Yulee, FL, USA) was filtered through a 20-μm mesh plankton net, and the concentrate was preserved in small plastic vials with 5% buffered formalin. The preserved samples were transported to the Oceanography Laboratory, Chattogram Veterinary and Animal Sciences University (CVASU) for further analysis. Quantitative estimation was performed using a Sedgewick–Rafter (S–R) cell consisting of 1000 compartments, each 1 mm^3 in volume (Asaduzzaman et al., 2020). A 1-mL subsample was placed in the chamber, and plankton were identified to the genus level and enumerated in 10 randomly chosen fields under a binocular microscope (Optika B-190 TB, Ponteranica, Italy) at objective magnifications ranging from 10× to 40×. Plankton density (cells or individuals L^{-1}) was then calculated using the equation: $N = (P \times C \times 100) / L$, where N = number of plankton cells or individuals per liter of ambient, unfiltered seawater, P = mean plankton count from 10 fields, C = final concentrate volume (mL), and L = volume of the original amount of water sample (L).

2.8. Statistical analysis

All statistical analyses were conducted in R (version 4.4.2; R Development Core Team, 2024). Data normality was examined using the Shapiro–Wilk test, while homogeneity of variances was assessed with Levene's test implemented in the onewaytests package (Dag et al., 2017). Monthly variations among datasets were analyzed through one-way ANOVA using the car package (Fox and Weisberg, 2019), and, where significant differences were detected, Tukey's HSD post hoc comparisons were performed with the multcompView package (Graves et al., 2024). For regression analyses, data were log-transformed to meet model assumptions. Statistical significance was evaluated at a 95% confidence level ($p < 0.05$). Multivariate analyses were applied to explore patterns within the dataset. Principal Component Analysis (PCA) was conducted using the FactoMineR package (Lê et al., 2008), with interpretation based on the first two principal components that explained the largest proportion of total variance. Canonical Variate Analysis (CVA) was further employed using the MASS package (Venables and Ripley, 2002) to discriminate among reproductive phases and assess group separations. Correlation structures among environmental, planktonic, and reproductive variables were investigated using Pearson's correlation matrices and visualized through the PerformanceAnalytics package (Peterson and Carl, 2024). All figures and graphical representations were generated with the ggplot2 package (Wickham, 2016).

3. Results

3.1. Biometric relationships and growth allometry of C. madrasensis

A significant positive relationship was observed between shell length and total weight ($R^2 = 0.444$), described by the equation $W = 8.79 \times L^{1.4141}$ (Fig. 2A). Similarly, shell length showed a positive correlation with wet soft tissue weight ($R^2 = 0.3434$), with an allometric exponent of 1.2394 (Fig. 2B). The correlation between shell height and total weight was notably stronger ($R^2 = 0.6674$), following the equation $W = 2.464 \times H^{1.8011}$ (Fig. 2C). Shell height also correlated with wet soft tissue weight ($R^2 = 0.3472$) with an exponent of 1.2914 (Fig. 2D). On the other hand, shell width had the weakest correlation with both total weight ($R^2 = 0.2829$) (Fig. 2E) and wet soft tissue weight ($R^2 = 0.1031$)

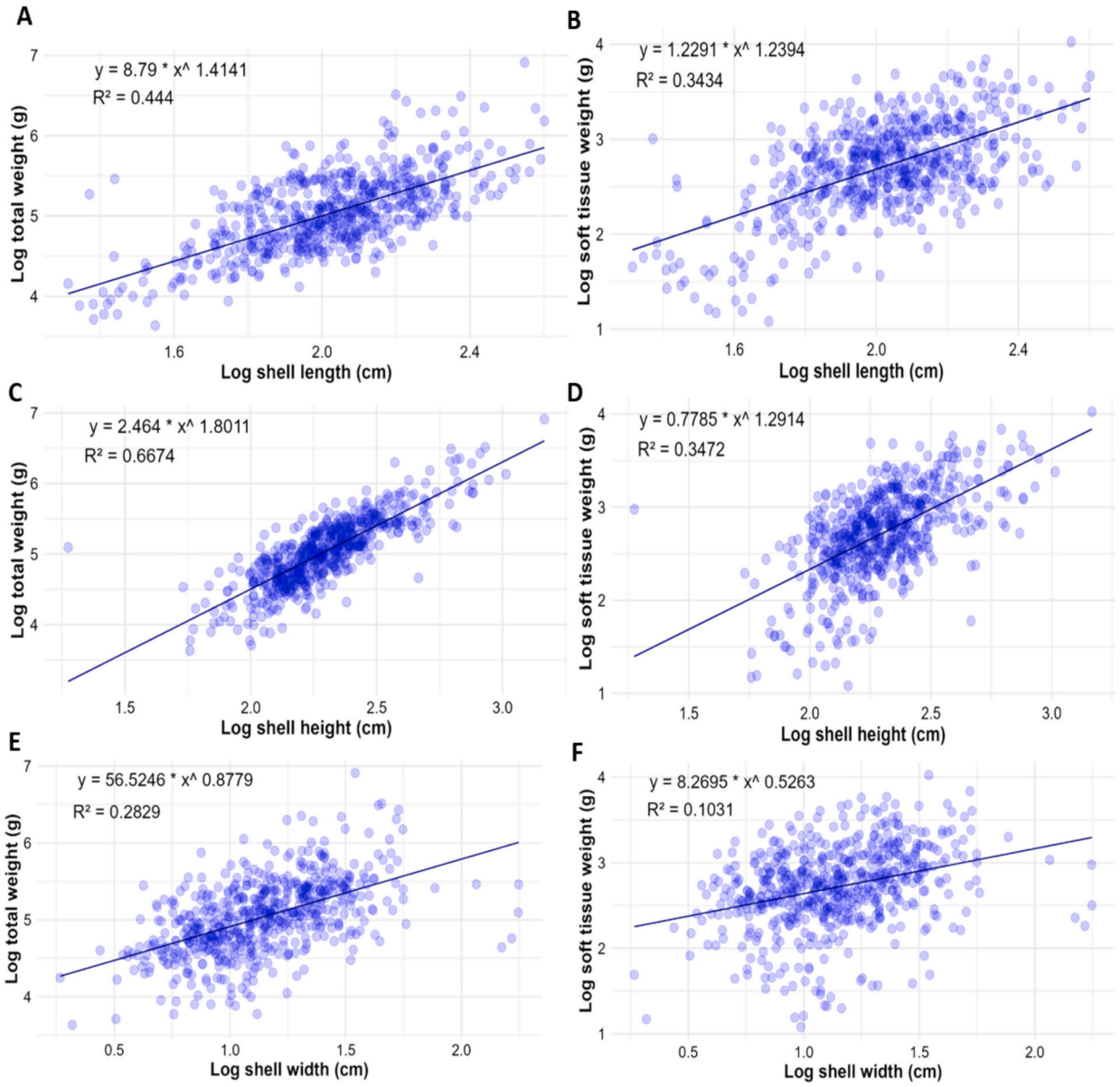

Fig. 2. Linear regression analyses depicting biometric relationships among morphometric parameters of oyster, *Crassostrea madrasensis* collected from the Moheshkhali Channel along the Southeast Coast of the Bay of Bengal, Bangladesh. (A) regression analysis between shell length (cm) and total weight (g); (B) regression analysis between shell length (cm) and soft tissue weight (g); (C) regression analysis between shell height (cm) and total weight (g); (D) regression analysis between shell height (cm) and soft tissue weight (g); (E) regression analysis between shell width (cm) and total weight (g); (F) regression analysis between shell width (cm) and soft tissue weight (g).

(Fig. 2F). Notably, total weight relationships consistently showed higher R^2 values than soft tissue weight, emphasizing the influence of shell dimensions on whole-body mass rather than edible content alone.

3.2. Macroscopic observation of gametogenic stages of C. madrasensis

Macroscopic examination of the gonads in *C. madrasensis* revealed distinct reproductive stages based on the size, colour, and visibility of the gonadal tissues within the mantle cavity (Fig. 3). In the resting stage (Fig. 3A), the gonads appeared inconspicuous with no visible reproductive tissue. During the early developing stage (Fig. 3B), a faint, translucent gonadal tissue became apparent along the mantle edge, indicating the onset of gametogenesis. The late developing stage (Fig. 3C) was characterized by thickened, more opaque gonadal tissue, occupying a broader area with a cream to light brown colouration. At the ripe stage (Fig. 3D-E), gonads appeared prominently enlarged and bulging, creamy-white to pale yellow in colour, clearly occupying significant space within the visceral area, indicating full maturity and readiness for spawning. Finally, the spent stage (Fig. 3F) exhibited flaccid, shrunken gonads with a watery appearance, due to the release of gametes. These visible morphological differences, marked by dashed lines (Fig. 3), allowed clear macroscopic identification and classification of reproductive stages.

3.3. Sex composition and temporal dynamics in C. madrasensis

The size-frequency distribution of *C. madrasensis* individuals ranged from 40 mm to 130 mm in shell length, exhibiting a unimodal pattern with the highest abundance recorded in the 80–90 mm class ($n = 79$) (Fig. 4A). Four reproductive categories have been identified: male, female, hermaphrodite, and undifferentiated (resting stage). (Fig. 4B). Out of the 240 specimens analyzed, 96 (40%) were identified as males, 106

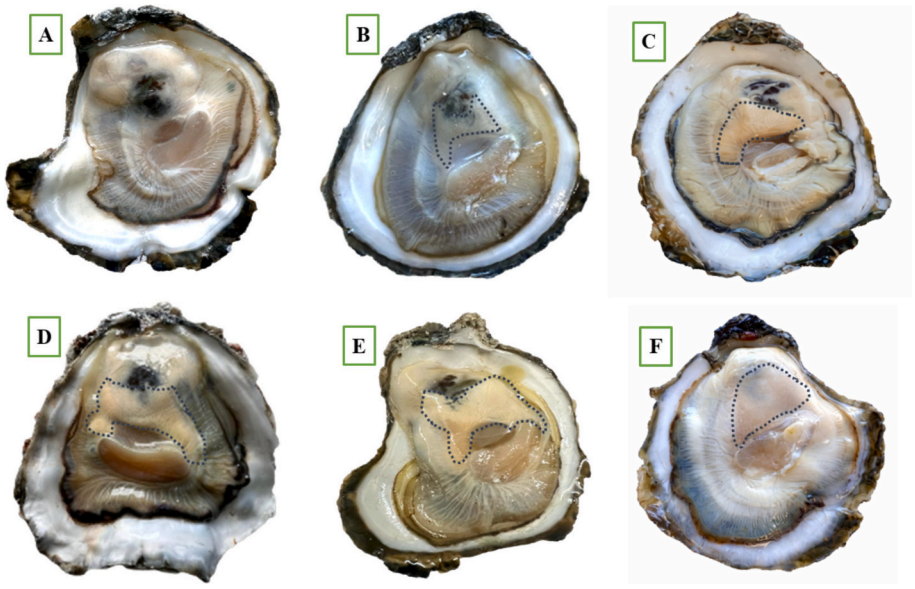

Fig. 3. Macroscopic view of gonadal maturation stages of oyster, *Crassostrea madrasensis* determined by direct visual inspection of specimens collected from the Moheshkhali Channel along the Southeast Coast of the Bay of Bengal, Bangladesh. The dashed lines indicate the most prominent boundaries of the gonadal area within the visceral mass. A: Indifferent sex stage; B-C: Developing stages; D-E: white gonad growing large in mature stage; and F: Spawning stage.

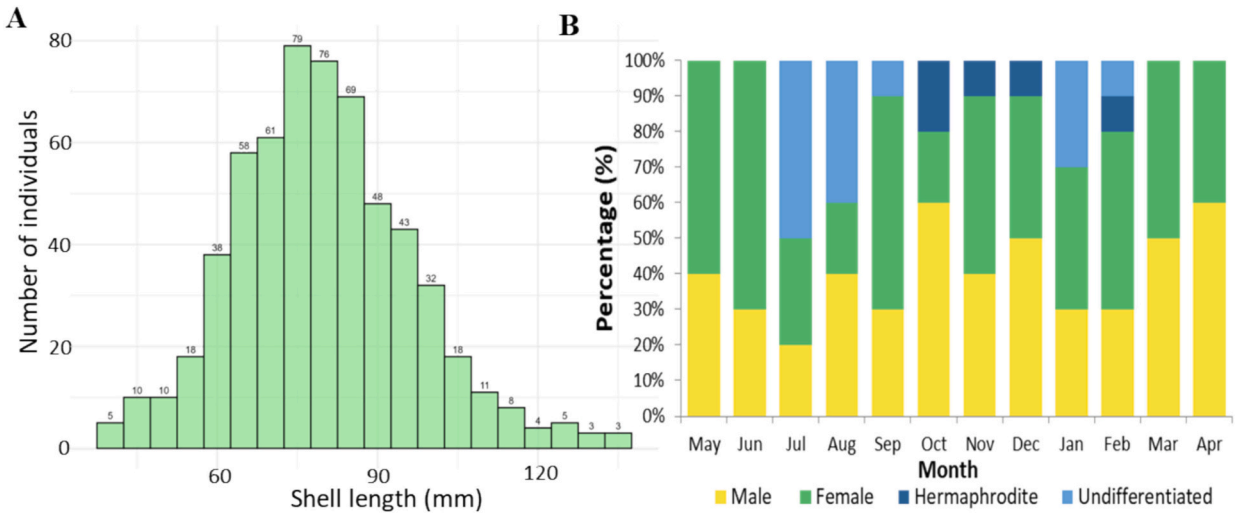

Fig. 4. Size-frequency distribution (A) and proportion of sex across month of the year (B) of oyster, *Crassostrea madrasensis* collected from the Moheshkhali Channel along the Southeast Coast of the Bay of Bengal, Bangladesh.

(44.2%) as females, 10 (4.17%) as hermaphrodites, and 28 (11.67%) as undifferentiated. Temporal variation in sex ratios was evident across the sampling period. Female dominance was observed during the pre-monsoon (March, April, May, June) and monsoon (July, August, September) months, with peak occurrences in June (70%), May (60%), and September (60%). Conversely, male prevalence was highest in April and October (each 60%). Hermaphroditic individuals were most abundant in October, accounting for 20% of the population during that month. Notably, undifferentiated individuals were more prevalent during the post-spawning and recovery phases, particularly from July – August and January to February. Despite month-to-month fluctuations in male and female proportions, the overall sex ratio did not significantly deviate from the expected 1:1 distribution. A Chi-square test ($\chi^2 = 0.49$, df $= 1$, $p > 0.05$) confirmed no statistically significant difference between male and female frequencies.

3.4. Reproductive phases, hermaphroditism, and seasonal synchrony

Histological analyses revealed that the reproductive development of male and female *C. madrasensis* followed a clear progression through five distinct stages: early developing, late developing, mature, spawning, and spent (Figs. 5–6). In the resting phase, the gonads were inactive and undifferentiated, with no visible gametes (Fig. 5A). As development began, females displayed small, scattered follicles containing early oocytes (Fig. 6A), while males had dense clusters of spermatogonia lining the tubule walls (Fig. 5B). This early stage was followed by late development, where female follicles became larger and filled with growing oocytes (Fig. 6B) and males showed a more advanced mix of spermatogenic cells, including spermatocytes and spermatozoa (Fig. 5C). In the mature stage, both sexes reached peak reproductive readiness where females had follicles packed with ripe, polygonal ova (Fig. 6C) and males had lumens filled with tightly arranged spermatozoa (Fig. 5D). The spawning phase was marked by the release of some gametes, leaving

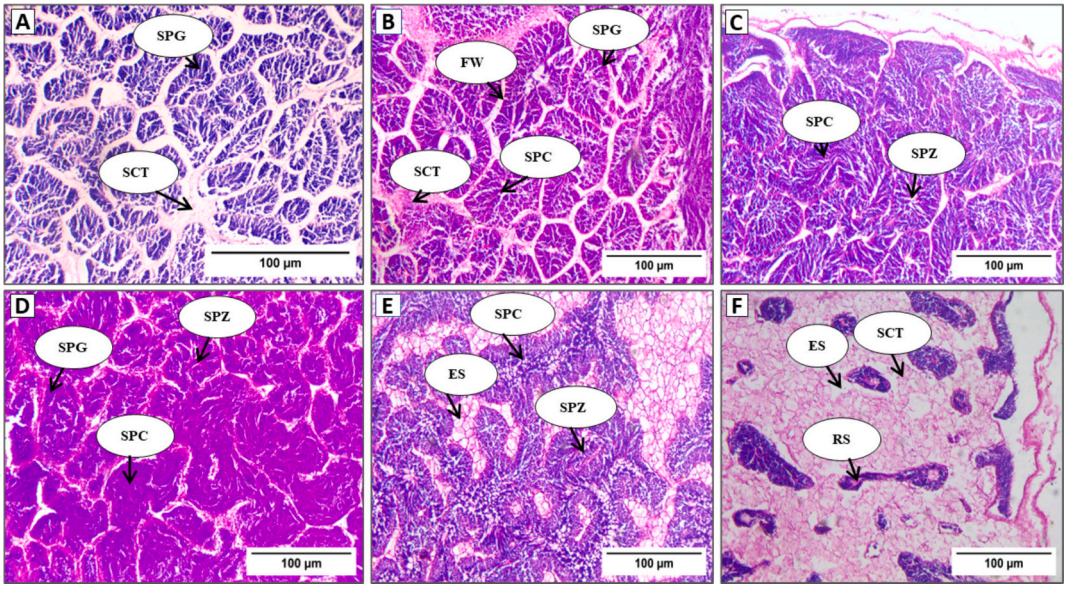

Fig. 5. Photomicrographs of the developmental stages of male gonads of oyster, *Crassostrea madrasensis* collected from the Moheshkhali Channel along the Southeast Coast of the Bay of Bengal, Bangladesh. A) Spent; B) Early developing; C) Late developing; D) Mature; E) Spawning A (early spawning); F) Spawning B (late spawning). Here, FW = follicle wall; SCT = storage connective tissue; SPG = spermatogonia; SPC = spermatocyte; SPZ = spermatozoa; ES = empty space; RS = residual spermatozoa.

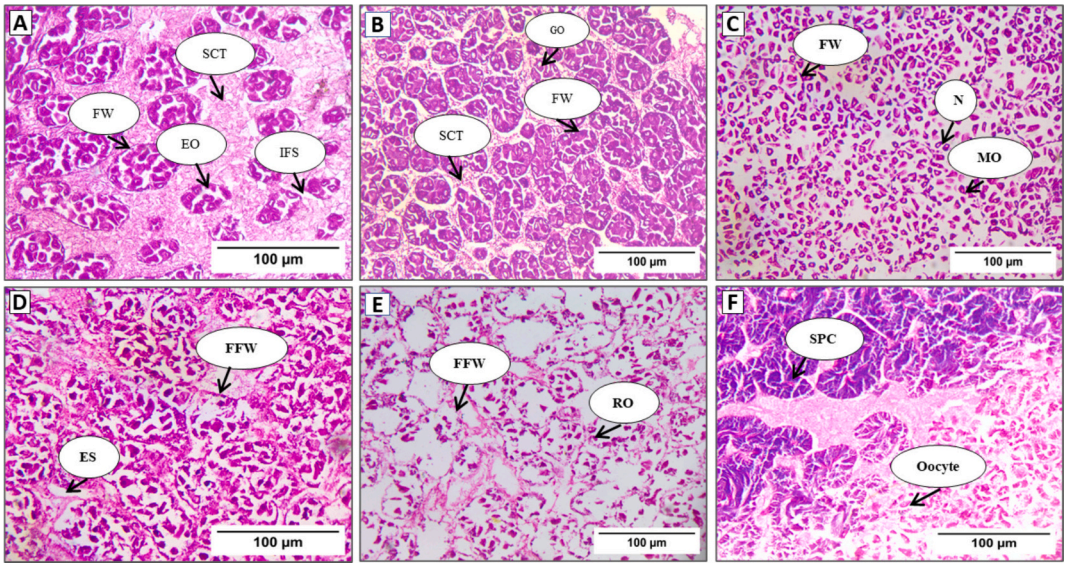

Fig. 6. Photomicrographs of the developmental stages of female gonads of oyster, *Crassostrea madrasensis* collected from the Moheshkhali Channel along the Southeast Coast of the Bay of Bengal, Bangladesh. A) Early developing; B) Late developing; C) Mature; D) Spawning A (early spawning); E) Spawning B (late spawning); F) Hermaphrodyte. Here, FW = follicle wall; SCT = storage connective tissue; IFS = interfollicular space; EO = early oocyte; GO = growing oocyte; FO = free oocyte inside lumen; MO = mature oocyte; N = nucleous; FFW = fragmented follicle wall; ES = empty space; RO = residual oocyte; SPC = Spermatocyte.

noticeable gaps in the follicles. Finally, in the spawning B stage, the gonads appeared depleted and regressed, with only a few residual gametes and disrupted follicular walls remaining (Figs. 5F, 6E). Additionally, histological analyses revealed instances of hermaphroditism, characterized by the simultaneous presence of oocytes and spermatocytes within the same gonadal tissue (Fig. 6F).

The monthly progression of gonadal development stages in *C. madrasensis* is illustrated in Fig. 7, showing clear temporal patterns across a reproductive cycle. *C. madrasensis* exhibited two spawning cycles over the 12-month study period. The proportion of early-developing and late-developing stages was predominant from June to October, indicating the onset of gametogenesis. A marked increase in mature and spawning stages was observed from September to December, peaking in November and December, suggesting active gamete release during the post-monsoon period. Subsequently, a higher percentage of spent individuals was recorded in January for males and February for females, reflecting post-spawning regression and reabsorption of residual gametes. From February to April, early and late developing stages re-emerged, indicating the initiation of a new reproductive cycle. The temporal pattern of gonadal development in *C. madrasensis* (Fig. 7) is well-supported by the CI and P.GSI trends (Fig. 8), highlighting two distinct spawning cycles. Elevated CI and P.GSI in May coincide with early gametogenic stages (May–August), while a sharp drop in June–July indicates spawning onset. A second peak in December

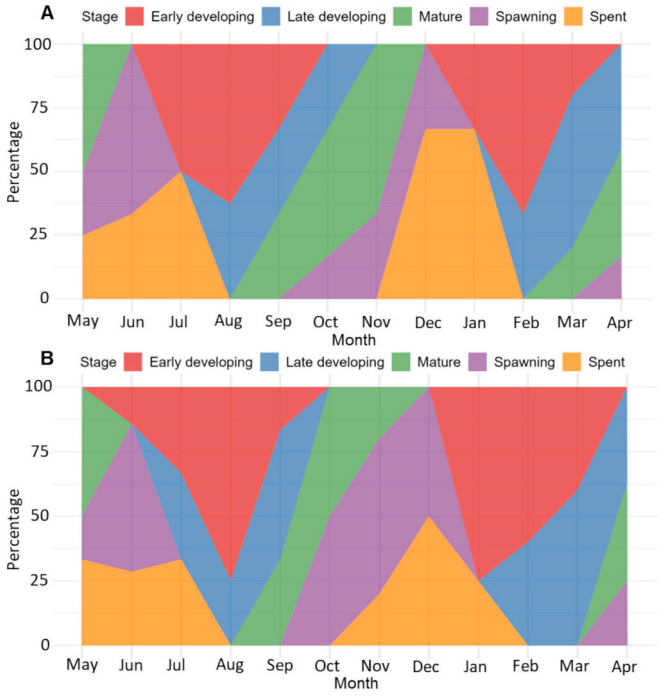

Fig. 7. Monthly fluctuations in the phases of gonadal maturity (%) in male (A) and female (B) of oyster, *Crassostrea madrasensis* collected from the Moheshkhali Channel along the Southeast Coast of the Bay of Bengal, Bangladesh.

corresponds with increased mature and spawning stages, confirming a post-monsoon reproductive event.

3.5. Multivariate evidence of stage-dependent dietary strategies of *C. madrasensis*

Canonical Variate Analysis (CVA) and Principal Component Analysis (PCA) were used to explore the associations between the gonadal developmental stages of *C. madrasensis* and the composition of ingested plankton across pre-monsoon (March–June) and post-monsoon (October–January) seasons (Fig. 9). The CVA results revealed a detectable separation among the gonadal stages (Fig. 9). In the pre-monsoon season, the first canonical variance (CV1) accounted for 75.8% of the total variance, effectively distinguishing early stages of gonadal development (early and late developing) from more advanced stages (mature, spawning, and spent). The second canonical variate (CV2), explaining 20.2% of the variance, captured more subtle differences in plankton ingestion within these broader stage groups. The density distributions (Fig. 9C) further supported this pattern, showing clear unimodal peaks along CV1 that corresponded with distinct clustering of the different gonadal stages. The post-monsoon CVA (Fig. 9B) revealed nearly equal contributions from CV1 (48.02%) and CV2 (46.06%).

Principal component analysis (PCA) biplots provided additional clarity on relationships between gonadal development stages and plankton ingestion of *C. madrasensis* during pre-monsoon (March–June) and post-monsoon (October–January) gametogenic cycle (Fig. 10). During the pre-monsoon season (Fig. 10A), Dim1 and Dim2 accounted for 21.1% and 15.8% of the variance, respectively. Early and late developing stages cluster toward plankton groups such as Cyanophyceae (G-Cyano), Bacillariophyceae (G-Baci), Fragilariophyceae (G-Fra), and zooplankton (G-Zoo). During the mature and spawning stage, oysters were predominantly associated with the ingestion of cholorophycae, while spent individuals exhibit a less distinct dietary preference. During the post-monsoon season (Fig. 10B), PCA patterns shifted notably, displaying stronger associations between mature and spawning stages with plankton groups such as Bacillariophyceae (G-Baci), Dinophyceae (G-Dino), and Fragilariophyceae (G-Fra). In contrast, early and late developing stages showed less defined plankton preferences.

3.6. Pre- and post-monsoon reproductive-environmental interactions

A correlation analysis was carried out linking the ecological factors with the CI and P.GSI values of *C. madrasensis* during the pre-monsoon (March–June) (Fig. 11) and post-monsoon (October–January) (Fig. 12) gametogenic cycles. During the pre-monsoon gametogenic cycle, CI exhibited a significant positive relationship with air temperature ($r = 0.33, p < 0.001$) and salinity ($r = 0.38$, $p < 0.001$), while showing strong negative correlations with chlorophyll-a ($r = -0.42$, $p < 0.001$), nitrate ($r = -0.52$, $p < 0.001$), phosphate ($r = -0.31$, $p < 0.01$), and DO ($r = -0.21$, $p < 0.01$). These inverse associations suggest that higher gonadal development (reflected in CI) is not directly driven by immediate phytoplankton abundance or nutrient enrichment (conservative schemes). Similarly, P.GSI demonstrated significant negative associations with most environmental parameters. In contrast, during the post-monsoon gametogenic cycle (Fig. 12), the CI exhibited a significant positive correlation with dissolved oxygen (DO; $r = 0.34$, $p < 0.001$), chlorophyll-a ($r = 0.41$, $p < 0.001$), nitrate ($r = 0.35$, $p < 0.001$), phosphate ($r = 0.45$, $p < 0.01$), and salinity ($r = 0.42$, $p < 0.001$).

To summarize the patterns observed in the datasets, a principal component analysis (PCA) was conducted to disentangle the complex interactions among environmental parameters, water-column plankton composition, ingested gut plankton, and the reproductive stages of *C. madrasensis* (Fig. 13). The first two principal components (Dim1 and Dim2) together explained 41.4% of the total variance, with Dim1 accounting for 24.7% and Dim2 for 16.7%. These axes distinctly separated the pre-monsoon (March–June), monsoon (July–September), and post-monsoon (October–January) periods. During the pre-monsoon months (March–June), no major environmental vectors projected into the corresponding grouping area. Nevertheless, the embedded bar chart of CI and P.GSI showed elevated values (Fig. 13), suggesting active gonadal development. This implies that *C. madrasensis* may rely on internal energy reserves to sustain reproductive processes (conservative schemes). Conversely, during the post-monsoon season (October–January), samples occupied the positive space of Dim1, reflecting favourable environmental conditions characterized by elevated salinity and higher dissolved oxygen (DO) concentrations. This period coincided with nutrient enrichment, as indicated by increased levels of nitrate (NO_3-N), phosphate (PO_4-P), and chlorophyll-a (Chlo-a). These factors were strongly correlated with a higher abundance of phytoplankton groups such as Coscinodiscophyceae, Bacillariophyceae, Fragillariophyceae, Dinophyceae and zooplankton in the water column, pointing to enhanced primary productivity. During the post-monsoon gametogenic cycle, oysters also exhibited higher ingestion of nearly all plankton groups in the gut, indicating opportunistic utilization of externally available energy inputs (opportunistic schemes).

4. Discussion

4.1. Growth dynamics of *C. madrasensis*

Understanding length–weight relationships in *C. madrasensis* offers valuable insights into growth dynamics, biomass estimation, and condition monitoring, particularly for resource management and mariculture planning. The current findings reveal a clear pattern of negative allometric growth, a trend frequently observed in tropical bivalves, where shell dimensions increase at a faster rate than soft tissue mass (Hemachandra and Thippeswamy, 2008; El-Sayed et al., 2011; Aban et al., 2017). Such growth indicates that *C. madrasensis* tends to invest more in structural development than in somatic tissue accumulation, possibly reflecting adaptive strategies to fluctuating environmental pressures in its natural habitat. This disproportionate investment may be influenced by several factors, including salinity fluctuations, nutrient

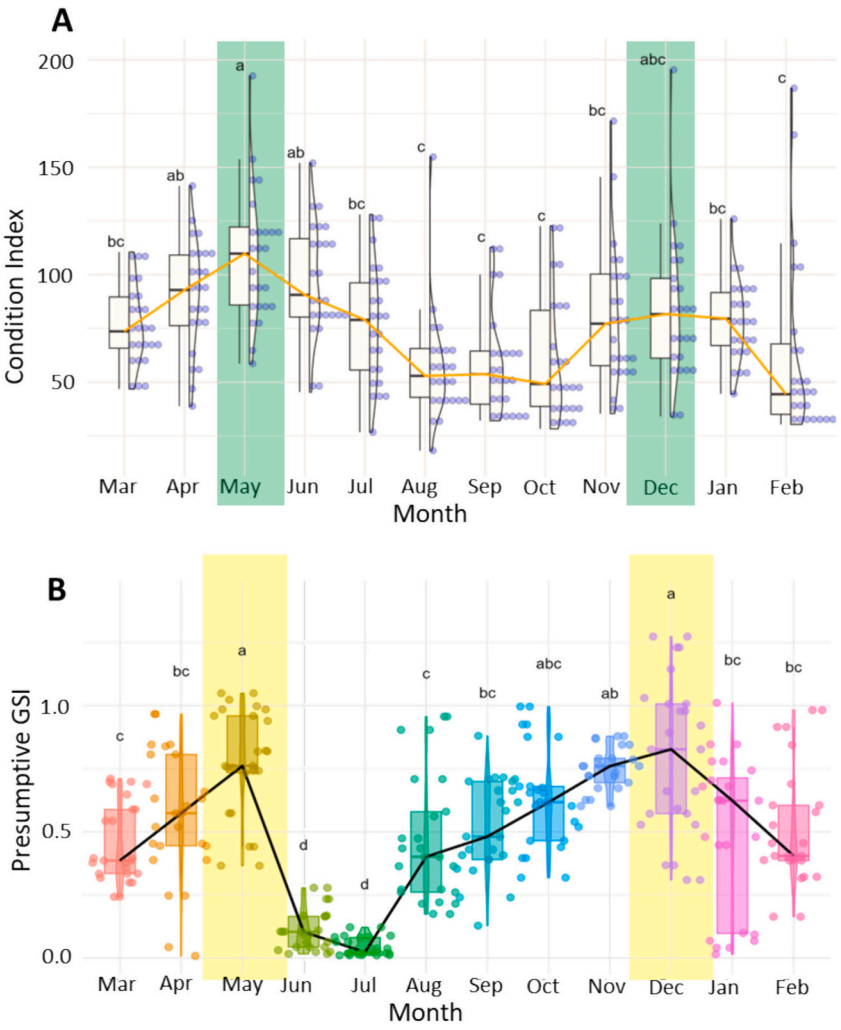

Fig. 8. Monthly variation of (A) condition index (CI) and (B) Presumptive GSI (P.GSI) of oyster, *Crassostrea madrasensis* collected from the Moheshkhali Channel along the Southeast Coast of the Bay of Bengal, Bangladesh. Boxplots represent the distribution of values, where the central line indicates the median, boxes denote the interquartile range (25th–75th percentiles), whiskers represent the minimum and maximum values excluding outliers, and dots indicate individual observations. Small letters indicate significant differences in CI and P.GSI values among months at $p < 0.05$.

availability, and reproductive cycles, common in estuarine environments like those of the southeast coast of Bangladesh (Çelik et al., 2015). In particular, seasonal spawning events and gametogenic development can temporarily alter tissue mass, resulting in inconsistent weight gain relative to shell expansion. These patterns also suggest energy reallocation between somatic maintenance and reproduction, a common phenomenon in bivalves subjected to shifting environmental and nutritional regimes in wild estuarine systems. (Dridi et al., 2007; Singh, 2017).

Among all morphometric predictors, shell height emerged as a more robust indicator of total biomass compared to length or width, reinforcing its utility in field-based assessments. Similar outcomes were reported by Nagi et al. (2011) for *C. madrasensis*, and by Derbali et al. (2023) for *Pinctada radiata*, where height-to-weight ratios demonstrated consistent predictive accuracy in growth evaluations. However, the weaker association of shell width with biomass suggests this trait is less functionally relevant for weight prediction, likely due to its limited role in overall energy storage or environmental buffering (Powell et al., 2016). The prevalence of negative allometry in this study aligns with observations from other estuarine bivalve species such as *Ruditapes decussatus* and *Mytilus galloprovincialis*, where shell elongation appears favoured under nutrient-limited or highly variable habitats (Béjaoui et al., 2008; Urrutia et al., 1999). Collectively, these growth tendencies underscore the species' physiological plasticity and ecological adaptability, allowing *C. madrasensis* to thrive under a wide range of environmental conditions while maintaining reproductive viability.

4.2. Size structure, sex ratios, and adaptive reproductive strategies of *C. madrasensis*

The observed population structure and reproductive dynamics of the *C. madrasensis* provide valuable insights into its ecological adaptability and reproductive strategy in the tropical estuarine environment of the southeast coast of Bangladesh. The unimodal size-frequency distribution centered around the 80–90 mm shell length class suggests a relatively synchronized population dominated by mid-sized, likely reproductively active individuals. Such a size structure is often indicative of successful recruitment and population stability (Gosling, 2015; Beukema and Cadée, 1996), particularly in environments where food availability and hydrological parameters remain within tolerable ranges for larval settlement and juvenile survival (Newell, 2004). The dominance of reproductively mature classes in the current study aligns with reports from other tropical oyster populations such as *C. rhizophorae* and *Saccostrea cucullata*, where similar unimodal distributions were associated with seasonal but consistent recruitment pulses (Lenz and Boehs, 2011; Aban et al., 2017). The presence of individuals exceeding 100 mm,

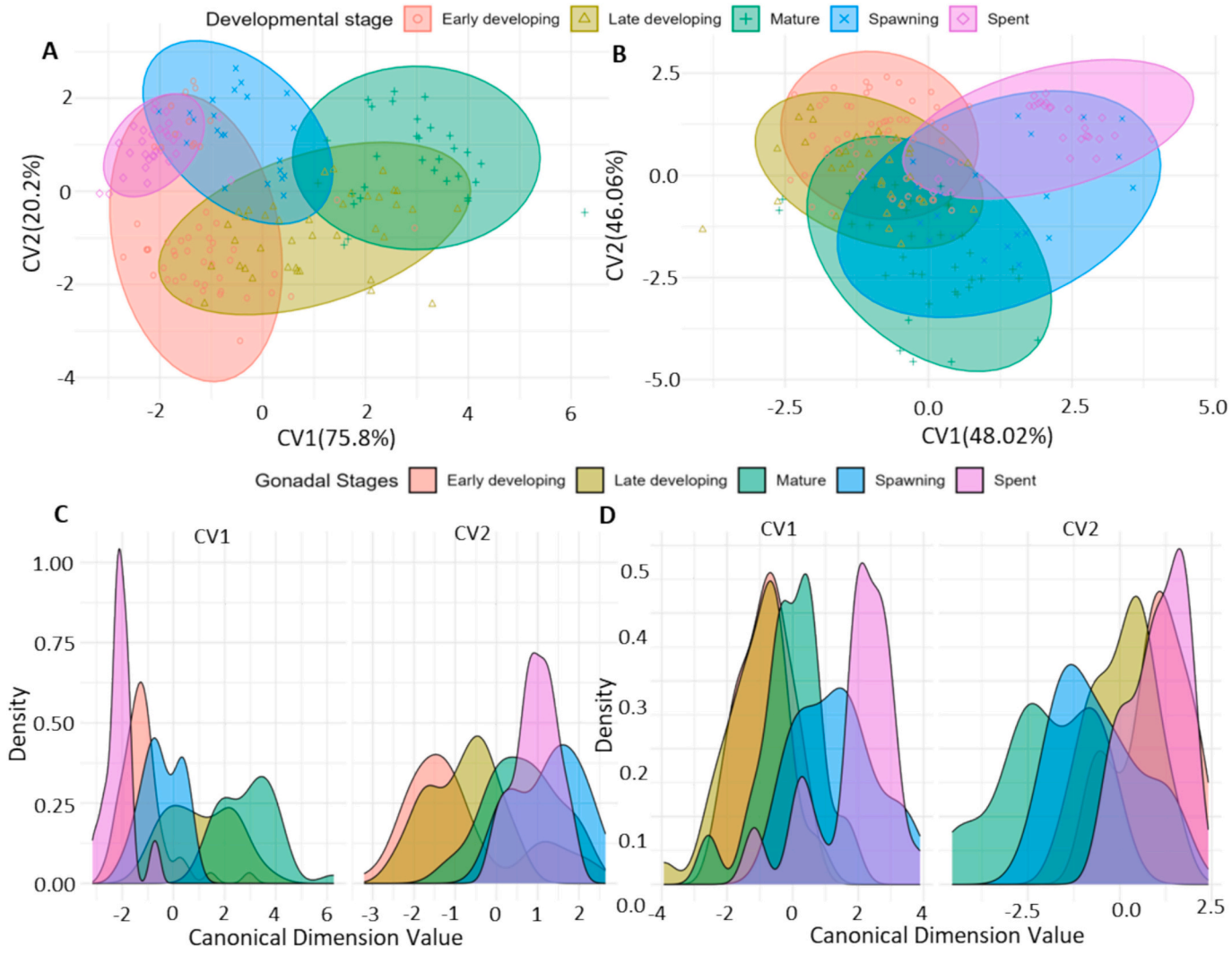

Fig. 9. Canonical Variate Analysis (CVA) of the gonad developmental stages and plankton ingestion during pre-monsoon and post-monsoon gametogenic cycle of oyster, *Crassostrea madrasensis* collected from the Moheshkhali Channel along the Southeast Coast of the Bay of Bengal, Bangladesh. The figure presents Canonical Variate Analysis (CVA) in panels A-D, demonstrating the separation of oyster developmental stages during pre-monsoon (A, C) and post-monsoon (B, D) periods.

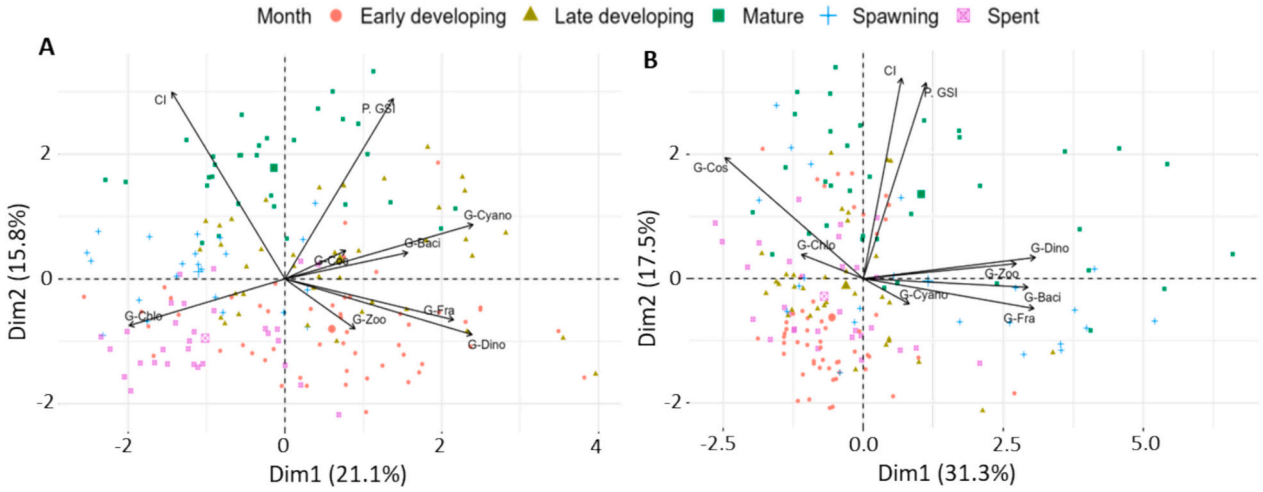

Fig. 10. Principal Component Analysis (PCA) biplots, illustrating the relationships between gut plankton composition, Condition Index (CI), and Presumptive Gonadosomatic Index (P.GSI) in oysters during pre-monsoon (A) and post-monsoon (B) gametogenic phases.

though fewer, suggests that some members of the population achieve faster growth, a trait associated with environmental stability and

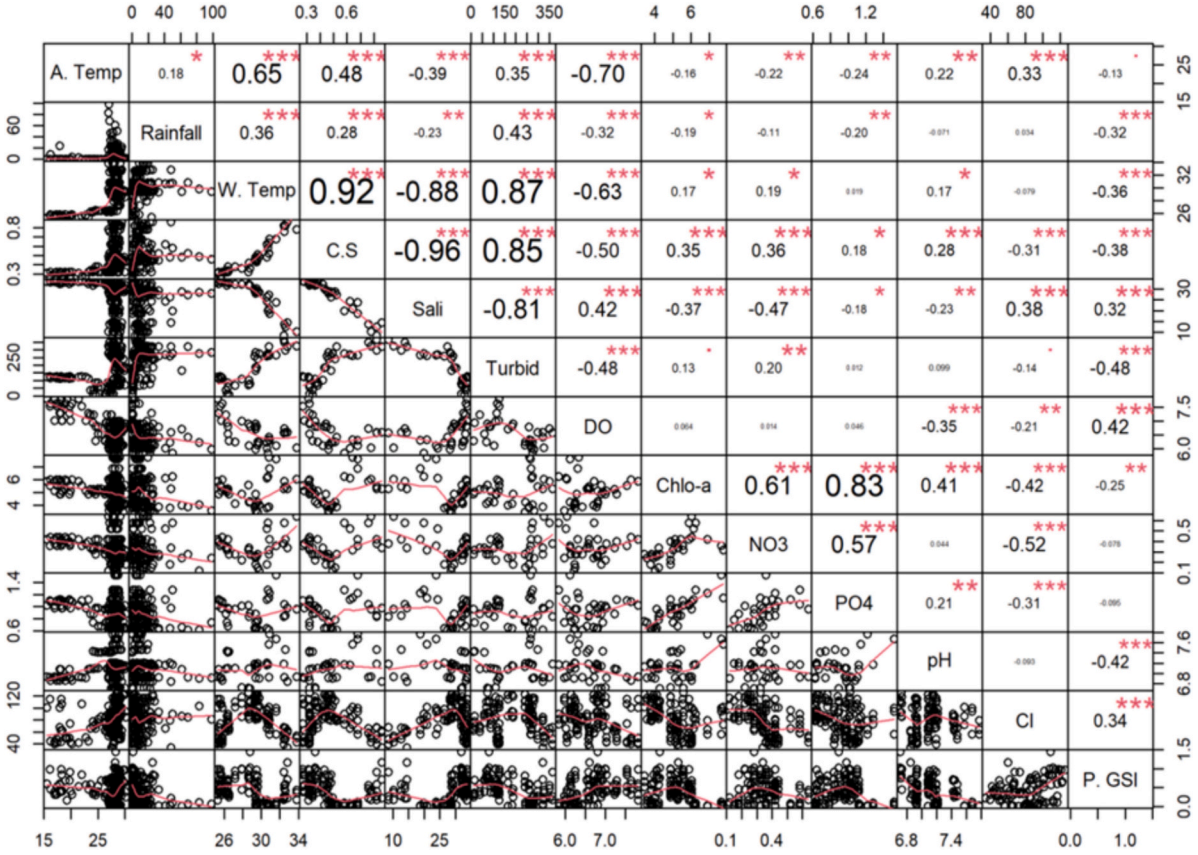

Fig. 11. Interrelations among various water quality parameters, condition index and presumptive gonadosomatic index values of oysters, *Crassostrea madrasensis* during pre-monsoon gametogenic cycle collected from the Moheshkhali Channel along the Southeast Coast of the Bay of Bengal, Bangladesh. Here, the variables' full forms: A.Temp- Air Temperature (°C); Rainfall; W. Temp - Water Temperature (°C); C.S.- water current speed (ms^{-1}); Sali- Salinity (ppt), Turbid- Turbidity (NTU); DO-Dissolved Oxygen (mg L^{-1}); Chlo.a- chlorophyll *a* (μg/L); NO3-Nitrate-nitrogen (mg L^{-1}); PO4-Phosphate phosphorus (mg L^{-1}); pH- water pH; CI- Condition Index; P.GSI- Presumptive gonadosomatic index (%). Values given around all axes are the range of the individual parameters' measured values. Correlation coefficients are represented numerically, with significance denoted by asterisks (*p < 0.05, **p < 0.01, ***p < 0.001).

reduced anthropogenic disturbance (Bayne, 2017).

The sex ratio and temporal distribution of reproductive stages highlight the complexity of sexual plasticity in *C. madrasensis*. The maintenance of a balanced sex ratio across seasons, despite monthly fluctuations, underscores the species' ability to sustain reproductive homeostasis, a trait similarly documented in *C. gigas* and *C. rhizophorae* populations in other tropical and subtropical regions (Lango-Reynoso et al., 1999; Lee et al., 2010; Lenz and Boehs, 2011). This equilibrium suggests that sex allocation in *C. madrasensis* is regulated by both internal physiological mechanisms and extrinsic environmental cues, including salinity, temperature, and food availability (Guo et al., 1998; Gosling, 2003).

A resource-mediated reproductive strategy is suggested by seasonal shifts in sex prevalence, which are characterized by female dominance during nutrient-rich pre-monsoon and monsoon months and increased male frequency during early and late post-monsoon as females need higher metabolic input for oogenesis, which aligns their reproductive effort with periods of elevated primary productivity (Ruiz et al., 1992; Murua and Saborido-Rey, 2003). In contrast, males, which recover faster due to lower energetic costs, predominate during regeneration phases. Furthermore, the finding of hermaphrodites, especially during transitional months, suggests the possibility of sequential hermaphroditism, a reproductive adaptation seen in a variety of oysters, such as *C. gigas* and *C. virginica*, which is frequently impacted by environmental cues, age, and energy levels (Lango-Reynoso et al., 2000; Vaschenko et al., 2013), highlighting the flexibility and ecological resilience of *C. madrasensis* in fluctuating estuarine environments. Additionally, the low frequency of undifferentiated individuals confined to post-spawning periods reflects synchronized reproductive timing, where gametogenic rest phases likely occur in response to re-establish energy reserves before the next gametogenic cycle, particularly in species with extended or multiple spawning episodes (Chávez-Villalba et al., 2002; Galtsoff, 1964). Overall, the stable sex ratio, combined with seasonal plasticity and the occurrence of intermediate and undifferentiated stages, reinforces the view that *C. madrasensis* employs a flexible, environment-sensitive reproductive strategy. These characteristics not only reflect evolutionary adaptation to estuarine dynamics but also position this species as a resilient candidate for sustainable aquaculture development in tropical regions (Southgate and Lucas, 2008; Helm et al., 2004).

4.3. Seasonal gametogenic dynamics and reproductive strategy of *C. madrasensis*

The reproductive biology of *C. madrasensis* reveals a seasonally synchronized yet environmentally responsive strategy, enabling successful propagation in tropical estuarine habitats. The species exhibited two distinct gametogenic cycles each year, coinciding with the pre- and post-monsoon periods, an adaptive reproductive strategy typical of tropical oysters thriving in environments with fluctuating ecological parameters and nutrient availability (Gosling, 2003; Southgate and Lucas, 2008). The cyclical pattern of reproductive phases seems closely linked to the availability of biological energy, demonstrated by the alignment among gonadal histology, CI, and P.GSI. Histological observations underscore a tightly regulated sequence of gonadal development, reflecting distinct developing, mature, spawning, and spent stages. This progression, observed in both males and females, supports

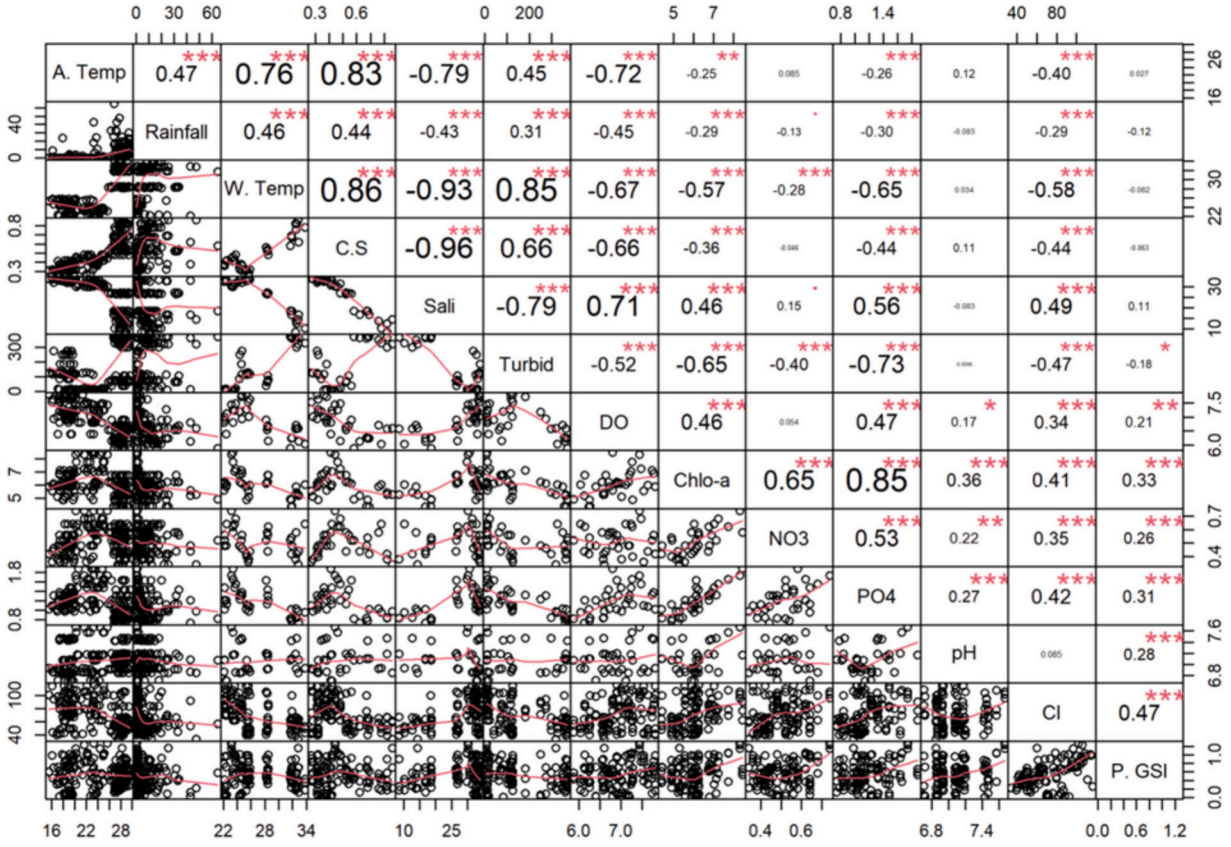

Fig. 12. Interrelations among various water quality parameters, condition index (CI) and presumptive gonadosomatic index (P.GSI) values oysters, *Crassostrea madrasensis* during post-monsoon gametogenic cycle collected from the Moheshkhali Channel along the Southeast Coast of the Bay of Bengal, Bangladesh. Here, the variables' full forms: A.Temp- Air Temperature (°C); Rainfall; W. Temp - Water Temperature (°C); C.S.- water current speed (m/s); Sali- Salinity (ppt), Turbid- Turbidity (NTU); DO-Dissolved Oxygen (mg l 1); Chlo.a- chlorophyll *a* (μg/L); NO3·N-Nitrate-nitrogen (mg l-1); PO4·P-Phosphate phosphorus (mg l-1); pH- water pH; CI- Condition Index; P.GSI- Presumptive gonadosomatic index (%). Values given around all axes are the range of the individual parameters' measured values. Correlation coefficients are represented numerically, with significance denoted by asterisks (*p < 0.05, **p < 0.01, ***p < 0.001).

the theory that oysters in tropical systems engage in continuous gametogenesis, punctuated by seasonally induced spawning events (Ruiz et al., 1992; Ojea et al., 2004). The presence of continuous gametogenesis aligns with patterns reported in other estuarine populations of *C. madrasensis* from Mulki Estuary and Korampallam Creek in India (Joseph et al., 1984; Palaniswamy, 1993), although minor temporal shifts are evident, reflecting regional climatic differences and local hydrographic variability. Notably, the sharp decline in GSI during the monsoon season (July–September), coupled with low CI values, reflects a temporary suppression of spawning activity. This period is likely driven by elevated freshwater inflow, reduced salinity, and nutrient dilution, which can impede gamete release despite the presence of developing gonads (Narváez et al., 2008; Paixão et al., 2013).

Temperature and food availability emerged as key modulators of reproductive effort. The pre-monsoon spawning event coincided with sea surface temperatures ranging from 28 to 33 °C, consistent with the optimal range (25–30 °C) for gametogenesis previously identified for *C. madrasensis* (Uddin et al., 2024; Mawa et al., 2023). Supporting this, both field and laboratory studies on *C. gasar* have shown a positive correlation between elevated temperatures and enhanced gonadal development (Gomes et al., 2014; Ramos et al., 2014; Castilho-Westphal et al., 2015; Legat et al., 2021). Subsequently, the post-monsoon spawning peak, marked by mature and spawning gonads alongside elevated P.GSI, reflects a secondary reproductive effort, potentially facilitated by stabilized salinity, nutrient recovery, increased abundance of plankton following monsoon flushing (Asaduzzaman et al., 2019, 2020; Noor et al., 2021). This bimodal spawning strategy enables reproductive assurance by distributing gamete release across multiple environmental windows, increasing larval survival probabilities under variable estuarine conditions (Galtsoff, 1964; Lango-Reynoso et al., 2000). Furthermore, the absence of spawning activity during peak monsoon months does not denote reproductive dormancy but rather a temporary pause in spawning as temperature rises to its maximum, but salinity and food availability decreased due to heavy rainfall and freshwater runoff (Narváez et al., 2008). Interestingly, histological sections still revealed ongoing gonadal development during this period, suggesting that gametogenesis and spawning may be uncoupled under environmental stress, allowing individuals to resume spawning rapidly once favourable conditions return (Ezgeta Balić et al., 2020; Bernard et al., 2011).

Importantly, the alignment between histological data and physiological indices reinforces the validity of using CI and P.GSI as proxy indicators of reproductive timing, especially where direct histological monitoring is logistically constrained. This integrative approach offers insights into the reproductive investment dynamics of *C. madrasensis*, revealing that this species modulates gametogenesis based on internal condition and external environmental signals. Collectively, these findings highlight the reproductive plasticity and seasonal adaptation of *C. madrasensis*, underscoring its resilience and potential for sustainable aquaculture in tropical coastal systems with pronounced hydrographic seasonality.

4.4. Gonadal stage-specific feeding strategies in C. madrasensis

The dynamic interplay between plankton composition and reproductive physiology in *C. madrasensis* reveals an intricate strategy of

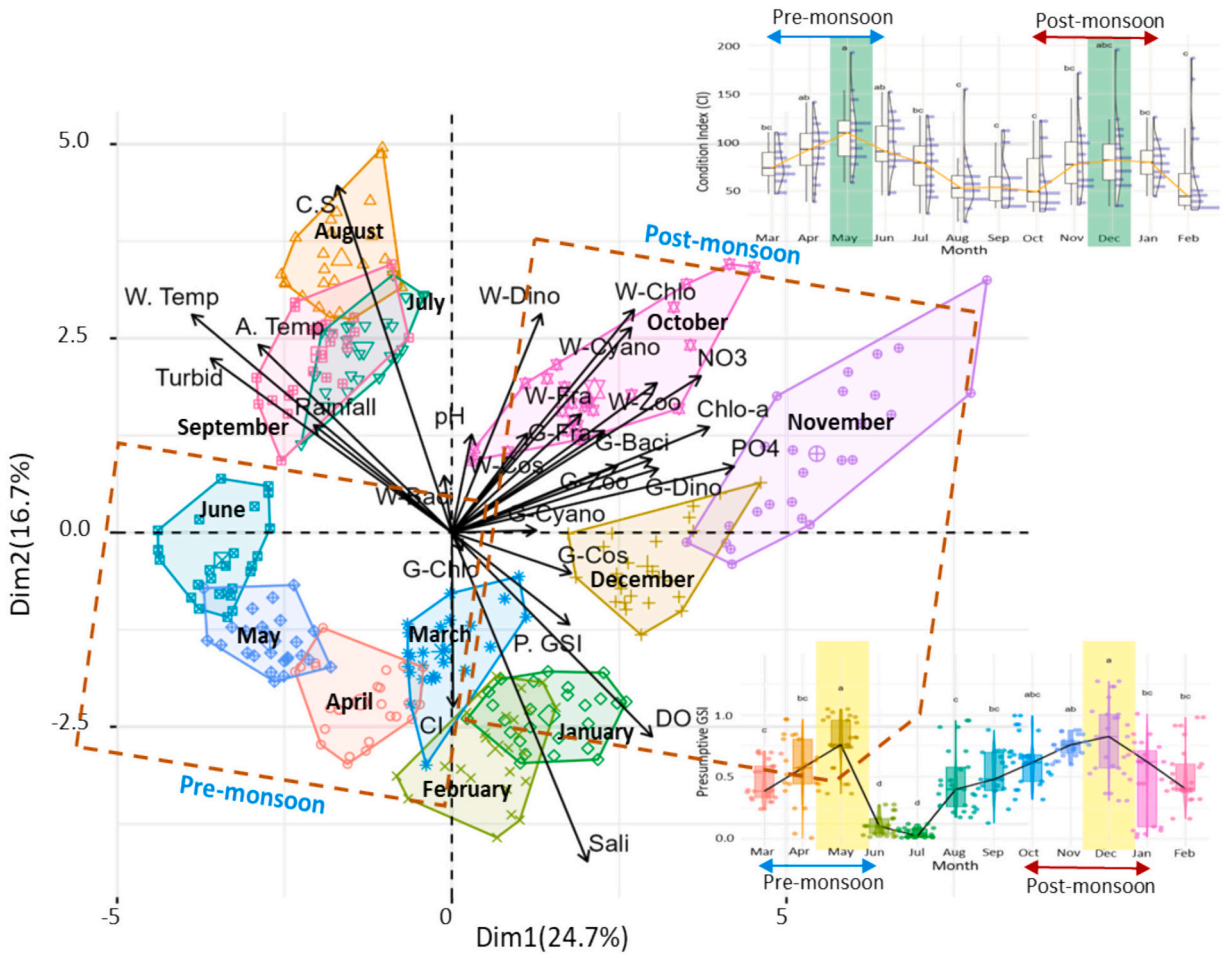

Fig. 13. Biplot of Principal Component Analysis (PCA) illustrating the relationships among the environmental parameters, water plankton, ingested gut plankton, condition index (CI) and presumptive gonadosomatic index (P.GSI) of oysters, *Crassostrea madrasensis* collected from the Moheshkhali Channel along the Southeast Coast of the Bay of Bengal, Bangladesh. The bar chart within the figure displays the month-to-month fluctuations in the CI and P.GSI of *C. madrasensis*. The abbreviations used represent the following variables: P.GSI- presumptive gonadosomatic index; CI- condition index; C.S- water current speed (m/s); W.Temp – water temperature (°C); A. Temp – air temperature (°C); Sali – salinity (ppt); Turbid – turbidity (NTU); DO – dissolved oxygen (ppm); Chl.a – chlorophyll *a* concentration (μg/L); NO3 – nitrate-nitrogen (ppm); PO4 – phosphate-phosphorus (ppm); W.Cos – water Coscinodiscophyceae; W.Fra – water Fragillariophyceae; W.Baci – water Bacillariophyceae; W.Chlo – water Chlorophyceae; W.Cyano – water Cyanophyceae; W.Dino –water Dinophyceae; W.Zoo –water Zooplankton; G.Cos – gut Coscinodiscophyceae; G.Fra – gut Fragilariophyceae; G.Baci – gut Bacillariophyceae; G.Chlo – gut Chlorophyceae; G.Cya – gut Cyanophyceae; G.Dino – gut Dinophyceae; G.Zoo – gut Zooplankton.

nutritional adaptation that aligns with gametogenic progression. Seasonal variability, particularly between pre- and post-monsoon phases, acts as a pivotal ecological driver shaping feeding preferences and energetic investments in oysters (Ren et al., 2000; Zhou et al., 2015). In our study, plankton ingestion was found to peak during the early to mid-gametogenic phases, while the spawning phase does not coincide with maximum ingestion. Such stage-specific dietary patterns are consistent with the energy-intensive nature of gametogenesis, where nutrient acquisition is tightly coupled with oocyte and spermatocyte formation (Enríquez-Díaz et al., 2009). This temporal decoupling between peak feeding and gamete release is consistent with the "feed-then-reproduce" strategy observed in other broadcast-spawning bivalves (Bayne et al., 1982; Pernet et al., 2007). Notably, early and late gametogenic phases are often associated with elevated assimilation of essential biochemical constituents, particulary polyunsaturated fatty acids (PUFAs) sourced from phytoplankton (Whyte et al., 1990; Pernet et al., 2007; Ferdous et al., 2025). These primary producers are known to be rich in eicosapentaenoic acid (EPA) and docosahexaenoic acid (DHA), which serve as critical precursors for reproductive tissue development (Langdon and Waldock, 1981; Gallager et al., 1986). The preferential ingestion of such taxa during early development stages may therefore act as a preparatory mechanism to stockpile energy reserves required for subsequent reproductive events.

Interestingly, the transition to mature and spawning stages did not exhibit a broadened planktonic spectrum but instead appeared to narrow toward specific taxa like Chlorophyceae during the pre-monsoon and Bacillariophyceae and Dinophyceae post-monsoon. This reduction in diversity may not necessarily indicate decreased feeding activity but rather a shift toward targeted ingestion of high-energy, bioavailable food sources optimally suited for final gamete maturation (Martínez-Pita et al., 2012). Moreover, the temporal decoupling between peak feeding and gamete release supports earlier findings in *C. gigas* and *Mytilus edulis*, where feeding intensity peaks weeks before spawning, allowing time for resource assimilation and gonadal buildup (Pazos et al., 1996; Beninger and Lucas, 1984; Pernet et al., 2007). Such anticipatory feeding is a hallmark of evolutionary optimization in broadcast spawners inhabiting seasonal environments. Taken together, these findings highlight an ecologically responsive and energetically efficient feeding strategy in *C. madrasensis*, finely tuned to seasonal plankton dynamics and reproductive imperatives.

4.5. Endogenous reserves and exogenous inputs: a biphasic reproductive strategy of C. madrasensis

The reproductive dynamics of *C. madrasensis* appear to be tightly linked to seasonal environmental oscillations and food availability, with oysters displaying a highly synchronized physiological strategy that aligns reproductive effort with prevailing ecological conditions. This seasonal alignment highlights how bivalve reproductive cycles have evolved to be more fit under changing environmental conditions (Bayne, 2017; Gosling, 2015). During the pre-monsoon period, oysters enter gametogenesis under moderate environmental forcing, notably in the absence of significant nutrient loading or phytoplankton blooms (Fig. 11). The lack of strong external cues during this phase implies that *C. madrasensis* may initiate reproductive development using endogenous reserves accumulated during earlier productive phases. This reserve-dependent reproductive strategy is well-documented in bivalves; for instance, Pacific oysters (*C. gigas*) use stored glycogen, and lipid reserves to fuel gametogenesis when external food is scarce (Dridi et al., 2007). The ability to capitalize on minimal resources during pre-monsoon months reflects physiological resilience and suggests that the gonadal development is not solely dependent on immediate planktonic intake but rather on a balance of prior energy acquisition and metabolic efficiency, a strategy similarly observed in Chesapeake Bay where reproductive investment often occurs before phytoplankton blooms, indicating reliance on stored energy (Newel, 1996). Such observations mirror the energy metabolism strategy described in *Ostrea angasi*, where gametogenic energy demands are met through both stored energy and instantaneous food intake across overlapping temporal windows (Mendo et al., 2016).

By contrast, the post-monsoon season offers a more resource-rich environment, characterized by elevated salinity, dissolved oxygen, and chlorophyll-a concentrations, alongside spikes in nitrate and phosphate. These environmental conditions collectively trigger post-monsoon phytoplankton blooms, which constitute nutritionally valuable planktonic groups. Among them, Coscinodiscophyceae are widely regarded as a high-quality food source for filter-feeding bivalves due to their richness in essential fatty acids, especially eicosapentaenoic acid (EPA), and the structural properties of their siliceous frustules that enhance digestibility (Celi et al., 2022; Ghobara et al., 2024). In addition, *C. madrasensis* may preferentially ingest Dinophyceae despite their smaller size or motility, likely influenced by chemical attractants or superior biochemical composition, as documented in other filter-feeding species (Cheng et al., 2020; Davenport et al., 2011). The availability of such high-quality phytoplankton during the post-monsoon period provides oysters with an enriched food base, effectively supporting peak gametogenic activity and reproductive success. This strategy, where active feeding and nutrient assimilation precede and support gamete maturation and spawning, has been described in several bivalve species, aligning with the concept of trophic synchronization (Luna-González et al., 2008; Utting and Millican, 1997).

These findings collectively illustrate that *C. madrasensis* follows a biphasic nutritional and reproductive strategy: a conservative phase during the pre-monsoon, where internal energy stores and moderate plankton support gametogenesis, followed by an externally fueled (opportunistic) phase during the post-monsoon, where abundant, high-quality plankton and improved water quality conditions sustain advanced maturation and spawning (Ferdous et al., 2025). This seasonal modulation of physiological effort, contingent on both internal and external cues, reflects an adaptive response to the coastal monsoonal regime, enhancing reproductive success in a highly dynamic estuarine ecosystem.

5. Conclusion

This study provides a comprehensive understanding of the reproductive biology, biometric growth patterns, and environmental interactions influencing *C. madrasensis* along the southeast coast of Bangladesh. The species exhibited bimodal spawning cycles during the pre-monsoon (April–June) and post-monsoon (October–December) periods, regulated by favourable thermal conditions and enhanced phytoplankton availability. The observed reproductive plasticity, including sequential hermaphroditism and stable sex ratios, underscores the species' adaptive resilience to dynamic estuarine environments. Moreover, multivariate analyses revealed strong associations between reproductive stages, condition indices, and environmental variables such as temperature, salinity, and nutrient levels, reinforcing the importance of trophic and hydrological cues in modulating reproductive investment. Importantly, spawning toward the end of the pre-monsoon likely results in larval development during the monsoon, when early life stages may experience heightened sensitivity to environmental stress. Larval survival under these conditions likely reflects a trade-off between increased food availability driven by nutrient enrichment and adverse factors such as reduced salinity, elevated turbidity, and strong hydrodynamic forcing. Further research should therefore aim to incorporate multi-year, multi-site studies to examine spatiotemporal variability and potential long-term effects of climate change on reproductive dynamics. Additionally, integrating biochemical approaches like lipid and fatty acid profiling with molecular techniques for sex determination and gametogenic regulation could yield deeper insights into energy allocation strategies and the physiological mechanisms underlying reproductive plasticity. In addition, these expanded approaches would strengthen precautionary conservation and management strategies, supporting the long-term resilience and sustainability of oyster population in fluctuating tropical estuarine ecosystems. Despite these limitations, the findings deepen our understanding of the life history traits of *C. madrasensis*, offering valuable insights for hatchery management, stock enhancement, and sustainable aquaculture development in tropical estuarine systems under changing environmental conditions.

Declaration of generative AI in scientific writing

During the preparation of this work, the authors used ChatGPT in the writing process to improve the readability and language of the manuscript. After using this tool/service, the authors reviewed and edited the content as needed and took full responsibility for the content of the published article

CRediT authorship contribution statement

Afshana Ferdous: Writing – original draft, Software, Methodology, Investigation, Formal analysis, Data curation. **Israt Jahan:** Writing – review & editing, Methodology, Formal analysis, Data curation. **Sourav Chowdhury:** Writing – review & editing, Methodology, Data curation. **Md Ramzan Ali:** Writing – review & editing, Methodology, Investigation. **Md Nayeem Hossain:** Software, Formal analysis, Data curation. **Md Moshiur Rahman:** Writing – review & editing, Software, Formal analysis, Data curation. **Mohammad Sadequr Rahman Khan:** Writing – review & editing, Supervision, Project administration, Funding acquisition. **Md Asaduzzaman:** Writing – review & editing, Supervision, Project administration, Funding acquisition, Data curation, Conceptualization.

Declaration of competing interest

The authors declare that they have no known competing financial interests or personal relationships that could have appeared to influence the work reported in this paper.

Acknowledgements

This work was conducted as a part of the research plan of the Bangladesh Academy of Sciences- United States Department of

Agriculture (BAS-USDA) Endowment 5th phase project implemented by Chattogram Veterinary and Animal Sciences University through a collaborative agreement with BAS (F 127). We would like to thank the director and other staff of the BAS-USDA Endowment Program for providing funding for this research work. We also thank the staff of the Oceanography Laboratory, Department of Marine Bioresource Science, Chattogram Veterinary and Animal Sciences University, for helping with oyster sampling and parameter analysis.

Data availability

Data will be made available on request.

References

Aban, M.S., Albert, T.F., Rey, S., Comelia, E., 2017. Length-weight relationships of the Asian green mussel, *Perna viridis* (Linnaeus, 1758) (Bivalvia: Mytilidae) population in Bolinao Bay, Pangasinan, Northern Philippines. J. Nat. Allied Sci. 1 (1), 1–6.

Alagarswami, K., Chellam, A., 1976. On fouling and boring organisms and mortality of pearl oysters in the farm at Veppalodai, Gulf of Mannar. Indian J. Fish 23 (1&2), 10–22.

Al-Kandari, M., Al-Yamani, F.Y., Al-Rifaie, K., 2009. Marine Phytoplankton Atlas of Kuwait's Waters. Kuwait Institute of Scientific Research, Kuwait, 351 pp.

APHA, 1992. Standard methods for the examination of water and wastewater, 18th ed. American Public Health Association (APHA), American Water Works Association (AWWA), Water Pollution Control Federation (WPCF), Washington, DC.

Arjarasirikoon, U., Kruatrachue, M., Sretarugsa, P., Chitramvong, Y., Jantataeme, S., Upatham, E.S., 2004. Gametogenic processes in the pearl oyster, *Pteria penguin* (Röding, 1798) (Bivalvia, Mollusca). J. Shellfish Res. 23, 403–410.

Asaduzzaman, M., Rahi, N.A., Rahman, M.M., Akter, S., Hoque, N.F., Shakil, A., Wahab, M.A., 2019. Reproductive biology and ecology of the green mussel *Perna viridis*: a multidisciplinary approach. Biology 8 (4), 88. https://doi.org/10.3390/biology8040088.

Asaduzzaman, M., Akter, S., Hoque, N.F., Shakil, A., Noor, A.R., Akter, M.N., Rahman, M. M., 2020. Multifaceted linkages among eco-physiological factors, seasonal plankton dynamics and selective feeding behavior of the green mussel (*Perna viridis*) in the south-east coast of the Bay of Bengal. J. Sea Res. 160, 101933. https://doi.org/10.1016/j.seares.2020.101933.

Asaduzzaman, M., Nahiduzzaman, M., Chowdhury, M.T.H., Rahman, M.M., Mamun, A. A., Hossain, M.M., 2025. Advancing low-trophic extractive mariculture (LTEM): strategies for a thriving blue economy in Bangladesh. Mar. Policy 173, 106557. https://doi.org/10.1016/j.marpol.2024.106557.

Bayne, B.L., 2017. Bivalve mariculture in two-way interaction with phytoplankton. Bull. Univ. Agric. Sci. Vet. Med. Cluj-Napoca 77 (2).

Bayne, B.L., Thompson, R.J., Widdows, J., 1982. Physiology I. In: The Mollusca, vol. 4. Academic Press, pp. 1–64.

Béjaoui, B., Harzallah, A., Moussa, M., Chapelle, A., 2008. Modèle couplé dynamique-écologie pour la lagune de Bizerte.

Beninger, P.G., Lucas, A., 1984. Seasonal variations in condition, reproductive activity, and gross biochemical composition of two species of adult clam reared in a common habitat: *Tapes decussatus* (L.) and *Tapes philippinarum* (Adams and Reeve). J. Exp. Mar. Biol. Ecol. 79, 19–37. https://doi.org/10.1016/0022-0981(84)90028-5.

Bernard, I., De Kermoysan, G., Pouvreau, S., 2011. Effect of phytoplankton and temperature on the reproduction of the Pacific oyster *Crassostrea gigas*: investigation through DEB theory. J. Sea Res. 66 (4), 349–360. https://doi.org/10.1016/j.seares.2011.07.009.

Beukema, J.J., Cadée, G.C., 1996. Consequences of the sudden removal of nearly all mussels and cockles from the Dutch Wadden Sea. Mar. Ecol. Prog. Ser. 17, 279–289. https://doi.org/10.1111/j.1439-0485.1996.tb00508.x.

Botes, L., 2001. Phytoplankton Identification Catalogue – Saldanha Bay, South Africa. GloBallast Monograph Series No. 7. IMO, London, 88 pp.

Boyd, C.E., 1979. Water Quality in Warm Water Fish Ponds. Auburn University, Auburn, AL, USA, p. 359.

Castilho-Westphal, G.G., Magnani, F.P., Ostrensky, A., 2015. Gonad morphology and reproductive cycle of the mangrove oyster Crassostrea brasiliana (Lamarck, 1819) in the baía de Guaratuba, Paraná, Brazil. Acta Zool. 96 (1), 99–107.

Celi, C., Fino, D., Savorani, F., 2022. *Phaeodactylum tricornutum* as a source of value-added products: a review on recent developments in cultivation and extraction technologies. Bioresour. Technol. Rep. 19, 101122. https://doi.org/10.1016/j.biteb.2022.101122.

Çelik, M.Y., Karayücel, S., Karayücel, İ., Eyüboğlu, B., Öztürk, R., 2015. The effects of environmental factors on survival, growth and biochemical composition of transplanted oysters (*Ostrea edulis* L innaeus, 1758) from Aegean Sea to southern Black Sea. Aquac. Res. 46 (4), 959–968. https://doi.org/10.1111/are.12253.

Chávez-Villalba, J., Cáceres-Martínez, J., Mazón-Suástegui, J.M., Enríquez-Espinoza, T., 2002. Gametogenic cycle of the pearl oyster *Pinctada mazatlanica* in the Gulf of California. Aquaculture 213 (1–4), 311–322. https://doi.org/10.1016/S0044-8486(02)00123-6.

Chávez-Villalba, J., Villelas-Ávila, R., Cáceres-Martínez, C., 2007. Reproduction, condition and mortality of the Pacific oyster *Crassostrea gigas* (Thunberg) in Sonora, México. Aquac. Res. 38 (3), 268–278. https://doi.org/10.1111/j.1365-2109.2007.01662.x.

Cheng, P., Zhou, C., Chu, R., Chang, T., Xu, J., Ruan, R., Chen, P., Yan, X., 2020. Effect of microalgae diet and culture system on the rearing of bivalve mollusks: nutritional properties and potential cost improvements. Algal Res. 51, 102076. https://doi.org/10.1016/j.algal.2020.102076.

Dag, O., Dolgun, A., Konar, N.M., 2017. One-Way Tests in Independent Groups Designs. R Package Version 1.5. Available from: https://CRAN.R-project.org/package=onewaytests (accessed 04.12.2019).

Davenport, J., Ezgeta-Balić, D., Peharda, M., Skejić, S., Ninčević-Gladan, Ž., Matijević, S., 2011. Size-differential feeding in *Pinna nobilis* L. (Mollusca: Bivalvia): exploitation of detritus, phytoplankton and zooplankton. Estuar. Coast. Shelf Sci. 92, 246–254. https://doi.org/10.1016/j.ecss.2010.12.033.

Delgado, M., Pérez-Camacho, A., 2005. Histological study of the gonadal development of *Ruditapes decussatus* (L.) (Mollusca: Bivalvia) and its relationship with available food. Sci. Mar. 69 (1), 87–97. https://doi.org/10.3989/scimar.2005.69n187.

Delgado, M., Pérez-Camacho, A., 2007. Comparative study of gonadal development of *Ruditapes philippinarum* (Adams and Revé) and *Ruditapes decussatus* (L.) (Mollusca, Bivalvia): influence of temperature. Sci. Mar. 71 (3), 471–481. https://doi.org/10.3989/scimar.2007.71n3471.

Derbali, A., Jarboui, O., Ghorbel, M., 2023. Comparative study of biometric characters in the pearl oyster *Pinctada radiata* from the islands of Kerkennah (Southern Tunisia). Bull. Inst. Natl. Sci. Tech. Mer 39, 5–13.

Dridi, S., Romdhane, M.S., Leitao, A., El Cafsi, M., 2006. Evidence for *Crassostrea gigas* reproduction in the Bizert lagoon of Tunisia. J. Biol. Res. 5, 35–45.

Dridi, S., Romdhane, M.S., El Cafsi, M., 2007. Seasonal variation in weight and biochemical composition of the Pacific oyster *Crassostrea gigas* in relation to the gametogenic cycle and environmental conditions of the Bizerta lagoon, Tunisia. Aquaculture 263, 238–248. https://doi.org/10.1016/j.aquaculture.2006.10.028.

El-Sayed, A.E.H., Razek, F.A.A., Abou-Zaid, M.M., Taha, S.M., 2011. Measures of allometric growth of black-lip pearl oyster *Pinctada margaritifera* (Linnaeus, 1758) Red Sea, Egypt. Int. J. Zool. Res. 7 (2), 201–211. https://doi.org/10.3923/ijzr.2011.201.211.

Enríquez-Díaz, M., Pouvreau, S., Chávez-Villalba, J., Le Pennec, M., 2009. Gametogenesis, reproductive investment, and spawning behavior of the Pacific giant oyster *Crassostrea gigas*: evidence of an environment-dependent strategy. Aquac. Int. 17 (5), 491–506. https://doi.org/10.1007/s10499-008-9219-1.

Etchian, O.A., Pellerin, J., Audet, C., Mathieu, M., 2004. Sexual maturation and related changes in aspartate transcarbamylase activity of gonad tissues in the soft shell clam (*Mya arenaria*). Comp. Biochem. Physiol. B Biochem. Mol. Biol. 139, 287–297. https://doi.org/10.1016/j.cbpc.2004.08.006.

Ezgeta Balić, D., Radonić, I., Bojanić Varezić, D., Zorica, B., Arapov, J., Stagličić, N., Jozić, S., Peharda, M., Briski, E., Lin, Y., Šegvić-Bubić, T., 2020. Reproductive cycle of a non-native oyster, *Crassostrea gigas*, in the Adriatic Sea. Mediterr. Mar. Sci. 21 (1), 146–156. https://doi.org/10.12681/mms.21304.

Fabioux, C., 2004. Origin and Development of Germ Cells in *Crassostrea gigas* Oyster: Relevance for Controlled Reproduction in Hatchery.

Ferdous, A., Jahan, I., Hossain, M.N., Chowdhury, S., Rahman, M.M., Asaduzzaman, M., 2025. Integrated insight into somato-gonadal fatty acid dynamics and environmental synchrony: unravelling post-monsoon gametogenic strategies of oysters Crassostrea madrasensis in raft-cultivation systems. Aquaculture 743576. https://doi.org/10.1016/j.aquaculture.2025.743576.

Ferreira, M.A.P., Paixão, L.F., Alcântara-Neto, C.P., Santos, S.S.D., Rocha, R.M., 2006. Morphological and morphometric aspects of *Crassostrea rhizophorae* (Guilding, 1828) oocytes in three stages of the gonadal cycle. Int. J. Morphol. 24 (3), 437–442.

Fox, J., Weisberg, S., 2019. An R Companion to Applied Regression, third ed. Sage Publications. https://doi.org/10.32614/CRAN.package.car.

Frías-Espericueta, M.G., Páez-Osuna, F., Osuna-López, J.I., 1997. Seasonal changes in the gonadal state of the oysters *Crassostrea iridescens* and *Crassostrea corteziensis* (Filibranchia: Ostreidae) in the northwest coast of México. Rev. Biol. Trop. 45 (3), 1061–1065. https://doi.org/10.15517/rbt.v45i3.32118.

Frías-Espericueta, M.G., Osuna-López, J.I., Páez-Osuna, F., 1999. Gonadal maturation and trace metals in the mangrove oyster *Crassostrea corteziensis*: seasonal variation. Sci. Total Environ. 231 (2–3), 115–123. https://doi.org/10.1016/S0048-9697(99)00097-2.

Gallager, S.M., Mann, R., Sasaki, G.C., 1986. Lipid as an index of growth and viability in three species of bivalve larvae. Aquaculture 56 (2), 81–103. https://doi.org/10.1016/0044-8486(86)90020-7.

Galtsoff, P.S., 1964. The American oyster *Crassostrea virginica* (Gmelin, 1791). Fish. Bull. Fish Wildl. Serv. 64, 1–480.

Gaughan, D.J., Mitchell, R.W.D., 2000. The Biology and Stock Assessment of the Tropical Sardine, *Sardinella lemuru*, off the Mid-West Coast of Western Australia. Fisheries Research Report. Published by Fisheries Western Australia, Perth.

Ghobara, M., El-Sheekh, M., Hamed, A.F., Abdelhamid, M.A.A., Pack, S.P., 2024. Diatom nanostructured biosilica. In: Abomohra, A., Ende, S. (Eds.), Value-Added Products from Algae. Springer, Cham, pp. 461–492. https://doi.org/10.1007/978-3-031-42026-9_14.

Gomes, C.H.A.M., Silva, F.C., Lopes, G.R., Melo, C.M.R., 2014. The reproductive cycle of the oyster *Crassostrea gasar*. Braz. J. Biol. 74 (4), 967–976. https://doi.org/10.1590/1519-6984.04912.

Gosling, E., 2003. Bivalve molluscs: Biology, ecology and culture. In: Fishing News Books. Blackwell Publishing. https://doi.org/10.1002/9780470995532, 443 pp.

Gosling, E., 2008. Bivalve Molluscs: Biology, Ecology and Culture. John Wiley & Sons, Hoboken, NJ, USA. ISBN 1405147571.

Gosling, E., 2015. Marine Bivalve Molluscs. John Wiley & Sons. https://doi.org/10.1002/9781119045212.

Graves, S., Piepho, H., Dorai-Raj, S., 2024. multcompView: Visualizations of Paired Comparisons. R Package Version 0.1–10. https://github.com/lselzer/multcompview.

Guo, X., Ford, S.E., Zhang, F.S., 1998. Molluscan aquaculture in China. J. Shellfish Res. 17 (1), 1–7.

Helm, M.M., Bourne, N., Lovatelli, A., 2004. Hatchery culture of bivalves: A practical manual. In: FAO Fisheries Technical Paper No. 471. https://doi.org/10.4060/y5720e.

Hemachandra, A., Thippeswamy, S., 2008. Allometry and condition index in green mussel *Perna viridis* (L.) from St Mary's Island off Malpe, near Udupi, India. Aquac. Res. 39, 1747–1758. https://doi.org/10.1111/j.1365-2109.2008.02051.x.

Hossain, K.Z., Jahan, I., Hossain, M.N., Ferdous, A., Ali, M.R., Rahman, M.M., Khan, M.S. R., Asaduzzaman, M., 2025. Feeding selectivity and gametogenic cycle of Crassostrea madrasensis in relation to seasonal plankton and environmental variability in the southeast coast of the Bay of Bengal, Bangladesh. J. Sea Res. 208, 102646. https://doi.org/10.1016/j.seares.2025.102646.

Jha, S., Mohan, P.M., 2014. Biometry and fouling study of intertidal black-lip pearl oyster, *Pinctada margaritifera* (Linnaeus, 1758) to determine their eligibility in the pearl culture industry. J. Res. Biol. 4 (2), 1264–1275.

Joseph, M.M., Stephen, R., Nair, V.R., 1984. Reproductive cycle of *Crassostrea madrasensis* in Mulki estuary. Indian J. Fish. 31 (1), 45–53.

Kim, B., Kang, D., Ko, D., Yang, H., Kim, D., Kang, C., Choi, K., 2010. Annual reproductive cycle of the oyster, *Saccostrea kegaki* (Torigoe & Inaba, 1981) on the southern coast of Jeju Island, Korea. Invertebr. Reprod. Dev. 54 (1), 19–26. https://doi.org/10.1080/07924259.2010.9652312.

Langdon, C.J., Waldock, M.J., 1981. The effect of algal and artificial diets on the growth and fatty acid composition of *Crassostrea gigas* spat. J. Mar. Biol. Assoc. UK 61 (2), 431–448. https://doi.org/10.1017/S0025315400047056.

Lango-Reynoso, F., Devauchelle, N., Le Pennec, M., Hatt, P.J., 1999. Elements of reproductive strategy in oyster, *Crassostrea gigas* from the "Rade de Brest", France. Invertebr. Reprod. Dev. 36, 141–144. https://doi.org/10.1080/07924259.1999.9652690.

Lango-Reynoso, F., Chávez-Villalba, J., Cochard, J.C., Le Pennec, M., 2000. Oocyte size, a means to evaluate the gametogenic development of the Pacific oyster, *Crassostrea gigas* (Thunberg). Aquaculture 190 (1–2), 183–199. https://doi.org/10.1016/S0044-8486(00)00392-6.

Le Pabic, L., Parrad, S., Koua, M.S., Nakasai, S., Saulnier, D., Devaux, D., Ky, C.L., 2016. Culture site dependence on pearl size realization in *Pinctada margaritifera* in relation to recipient oyster growth and mantle graft biomineralization gene expression using the same donor phenotype. Estuar. Coast. Shelf Sci. 182, 294–303. https://doi.org/10.1016/j.ecss.2016.03.009.

Lê, S., Josse, J., Husson, F., 2008. FactoMineR: an R package for multivariate analysis. J. Stat. Softw. 25 (1), 1–18. https://doi.org/10.18637/jss.v025.i01.

Lee, J.S., Lee, Y.G., Kang, S.W., Park, J.S., Lee, D.G., Jeon, M.A., Ju, S.M., 2010. Intersexuality of *Crassostrea gigas* and *Ruditapes philippinarum* in southern coastal waters of Korea. Environ. Health Toxicol. 25, 287–294.

Legat, J.F.A., Puchnick-Legat, A., Sühnel, S., Pereira, A.L.M., Magalhães, A.R.M., de Melo, C.M.R., 2021. Reproductive cycle of the mangrove oyster, *Crassostrea gasar* (Adanson, 1757), in tropical and temperate climates. Aquac. Res. 52 (3), 991–1000. https://doi.org/10.1111/are.14954.

Lenz, T.M., 2008. Biologia reprodutiva da ostra-do-mangue *Crassostrea rhizophorae* (Guilding, 1828) (Bivalvia: Ostreidae) como subsídio à implantação de ostreicultura na Baía de Camamu (BA). Ilhéus-BA, 54 f. Dissertação (Mestrado em Sistemas Aquáticos Tropicais – Ecologia), Universidade Estadual de Santa Cruz.

Lenz, T., Boehs, G., 2011. Ciclo reproductivo del ostión de manglar *Crassostrea rhizophorae* (Bivalvia: Ostreidae) en la Bahía de Camamu, Bahia, Brasil. Rev. Biol. Trop. 59, 137–149.

Liang, F., Xie, S., Fu, S., Li, J., Deng, Y., 2016. Growth pattern and biometric relationship of pearl oyster *Pinctada maxima* cultured in Beibu Bay, China. J. Appl. Aquac. 28 (2), 110–118. https://doi.org/10.1080/10454438.2016.1172535.

Luna-González, A., De Jesús Romero-Geraldo, M., Campa-Córdova, Á., Orduña-Rojas, J., Valles-Jiménez, R., Ruíz-Verdugo, C.A., 2008. Seasonal variations in the immunological and physiological parameters of the Pacific oyster *Crassostrea gigas* cultured in Bahía de Macapule (Sinaloa, Mexico). Aquac. Res. 39 (14), 1488–1497. https://doi.org/10.1111/j.1365-2109.2008.02017.x.

Martínez-Pita, I., Sánchez-Lazo, C., Ruíz-Jarabo, I., Herrera, M., Mancera, J.M., 2012. Biochemical composition, lipid classes, fatty acids and sexual hormones in the mussel *Mytilus galloprovincialis* from cultivated populations in South Spain. Aquaculture 358, 274–283. https://doi.org/10.1016/j.aquaculture.2012.06.003.

Mawa, J., Rana, S., Sultana, N., Al-Nahid, S.A., 2023. Crustacean (Malacostraca) plankton assemblages in the northern Bay of Bengal: a comparison of seasonal and geographical patterns. Ukr. J. Ecol. 13 (2). https://doi.org/10.15421/2023_423.

Mendo, T., Semmens, J.M., Lyle, J.M., Tracey, S.R., Moltschaniwskyj, N., 2016. Reproductive strategies and energy sources fuelling reproductive growth in a protracted spawner. Mar. Biol. 163, 2. https://doi.org/10.1007/s00227-015-2785-7.

Murua, H., Saborido-Rey, F., 2003. Female reproductive strategies of marine fish species of the North Atlantic. J. Northwest Atl. Fish. Sci. 33, 23–31. https://doi.org/10.2960/J.v33.a2.

Nagi, H.M., Shenai-Tirodkar, P.S., Jagtap, T.G., 2011. Dimensional relationship in *Crassostrea madrasensis* (Preston) and *C. gryphoides* (Schlotheim) in mangrove ecosystem. Indian J. Geomar. Sci. 40 (4), 559–566.

Narasimham, K.A., 1980. Fishery and biology of the green mussel, *Perna viridis* (Linnaeus). CMFRI Bull. 29, 10–16.

Narváez, M., Freites, L., Guevara, M., Mendoza, J., Guderley, H., Lodeiros, C.J., Salazar, G., 2008. Food availability and reproduction affects lipid and fatty acid composition of the brown mussel, *Perna perna*, raised in suspension culture. Comp. Biochem. Physiol. B Biochem. Mol. Biol. 149 (2), 293–302. https://doi.org/10.1016/j.cbpb.2007.09.018.

Newel, R.I.E., 1996. Mechanisms and Physiology of Larval and Adult Feeding. The Eastern Oyster.

Newell, R.I., 2004. Ecosystem influences of natural and cultivated populations of suspension-feeding bivalve molluscs: a review. J. Shellfish Res. 23 (1), 51–62.

Noor, A.R., Shakil, A., Hoque, N.F., Rahman, M.M., Akter, S., Talukder, A., Ahmad-Al-Nahid, S., Wahab, M.A., Nahiduzzaman, M., Rahman, M.J., Asaduzzaman, M., 2021. Effect of eco-physiological factors on biometric traits of green mussel *Perna viridis* cultured in the south-east coast of the Bay of Bengal. Bangladesh. Aquacult. Rep. 19, 100562. https://doi.org/10.1016/j.aqrep.2020.100562.

Normand, J., Le Pennec, M., Boudry, P., 2008. Comparative histological study of gametogenesis in diploid and triploid Pacific oysters (*Crassostrea gigas*) reared in an estuarine farming site in France during the 2003 heatwave. Aquaculture 282 (1–4), 124–129. https://doi.org/10.1016/j.aquaculture.2008.06.026.

Octavina, C., Afriana, S., 2024. The length-weight relationship of *Magallana gigas* in Krueng Cut, Province of Aceh, Indonesia. BIO Web Conf. 87, 01004. https://doi.org/10.1051/bioconf/20248701004.

Octavina, C., Yulianda, F., Krisanti, M., Muchlisin, Z.A., 2015. Length-weight relationship of *Ostreidae* in the Kuala Gigieng estuary, Aceh Besar District, Indonesia. Aquacult. Aquarium Conserv. Legis. 8 (5), 817–823. https://doi.org/10.54115/jmi.v5i1.3.

Ojea, J., Pazos, A.J., Martínez, D., Novoa, S., Sanchez, J.L., Abad, M., 2004. Seasonal variation in weight and biochemical composition of the tissues of *Ruditapes decussatus* in relation to the gametogenic cycle. Aquaculture 238 (1–4), 451–468. https://doi.org/10.1016/j.aquaculture.2004.05.022.

Paixão, L., Ferreira, M.A., Nunes, Z., Fonseca-Sizo, F., Rocha, R., 2013. Effects of salinity and rainfall on the reproductive biology of the mangrove oyster (*Crassostrea gasar*): implications for the collection of broodstock oysters. Aquaculture 380, 6–12. https://doi.org/10.1016/j.aquaculture.2012.11.019.

Palaniswamy, R., 1993. Reproductive biology of *C. Madrasensis* in Tuticorin coast. J. Mar. Biol. Assoc. India 35 (1–2), 17–22.

Pazos, A.J., Ruíz, C., García-Martin, O., Abad, M., Sánchez, J., 1996. Seasonal variations of the lipid content and fatty acid composition of *Crassostrea gigas* cultured in E1 Grove, Galicia, NW Spain. Comp. Biochem. Physiol. B Biochem. Mol. Biol. 114 (2), 171–179. https://doi.org/10.1016/0305-0491(96)00017-X.

Pearse, A.G.E., 1985. Histochemistry: Theoretical and Applied, 4th ed. Churchill Livingstone, Edinburgh, London, Melbourne, New York. https://www.scirp.org/reference/referencespapers?referenceid=1513327.

Pernet, F., Gauthier, C.S., Elise, M., 2007. Change in lipid composition in eastern oyster (*Crassostrea virginica* Gmelin) exposed to constant or fluctuating temperature regimes. Comp. Biochem. Physiol. B Biochem. Mol. Biol. 147 (3), 557–565. https://doi.org/10.1016/j.cbpb.2007.03.009.

Peterson, B., Carl, P., 2024. Performance Analytics: Econometric Tools for Performance and Risk Analysis. R Package Version 2.0.8. https://cran.r-project.org/package=PerformanceAnalytics.

Powell, E.N., Mann, R., Ashton-Alcox, K.A., Kim, Y., Bushek, D., 2016. The allometry of oysters: spatial and temporal variation in the length–biomass relationships for *Crassostrea virginica*. J. Mar. Biol. Assoc. UK 96 (5), 1127–1144. https://doi.org/10.1017/S0025315415000703.

R Core Team, 2024. R: A Language and Environment for Statistical Computing. R Foundation for Statistical Computing, Vienna, Austria. https://www.R-project.org/.

Ramos, C.D.O., Gomes, C.H.A.D.M., Magalhães, A.R.M., Dos Santos, A.I., De Melo, C.M. R., 2014. Maturation of the mangrove oyster *Crassostrea gasar* at different temperatures in the laboratory. J. Shellfish Res. 33 (1), 187–194. https://doi.org/10.2983/035.033.0118.

Ren, J.S., Ross, A.H., Schiel, D.R., 2000. Functional descriptions of feeding and energetics of the Pacific oyster *Crassostrea gigas* in New Zealand. Mar. Ecol. Prog. Ser. 208, 119–130. https://doi.org/10.3354/meps208119.

Ruiz, C., Abad, M., Sedano, F.J., Omena, L., Ibarrola, I., 1992. Seasonal variations in condition, reproductive activity and biochemical composition of the flat oyster *Ostrea edulis* from San Cibrán (Galicia, NW Spain). Mar. Biol. 112 (1), 67–74. https://doi.org/10.1007/BF00349731.

Sanjeeva Raj, P.J., 2008. Oysters in a new classification of keystone species. Resonance 13 (7), 648–654. https://doi.org/10.1007/s12045-008-0071-4.

Singh, Y.T., 2017. Relationships between environmental factors and biological parameters of Asian wedge clam, *Donax scortum*, morphometric analysis, length-weight relationship and condition index: a first report in Asia. J. Mar. Biol. Assoc. UK 97 (8), 1617–1633. https://doi.org/10.1017/S002531541600103X.

Solon, E.M., 1984. Hatchery Development of Marine Bivalve Molluscs, 59 f. Dissertação (Mestrado em Ciências). Oregon State University School of Oceanography.

Southgate, P.C., Lucas, J.S., 2008. The Pearl Oyster. Elsevier, Oxford, UK. ISBN 978–0–444-52976-3.

Steele, S., Mulcahy, M.F., 1999. Gametogenesis of the oyster *Crassostrea gigas* in southern Ireland. J. Mar. Biol. Assoc. UK 79, 673–686. https://doi.org/10.1017/S0025315498000836.

Uddin, M.J., Jeung, H.D., Yang, H.S., Kim, B.K., Ju, S.J., Choi, K.S., 2013. Quantitative assessment of reproductive effort of the Manila clam *Ruditapes philippinarum* in a lagoon on Jeju Island (Korea) using enzyme–linked immunosorbent assay. Invertebr. Reprod. Dev. 57 (4), 316–324. https://doi.org/10.1080/07924259.2013.793219.

Uddin, M.J., Rahman, M.S., Sonia, S.S., Kubra, S.K., Mia, M.S., Yeasmine, S., 2024. Annual gametogenic phenology of oyster, *Magallana bilineata* (Röding, 1798) collected from the west coast of Moheshkhali Island, Cox's Bazar, Bangladesh. Heliyon 10 (7). https://doi.org/10.1016/j.heliyon.2024.e28753.

Urrutia, M.B., Ibarrola, I., Iglesias, J.I.P., Navarro, E., 1999. Energetics of growth and reproduction in a high-tidal population of the clam *Ruditapes decussatus* from

Urdaibai Estuary (Basque Country, N. Spain). J. Sea Res. 42 (1), 35–48. https://doi.org/10.1016/S1385-1101(99)00017-9.

Utting, S.D., Millican, P.F., 1997. Techniques for the hatchery conditioning of bivalve broodstocks and the subsequent effect on egg quality and larval viability. Aquaculture 155, 45–54. https://doi.org/10.1016/S0044-8486(97)00108-7.

Vaschenko, M.A., Syasina, I.G., Lukyanova, O.N., 2013. The reproductive cycle and sex ratio of *Crassostrea angulata* in southern Primorye. Russ. J. Mar. Biol. 39 (1), 32–39. https://doi.org/10.1134/S1063074013010124.

Vasconcelos, P., Moura, P., Pereira, F., Pereira, A.M., Gaspar, M.B., 2018. Morphometric relationships and relative growth of 20 uncommon bivalve species from the Algarve Coast (southern Portugal). J. Mar. Biol. Assoc. UK 98 (3), 463–474. https://doi.org/10.1017/S002531541600165X.

Venables, W.N., Ripley, B.D., 2002. Modern Applied Statistics with *S*, 4th ed. Springer, p. 498. https://doi.org/10.1007/978-0-387-21706-2.

Waite, R., Beveridge, M., Brummett, R., Castine, S., Chaiyawannakarn, N., Kaushik, S., Phillips, M., 2014. Improving Productivity and Environmental Performance of Aquaculture. WorldFish.

Whyte, J.N.C., Englar, J.R., Carswell, B.L., 1990. Biochemical composition and energy reserves in *Crassostrea gigas* exposed to different levels of nutrition. Aquaculture 90 (2), 157–172. https://doi.org/10.1016/0044-8486(90)90338-N.

Wickham, H., 2016. ggplot2: Elegant Graphics for Data Analysis. Springer. https://doi.org/10.1007/978-3-319-24277-4.

Willer, D.F., Aldridge, D.C., 2019. Microencapsulated diets to improve bivalve shellfish aquaculture for global food security. Glob. Food Secur. 23, 64–73. https://doi.org/10.1016/j.gfs.2019.04.007.

Willett, W., Rockström, J., Loken, B., Springmann, M., Lang, T., Vermeulen, S., Murray, C.J., 2019. Food in the Anthropocene: the EAT–lancet commission on healthy diets from sustainable food systems. Lancet 393 (10170), 447–492. https://doi.org/10.1016/S0140-6736(18)31788-4.

Yap, C.K., Ismail, A., Tan, S.G., 2002. Condition index of green-lipped mussel *Perna viridis* (Linnaeus) as a potential physiological indicator of ecotoxicological effects of heavy metals (Cd and pb). Malays. Appl. Biol. 31, 37–45.

Zhou, L., Xie, X., Sun, X., 2015. Seasonal and size-dependent variations in phytoplankton under monsoonal influence. Biogeosciences 12, 6285–6298. https://doi.org/10.5194/bg-12-6285-2015.

Aquaculture and Fisheries xxx (xxxx) xxx

Contents lists available at ScienceDirect

Aquaculture and Fisheries

journal homepage: www.keaipublishing.com/en/journals/aquaculture-and-fisheries

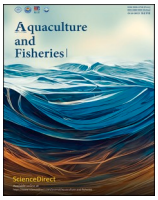

Original research article

Environmental fingerprints of cultivation site and depth: Variation in shell shape and coloration of the green mussel (*Perna viridis*) from the southeast coast of the Bay of Bengal, Bangladesh

Kanij Fatema Eti [a], Rahanuma Tasnim [a], Afshana Ferdous [a,b], Md Mohiuddin [a], Md Nayeem Hossain [a,c], Md Moshiur Rahman [d], Md Asaduzzaman [a,*]

[a] Department of Marine Bioresource Science, Faculty of Fisheries, Chattogram Veterinary and Animal Sciences University, Khulshi, Chittagong, 4225, Bangladesh
[b] Department of Marine Fisheries and Oceanography, Sher-e-Bangla Agricultural University, Sher-e-Bangla Nagar, Dhaka, 1207, Bangladesh
[c] Department of Marine Fisheries and Aquaculture, Faculty of Earth and Ocean Science, Bangladesh Maritime University, Dhaka, 1216, Bangladesh
[d] Fish Conversation and Culture Laboratory, Department of Biological and Agricultural Engineering, University of California Davis, 17501 Byron Hwy, Byron, CA, 94514, USA

ARTICLE INFO

Keywords:
Green mussel
Shell morphology
Shell coloration
Geometric morphometrics
Phenotypic plasticity
Coastal aquaculture

ABSTRACT

Understanding how environmental gradients influence bivalve shell characteristics is essential for developing ecological knowledge, strengthening consumer preferences, and increasing market value. This study employed geometric morphometrics and digital color profiling to assess the impact of cultivation sites (Khurushkul, Moheshkhali, and Chowfaldandi) and depths (0.5, 1.0, and 1.5 m) in raft-based mariculture on the shell morphology and coloration of the green mussel *Perna viridis* along the southeastern coast of the Bay of Bengal, Bangladesh. At each site, a total of 150 mussels were collected directly from raft-culture socks, with 50 individuals sampled from each of the three depths, resulting in a total sample size of 450 mussels. Morphometric variation was assessed by geometric techniques, and coloring was measured using RGB, HSV, and CIELAB models under standardized imaging conditions. Environmental and trophic conditions varied across sites and depths, producing distinct phenotypic patterns in mussels. Khurushkul individuals were more elongated with the most saturated and brilliant green hues of coloration, Chowfaldandi mussels were compact and appeared pale and chalky in color, and Moheshkhali populations showed intermediate traits. Multivariate analyses supported strong spatial separation with >90 % classification accuracy. Depth gradients further shaped morphology and color: shallow mussels were larger and greener, mid-depth individuals exhibited a more vivid brownish tone, and deeper mussels were smaller, dorsally compressed, and weakly pigmented, reflecting reduced light, food availability, and hydrodynamic differences. These findings indicate that site-specific hydrographic conditions, associated food availability, and vertical gradients collectively shaped mussel phenotype, underscoring the adaptive plasticity of *P. viridis* to local ecological conditions. These findings also provide compelling evidence that *P. viridis* exhibits pronounced adaptive plasticity, enabling its phenotype to mirror localized ecological conditions. Ecologically, the study demonstrates that shell traits serve as sensitive integrators of environmental variability, making them powerful bioindicators for detecting habitat quality, trophic shifts, and environmental stress in tropical coastal systems. From a practical perspective, the phenotypic indicators identified in this study can inform site selection, optimize culture depth, and improve broodstock and farming management for green mussel mariculture. Overall, the study provides a framework for integrating shell-based phenotypic traits into aquaculture planning and coastal environmental monitoring in the Bay of Bengal region.

Peer review under the responsibility of Editorial Board of Aquaculture and Fisheries.

* Corresponding author. Department of Marine Bioresource Science, Faculty of Fisheries, Chattogram Veterinary and Animal Sciences University, Khulshi, Chattogram, 4225, Bangladesh.
E-mail address: a_zamanbau@yahoo.com (M. Asaduzzaman).

https://doi.org/10.1016/j.aaf.2026.01.003
Received 28 October 2025; Received in revised form 29 December 2025; Accepted 4 January 2026

1. Introduction

Endowed with an extensive network of inland rivers and a dynamic tidal coastline, Bangladesh offers fertile grounds for aquaculture that contribute substantially to food security, rural livelihoods, and export revenues (AftabUddin et al., 2021; Samanta Chandan & Roy, 2024). While diverse aquatic resources support this sector, coastal systems are particularly important due to their biological productivity and suitability for bivalve mariculture. Among the suite of coastal bivalves, the green mussel *Perna viridis* has emerged as a species of notable commercial and ecological importance due to its rapid growth, broad environmental tolerance, high nutritional value, and expanding market demand across Asia (Appukuttan et al., 2003; Asaduzzaman et al., 2025; Saleh et al., 2021; Shahabuddin et al., 2010). Beyond its role in human nutrition and income generation, *P. viridis* contributes to ecosystem services, filtration, nutrient cycling, and habitat structuring, which strengthen the argument for its inclusion in sustainable mariculture and integrated coastal management (Hickman, 1992; Wijsman et al., 2019). With global interest in low-carbon, climate-resilient seafood and scalable molluscan production, mussel farming has been identified as a strategic avenue for sustainable seafood production under climate-resilient coastal development initiatives (Gentry et al., 2017).

Shell traits, shape, size, and coloration encode the integrated outcome of genetic potential and local environmental influence and therefore constitute an accessible record of organismal responses to habitat heterogeneity. While genetic control contributes to morphological baseline (Inoue et al., 2013, 2014; Marinho & Arruda, 2021), a broad literature demonstrates that environmental drivers such as hydrodynamics, salinity, turbidity, food supply, temperature and predation pressure frequently exert dominant and plastic effects on bivalve shell form and pigmentation (Haag, 2012; Martin et al., 2019; Rajagopal et al., 1998; Siddall, 1980; Vermeij, 2002; Wilke et al., 2010; Williams, 2017). Ecologically, these phenotypic responses can signal habitat quality, trophic regimes, and environmental stress. Commercially, shell appearance and form influence consumer choice and therefore product value. Despite this dual relevance, many regional studies of *P. viridis* have focused on growth, reproduction, and basic biometric descriptors, leaving integrative phenotype–environment relationships underexplored in tropical mariculture contexts.

Methodological advances in shape analysis and colour quantification now permit much finer inference of phenotype–environment linkages. Traditional linear morphometrics, while useful for many applications, suffer from limitations including multicollinearity and an inability to resolve subtle, localized shape variation (Adams et al., 2004; Noor et al., 2021; Zelditch et al., 2012). Geometric morphometrics (GM) addresses these limitations by capturing complex form through landmark and semi-landmark configurations and analysing shape in a statistically rigorous framework (Beyett et al., 2020; Bookstein, 1997; Fruciano et al., 2011). Similarly, calibrated digital colour profiling across RGB, HSV, and CIELAB spaces, when combined with objective imaging protocols, enables quantification of shell pigmentation beyond subjective description (Stevens et al., 2007; Troscianko & Stevens, 2015; Weller & Westneat, 2019). Although GM and quantitative colour metrics have been successfully deployed in diverse taxa and contexts (Costa et al., 2010; Krapivka et al., 2007; Rufino et al., 2006; Sahidin et al., 2022; Sousa et al., 2007; Stenger et al., 2019, 2021), their joint application to *P. viridis* within tropical raft-culture systems remains sparse (Gamier et al., 2019), and studies that explicitly link shape and colour variation across both horizontal (sites) and vertical (depths) cultivation gradients are notably absent in the Bangladeshi context and other regions of the world.

This knowledge gap is important for three reasons. First, without integrated morpho-chromatic baselines, it remains difficult to interpret shell variation as either environmentally induced plasticity or as a heritable trait, an ambiguity that limits the development of shell-based bioindicators for habitat monitoring (Gefaell et al., 2023; Haag, 2012; Vermeij, 2002; Williams, 2017). Second, the absence of fine-scale phenotype–environment mapping restricts informed decisions on site selection, culture-depth optimization, and broodstock selection, practices that directly affect yield, product appearance, and marketability (Marma et al., 2021; Rajagopal et al., 2006; Tan & Ransangan, 2014). Third, lacking multi-trait phenotypic baselines constrains our capacity to detect and manage environmental change, such as shifts in turbidity, productivity, or hydrodynamics, which will be increasingly relevant under climate variability and coastal development pressures (Asaduzzaman et al., 2019; Kapsenberg et al., 2018; Noor et al., 2021).

The present study responds directly to these gaps by delivering a first-of-its-kind, integrated assessment of shell morphology and pigmentation in *P. viridis* across multiple cultivation sites (Moheshkhali, Khurushkul, and Chowfaldandi) and discrete depth (0.5, 1.0, and 1.5 m) strata in the southeastern Bay of Bengal. We hypothesize that shell morphology and pigmentation in *P. viridis* will vary significantly with cultivation depth and across sites, reflecting differential responses to hydrodynamic stress, light exposure, and local ecological conditions. Therefore, using landmark-based GM, including sliding semi-landmarks to capture outline variation, together with standardized digital colour profiling (RGB, HSV, and CIELAB), we quantify how site-specific hydrographic regimes and vertical gradients shape shell form and hue (Bookstein, 1997; Fruciano et al., 2011; Zelditch et al., 2012). We also examine the degree to which these phenotypic signals can discriminate cultivation environments (Krapivka et al., 2007; Rufino et al., 2006). Importantly, our approach couples objective multivariate shape analysis with calibrated color metrics and environmental/trophic measurements, thereby moving beyond single-trait descriptions to a multivariate phenotype perspective that is directly actionable for ecological monitoring and aquaculture management (Beyett et al., 2020; Vermeij, 2002; Williams, 2017).

2. Materials and methods

2.1. Study area and sample collection

In Bangladesh, the natural distribution of *P. viridis* is largely confined to the southeastern coastal belt, particularly the Moheshkhali Channel, which directly connects with the Bay of Bengal (Shahabuddin et al., 2010). This channel provides highly favorable conditions for mussel aquaculture, characterized by suitable water depths, moderate currents, stable salinity, and optimal temperature regimes. Moreover, the presence of abundant natural seed stocks and established wild populations further strengthens its potential for large-scale mussel farming (Asaduzzaman et al., 2025; Marma et al., 2021; Noor et al., 2021; Shahabuddin et al., 2010). The present study was conducted at three sites within this coastal zone: Khurushkul (21°30′40.13″N; 91°59′53.3″E), Moheshkhali (21°31′58.8″N; 91°58′52.5″E), and Chowfaldandi (21°30′42.3″N; 92°0′56.9″E) (Fig. 1). All three locations lie close to the shoreline and are considered environmentally suitable for mussel aquaculture activities owing to their supportive water quality parameters.

For this study, floating bamboo raft systems (36 m^2 each) were established at the above three sites and deployed in shallow near-shore waters (~2.0 m depth) to avoid navigational conflicts. Each raft was constructed in a square configuration, with each side measuring 6 m. The bamboo culms used for construction had an average diameter of 12.0 ± 2.4 cm and a wall thickness of 1.2 ± 0.1 cm. Buoyancy was maintained using 12 plastic drums, each with a capacity of 220 L, securely attached to the raft framework. Mussels were cultured at three depths (0.5, 1.0, and 1.5 m) using nylon net socks (1.5 m × 15 cm, mesh size 0.8 cm) suspended vertically from the rafts. Spats (2.9 ± 0.08 g) were collected from a wild settlement, detached from byssus threads, and 20 uniform-sized spats were stocked into each sock. At each site, ten replicate socks per depth were hung independently to ensure replication, and cultivation continued for six months (October 2023–March

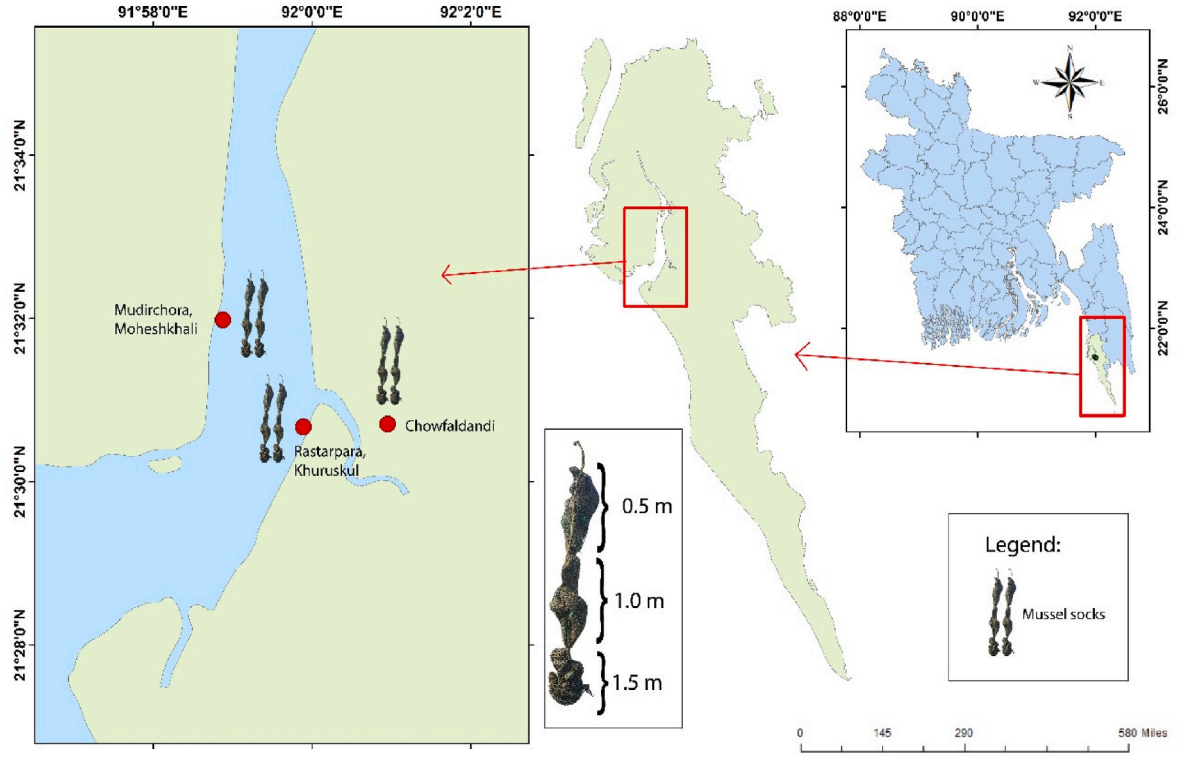

Fig. 1. Map of the study area along the Moheshkhali Channel in Cox's Bazar, Bangladesh, showing the three experimental sites: Moheshkhali, Khurushkul, and Chowfaldandi. The inset map highlights the location of the study sites along the south-east coast of the Bay of Bengal, Bangladesh. The culture setup illustrates floating raft systems with mussel socks suspended at three depths (0.5 m, 1.0 m, and 1.5 m).

2024). From each location, 150 individuals were collected, with 50 specimens taken from each depth, producing a total sample size of 450 mussels. Following the collection, the samples were carefully processed in the laboratory. Mussels from each depth and location were measured for shell length, width, and height using vernier calipers with an accuracy of 0.01 mm. The weight of each mussel was then determined with an electronic balance (PS 1200.R2, Radwag, Poland) to the nearest 0.1 g, after draining fluids from the intervalvar cavity. The shell length of the collected specimens ranged from 26.2 to 89.5 mm, shell width from 19.5 to 43.5 mm, shell height from 13.2 to 30.2 mm, and individual weight from 7.9 to 58.5 g. After biometric measurements, gut contents were removed, and the posterior adductor muscle, along with other tissues, was dissected to avoid soft-tissue interference. For geometric morphometric assessments, the left valve of each mussel was isolated and used. This methodological framework allowed us to assess morphological variation and evaluate the suitability of green mussel aquaculture across the selected sites in southeastern Bangladesh.

2.2. Digital imaging/photographic documentation

The left valves of all mussel samples were photographed under standardized laboratory conditions to ensure uniformity in distance and orientation, which is essential for reliable geometric morphometric and color analysis. Moreover, consistency in illumination and orientation was maintained to prevent artificial color shifts and ensure reproducibility (Akkaynak et al., 2014). Each shell was assigned a unique identification code to maintain accurate documentation and tracking throughout the study. Digital images were captured using a Canon EOS 60D DSLR camera (18.0 MP) equipped with an 18–55 mm lens (Canon Inc., USA). This camera system was selected for its high resolution and proven reliability, providing detailed and reproducible images of shell valves (Cadrin & Friedland, 1999).

2.3. Water quality parameter analysis

Physicochemical parameters, temperature, pH, dissolved oxygen (DO), salinity, and turbidity, were monitored fortnightly, and other parameters (Chlo-a, NO_2–N, NO_3–N, NH_3–N, and PO_4–P) were recorded monthly in triplicate at low tide across three cultivation sites and depths. In situ measurements of physical parameters included water temperature (Celsius thermometer), pH (digital pH meter, EcoSense pH10A; YSI, USA), dissolved oxygen (digital dissolved oxygen meter, PDO-519; Lutron, Taiwan), salinity (Bellingham and Stanley E-Line refractometer; Xylem, UK), and turbidity (digital turbidity meter, Turb430 IR; WTW, Germany). DO was recorded in situ by submerging the probe, while other parameters were measured on boat from composite water samples collected at each depth using a horizontal water sampler (Alpha™ Bottles, WildCo, USA). About 800 ml of water from each depth and site was transported on ice to the laboratory for nutrient and chlorophyll-a analysis. Samples were filtered through Whatman GF/C filters, and nutrients (NO_2–N, NO_3–N, NH_3–N, PO_4–P) were quantified spectrophotometrically (WTW PhotoFlex STD) following APHA (1992). Chlorophyll-a was measured at 664, 647, and 630 nm using an Optizen Pop 2102 spectrophotometer following Boyd (1979). The data of the water quality parameters were analyzed by using two-way ANOVA using the 'car' package of R.

2.4. Quantitative estimation of water plankton

Monthly assessments of the quantitative composition of plankton were carried out in triplicate at each depth and sampling location. For each sampling location, 20 L of composite water samples were obtained from each cultivation depth using a horizontal water sampler (1120–1180 Horizontal Alpha™ Bottles, WildCo, FL, USA). The obtained water samples (20 L) were filtered through a 25-μm mesh plankton net, and the concentrate was preserved in small plastic vials

with 5% buffered formalin. The preserved samples were transported to the Oceanography Laboratory, Chattogram Veterinary and Animal Sciences University (CVASU) for further analysis. Quantitative estimation was performed using a Sedgewick–Rafter (S–R) cell consisting of 1000 compartments, each 1 mm^3 in volume (Asaduzzaman et al., 2020). A 1-mL subsample was placed in the chamber, and plankton were identified to the genus level and enumerated in 10 randomly chosen fields under a binocular microscope (Optika B-190TB, Ponteranica, Italy) at objective magnifications ranging from 10 × to 40 × . Plankton density (cells or individuals / L) was then calculated using the equation: $N = (P \times C \times 100)/L$, where N = number of plankton cells or individuals per liter of original water, P = mean plankton count from 10 fields, C = final concentrate volume (mL), and L = volume of the original water sample (L). The data of the water quality parameters were analyzed by using two-way ANOVA using the 'car' package of R.

2.5. Landmark-based geometric morphometric analysis

Shell morphology of *P. viridis* was analyzed using landmark-based geometric morphometric (GM) techniques (Fig. 2). Digital landmarks were first established in TPSdig2 (Rohlf, 2005), where five fixed landmarks and 36 semi-landmarks were digitized to capture shell geometry. The configuration included: (1) the umbo, marking the initiation point of the hinge plate; (2) the ligament, denoting the hinge plate endpoint; (3) the midpoint of the ventral margin; (4) the midpoint of the dorsal margin; and (5) ventral midpoint at the lowest point of the shell outline (Fig. 2). The semi-landmarks (6-40) distributed along the shell's curvature (Supp. Table 1). Landmark datasets were managed in TPSUtil to separate fixed from semi-fixed landmarks. To ensure reproducibility and quantify potential operator bias, a subset of 30 shells was digitized twice by the primary operator with a one-week interval. Intraclass correlation coefficients (ICCs) were calculated for all landmarks, yielding high repeatability (ICC >0.95). Additionally, a second independent operator digitized the same subset, and Procrustes distances between configurations indicated minimal inter-operator variability (<2% of total shape variance). These steps confirmed that landmark placement was robust and reproducible.

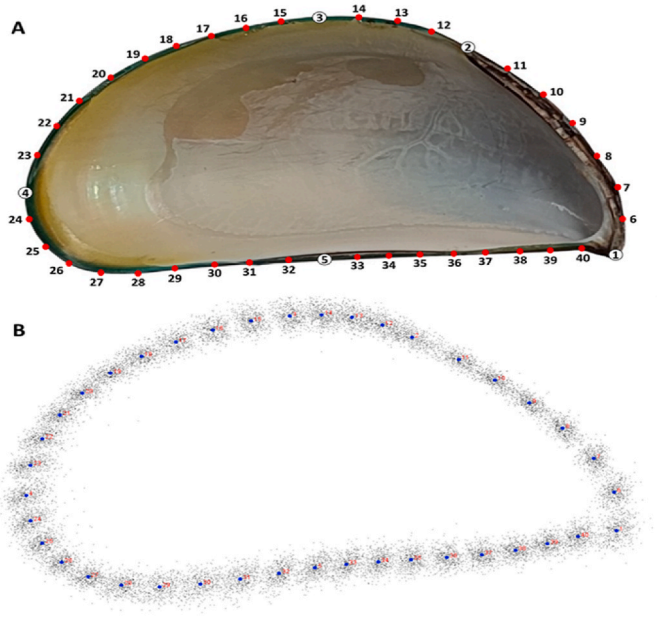

Fig. 2. Key geometric morphometric landmarks used to analyze shell morphology of green mussels (*Perna viridis*) collected from three coastal sites (Chowfaldandi, Khurushkul, and Moheshkhali). (A) Forty-two-dimensional (2D) landmarks were digitized along the shell outline, comprising five fixed landmarks and 35 semi-landmarks. The fixed landmarks include: (1) anterior-ventral tip, marking the initiation of the shell hinge; (2) ligament region at the upper anterior curve (transition to dorsal arc); (3) maximum shell height located at the dorsal mid-point; (4) posterior midpoint along the dorsal margin (transition from dorsal to posterior curvature); and (5) ventral midpoint at the lowest point of the shell outline. The semi-landmarks (6–40) were distributed along the anterior, dorsal, posterior, and ventral margins to capture curvature and shell outline variation, with detailed anatomical positions provided in Table 1. (B) Procrustes superimposition of landmark configurations for *P. viridis*, illustrating shape variation after translation, rotation, and scaling.

To remove variation caused by non-shape factors such as rotation, translation, and scaling, a generalized Procrustes analysis (GPA) was performed in TPSRelw following the protocols of Rohlf and Slice (1990) and Slice (1996). The software also employed an algorithm that allowed semi-landmarks to slide along tangent directions, minimizing bending energy and optimizing their alignment with a reference configuration (Bookstein, 1997). Relative Warp (RW) scores were then generated, quantifying deviations from a consensus shape and functioning analogously to principal components in Principal Component Analysis (PCA) (Adams et al., 2004). MorphoJ (Klingenberg, 2011) was subsequently used to visualize group-level variations in shell shape using the RW scores. For advanced statistical treatment, the GM dataset was exported to the R environment (v. 4.0.5), where multivariate analyses were conducted. Variables were first centered and scaled prior to ordination. The PCA was performed using the FactoMineR package (Lê et al., 2008), and component retention was guided by eigenvalues >1, scree plot examination, and cumulative explained variance thresholds exceeding 70%. Canonical Variate Analysis (CVA) was then used to maximize inter-group separation, with Mahalanobis distances and permutation tests (1000 iterations) applied to assess statistical significance among mussel groups. Discriminant Function Analysis (DFA) was implemented using the MASS package (Venables & Ripley, 2013) to determine which shape variables contributed most strongly to group discrimination. To ensure the robustness of multivariate inference, underlying analytical assumptions, including multicollinearity, homogeneity of covariance matrices (Box's M test), and normality of residuals (Shapiro–Wilk test), were checked prior to model interpretation. DFA model performance was validated using leave-one-out cross-validation, and classification accuracy was reported for each group to avoid overfitting. This integrated workflow ensured statistically rigorous detection, visualization, and testing of shell shape differences among mussel populations.

2.6. Shell coloration analysis

The mussels color measurements were conducted following the standardized protocols of the *Image Calibration and Analysis Toolbox* (Troscianko & Stevens, 2015). Following the recommended workflow, all images were first white balanced using a standardized grey reference card placed in each frame to correct illumination bias. Image files were linearized and converted to a calibrated color space prior to extraction of pixel values. Backgrounds were then manually removed in Adobe Photoshop to isolate the whole outer surface of the left valve, ensuring that only biologically relevant shell pigmentation was quantified (Stevens et al., 2007). Each processed image was imported into ImageJ (Schneider et al., 2012), where regions of interest (ROI) encompassing the entire outer surface of the left valve were defined, and mean pixel values were extracted for each color channel. *These calibrated values were subsequently analyzed in R using* the packages *pavo* (Maia et al., 2013) and *colordistance* (Weller & Westneat, 2019). *Colour metrics were converted into three commonly used perceptual spaces, RGB* (Red, Green, Blue)*, HSV (Hue, Saturation, Value), and CIELAB (L*, a*, b*), to capture brightness, hue shifts, chromatic components, and pigment intensity. These workflows enabled the extraction of color data (Fairchild, 2013; Westland et al., 2012). Color datasets were compiled and statistically analyzed in R. In recognition of the multivariate nature of color data, we initially explored the joint structure of RGB, HSV, and CIELAB variables using PCA (*FactoMineR* package) and CVA (*MASS* package) and cluster

analyses to assess whether site- and depth-specific differences yielded coherent multivariate separation. Although these ordinations revealed broad tendencies, PCA and CVA did not yield clear discriminatory axes. *Following this multivariate screening, one-way ANOVA was applied to individual color channels (e.g., L,* a*, b*, R, G, B, H, S, V indices) to determine which specific parameters differed significantly among sites and depths, followed by Tukey's HSD to control Type I error in post-hoc comparisons. This two-tiered strategy ensured that both multivariate relationships and channel-specific responses were appropriately assessed. Group means with standard deviations were displayed in bar plots, with error bars representing within-group variability (Quinn & Keough, 2002; Zar, 2010). Additionally, multivariate hierarchical clustering (Euclidean distance, Ward's linkage) was conducted on the color profiles, providing insights into site- and depth-specific grouping patterns (Borcard et al., 2018; Murtagh & Legendre, 2014). This integrated workflow, combining standardized imaging, ImageJ preprocessing, and R-based statistical analyses, provides an objective and reproducible framework for quantifying shell coloration on the outer surface of the left valve in bivalves.

3. Results

3.1. Spatial and vertical variability in water quality and plankton abundance

Water quality (Table 1) and plankton composition (Table 2) of *P. viridis* culture exhibited significant spatial and depth-related variations. Temperature and pH remained relatively uniform across sites and depths ($P > 0.05$). Dissolved oxygen (DO) was markedly higher at Khurushkul and Moheshkhali than at Chowfaldandi ($P < 0.001$), while salinity followed a similar trend, being highest at the former two locations. Turbidity was significantly greater at Chowfaldandi ($P < 0.001$). Nutrient patterns varied, with phosphate (PO_4-P) increasing at shallower depths ($P < 0.001$) and nitrate (NO_3-N) exhibiting both locational and depth-related effects ($P < 0.01$). Chlorophyll-a concentration differed significantly between both factors ($P < 0.001$), attaining higher values at Moheshkhali and at 0.5 m depth, suggesting enhanced primary productivity near the surface. Phytoplankton assemblages were dominated by diatoms (Coscinodiscophyceae, Fragilariophyceae, and Bacillariophyceae), with abundance significantly higher at Khurushkul and in upper-water layers ($P < 0.05$–0.001). Chlorophyceae and Dinophyceae also declined with increasing depth, while Cyanophyceae showed moderate spatial variability. Total phytoplankton and total plankton exhibited significant differences across both sites and depths, peaking at 0.5 m and at Khurushkul ($P < 0.01$). Zooplankton abundance, however, remained relatively consistent ($P > 0.05$).

3.2. Centroid size and shell morphometric divergence across cultivation sites

Centroid size shows distinct variation among cultivation sites (Fig. 3A). Mussels from Khurushkul (green) exhibited the largest centroid sizes, those from Moheshkhali (blue) were intermediate, while Chowfaldandi (red) typically showed the smallest values. Despite a little overlap in the 95 % confidence ellipses, the distinction of group centroids demonstrated significant habitat-specific size differentiation. Procrustes deformation plots (Fig. 3B) indicated that bigger shells (positive centroid-size direction) expanded outward along the dorsal and ventral borders, whereas smaller shells (negative direction) constricted along these same axes. Wireframe diagrams (Fig. 3C) illustrated localized expansions and compressions that align with these tendencies. Khuruskul mussels exhibit significant elongation and posterior expansion correlating with greater centroid sizes, while Chowfaldandi specimens provide a more compact and rounded shell contour. Moheshkhali is once more positioned as intermediate in form, connecting the morphological continuum between the Chowfaldandi and Khuruskul clusters.

Principal component analysis (PCA) demonstrated significant overlap in shell morphology across populations with site-specific tendencies (Fig. 4A–C). PC1, the predominant axis, signifies variations in shell elongation and ventral curvature. Along PC1, Khurushkul (green) individuals exhibit higher positive scores, aligning with their comparatively extended and ventrally expanded outlines, but Chowfaldandi (red) and Moheshkhali (blue) are situated nearer to the center cloud, with Moheshkhali displaying a greater within-site variation. PC2 and PC3 encompass supplementary variance in the dorsal and posterior margins. Khurushkul displays some dorsal flattening along these axes, while Chowfaldandi and Moheshkhali demonstrate greater variability at the dorsal/posterior borders. CVA generated a more distinct separation by location (Fig. 4D). Khurushkul (green) clusters on the negative side of CV1, characterized by an elongated shell outline with significant anterior–posterior extension and ventral elongation (CV1 −ve). Chowfaldandi (red) is positioned on the positive CV1, displaying relatively shorter, more rounded outlines with moderate anterior–posterior compression and slight ventral flattening (CV1 +ve). In contrast, Moheshkhali (blue) occupies elevated CV2 values, exhibiting enhanced dorsal–ventral expansion and increased shell height. The CVA results align with PCA, wherein the principal axes of variation characterize elongation and ventral curvature. Pairwise testing validated these differences, with all Procrustes and Mahalanobis distances exhibiting high significance ($P < 0.0001$; Supp. Table 2), and the most pronounced divergence noted between Chowfaldandi and Khurushkul.

Discriminant Function Analysis (Fig. 5) indicates that pairwise morphological variations are mostly influenced by dorsal height, posterior taper (elongation), and ventral-margin curvature. In the

Table 1
Variations in water quality parameters among different depths and locations based on two-way ANOVA.

Variables	Means (Tukey test)						Sig. (*P*-value)		
	Location (L)			Depth (D)			L	D	D × L
	Khurushkul	Moheshkhali	Chowfaldandi	0.5 m	1 m	1.5 m			
Temp (°C)	28.24 ± 1.33^{a}	27.74 ± 1.41^{a}	29.10 ± 1.16^{a}	28.34 ± 1.78^{a}	28.12 ± 1.58^{a}	28.04 ± 1.42^{a}	NS	NS	NS
pH	7.48 ± 0.82^{a}	7.79 ± 0.81^{a}	7.64 ± 0.58^{a}	7.78 ± 0.82^{a}	7.71 ± 0.92^{a}	7.52 ± 0.68^{a}	NS	NS	NS
DO (mg/L)	5.98 ± 0.12^{a}	5.92 ± 0.12^{a}	5.28 ± 0.12^{b}	5.93 ± 0.28^{a}	5.73 ± 0.32^{ab}	5.23 ± 0.22^{b}	***	**	NS
Salinity (ppt)	26.09 ± 0.72^{a}	26.66 ± 0.58^{a}	20.57 ± 1.22^{b}	24.24 ± 1.04^{a}	24.44 ± 1.08^{a}	24.65 ± 1.28^{a}	***	NS	NS
Turb (NTU)	9.86 ± 0.69^{b}	9.57 ± 0.64^{b}	17.6 ± 1.40^{a}	12.35 ± 1.16^{a}	12.46 ± 1.18^{a}	12.06 ± 1.04^{a}	***	NS	NS
PO_4-P (mg/L)	1.49 ± 0.12^{a}	1.23 ± 0.32^{ab}	1.06 ± 0.28^{b}	1.55 ± 0.22^{a}	1.11 ± 0.12^{b}	1.09 ± 0.22^{b}	**	***	NS
NO_2-N (mg/L)	0.14 ± 0.02^{a}	0.18 ± 0.01^{a}	0.18 ± 0.01^{a}	0.19 ± 0.01^{a}	0.15 ± 0.01^{a}	0.16 ± 0.02^{a}	NS	NS	NS
NO_3-N (mg/L)	1.35 ± 0.19^{a}	0.99 ± 0.16^{ab}	0.65 ± 0.09^{b}	1.11 ± 0.11^{a}	0.84 ± 0.09^{b}	0.75 ± 0.16^{b}	**	**	*
NH_3-N (mg/L)	0.22 ± 0.04^{a}	0.17 ± 0.02^{a}	0.19 ± 0.03^{a}	0.17 ± 0.05^{a}	0.23 ± 0.04^{a}	0.18 ± 0.02^{a}	NS	NS	NS
Chlorophyll-a (μg/L)	5.02 ± 0.15^{b}	5.70 ± 0.22^{a}	4.06 ± 0.18^{c}	5.67 ± 0.26^{a}	4.75 ± 0.20^{b}	4.27 ± 0.19^{b}	***	***	NS

The significance levels (*P*) are denoted by asterisks (*<0.05, **<0.01, ***<0.001, NS= Not significant). Significant variations among various depths and locations are shown by several superscripts in the same row at $p < 0.05$ level.

Table 2
Variations of different plankton groups ($\times 10^2$ cells or individuals L^{-1}) abundance in water among different depths and green mussel cultivation sites based on two-way ANOVA.

Variables	Means (Tukey test)						Sig. (*P*-value)		
	Location (L)			Depth (D)			L	D	D × L
	Khurushkul	Moheshkhali	Chowfaldandi	0.5 m	1 m	1.5 m			
Coscinodiscophyceae	128.92 ± 7.1^{a}	118.7 ± 7.1^{ab}	103.22 ± 8.0^{b}	134.6 ± 8.0^{a}	114.6 ± 7.3^{ab}	101.7 ± 6.6^{b}	*	**	NS
Fragilariophyceae	20.57 ± 3.5^{a}	17.88 ± 2.6^{a}	15.45 ± 2.8^{a}	20.28 ± 3.4^{a}	17.72 ± 2.9^{a}	15.91 ± 2.7^{a}	NS	NS	NS
Bacillariophyceae	135.5 ± 5.3^{a}	124.5 ± 5.9^{ab}	104.5 ± 6.6^{b}	139.6 ± 6.2^{a}	119.3 ± 6.1^{b}	105.6 ± 5.4^{b}	**	***	NS
Chlorophyceae	36.09 ± 2.1^{a}	34.29 ± 2.4^{a}	29.72 ± 2.5^{a}	38.12 ± 2.4^{a}	32.9 ± 2.3^{ab}	29.12 ± 2.1^{b}	NS	*	NS
Cyanophyceae	27.16 ± 2.4^{a}	23.53 ± 2.2^{ab}	18.69 ± 1.9^{b}	26.45 ± 2.5^{a}	22.7 ± 2.2^{a}	20.23 ± 1.9^{a}	*	NS	NS
Dinophyceae	62.85 ± 3.4^{a}	57.35 ± 3.8^{ab}	47.35 ± 3.6^{b}	63.55 ± 3.9^{a}	54.9 ± 3.8^{ab}	49.16 ± 3.3^{b}	*	*	NS
Total Phytoplankton	410.8 ± 15.0^{a}	376.3 ± 17.1^{ab}	318.9 ± 20.8^{b}	422.5 ± 18.0^{a}	362.1 ± 18.3^{b}	321.4 ± 16.6^{b}	**	***	NS
Total zooplankton	98.66 ± 10.7^{a}	94.85 ± 11.2^{a}	84.22 ± 10.2^{a}	103.3 ± 11.7^{a}	92.10 ± 10.7^{a}	82.36 ± 9.6^{a}	NS	NS	NS
Total Plankton	509.5 ± 23.8^{a}	471.2 ± 27.4^{ab}	403.1 ± 30.1^{b}	525.8 ± 27.8^{a}	454.2 ± 27.9^{ab}	403.7 ± 25.2^{b}	*	**	NS

The significance levels (*P*) are denoted by asterisks (*<0.05, **<0.01, ***<0.001, NS= Not significant). Significant variations among various depths and locations are shown by different superscripts in the same row at $p < 0.05$ level.

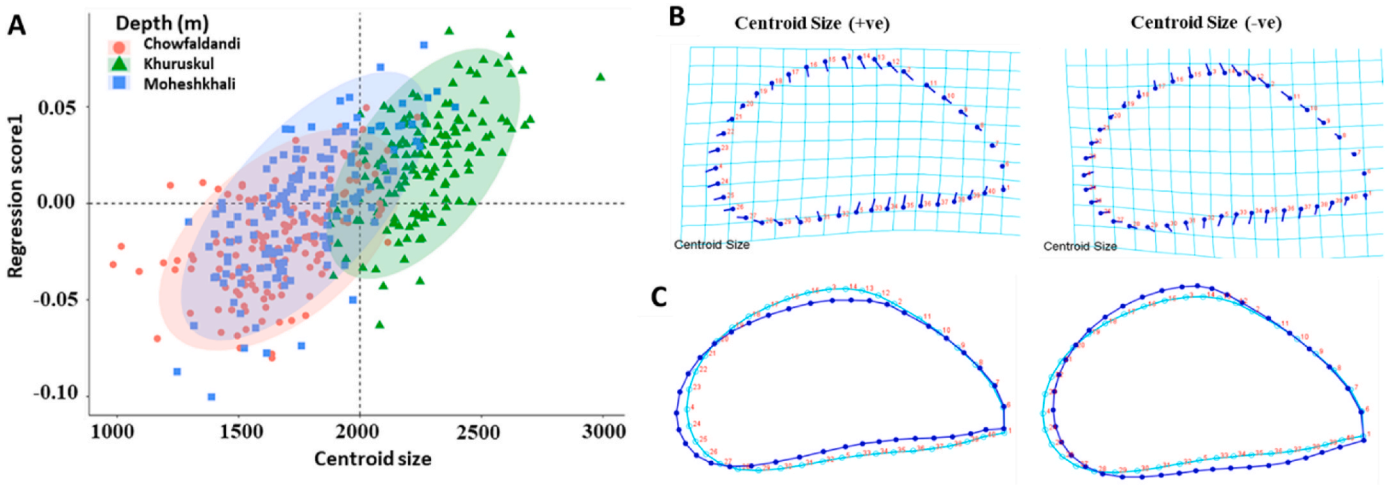

Fig. 3. (A)Variation in centroid size in *Perna viridis* population from three coastal habitats (Chowfaldandi, Khuruskul, Moheshkhali). (B) Procrustes deformations based on centroid size for both positive and negative values, where each dot indicates the mean and the line indicates the shape variation from the mean. (C) Shape variation in positive and negative wireframe plots for centroid size due to habitat variation.

comparison between Chowfaldandi and Khuruskul (Fig. 5A), positive DFA values are associated with Khuruskul (left wireframes), whereas negative values pertain to Chowfaldandi (right). Khuruskul mussel shells are comparatively slimmer and more elongated, exhibiting a lower dorsal bulge, while Chowfaldandi shells are more dorsally expanded, featuring a higher dome and a slightly deeper ventral profile. In Chowfaldandi–Moheshkhali (Fig. 5B), Chowfaldandi (negative/right) displays a larger, more domed configuration, whereas Moheshkhali (positive/left) is somewhat more tapered. In Khuruskul–Moheshkhali (Fig. 5C), Moheshkhali (positive/left) exhibits more dorsal expansion compared to Khuruskul (negative/right), which retains the most elongated form. Thin-plate splines and wireframes validate these regular alterations, with breadth (dorsal expansion) and elongation (posterior taper) underpinning inter-population variations. All Procrustes and Mahalanobis distances, together with T^2 statistics, exhibited strong significance ($P < 0.0001$; Supp. Table 2). Cross-validation revealed substantial classification accuracy: Chowfaldandi = 92 %, Khurushkul = 91.3 %, and Moheshkhali = 86.7 % (Supp Table 3).

3.3. Centroid size and shell morphometric divergence across cultivation depths

Depth-stratified analysis yielded an important insight into centroid size (Fig. 6A–C). At Chowfaldandi cultivation site (Fig. 6A), mussels from deeper strata displayed comparatively greater centroid sizes with slight ventral expansion, while shallow specimens were marginally dorsally compressed. Conversely, Khurushkul (Fig. 6B) exhibited an inverse trend, wherein shallow mussels were predominantly larger, whereas deeper specimens demonstrated diminished centroid sizes, with only negligible morphological variations across depths. A comparable trend was observed at Moheshkhali (Fig. 6C), where shallow mussels displayed higher centroid sizes, whereas deeper specimens were grouped towards smaller sizes, with dorsal-ventral compressions evident in the deformation and wireframe plots.

Depth-stratified PCA at each site (Fig. 7A–C) revealed further distinction. At Chowfaldandi, deeper mussels exhibited slight ventral growth compared to shallow specimens. At Khurushkul, the depth effects were minimal, exhibiting considerable overlap among the groups. Conversely, Moheshkhali demonstrated the most pronounced depth-related variations. Mussels at 0.5 m exhibited clustering towards compact morphologies, whilst those at 1.5 m demonstrated significant dorsal-ventral expansion. Depth-based CVA further elucidated grouping tendencies over the vertical gradient. Canonical Variate Analysis (CVA) demonstrated depth-related variations in the shell morphology of *P. viridis* among locations (Fig. 8). At Chowfaldandi, CV1 (66.1 % variance) distinguished between shallow (0.5 m) and deep (1.5 m) mussels, whereas individuals at 1.0 m exhibited overlap between the two categories (Fig. 8A). Deformation grids revealed that shallow mussels exhibited broader shells with pronounced ventral curvature, whereas deep mussels were narrower and more elongated, with the 1.0 m group

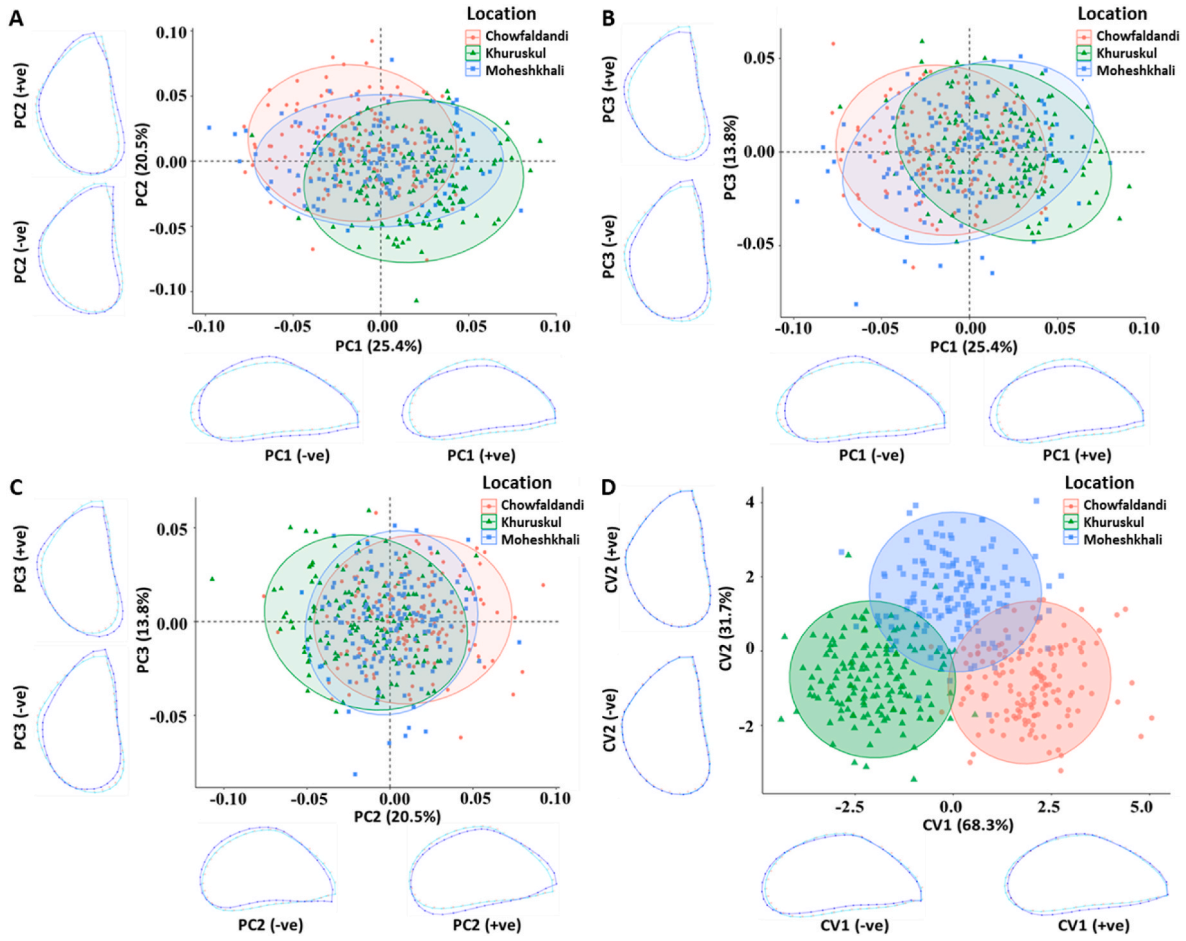

Fig. 4. Principal component analysis (PCA), Canonical variate analysis (CVA), and wireframe plots showing the morphological change described by each component due to habitat variation through geometric morphometrics of green mussel (*Perna viridis)*. (A–C) Principal component analysis (PCA) plot for the first three principal components showed percent contribution with shape variation in positive and negative wireframe plots, and (D) Canonical variate analysis (CVA) plots with percent comparison between CV1 and CV2 revealed the population shape variation with positive and negative wireframe plots. In wireframe plots, light blue outlines represent the average shape, and dark blue outlines represent extreme shape changes.

displaying transitional morphologies (Fig. 8B and C). The depth effects were most pronounced at Khurushkul. CV1 (75.97 % variance) clearly differentiated mussels based on depth (Fig. 8D). Morphological changes exhibited a progression from wider, more curved shells in shallow seas to narrower, elongated forms at greater depths, with intermediate mussels appearing transitional (Fig. 8E and F). The discrimination in Moheshkhali was less pronounced. CV1 (61.58 %) and CV2 (38.42 %) exhibited significant overlap among the groups (Fig. 8G). Deformation grids indicated minor variations, with shallow mussels being marginally broader and deeper mussels being more elongated, although the extent of change was minimal (Fig. 8H and I).

The pairwise DFA comparisons across each location, revealing a consistent, depth-dependent alteration in shell morphology (Fig. 9). In Chowfaldandi (Fig. 9A–C), Khuruskul (Fig. 9D–F), and Moheshkhali (Fig. 9G–I), deeper samples (the DFA-positive clusters in most comparisons: 1.0–1.5 m) exhibit enhanced dorsal convexity and overall shell breadth, accompanied by a more prominent ventral curvature. In contrast, shallower samples (DFA-negative clusters: 0.5–1.0 m) are generally narrower, more elongated, and taper posteriorly. The most significant morphological differences arise in greater depth contrasts (0.5 vs 1.5 m), where histograms indicate pronounced score separation and the wireframes (DFA ± ve) exhibit distinct dorsal uplift and rounder contours in the deeper group. Light-blue outlines represent the mean form, while dark-blue outlines denote the extremes, affirming that the primary axes of variation are dorsal height (degree of doming), shell breadth, and posterior taper. Depth predominantly effects shell morphology by modifying dorsal expansion and elongation, with effect size differing between locations. DFA pairwise testing indicated substantial Procrustes and Mahalanobis distances among most categories, with the most pronounced separation observed between shallow (0.5 m) and deep (1.5 m) strata (Supp. Table 4). Nonetheless, classification accuracy was significantly inferior to that of site-based comparisons (52.7 %–66 %; Supp. Table 5), indicating that depth-driven variations were more nuanced and overlapped. These data collectively indicate a pronounced spatial structure of shell morphology, whereas depth has a lesser nevertheless ecologically significant impact.

3.4. Shell color divergence across cultivation sites

The shell coloration parameters of *P. viridis* exhibited distinct site-specific variations among Chowfaldandi, Khurushkul, and Moheshkhali (Fig. 10). The chromatic variable “a” (green–red axis) exhibited substantial variation between sites ($P < 0.05$). Khurushkul mussels had elevated values (-1.82 ± 0.16), signifying a more pronounced reddish component relative to Chowfaldandi (-2.43 ± 0.18), while Moheshkhali showed intermediate values (-2.17 ± 0.17). The “b” parameter (blue–yellow axis) also differed significantly ($P < 0.01$), with Khurushkul individuals exhibiting the greatest yellowness (9.18 ± 0.42), Moheshkhali the lowest (7.73 ± 0.38), and Chowfaldandi occupying a median position (8.70 ± 0.49). This pattern underscores a trend toward

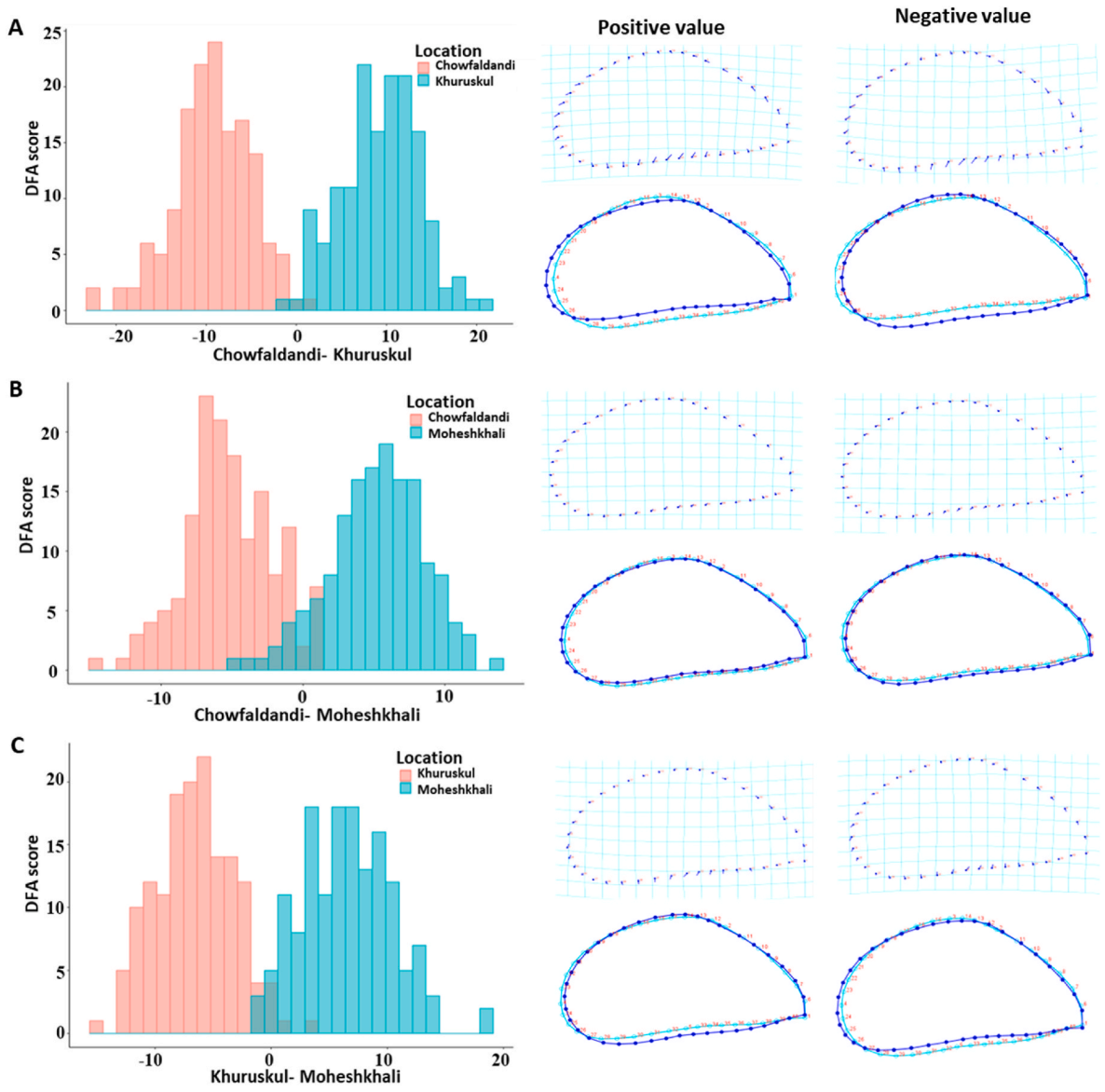

Fig. 5. Discriminant Function Analysis (DFA) for pairwise comparison and corresponding thin-plate spline of Procrustes deformations and wireframe plots illustrating shape variation of green mussel (*Perna viridis*). DFA histogram with positive and negative wireframe plots showed mean shape variation between Chowfaldandi-Khurushkul (A), Chowfaldandi-Moheshkhali (B), Khurushkul-Moheshkhali (C) populations. Light blue outlines represent the average shape, and dark blue outlines represent extreme shape changes.

warmer shell hues in Khurushkul mussels. Among brightness-related variables, most parameters (B, R, L-1, L-2, V) did not differ significantly among sites. However, the green component (G) exhibited a significant difference ($P < 0.05$), with Khurushkul mussels showing notably higher values compared to Chowfaldandi and Moheshkhali, reflecting the visually strong green pigmentation observed in shells from this site. Both hue descriptors (H-1 and H-2) showed pronounced site effects ($P < 0.001$). Moheshkhali mussels consistently displayed elevated hue values (H-1 = 60.41 ± 1.01; H-2 = 106.36 ± 0.88) compared to Chowfaldandi (H-1 = 55.49 ± 0.88; H-2 = 102.09 ± 0.91) and Khurushkul (H-1 = 55.10 ± 0.92; H-2 = 101.86 ± 0.82). Saturation (S) also differed significantly ($P < 0.001$), being highest in Khurushkul (26.71 ± 0.43) relative to Chowfaldandi (22.32 ± 0.37) and Moheshkhali (21.68 ± 0.40). This elevated saturation corresponds to the visibly brighter and more vivid greenish coloration recorded from Khurushkul mussels (Fig. 10B). The site-based dendrogram (Fig. 10C) corroborates these patterns, revealing closer color similarity between Chowfaldandi and Moheshkhali, while Khurushkul forms a distinct cluster. This grouping indicates that Khurushkul mussels exhibit greater divergence, primarily driven by elevated saturation and green chroma, whereas Chowfaldandi and Moheshkhali maintain comparable hue–lightness profiles. Collectively, these results suggest that although baseline lightness and reflectance remain stable across regions, the coloration of *P. viridis* displays notable plasticity in response to local environmental conditions, with hue, saturation, and green intensity emerging as key indicators of site-specific ecological influences.

3.5. Depth-specific variation in shell coloration

The shell coloration parameters of *Perna viridis* showed significant depth-specific variation across 0.5, 1.0 and 1.5 m (Fig. 11). Chromatic variables a (green–red) and b (blue–yellow) did not differ significantly with depth (both NS). Likewise, most lightness and primary channel indices (R, B, L-1, L-2, V) remained statistically stable. However, the green channel (G) exhibited a significant depth effect ($P < 0.05$), with the highest green intensity recorded at 0.5 m relative to 1.0 and 1.5 m,

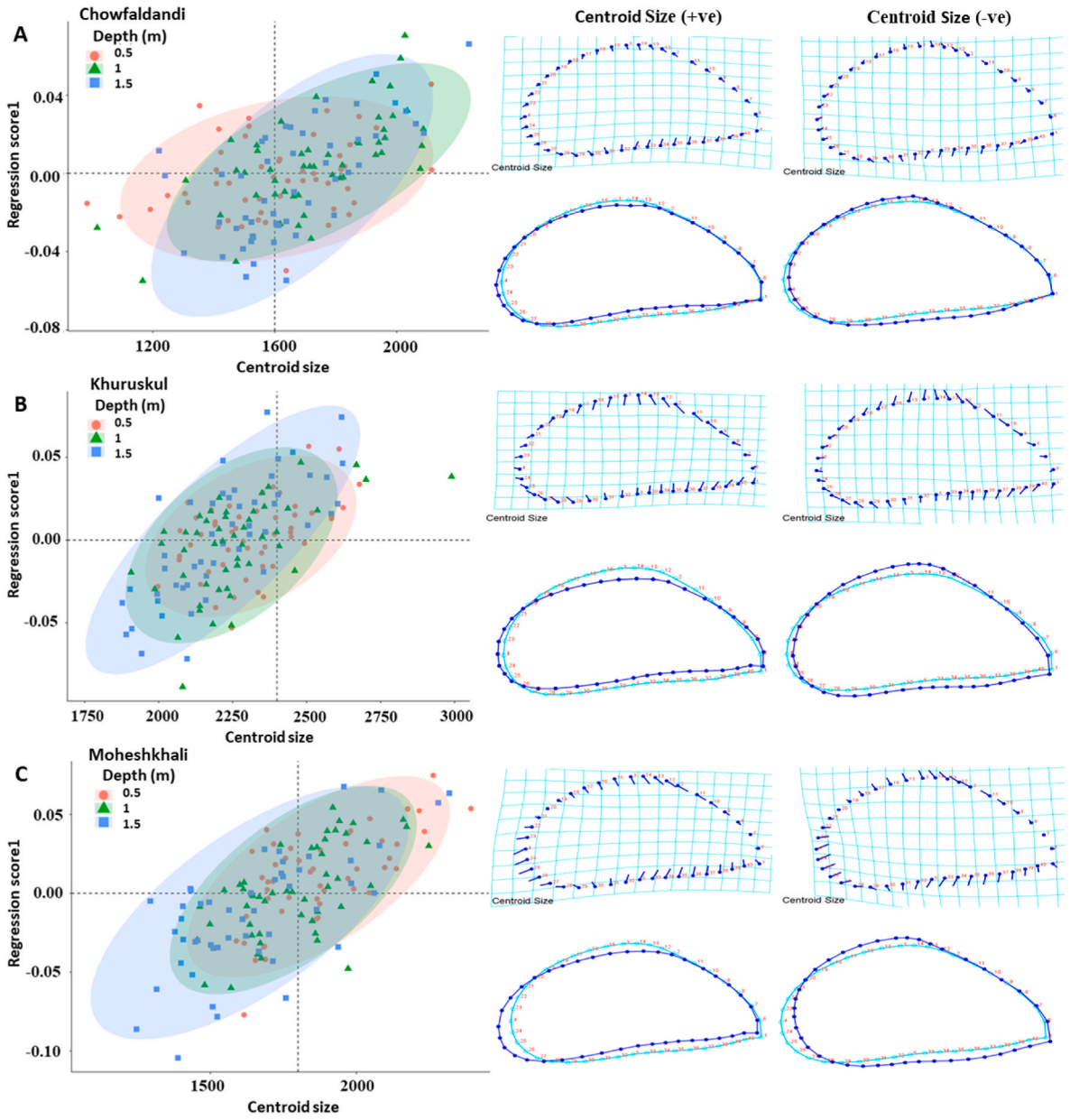

Fig. 6. Centroid size variation of *Perna viridis* across depth strata within three coastal sites: (A) Chowfaldandi, (B) Khurushkul, and (C) Moheshkhali. Mean centroid size values (dots) and corresponding Procrustes deformation plots (lines) illustrate depth-related shell size changes and associated shape variation. Wireframe diagrams indicate localized expansions and compressions in shell morphology, potentially driven by habitat conditions at varying depths.

consistent with the visibly greener shells at shallow culture depth. Both hue descriptors (H-1, H-2) varied strongly with depth ($p < 0.001$). Mussels at 1.0 m showed reduced hue values (H-1 = 53.45 ± 0.91; H-2 = 100.09 ± 0.91) compared with 0.5 m (H-1 = 57.48 ± 0.95; H-2 = 103.70 ± 0.90) and 1.5 m (H-1 = 60.07 ± 0.94; H-2 = 106.53 ± 0.79), indicating a mid-depth shift toward browner tones. Saturation (S) also differed with depth ($p < 0.001$), peaking at 1.0 m (25.50 ± 0.42) versus 0.5 m (23.22 ± 0.39) and 1.5 m (21.99 ± 0.42), implying more vivid chroma at mid-depth. The depth-based dendrogram (Fig. 11C) supports these patterns: 0.5 m mussels are the most distinct group (driven largely by elevated G), while 1.0 m forms a separate branch driven by hue and saturation differences, and 1.5 m clusters more closely with the others. Overall, although baseline brightness and major reflectance indices remain relatively constant with depth, green intensity, hue and saturation are the most responsive color metrics to culture depth in *P. viridis*.

4. Discussion

4.1. Cultivation site- and depth-specific divergence in shell morphology of *P. viridis*

In bivalves, shell morphology is significantly influenced by hydrodynamics, food availability, salinity, turbidity, and oxygen gradients, which serve as selection forces that promote adaptive plasticity (Hornbach et al., 2010; Keogh et al., 2024). The current study demonstrated distinct variations in *P. viridis* morphology based on site and depth, which closely aligned with the environmental variables assessed at different locations and depths. The larger and more resilient morphotypes at Khurushkul align with advantageous environmental conditions marked by elevated dissolved oxygen and consistent salinity. Increased oxygen availability improves aerobic metabolism and calcification efficiency (Telesca et al., 2018), while elevated nitrate and phosphate concentrations promote primary production, ensuring a

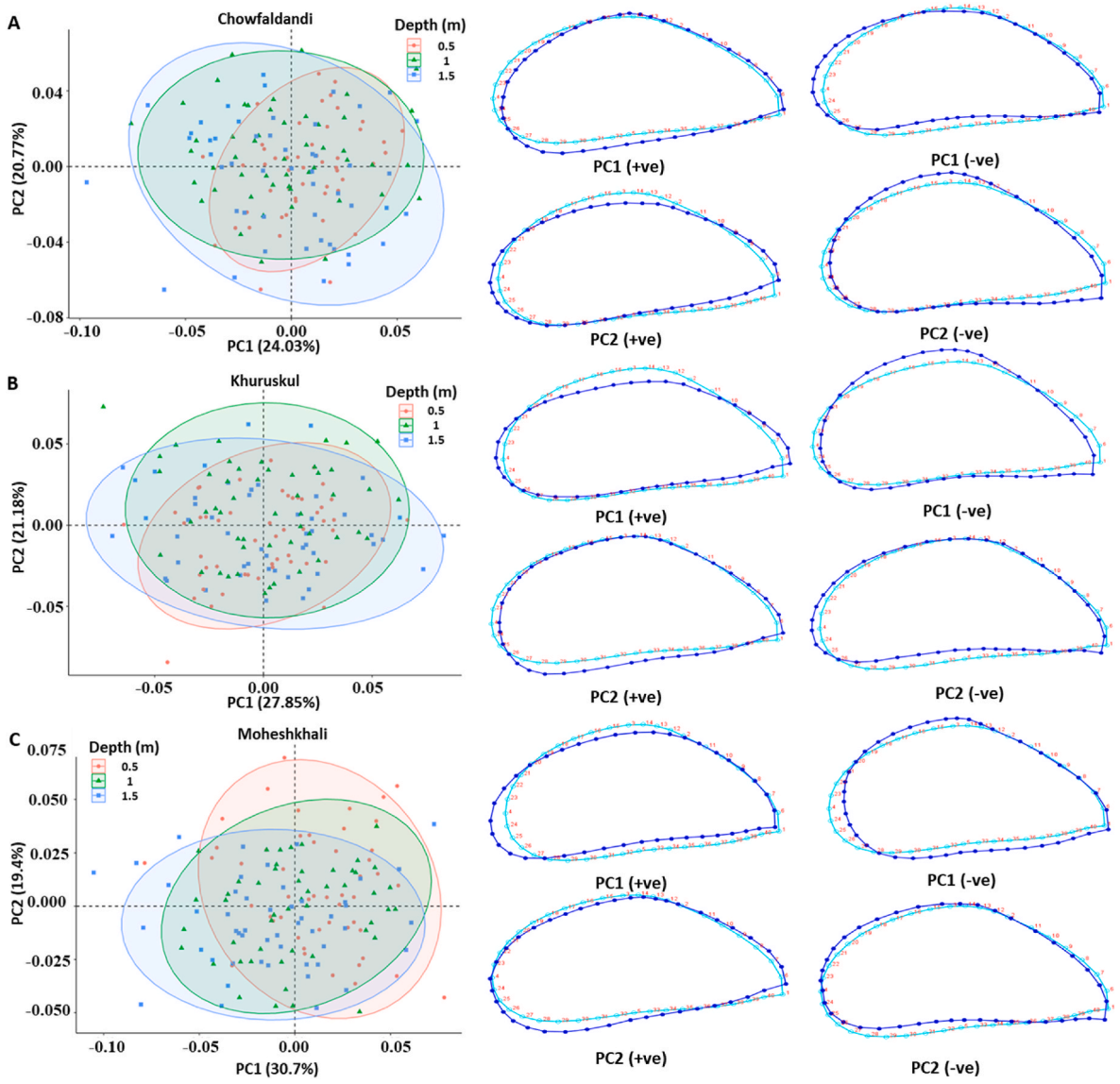

Fig. 7. Principal Component Analysis (PCA) of shell shape variation in *Perna viridis* across depth levels (0.5 m, 1.0 m, 1.5 m) at: **(A)** Chowfaldandi, **(B)** Khurushkul, and **(C)** Moheshkhali. Each PCA plot shows PC1 vs. PC2 with associated variance percentages. Wireframe plots display representative shape deformations along each principal axis, indicating site-specific depth-induced changes in dorsal and ventral shell margins.

consistent supply of phytoplankton for suspension feeding. The interplay of food availability and metabolic efficiency fosters conditions that enable mussels to direct energy towards shell formation, leading to thicker and broader shells (Schotanus et al., 2019; Wang et al., 2011). In contrast, Chowfaldandi mussels displayed compressed and elongated morphologies indicative of harsher conditions at this location. The markedly reduced salinity noted here elevates osmotic stress, augmenting the energetic expenditures of ionic control and diminishing the energy allocated for calcification (Sanders et al., 2018; Zeng et al., 2024). Concurrently, elevated turbidity levels diminish feeding efficiency by obstructing gills and hindering oxygen absorption (Firth et al., 2024), while insufficient chlorophyll-a further restricts food availability. In these circumstances, mussels must reallocate resources from growth to maintenance, resulting in thinner, elongated shells that demonstrate adaptive plasticity in reaction to environmental stressors (Seitz et al., 2023; Telesca et al., 2018). Moheshkhali exhibited intermediate conditions, characterized by moderate salinity, low turbidity, and comparatively high chlorophyll-a, hence sustaining mussels with intermediate morphologies. This underscores the notion that mussel shell morphology incorporates many environmental signals, resulting in morphologies that embody local compromises between growth efficiency and stress resilience (Bergström et al., 2015).

Depth effects, while less pronounced than site influences, were also apparent in the studied patterns. Dissolved oxygen and chlorophyll-a exhibited a marked decrease with depth, but nitrate concentrations were elevated in shallower waters. These observed depth-related shell variations are consistent with patterns reported in temperate mussel systems (*Mytilus edulis*, *M. trossulus*), where shell shape reflects environmental gradients such as food availability, salinity, and temperature (Carboni et al., 2021). While hydrodynamic factors may contribute to shell morphology in our sites, the absence of direct in-situ measurements of current velocity, wave orbital motion, or bottom shear stress limits mechanistic inference, and the observed patterns should therefore be interpreted as correlative rather than causative. Furthermore, shell strength and morphology in bivalves are known to be phenotypically plastic, responding to local water chemistry (*e.g.*, salinity, pH, dissolved inorganic carbon) rather than being strictly genetically determined (Telesca et al., 2018). Mussels inhabiting shallow waters typically possess compact, streamlined shells designed to endure wave action and minimize dislodgement risk, whereas those in deeper waters display

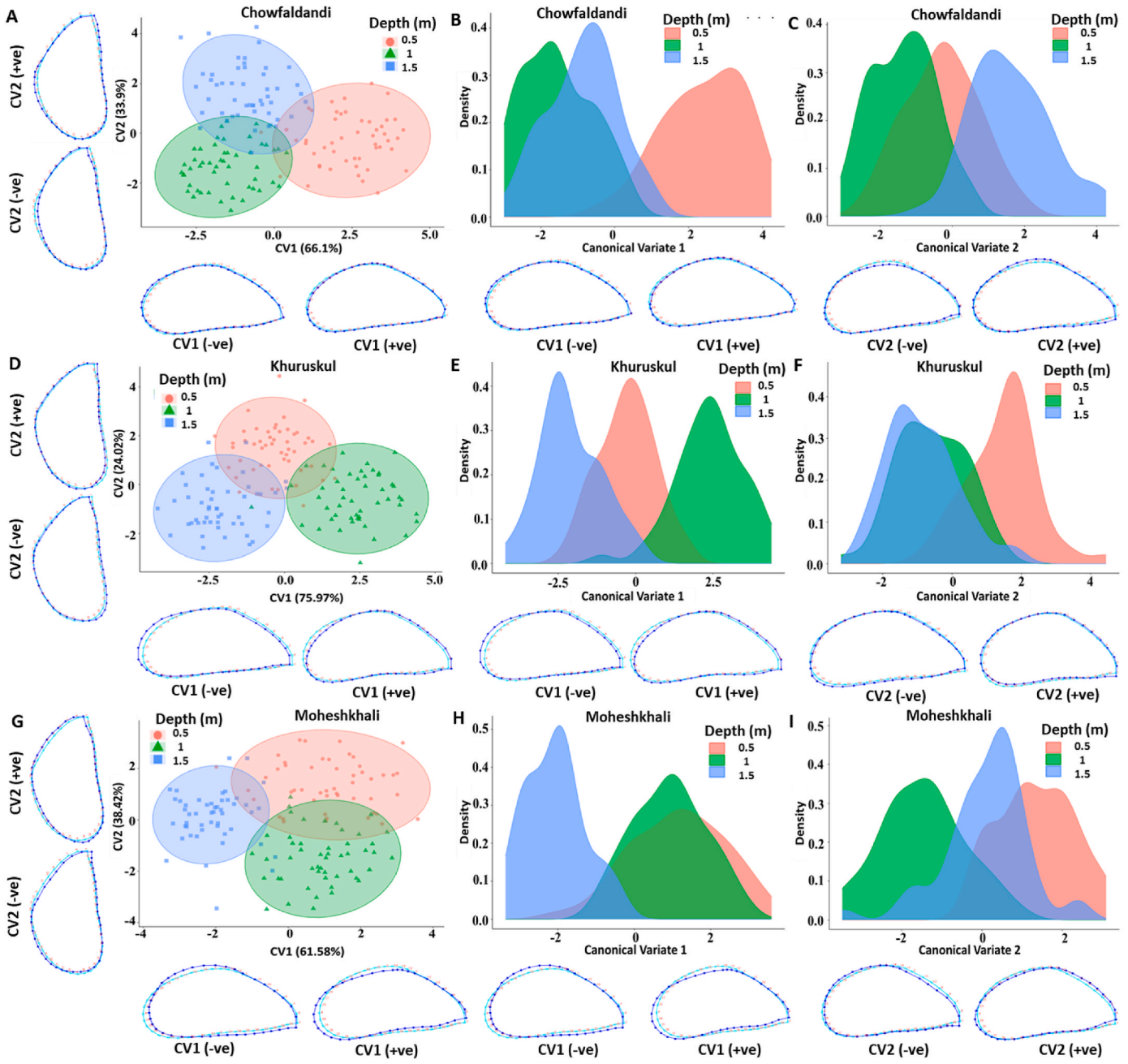

Fig. 8. Canonical Variate Analysis (CVA) of *Perna viridis* shell shape variation across depth gradients in (A–C) Chowfaldandi, (D–F) Khuruskul, and (G–I) Moheshkhali. CVA scatterplots (A, D, G) contrast CV1 and CV2 scores, revealing group clustering by depth. Corresponding density plots (B–C, E–F, H–I) highlight phenotypic overlap among depth groups, with the highest convergence at intermediate depths (1.0 m), suggesting moderate morphological plasticity.

rounder, inflated shapes more appropriate for tranquil, low-disturbance settings with softer substrates (Hermanson, 2011; Peyer et al., 2010). Together, these observations suggest depth-related phenotypic plasticity consistent with hydrodynamic gradients, although direct mechanistic inference remains limited in the absence of site-specific flow measurements, wherein shell morphology reflects trade-offs between stability and growth efficiency across depth strata (Elgin et al., 2022; Longman & Sanford, 2025).

The amalgamation of morphometric and environmental data indicates that site-specific elements, notably salinity, turbidity, oxygen, and food availability, have a more significant influence on mussel morphology than depth alone. The observed variation in shell morphology across locations and depths underscores the phenotypic plasticity of *P. viridis*, allowing it to endure in diverse coastal ecosystems. This plasticity holds ecological importance, enabling mussels to enhance performance amid varying hydrological and trophic conditions, thereby illustrating their function as sensitive bioindicators of environmental fluctuations in dynamic tropical ecosystems (Longman & Sanford, 2025; Telesca et al., 2018).

4.2. Cultivation site- and depth-specific divergence in shell coloration of *P. viridis*

Shell coloration in *P. viridis* also emerged as a highly site-dependent trait, strongly shaped by local environmental conditions. The differences in shell color and intensity among locations are mostly influenced by environmental factors, especially food supply and light penetration. This corroborates previous research indicating that pigmentation patterns in

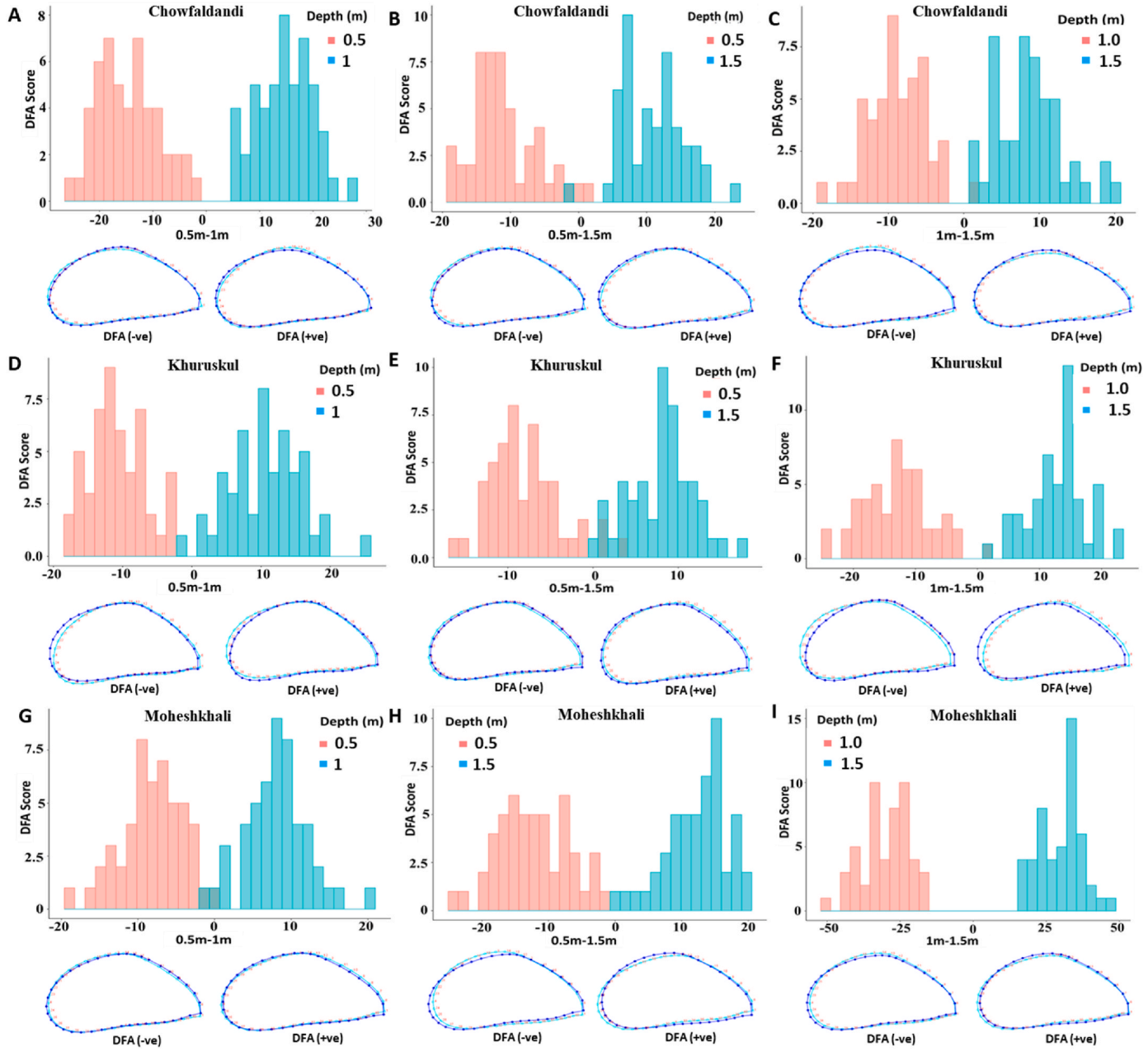

Fig. 9. Discriminant Function Analysis (DFA) for pairwise comparison and corresponding wireframe plots for both positive and negative values illustrating shape variation for three distinct regions: Chowfaldandi (A–C), Khuruskul (D–F), and Moheshkhali (G–I). Each region has three plots comparing two depth levels within specific depth ranges. Chowfaldandi's plots (A–C) reveal the DFA score distribution for depths 0.5m and 1m (A), 0.5m and 1.5m (B), and a comparison between 1m and 1.5m (C). Khuruskul's distributions (D–F) follow a similar pattern with scores between 0.5m and 1m (D), 0.5m and 1.5m (E), and 1m versus 1.5m (F). Moheshkhali (G–I) mirrors this depth analysis with plots for 0.5m and 1m (G), 0.5m and 1.5m (H), and a 1m–1.5m comparison (I). Light blue outlines represent the average shape, and dark blue outlines represent extreme shape changes.

bivalves are integrative features that reflect ecological pressures and physiological performance (Alma et al., 2023; Fitzer et al., 2015; Louis et al., 2022; Purroy Albet, 2017). Mussels from Khurushkul consistently exhibited the most vibrant coloration, aligning with optimal hydrodynamic and trophic conditions. The significantly higher dissolved oxygen (DO), salinity, and chlorophyll-a concentration recorded at this site indicate a favorable environment supporting higher primary productivity and planktonic food availability (Tables 1 and 2). These enhanced trophic and oxygenic conditions likely promote chlorophyll-a assimilation and boost pigment biosynthesis, leading to deeper and more saturated shell hues (He et al., 2024; McMahon et al., 2024; Olivier et al., 2020). The elevated saturation and green (G) values observed in Khurushkul mussels therefore indicate a clear correlation between food availability and pigment accumulation (Saurel, 2008). The high abundance of diatoms and total phytoplankton at Khurushkul further reinforces this relationship, as diatom-dominated diets are rich in carotenoids and chlorophyll derivatives that can enhance shell pigmentation and green chroma expression. Conversely, Chowfaldandi individuals had pale and chalky shells, indicative of consistently murky conditions that restrict light penetration due to higher suspended particles and turbidity (Table 1), hence diminishing phytoplankton development and inhibiting pigment absorption (Alexander Jr et al., 1994; Tuttle-Raycraft & Ackerman, 2019). Turbidity inhibits chlorophyll precursors and induces extra stress, redirecting energy towards survival

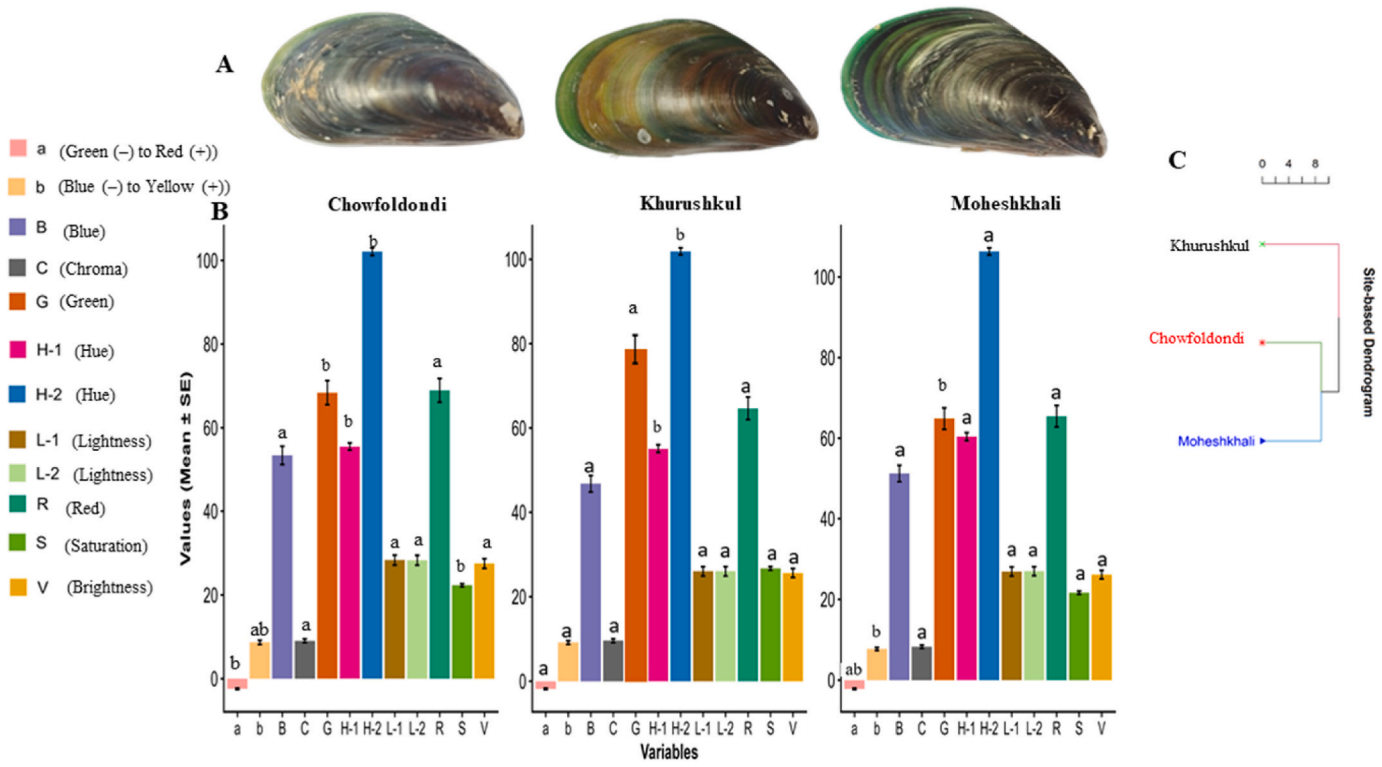

Fig. 10. Variation in shell coloration of *Perna viridis* across three coastal sites in Bangladesh. (A) Representative shell images from Choufaldondi, Khurushkul, and Moheshkhali showing site-specific differences in external coloration. (B) Site-wise comparisons of color parameters derived from multiple color models (CIELAB: a, b, L-1, L-2; RGB: R, G, B; HSV: H-1, H-2, S, V; Chroma = C), with bars representing mean ± SD. Different letters above bars indicate significant differences among variables within sites (Tukey's HSD, $P < 0.05$). (C) Site-based dendrogram constructed from color metrics, showing greater similarity between Chowfaldondi and Moheshkhali, while Khurushkul mussels form a distinct cluster. Collectively, these results demonstrate that mussel shell coloration is influenced by site-specific environmental conditions.

and maintenance instead of pigment synthesis (Buczek et al., 2018; Cloern, 1987; Nunes et al., 2022; Wang et al., 2019). Comparable pigment depletion and lackluster appearance have been documented in bivalves from sediment-rich environments (Jones et al., 2011; Scanes et al., 2024; Volety et al., 2006). The mussels of Moheshkhali exhibited an intermediate condition, aligned with variable environmental influences. Although DO and salinity were comparatively high, fluctuating turbidity and nutrient regimes likely created alternating favorable and stressful phases for pigment deposition. Intermittent access to phytoplankton-dense waters facilitated partial pigment expression (Becker et al., 2021; Jiang et al., 2022), whereas repeated turbidity events disrupted uniform deposition. This variability was apparent in intermediate hue values, indicating that coloration at this location is influenced by alternating periods of advantageous feeding conditions and sediment stress (Norkko et al., 2006; Scanes et al., 2024). These findings collectively indicate that shell coloration in *P. viridis* is a dynamic trait that adapts to ecological conditions, reflecting variations in food availability, light penetration, and sediment stress, thereby acting as a significant bioindicator of localized environmental quality in coastal ecosystems (Carroll et al., 2009; Steinhardt et al., 2016; Strehse & Maser, 2020).

The significance of depth as an ecological filter was especially apparent in shell pigmentation. Hue and saturation were affected by vertical variations in light and food availability, aligning with depth-related ecological gradients such as light penetration, food resources, and suspended materials (Stenger et al., 2021; Rousseau & Rollion-Bard, 2012). At 0.5 m, where water quality data indicated the highest chlorophyll-a and total plankton abundance, the more vibrant and saturated colors likely indicate increased light penetration and higher availability of chlorophyll *a*, which promotes feeding efficiency and pigment assimilation (Diana et al., 2021). Elevated light intensity at shallow depths facilitates phytoplankton proliferation, hence providing a substantial food source for filter-feeding mussels, which amplifies pigmentation intensity (Trottet et al., 2008). The significantly higher green (G) values at this depth confirm that shallower mussels assimilate more phytoplankton-derived pigments, particularly from diatom-rich assemblages abundant near the surface. Reduced suspended sediments at this level facilitate clearer color expression, as sediment load influences lighter, chalkier shell appearances (Fu et al., 2016; Saenko & Schilthuizen, 2021). At 1.0 m, mussels displayed a significant transition to brownish and more saturated tones, indicative of distinct intermediate circumstances. Moderate light penetration at this mid-water depth supports photosynthetic biofilms, which enhance food availability and provide cues for pigment synthesis. Simultaneously, variable dissolved oxygen and nutrient concentrations can induce physiological stress, leading to upregulated melanin and other pigment production as part of antioxidant and photoprotective responses (Comfort, 1951; Gefaell et al., 2023; Williams, 2017). These combined ecological and physiological factors likely explain why mussels at this level had a distinct cluster in the dendrogram, indicating unique environmental stresses that heightened pigmentation. In contrast, mussels at 1.5 m had the most pallid and least saturated shells. Decreased light availability limits photosynthetically active radiation, resulting in reduced phytoplankton biomass and food consumption (Dolmer, 2000; Hoque et al., 2021), which leads to a decline in pigment assimilation and shell vibrancy (Zieritz et al., 2019). Increased turbidity and suspended particles at greater depths disrupt feeding and shell deposition (Melzner et al., 2011), whereas oxygen deficiency may impair mussel metabolism and pigment production (Sanders et al., 2018; Wang et al., 2011). These factors collectively elucidate the muted shell colors noted in deeper mussels. In summary, depth-specific variation in shell coloration signifies a cohesive reaction to light, food accessibility, and water column

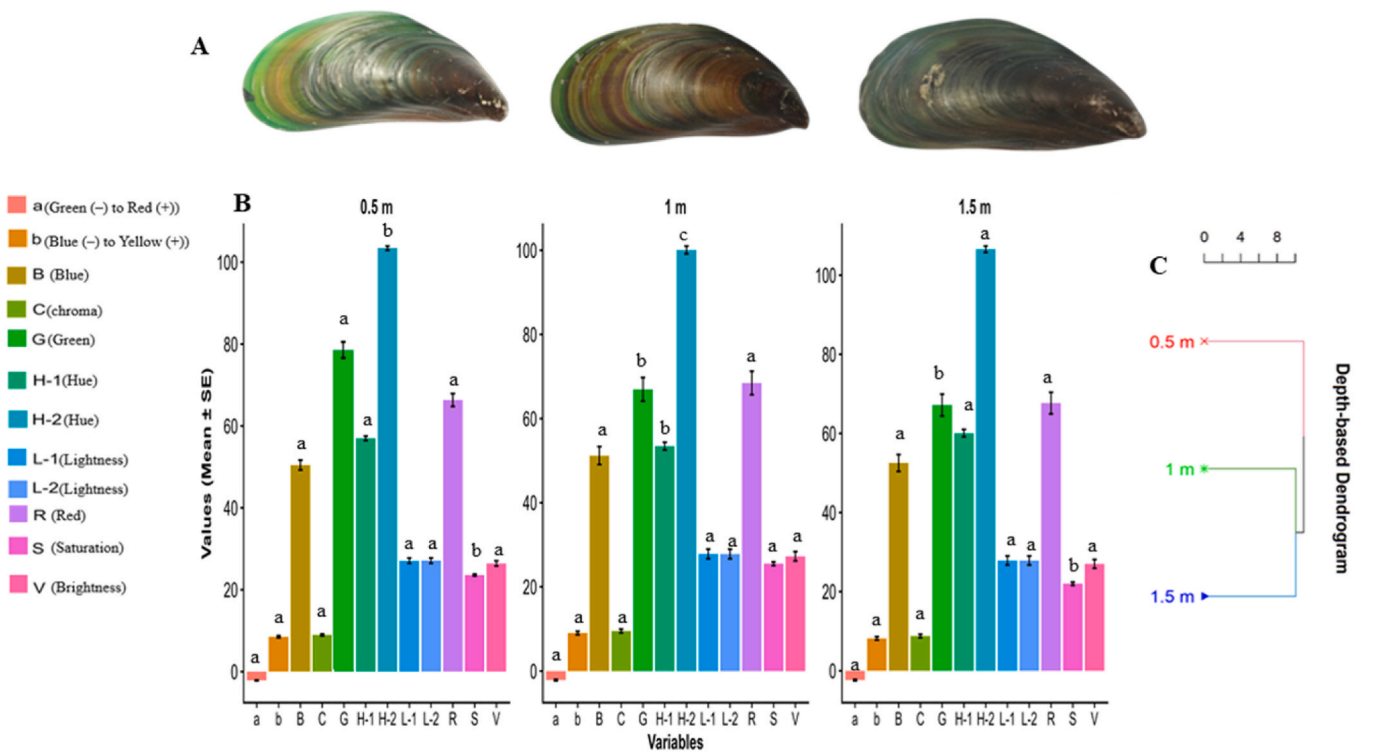

Fig. 11. Variation in shell coloration of *Perna viridis* across three culture depths. (A) Representative shell images from 0.5 m, 1 m, and 1.5 m showing depth-specific differences in external coloration. (B) Depth-wise comparisons of color parameters derived from multiple color models (CIELAB: a, b, L-1, L-2; RGB: R, G, B; HSV: H-1, H-2, S, V; Chroma = C), with bars representing mean ± SD. Different letters above bars indicate significant differences among variables within depths (Tukey's HSD, $P < 0.05$). (C) Depth-based dendrogram constructed from color metrics, showing clear clustering by depth, with 0.5 m mussels forming the most distinct group. Collectively, these results indicate that shell coloration is influenced by cultivation depth.

stability. The shallow and deeper mussels exhibited greener yet less saturated hues, whereas the mid-depth population manifested noticeably brownish and more vibrant shells. This indicates that shell pigmentation in *P. viridis* is markedly responsive to vertical gradients, underscoring its significance as a bioindicator of ecological variability in both aquaculture and wild environments (Asaduzzaman et al., 2019; Yap et al., 2023).

5. Conclusion

This study revealed that the shell morphology and coloration of *P. viridis* are significantly variable features affected by the cultivation site and depth in raft-based mariculture systems along the southeastern coast of Bangladesh. Geometric morphometric investigations indicated significant site-specific divergence: Khurushkul mussels were elongated and thin, Chowfaldandi individuals were compact and rounded, whilst Moheshkhali mussels exhibited increased dorsal-ventral expansion with intermediate forms. Depth effects were nuanced yet biologically significant, as shallow mussels displayed bigger, streamlined morphologies, while deeper mussels presented smaller, dorsally compressed forms. Shell coloration exhibited significant variation across locations and depths, with Khurushkul mussels displaying the most intense pigmentation, Chowfaldandi mussels appearing subdued under murky conditions, and Moheshkhali populations presenting intermediate shades. Vertical gradients influenced pigmentation, with mid-depth mussels exhibiting more vivid brownish hues, whereas surface individuals presented greener yet less saturated shells. Additionally, direct measurements of water flow velocity, wave orbital motion, or bottom shear stress were not conducted, which limits empirical support for the proposed mechanistic link between hydrodynamics and observed shell plasticity. This study, while robust, was confined to three locations and a single culture cycle, neglecting seasonal or genetic factors affecting phenotypic variation. Nevertheless, the findings had practical implications for aquaculture, offering a scientific foundation for site selection, depth optimization, and selective breeding procedures to improve production and market attractiveness. Future research should encompass multi-seasonal evaluations, extensive geographic comparisons, and genomic analysis to elucidate genetic and environmental influences, and experimental trials examining specific ecological factors, including hydrodynamic conditions. These initiatives will enhance ecological comprehension and facilitate the sustainable growth of mussel aquaculture in tropical coastal habitats.

CRediT authorship contribution statement

Kanij Fatema Eti: Writing – original draft, Software, Methodology, Investigation, Formal analysis, Data curation. **Rahanuma Tasnim:** Methodology, Investigation, Formal analysis, Data curation. **Afshana Ferdous:** Writing – review & editing, Methodology, Data curation. **Md Mohiuddin:** Writing – review & editing, Resources, Methodology, Investigation, Data curation. **Md Nayeem Hossain:** Writing – review & editing, Visualization, Formal analysis, Data curation. **Md Moshiur Rahman:** Visualization, Software, Formal analysis, Data curation. **Md Asaduzzaman:** Writing – original draft, Visualization, Software, Resources, Project administration, Funding acquisition, Conceptualization.

Ethics statement

This research involved working with marine bivalves (invertebrates) and did not require approval from the Chattogram Veterinary and Animal Sciences University Welfare Committee according to the Bangladesh Code for the Care and Use of Animals for Scientific Purposes.

Data availability statement

Data will be made available on request.

Declaration of generative AI in scientific writing

During the preparation of this work, the authors used ChatGPT in the writing process to improve the readability and language of the manuscript. After using this tool/service, the authors reviewed and edited the content as needed and took(s) full responsibility for the content of the published article.

Declaration of competing interest

The authors declare that they have no known competing financial interests or personal relationships that could have appeared to influence the work reported in this paper.

Acknowledgements

This work was conducted as a part of the research plan of the Bangladesh Academy of Sciences- United States Department of Agriculture (BAS-USDA) Endowment 5th phase project implemented by Chattogram Veterinary and Animal Sciences University through a collaborative agreement with BAS (F 127). We would like to thank the director and other staff of the BAS-USDA Endowment Program for providing funding for this research work. We also thank the staff of the Oceanography Laboratory, Department of Marine Bioresource Science, Chattogram Veterinary and Animal Sciences University, for helping with oyster sampling and parameter analysis.

Appendix A. Supplementary data

Supplementary data to this article can be found online at https://doi.org/10.1016/j.aaf.2026.01.003.

References

Adams, D. C., Rohlf, F. J., & Slice, D. E. (2004). Geometric morphometrics: Ten years of progress following the "revolution.". *Italian Journal of Zoology, 71*(1), 5–16.

AftabUddin, S., Hussain, M. G., Abdullah, A. M., Failler, P., & Drakeford, B. M. (2021). On the potential and constraints of mariculture development in Bangladesh. *Aquaculture International, 29*, 575–593.

Akkaynak, D., Treibitz, T., Xiao, B., Gürkan, U. A., Allen, J. J., Demirci, U., & Hanlon, R. T. (2014). Use of commercial off-the-shelf digital cameras for scientific data acquisition and scene-specific color calibration. *Journal of the Optical Society of America A, 31*(2), 312–321.

Alexander Jr, J. E., Thorp, J. H., & Fell, R. D. (1994). Turbidity and temperature effects on oxygen consumption in the zebra mussel (*Dreissena polymorpha*). *Canadian Journal of Fisheries and Aquatic Sciences, 51*(1), 179–184.

Alma, L., Fiamengo, C. J., Alin, S. R., Jackson, M., Hiromoto, K., & Padilla-Gamiño, J. L. (2023). Physiological responses of scallops and mussels to environmental variability: Implications for future shellfish aquaculture. *Marine Pollution Bulletin, 194*, Article 115356.

Appukuttan, K. K., Asokan, P. K., Mohamed, K. S., Subramanian, S., & George Joseph, K. (2003). *Manual on mussel farming (Technical bulletin no. 3)* (pp. 1–23).

Asaduzzaman, M., Akter, S., Hoque, N. F., Shakil, A., Noor, A. R., Akter, M. N., & Rahman, M. M. (2020). Multifaceted linkages among eco-physiological factors, seasonal plankton dynamics and selective feeding behavior of the green mussel (*Perna viridis*) in the south-east coast of the Bay of Bengal. *Journal of Sea Research, 160*, Article 101933.

Asaduzzaman, M., Mohiuddin, M., Rahman, M. M., Kabir, I. E., & Nahiduzzaman, M. (2025). Ecology intersects with mariculture: How cultivation depth and site-specific environmental factors shape growth and nutritional profile of green mussels (*Perna viridis*). *Regional Studies in Marine Science, 81*, Article 103981.

Asaduzzaman, M., Noor, A. R., Rahman, M. M., Akter, S., Hoque, N. F., Shakil, A., & Wahab, M. A. (2019). Reproductive biology and ecology of the green mussel *Perna viridis*: A multidisciplinary approach. *Biology, 8*(4), 88.

Becker, K. W., Harke, M. J., Mende, D. R., Muratore, D., Weitz, J. S., DeLong, E. F., Dyhrman, S. T., & Van Mooy, B. A. (2021). Combined pigment and metatranscriptomic analysis reveals highly synchronized diel patterns of phenotypic light response across domains in the open oligotrophic ocean. *The ISME Journal, 15*(2), 520–533.

Bergström, P., Lindegarth, S., & Lindegarth, M. (2015). Modeling and predicting the growth of the mussel, Mytilus edulis: Implications for planning of aquaculture and eutrophication mitigation. *Ecology and Evolution, 5*(24), 5920–5933.

Beyett, T. W., McNichols-O'Rourke, K., Morris, T. J., & Zanatta, D. T. (2020). Use of morphometric analyses and DNA barcoding to distinguish *Truncilla donaciformis* and *Truncilla truncata* (Bivalvia: Unionidae). *Freshwater Mollusk Biology and Conservation, 23*(2), 99–108.

Bookstein, F. L. (1997). Landmark methods for forms without landmarks: Morphometrics of group differences in outline shape. *Medical Image Analysis, 1*(3), 225–243.

Borcard, D., Gillet, F., & Legendre, P. (2018). Spatial analysis of ecological data. In *Numerical ecology with R* (pp. 299–367). Springer.

Boyd, C. E. (1979). *Water quality in warm water fish ponds*. Auburn, AL, USA: Auburn University.

Buczek, S. B., Cope, W. G., McLaughlin, R. A., & Kwak, T. J. (2018). Effects of turbidity, sediment, and polyacrylamide on native freshwater mussels. *JAWRA Journal of the American Water Resources Association, 54*(3), 631–643.

Cadrin, S. X., & Friedland, K. D. (1999). The utility of image processing techniques for morphometric analysis and stock identification. *Fisheries Research, 43*(1–3), 129–139.

Carboni, S., Evans, S., Tanner, K. E., Davie, A., Bekaert, M., & Fitzer, S. C. (2021). Are shell strength phenotypic traits in mussels associated with species alone? *Aquaculture Journal, 1*(1), 3–13.

Carroll, M. L., Johnson, B. J., Henkes, G. A., McMahon, K. W., Voronkov, A., Ambrose Jr, W. G., & Denisenko, S. G. (2009). Bivalves as indicators of environmental variation and potential anthropogenic impacts in the southern Barents Sea. *Marine Pollution Bulletin, 59*(4–7), 193–206.

Cloern, J. E. (1987). Turbidity as a control on phytoplankton biomass and productivity in estuaries. *Continental Shelf Research, 7*(11–12), 1367–1381.

Comfort, A. (1951). The pigmentation of molluscan shells. *Biological Reviews, 26*(3), 285–301.

Costa, C., Menesatti, P., Aguzzi, J., D'Andrea, S., Antonucci, F., Rimatori, V., Pallottino, F., & Mattoccia, M. (2010). External shape differences between sympatric populations of commercial clams *Tapes decussatus* and *T. philippinarum*. *Food and Bioprocess Technology, 3*(1), 43–48.

Diana, A., Zahro, N., Sari, L. A., Arsad, S., Pursetyo, K. T., & Cahyoko, Y. (2021). Monitoring of phytoplankton abundance and chlorophyll-a content in the estuary of Banjar Kemuning river, Sidoarjo regency, East Java. *Journal of Ecological Engineering, 22*(1).

Dolmer, P. (2000). Feeding activity of mussels Mytilus edulis related to near-bed currents and phytoplankton biomass. *Journal of Sea Research, 44*(3–4), 221–231.

Elgin, A. K., Glyshaw, P. W., & Weidel, B. C. (2022). Depth drives growth dynamics of dreissenid mussels in Lake Ontario. *Journal of Great Lakes Research, 48*(2), 289–299.

Fairchild, M. D. (2013). *Color appearance models* (3rd ed.). John Wiley & Sons.

Firth, B. L., Craig, P. M., Drake, D. A. R., & Power, M. (2024). Impact of turbidity on the gill morphology and hypoxia tolerance of eastern sand darter (*Ammocrypta pellucida*). *Journal of Fish Biology, 104*(6), 1888–1898.

Fitzer, S. C., Vittert, L., Bowman, A., Kamenos, N. A., Phoenix, V. R., & Cusack, M. (2015). Ocean acidification and temperature increase impact mussel shell shape and thickness: Problematic for protection? *Ecology and Evolution, 5*(21), 4875–4884.

Fruciano, C., Tigano, C., & Ferrito, V. (2011). Traditional and geometric morphometrics detect morphological variation of lower pharyngeal jaw in *Coris julis* (Teleostei, Labridae). *Italian Journal of Zoology, 78*(3), 320–327.

Fu, M., Wang, Z., Pu, X., Qu, P., Li, Y., Wei, Q., & Jiang, M. (2016). Response of phytoplankton community to nutrient enrichment in the subsurface chlorophyll maximum in Yellow Sea Cold Water Mass. *Acta Ecologica Sinica, 36*(1), 39–44.

Gamier, D. E. F., Velasco, D. A. B., Dalisaya, T. M. A., & Saco, J. A. (2019). Geometric morphometric analysis on the shell of green mussel (*Perna viridis*) from two culturing sites in Cavite province. *International Research Journal of Innovations in Engineering, Science and Technology (IRJIEST), 5*, 1–4.

Gefaell, J., Galindo, J., & Rolán-Alvarez, E. (2023). Shell color polymorphism in marine gastropods. *Evolutionary Applications, 16*(1), 202–222.

Gentry, R. R., Froehlich, H. E., Grimm, D., Kareiva, P., Parke, M., Rust, M., Gaines, S. D., & Halpern, B. S. (2017). Mapping the global potential for marine aquaculture. *Nature Ecology & Evolution, 1*, 1317–1324.

Haag, W. R. (2012). *North American freshwater mussels: Natural history, ecology, and conservation*. Cambridge University Press.

He, C., Ye, T., Zeng, J., Zhang, H., Sun, Y., Zhang, C., He, X., Qiu, J., & Zheng, H. (2024). Nutrient comparisons among the noble scallops *Chlamys nobilis* with three different shell colours to provide advice for consumers to choose high-quality food. *Frontiers in Marine Science, 11*, Article 1395339.

Hermanson, J. C. (2011). Effects of shell morphology on mechanics of zebra and quagga mussel locomotion. *Journal of Experimental Biology, 214*(6), 933–941.

Hickman, R. W. (1992). Mussel cultivation. *Developments in Aquaculture and Fisheries Science, 25*, 465–510.

Hoque, N. F., Shakil, A., Sultana, F., Wahab, M. A., Rahman, M. J., Nahiduzzaman, M., Akter, S., & Asaduzzaman, M. (2021). Feasibility study of green mussel *Perna viridis* farming in the southeast coast of the Bay of Bengal of Bangladesh. *Journal of the Indian Society of Coastal Agricultural Research, 39*(2), 45–53.

Hornbach, D. J., Kurth, V. J., & Hove, M. C. (2010). Variation in freshwater mussel shell sculpture and shape along a river gradient. *The American Midland Naturalist, 164*(1), 22–36.

Inoue, K., Hayes, D. M., Harris, J. L., & Christian, A. D. (2013). Phylogenetic and morphometric analyses reveal ecophenotypic plasticity in freshwater mussels *Obovaria jacksoniana* and *Villosa arkansasensis* (Bivalvia: Unionidae). *Ecology and Evolution, 3*(8), 2670–2683.

Inoue, K., McQueen, A. L., Harris, J. L., & Berg, D. J. (2014). Molecular phylogenetics and morphological variation reveal recent speciation in freshwater mussels of the genera *Arcidens* and *Arkansia* (Bivalvia: Unionidae). *Biological Journal of the Linnean Society, 112*(3), 535–545.

Jiang, T., Pan, H., Steeves, L., Jiang, Z., Filgueira, R., Strand, Ø., Strohmeier, T., Cranford, P. J., & Cui, Z. (2022). Effect of *Mytilus coruscus* selective filtration on phytoplankton assemblages. *Frontiers in Marine Science, 9*, Article 1070737.

Jones, H. F., Pilditch, C. A., Bruesewitz, D. A., & Lohrer, A. M. (2011). Sedimentary environment influences the effect of an infaunal suspension feeding bivalve on estuarine ecosystem function. *PLoS One, 6*(10), Article e27065.

Kapsenberg, L., Miglioli, A., Bitter, M. C., Tambutté, E., Dumollard, R., & Gattuso, J. P. (2018). Ocean pH fluctuations affect mussel larvae at key developmental transitions. Proceedings of the royal society B. *Biological Sciences, 285*(1893), Article 20182381.

Keogh, S. M., Pfeiffer, J. M., Simons, A. M., & Edie, S. M. (2024). Riverine flow rate drives widespread convergence in the shell morphology of imperiled freshwater mussels. *Evolution, 78*(1), 39–52.

Klingenberg, C. P. (2011). MorphoJ: An integrated software package for geometric morphometrics. *Molecular Ecology Resources, 11*(2), 353–357.

Krapivka, S., Toro, J. E., Alcapán, A. C., Astorga, M., Presa, P., Pérez, M., & Guiñez, R. (2007). Shell-shape variation along the latitudinal range of the Chilean blue mussel *Mytilus chilensis* (Hupe 1854). *Aquaculture Research, 38*(16), 1770–1777.

Lê, S., Josse, J., & Husson, F. (2008). FactoMineR: An R package for multivariate analysis. *Journal of Statistical Software, 25*, 1–18.

Longman, E. K., & Sanford, E. (2025). Biogeographic variation in mussel shell thickness and drilling predation on rocky shores. *Oecologia, 207*(8), 126.

Louis, V., Besseau, L., & Lartaud, F. (2022). Step in time: Biomineralisation of bivalve's shell. *Frontiers in Marine Science, 9*, Article 906085.

Maia, R., Eliason, C. M., Bitton, P. P., Doucet, S. M., & Shawkey, M. D. (2013). Pavo: An R package for the analysis, visualization and organization of spectral data. *Methods in Ecology and Evolution, 4*(10), 906–913.

Marinho, T. A., & Arruda, E. P. (2021). Shell-specific differentiation: How geometric morphometrics can add to knowledge of *Macominae* species (Tellinidae, Bivalvia). *Marine Biodiversity, 51*, 1–14.

Marma, M. C., Asaduzzaman, M. D., Barua, U., Akter, S., & Noor, A. R. (2021). Spat settlement and growth performance of green mussel *Perna viridis* in different culture system at Moheshkhali channel. *Cox's Bazar. Journal of Global Biosciences, 10*(1), 8243–8259.

Martin, V. A., Gelcich, S., Vásquez-Lavín, F., Ponce Oliva, R. D., Hernández, J. I., Lagos, N. A., Birchenough, S. N., & Vargas, C. A. (2019). Linking social preferences and ocean acidification impacts in mussel aquaculture. *Scientific Reports, 9*(1), 4719.

McMahon, T., Thatcher, D., Williams, B., Wanamaker, A., Jellison, B., Franklin, H., Guay, K., Whitney, N. M., Stewart, J. A., & LaVigne, M. (2024). Contrasting responses of commercially important Northwest Atlantic bivalve species to ocean acidification and temperature conditions. *PLOS Climate, 3*(11), Article e0000509.

Melzner, F., Stange, P., Trübenbach, K., Thomsen, J., Casties, I., Panknin, U., … Gutowska, M. A. (2011). Food supply and seawater p CO2 impact calcification and internal shell dissolution in the blue mussel *Mytilus edulis*. *PLoS One, 6*(9), Article e24223.

Murtagh, F., & Legendre, P. (2014). Ward's hierarchical agglomerative clustering method: Which algorithms implement Ward's criterion? *Journal of Classification, 31*, 274–295.

Noor, A. R., Shakil, A., Hoque, N. F., Rahman, M. M., Akter, S., Talukder, A., Ahmad-Al-Nahid, S., Wahab, M. A., Nahiduzzaman, M., Rahman, M. J., & Asaduzzaman, M. (2021). Effect of eco-physiological factors on biometric traits of green mussel *Perna viridis* cultured in the south-east coast of the Bay of Bengal, Bangladesh. *Aquaculture Reports, 19*, Article 100562.

Norkko, J., Hewitt, J. E., & Thrush, S. F. (2006). Effects of increased sedimentation on the physiology of two estuarine soft-sediment bivalves, *Austrovenus stutchburyi* and *Paphies australis*. *Journal of Experimental Marine Biology and Ecology, 333*(1), 12–26.

Nunes, P., Roland, F., Amado, A. M., Resende, N. D. S., & Cardoso, S. J. (2022). Responses of phytoplanktonic chlorophyll-a composition to inorganic turbidity caused by mine tailings. *Frontiers in Environmental Science, 9*, Article 605838.

Olivier, F., Gaillard, B., Thébault, J., Meziane, T., Tremblay, R., Dumont, D., Bélanger, S., Gosselin, M., Jolivet, A., Chauvaud, L., & Martel, A. L. (2020). Shells of the bivalve *Astarte moerchi* give new evidence of a strong pelagic–benthic coupling shift occurring since the late 1970s in the North Water polynya. *Philosophical Transactions of the Royal Society A: Mathematical, Physical and Engineering Sciences, 378*(2181), Article 20190353.

Peyer, S. M., Hermanson, J. C., & Lee, C. E. (2010). Developmental plasticity of shell morphology of quagga mussels from shallow and deep-water habitats of the Great Lakes. *Journal of Experimental Biology, 213*(15), 2602–2609.

Purroy Albet, A. (2017). *The biological and ecological drivers of shell growth in bivalves*. Doctoral dissertation, University of Split.

Quinn, G. P., & Keough, M. J. (2002). *Experimental design and data analysis for biologists*. Cambridge University Press.

Rajagopal, S., Venugopalan, V. P., Nair, K. V. K., Van der Velde, G., Jenner, H. A., & Den Hartog, C. (1998). Reproduction, growth rate, and culture potential of the green mussel *Perna viridis* (Linnaeus) in Edaiyur backwaters, east coast of India. *Aquaculture, 162*(3–4), 187–202.

Rajagopal, S., Venugopalan, V. P., Van der Velde, G., & Jenner, H. A. (2006). Greening of the coasts: A review of the *Perna viridis* success story. *Aquatic Ecology, 40*(2), 273–297.

Rohlf, F. J. (2005). *tpsDig, digitize landmarks and outlines (version 2.05)*. Department of Ecology and Evolution, State University of New York at Stony Brook.

Rohlf, F. J., & Slice, D. (1990). Extensions of the Procrustes method for the optimal superimposition of landmarks. *Systematic Zoology, 39*(1), 40–59.

Rousseau, M., & Rollion-Bard, C. (2012). Influence of the depth on the shape and thickness of nacre tablets of Pinctada margaritifera pearl oyster, and on oxygen isotopic composition. *Minerals, 2*(1), 55–64.

Rufino, M. M., Gaspar, M. B., Pereira, A. M., & Vasconcelos, P. (2006). Use of shape to distinguish *Chamelea gallina* and *Chamelea striatula* (Bivalvia: Veneridae): Linear and geometric morphometric methods. *Journal of Morphology, 267*(12), 1433–1440.

Saenko, S. V., & Schilthuizen, M. (2021). Evo-devo of shell colour in gastropods and bivalves. *Current Opinion in Genetics & Development, 69*, 1–5.

Sahidin, A., Muhammad, G., Hasan, Z., Arief, M. C. W., & Komaru, A. (2022). Color profile and microstructure of the nacre shell of an invasive freshwater mussel, *Sinanodonta woodiana*, at different elevations in West Java, Indonesia. *Aquaculture, 561*, Article 738643.

Saleh, I., Syamsir, S., Pramaningsih, V., & Hansen, H. (2021). The use of green mussel as bioindicator of heavy metal pollution in Indonesia: A review. *Environmental Analysis, Health and Toxicology, 36*(4), Article e2021026.

Samanta Chandan, C. S., & Roy, P. (2024). Aquaculture practices in Bangladesh: A synopsis on prospects, productivity, and problems. *Journal of the World Aquaculture Society, 55*(1), 4–25.

Sanders, T., Schmittmann, L., Nascimento-Schulze, J. C., & Melzner, F. (2018). High calcification costs limit mussel growth at low salinity. *Frontiers in Marine Science, 5*, 352.

Saurel, C. (2008). *Mussel production carrying capacity: The need for an in situ and multidisciplinary approach*. United Kingdom: Bangor University.

Scanes, E., Kutti, T., Fang, J. K., Johnston, E. L., Ross, P. M., & Bannister, R. J. (2024). The long-lived deep-sea bivalve *Acesta excavata* is sensitive to the dual stressors of sediment and warming. *Marine Pollution Bulletin, 202*, Article 116323.

Schneider, C. A., Rasband, W. S., & Eliceiri, K. W. (2012). NIH image to ImageJ: 25 years of image analysis. *Nature Methods, 9*(7), 671–675.

Schotanus, J., Capelle, J. J., Leuchter, L., Van De Koppel, J., & Bouma, T. J. (2019). Mussel seed is highly plastic to settling conditions: The influence of waves versus tidal emergence. *Marine Ecology Progress Series, 624*, 77–87.

Seitz, C., Scordo, F., Suenaga, E., Carlson, E. M., McMillen, S., Gregory, L., & Chandra, S. (2023). Salinity and pH effects on survival, growth, and reproduction of quagga mussels. *PeerJ, 11*, Article e15450.

Shahabuddin, A. M., Wahab, M. A., Miah, M. I., & Salam, M. A. (2010). *Abundance, distribution and culture potentials of three commercially important mollusks species along the coast of Bay of Bengal*.

Siddall, S. E. (1980). A clarification of the genus *Perna* (Mytilidae). *Bulletin of Marine Science, 30*(4), 858–870.

Slice, D. E. (1996). Three-dimensional generalized resistant fitting and the comparison of least-squares and resistant-fit residuals. In *Advances in morphometrics* (pp. 179–199). Springer US.

Sousa, R., Freire, R., Rufino, M., Méndez, J., Gaspar, M., Antunes, C., & Guilhermino, L. (2007). Genetic and shell morphological variability of the invasive bivalve *Corbicula fluminea* (Müller, 1774) in two Portuguese estuaries. *Estuarine, Coastal and Shelf Science, 74*(1–2), 166–174.

Steinhardt, J., Butler, P. G., Carroll, M. L., & Hartley, J. (2016). The application of long-lived bivalve sclerochronology in environmental baseline monitoring. *Frontiers in Marine Science, 3*, 176.

Stenger, P. L., Ky, C. L., Reisser, C. M. O., Cosseau, C., Grunau, C., Mege, M., Planes, S., & Vidal-Dupiol, J. (2021). Environmentally driven color variation in the pearl oyster *Pinctada margaritifera var. cumingii* (Linnaeus, 1758) is associated with differential methylation of CpGs in pigment- and biomineralization-related genes. *Frontiers in Genetics, 12*, Article 630290.

Stenger, P. L., Vidal-Dupiol, J., Reisser, C., Planes, S., & Ky, C. L. (2019). Colour plasticity in the shells and pearls of animal graft model *Pinctada margaritifera* assessed by HSV colour quantification. *Scientific Reports, 9*(1), 7520.

Stevens, M., Párraga, C. A., Cuthill, I. C., Partridge, J. C., & Troscianko, T. S. (2007). Using digital photography to study animal coloration. *Biological Journal of the Linnean Society, 90*(2), 211–237.

Strehse, J. S., & Maser, E. (2020). Marine bivalves as bioindicators for environmental pollutants with focus on dumped munitions in the sea: A review. *Marine Environmental Research, 158*, Article 105006.

Tan, K. S., & Ransangan, J. (2014). Feeding behavior of green mussel, *Perna viridis* farmed in Marudu Bay, Malaysia. *Aquaculture Research, 48*(3), 1216–1231.

Telesca, L., Michalek, K., Sanders, T., Peck, L. S., Thyrring, J., & Harper, E. M. (2018). Blue mussel shell shape plasticity and natural environments: A quantitative approach. *Scientific Reports, 8*(1), 2865.

Troscianko, J., & Stevens, M. (2015). Image calibration and analysis toolbox–a free software suite for objectively measuring reflectance, colour and pattern. *Methods in Ecology and Evolution, 6*(11), 1320–1331.

Trottet, A., Roy, S., Tamigneaux, E., Lovejoy, C., & Tremblay, R. (2008). Impact of suspended mussels (Mytilus edulis L.) on plankton communities in a Magdalen islands lagoon (Québec, Canada): A mesocosm approach. *Journal of Experimental Marine Biology and Ecology, 365*(2), 103–115.

Tuttle-Raycraft, S., & Ackerman, J. D. (2019). Living the high turbidity life: The effects of total suspended solids, flow, and gill morphology on mussel feeding. *Limnology & Oceanography, 64*(6), 2526–2537.

Venables, W. N., & Ripley, B. D. (2013). *Modern applied statistics with S*. Springer Science & Business Media.

Vermeij, G. J. (2002). Characters in context: Molluscan shells and the forces that mold them. *Paleobiology, 28*(1), 41–54.

Volety, A. K., Encomio, V. G., & Myers, F. (2006). Biological effects of suspended sediments on shellfish in the Charlotte Harbor Watershed–implications for water releases and dredging activities. *Final Report Submitted to Charlotte Harbor National Estuary Program* (p. 47).

Wang, N., Consbrock, R. A., Ingersoll, C. G., & Barn-hart, M. C. (2011). Evaluation of influence of sediment on the sensi-tivity of a unionid mussel (*Lampsilis siliquoidea*) to ammo-nia in 28-day water exposures. *Environmental Toxicologyand Chemistry, 30*, 2270–2276.

Wang, Y., Hu, M., Wong, W. H., Shin, P. K., & Cheung, S. G. (2011). The combined effects of oxygen availability and salinity on physiological responses and scope for growth in the green-lipped mussel *Perna viridis*. *Marine Pollution Bulletin, 63*(5–12), 255–261.

Wang, Y., Wu, H., Lin, J., Zhu, J., Zhang, W., & Li, C. (2019). Phytoplankton blooms off a high turbidity estuary: A case study in the Changjiang river Estuary. *Journal of Geophysical Research. Oceans, 124*(11), 8036–8059.

Weller, H. I., & Westneat, M. W. (2019). Quantitative color profiling of digital images with earth mover's distance using the R package colordistance. *PeerJ, 7*, Article e6398.

Westland, S., Ripamonti, C., & Cheung, V. (2012). *Computational colour science using MATLAB*. John Wiley & Sons.

Wijsman, J. W. M., Troost, K., Fang, J., & Roncarati, A. (2019). Global production of marine bivalves. Trends and challenges. In *Goods and services of marine bivalves* (pp. 7–26).

Wilke, T., Schultheiß, R., Albrecht, C., Bornmann, N., Trajanovski, S., & Kevrekidis, T. (2010). Native *Dreissena* freshwater mussels in the Balkans: In and out of ancient lakes. *Biogeosciences, 7*(10), 3051–3065.

Williams, S. T. (2017). Molluscan shell colour. *Biological Reviews, 92*(2), 1039–1058.

Yap, C. K., Ahmad Wakid, S., Chew, J. M., Sutra, J., Syazwan, W. M., Aziz, N. A. A., … Cheng, W. H. (2023). Shell deformities in the green-lipped mussel perna viridis: Occurrence and potential environmental stresses on the West Coast of peninsular Malaysia. *Pollutants, 3*(3), 406–418.

Zar, J. H. (2010). *Biostatistical analysis pearson prentice-hall, Upper Saddle River, NJ* (p. 944).

Zelditch, M. L., Swiderski, D. L., & Sheets, H. D. (2012). *Geometric morphometrics for biologists: A primer* (2nd ed.). Academic Press.

Zeng, X., Zeng, Y., Yee, J. C., & Yang, H. (2024). Biochemical and molecular responses to long-term salinity challenges in northern quahogs *Mercenaria mercenaria*. *Fish & Shellfish Immunology, 154*, Article 109888.

Zieritz, A., Mahadzir, F. N., Chan, W. N., & McGowan, S. (2019). Effects of mussels on nutrient cycling and bioseston in two contrasting tropical freshwater habitats. *Hydrobiologia, 835*(1), 179–191.

Aquaculture 622 (2026) 744083

Contents lists available at ScienceDirect

Aquaculture

journal homepage: www.elsevier.com/locate/aquaculture

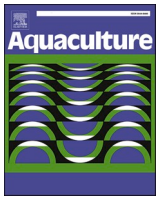

Depuration efficiency of raft-cultivated *Perna viridis*: Interactive effects of salinity, exposure time, and body size on the removal of microbial pathogens and trace/toxic elements for seafood safety

Md Asaduzzaman [a,*], Khandakar Zakir Hossain [a], Sabrina Jahan [a], Israt Jahan [a], Kanij Fatema Ety [a], Md. Ramzan Ali [a], Md Nahiduzzaman [b], Yeasmin Nahar Jolly [c], Shirin Akter [c], Mohammad Sadequr Rahman Khan [a], Md Moshiur Rahman [d]

[a] *Department of Marine Bioresource Science, Faculty of Fisheries, Chattogram Veterinary and Animal Sciences University, Khulshi, 4225 Chittagong, Bangladesh*
[b] *WorldFish, Bangladesh and South Asia Office, Gulshan-2, Dhaka, Bangladesh*
[c] *Atmospheric and Environmental Chemistry Laboratory, Chemistry Division, Atomic Energy Center, Dhaka 1000, Bangladesh*
[d] *Fish Conservation and Culture Laboratory, Department of Biological and Agricultural Engineering, University of California Davis, 17501 Byron Hwy, Byron, CA 94514, USA*

ARTICLE INFO

Keywords:
Green mussel (*Perna viridis*)
Depuration efficiency
Salinity-driven purification
Microbial contamination
Toxic heavy metals detoxification
Post-harvest sanitation

ABSTRACT

Bangladesh has been emerging as a significant producer of farmed green mussels (*Perna viridis*) along the southeastern coast of the Bay of Bengal, driven by increasing domestic demand and expanding export potential. However, despite increasing production volumes, market access remains severely constrained because farmers lack a scientifically validated depuration protocol tailored to local tropical conditions, leading to persistent concerns over microbial contamination and the accumulation of toxic heavy metals and trace elements. Addressing this critical bottleneck, the present study evaluated depuration efficiency in raft-cultivated *P. viridis*, with particular emphasis on the interactive roles of salinity, exposure duration, and mussel body size in removing microbial pathogens and toxic heavy metals and trace elements. Using a controlled static fill-and-draw depuration system with UV-treated seawater, mussels were subjected to four salinity regimes (15, 20, 25, and 30 psu) for up to 72 h, alongside size-based trials (small: 35–45 mm; medium: 45–60 mm; large: >60 mm shell length) conducted at 30 psu as the optimal salinity. Microbial loads were quantified using culture-based enumeration and PCR-confirmed detection of *Salmonella*, *Shigella*, *Escherichia coli*, and *Vibrio cholerae*, while elemental concentrations (Cr, Mn, Fe, Ni, Cu, Zn, As, Se, Hg, Pb) were determined by energy-dispersive X-ray fluorescence (EDXRF). Advanced generalized and linear mixed-effects models were applied to disentangle time-dependent, salinity-driven, and size-mediated responses. Depuration time emerged as the dominant driver of microbial clearance, achieving >4-log reductions in total viable bacteria and near-complete elimination of *Salmonella* and *Shigella* within 24–48 h at ≥25 psu. Elevated salinity significantly accelerated pathogen removal through strong salinity × time interactions, whereas body size influenced clearance trajectories without altering final depuration efficacy at 72 h. Toxic heavy metals and trace elements depuration was element-specific: notable reductions were observed for several elements (e.g., Fe, Pb, Cu, Zn, Hg, and Cr), whereas Ni, As, and Se showed limited responsiveness. Overall, depuration under elevated salinity (25–30 psu) over 72 h substantially improved microbial and chemical quality, approaching levels consistent with international food safety standards. These findings establish a robust, evidence-based depuration framework for tropical mussel aquaculture, directly supporting seafood safety, public health protection, and the sustainable growth of the blue economy in the Bay of Bengal and comparable regions.

* Corresponding author at: Department of Marine Bioresource Science, Faculty of Fisheries, Chattogram Veterinary and Animal Sciences University, Khulshi, 4225 Chattogram, Bangladesh.
E-mail address: a_zamanbau@yahoo.com (M. Asaduzzaman).

https://doi.org/10.1016/j.aquaculture.2026.744083
Received 18 January 2026; Received in revised form 15 April 2026; Accepted 23 April 2026
Available online 24 April 2026

1. Introduction

Marine bivalves play a vital role as biofilters in coastal ecosystems, contributing to nutrient recycling and water clarification while supporting global seafood supply chains (Cranford et al., 2011). Among them, mussels (family Mytilidae) dominate production, with annual yields increasing by about 5% since 1990 (FAO, 2016). The Asian green mussel (*Perna viridis*, Linnaeus, 1758) is widely distributed across tropical and subtropical Indo-Pacific estuaries and coastal waters (Rajagopal et al., 2006; McGuire and Stevely, 2009). In Bangladesh, *P. viridis* aquaculture has expanded rapidly in southeastern estuarine areas, particularly around Moheshkhali channel in Cox's Bazar, driven by favorable hydrographic conditions and increasing market demand (Asaduzzaman et al., 2019; Asaduzzaman et al., 2025a; Eti et al., 2026). In line with the country's blue economy agenda, the government has emphasized sustainable management of wild stocks and the development of mussel farming technologies to support coastal livelihoods (Hoque et al., 2021; Asaduzzaman et al., 2025a). Beyond these socio-economic benefits, this fast-growing species provides a cost-effective source of high-quality protein, minerals, and essential fatty acids, contributing to rising nutritional demands (Saritha et al., 2015; Taib et al., 2016; Asaduzzaman et al., 2025b). However, these estuarine systems are increasingly exposed to anthropogenic pressures, including untreated effluents, agricultural runoff, and port activities, leading to elevated microbial and toxic heavy metals and trace elements contamination. This contamination threatens seafood safety and the sustainability of Bangladesh's emerging blue economy.

Edible green mussels can bioaccumulate microbial pathogens such as *Escherichia coli*, *Vibrio* spp., *Salmonella* spp., and other enteric bacteria from contaminated waters during filter feeding. Contamination levels are strongly influenced by environmental conditions, posing significant public health risks, including gastrointestinal illness and mortality in vulnerable populations (Strubbia et al., 2020; Chinnadurai et al., 2021). *Vibrio* species are detected year-round in bivalves from southeast estuaries (Chinnadurai et al., 2023). Pathogenic *E. coli* is associated with approximately 1.7 billion diarrheal cases globally (Yang et al., 2017), while *S. typhi* causes enteric fever with an incidence of 913 per 100,000 in Bangladesh (Garrett et al., 2022). These risks are exacerbated by coastal pollution from untreated sewage, industrial effluents, and aquaculture discharges (Jannatun et al., 2023). Effective post-harvest measures are therefore essential to ensure microbial and chemical safety, particularly given increasing domestic demand and export potential. Depuration, whereby bivalves are held in clean, filtered seawater to eliminate contaminants, has been shown to significantly reduce indicator bacteria such as *E. coli* and coliphages (Power and Collins, 1990). This process enables self-purification under controlled conditions, facilitating microbial removal. Studies indicate that artificially contaminated bivalves can reduce pathogens to undetectable levels within 48 h of depuration (Muniain-Mujika et al., 2000). However, despite its effectiveness under temperate conditions, depuration performance in tropical coastal systems remains poorly understood due to complex environmental and physiological interactions (Chinnadurai et al., 2022).

Depuration efficiency primarily depends on mussel pumping activity (Chae et al., 2009; Lewis et al., 2010). While initial microbial load is a key determinant, performance is also influenced by temperature, salinity, flow rate, bivalve size, health status, and system design (Phuvasate et al., 2012; Anacleto et al., 2013a; Anacleto et al., 2013b; Chinnadurai et al., 2021b). Among these, salinity is particularly critical for osmoconforming organisms such as mussels, as deviations from ambient levels can disrupt filtration and metabolism (Shumway and Koehn, 1982; Rajesh et al., 2001). Optimal conditions therefore approximate natural salinity ranges, sustaining filtration while imposing osmotic stress on bacteria that accelerates their removal (Shumway, 1977). Despite this understanding, empirical evidence on salinity-driven microbial clearance in tropical mussels remains limited. Studies on *Crassostrea madrasensis* and *Anadara granosa* indicate that elevated salinity (25–35 psu) enhances microbial elimination within 48–72 h (Chinnadurai et al., 2021a, 2023). Whether similar responses occur in *P. viridis* populations from the Bay of Bengal, where salinity fluctuates seasonally, remains unclear.

In addition to microbial hazards, accumulation of toxic and essential trace elements in bivalve tissues presents a major food safety concern (Oranusi et al., 2018; Wright et al., 2018; Pasinszki et al., 2023). Bivalves bioconcentrate essential elements (iron, Fe; copper, Cu; zinc, Zn; manganese, Mn) and non-essential/toxic elements (lead, Pb; mercury, Hg; arsenic, As; nickel, Ni; chromium, Cr) through ingestion and absorption across gill epithelia (Bonneris et al., 2005; Esposito et al., 2022). Chronic exposure, even at low concentrations, can cause genotoxic and neurotoxic effects in humans (Engwa et al., 2019). Depuration offers a potential route for reducing tissue metal burdens, although its effectiveness varies with metal speciation, binding affinity, and physiological regulation (Martinez-Albores et al., 2020). Essential elements such as Cu and Zn are actively regulated, whereas elements like Ni and As tend to persist due to strong intracellular binding (Bánfalvi, 2011). Studies in India and Malaysia report 70–90% reduction of labile metals within 2–4 days under static systems, although complete removal of As and Ni is rarely achieved (Chinnadurai et al., 2022; Firdaus et al., 2020). However, such evidence is lacking for Bangladeshi *P. viridis*, where distinct hydrochemical conditions may influence depuration dynamics.

Another important but underexplored factor is body size, which affects filtration capacity, metabolism, and contaminant burden (El-Shenawy, 2004; Mokrani et al., 2025). Larger mussels generally exhibit higher filtration volumes (Tantanasarit et al., 2013; Fernández and Albentosa, 2019) but may retain greater contaminant loads due to increased tissue mass. Evidence from *Mytilus edulis* and *Ruditapes decussatus* suggests that smaller bivalves may depurate certain metals more rapidly, whereas larger individuals achieve more efficient microbial removal (El-Shenawy, 2004). Thus, interactions among size, salinity, and contaminant type require systematic evaluation.

Despite growing global evidence supporting depuration, its direct applicability to Bangladesh remains uncertain due to context-specific contamination profiles shaped by hydrography, pollution sources, and aquaculture practices. Although Bangladesh has a potential to be a major producer of farmed green mussels, market expansion is constrained by the lack of a scientifically validated depuration protocol tailored to local conditions. Persistent concerns over microbial contamination and toxic heavy metals and trace elements accumulation continue to limit consumer confidence and compliance with international standards. Accordingly, this study provides a comprehensive evaluation of microbial and toxic and essential trace element depuration in raft-cultivated *P. viridis* from the southeast coast of Bangladesh. Using a controlled depuration system with UV-treated seawater, we assessed the effects of salinity (15, 20, 25, and 30 psu), mussel body size (small: 35–45 mm; medium: 45–60 mm; large: >60 mm shell length), and depuration duration (0–72 h) on contaminant removal. Mixed-effects modeling was applied to quantify main and interactive effects. Specifically, the study aimed to (i) quantify the relative contributions of salinity, body size, and time to microbial and metal clearance; (ii) identify element-specific depuration responses; and (iii) evaluate whether optimized salinity–size combinations can achieve international food safety compliance. By generating Bangladesh-specific evidence, this work provides a scientific basis for shellfish sanitation protocols and supports sustainable green mussel aquaculture in the Bay of Bengal and comparable tropical regions.

2. Materials and methods

2.1. Sample collection and transportation

Raft-cultivated mussels were collected from estuarine sites in Khurushkul, Cox's Bazar (21°30′40″N, 91°59′53″E) between February and

May 2024 (Fig. 1). Samples were transported alive to the Coastal Biodiversity, Marine Fisheries and Wildlife Research Centre, CVASU, within 1 h of collection in containers filled with ambient seawater to maintain viability for depuration trials. A total of 420 individuals were measured for morphometric parameters, including shell length (SL), shell height (SH), shell width (SW), and total fresh weight (TFW). Mussels were weighed individually (±0.01 g), and shell dimensions (length, height, and width) were measured to the nearest 0.1 mm using a slide caliper. Of these, 240 individuals were used for salinity-based experiments and 180 for size-based experiments. Mussels were subsequently classified into three size groups based on shell length: small (35–45 mm), medium (45–60 mm), and large (>60 mm).

2.2. Depuration experiments

The fill-and-draw (static) depuration method was applied following the procedures of Chinnadurai et al. (2014, 2021a). Experimental seawater was sequentially filtered through cartridges (10, 5, 2, and 0.2 μm) and subsequently disinfected using UV irradiation (MOC: SS-313, UV intensity 1200 mW/min/cm^2) in 1000 L fiberglass tanks (1.25 × 0.75 × 0.75 m) for 8 h. The dissolved oxygen concentration of the seawater ranged from 5.3 to 6.6 mg/L. Before the depuration experiments, mussels were scrubbed to remove barnacles and other fouling organisms, then washed with high-pressure water to eliminate sand and adhering materials. Two separate depuration experiments were conducted to evaluate the effects of salinity and body size on the removal of microbes and toxic heavy metals and trace elements from raft-cultured green mussels. In the salinity experiment, four salinity levels (15, 20, 25, and 30 psu) were tested using market-sized (MS) mussels (shell length: 45–60 mm) for a duration of 72 h. In the size-based experiment, three size groups, small (SS: 35–45 mm), medium (MS: 45–60 mm), and large (LS: > 60 mm), were tested at 30 psu for 72 h. Each treatment included three replicates, with 20 mussels per replicate maintained in 100 L Carbo boxes. The cleaned mussels were directly placed in the depuration tanks (Carbo boxes) with continuous aeration to maintain adequate dissolved oxygen and water circulation. The depuration system was operated as a static fill-and-draw system, in which the entire tank volume was replaced with fresh UV-treated seawater at 8-h intervals. Mussels were not fed during depuration, and dead individuals were removed during each water exchange. Mussels were also continuously monitored during the depuration period, and no spawning activity was observed in any treatment. The ambient temperature was maintained at 29.0 ± 1.5 °C throughout the study. Mussels were sampled at 0, 24, 48, and 72 h for microbial analysis. At each sampling time, three individuals per replicate tank (nine individuals per treatment) were collected for microbial enumeration and identification. For

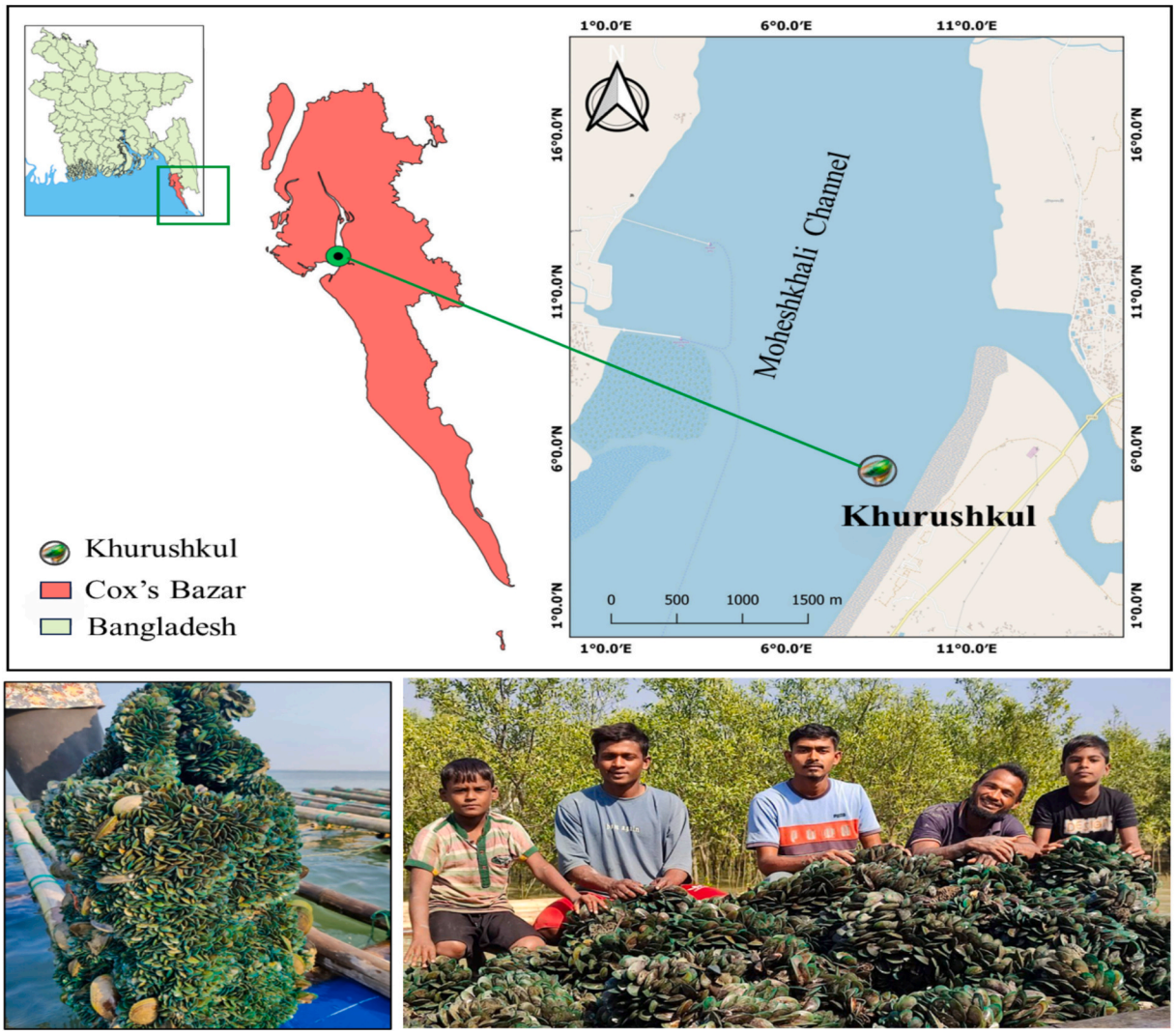

Fig. 1. Study area map illustrating the sampling site of the green mussel (*Perna viridis*) for the depuration experiment collected from the estuarine farming sites at Khurushkul (21°30′40″N, 91°59′53″E), Cox's Bazar, Bangladesh. The lower two images showed raft-cultivated green mussels. (For interpretation of the references to colour in this figure legend, the reader is referred to the web version of this article.)

toxic heavy metals and trace elements analysis, sampling was conducted only at the start (0 h) and the end (72 h) of the depuration period. Twelve mussels were collected initially as the baseline sample, and six individuals per replicate tank (18 individuals per treatment) were collected as the final sample for both experiments.

2.3. Microbiological analysis

Microbial contamination levels were quantitatively determined using culture-based enumeration (CFU/g) across selective media, providing estimates of presumptive bacterial groups. As selective media cannot confirm specific pathogens, representative isolates were further verified using PCR-based assays to ensure accurate identification of target pathogenic bacteria. For microbial analysis, mussels were shucked aseptically. The isolated soft tissues were sealed in sterile zipper bags, transported on ice, and processed within four hours at the Laboratory of Microbiology, Chattogram Veterinary and Animal Sciences University. Microbial loads were determined using the standard plate count method and included total viable bacteria (TVB), presumptive *Salmonella/Shigella* and other enteric gram-negative bacilli counts (PSS-BC), presumptive *Vibrio* bacteria (PVB), and presumptive gram-negative/coliform counts (PGN-CC). For sample preparation, 5 g of homogenized mussels tissue was mixed with 45 mL of buffered peptone water (BPW) to give a 1:9 (*w/v*) suspension, followed by serial ten-fold dilutions. Aliquots (1 mL) of appropriate dilutions were spread-plated on Plate Count Agar (PCA) for total viable count (TVC). For selective bacterial enumeration, aliquots were plated onto Thiosulfate–Citrate–Bile Salts–Sucrose (TCBS) agar for presumptive *Vibrio* counts (PVC), Xylose–Lysine–Deoxycholate (XLD) agar for presumptive *Salmonella/Shigella* and other enteric gram-negative bacilli counts (PSS-BC), and MacConkey agar for presumptive gram-negative/coliform counts (PGN-CC). All colonies that grew on each selective medium were counted and included in the respective plate counts. Plates were incubated at 37 °C for 24 h. After incubation, colonies were enumerated, and bacterial loads were expressed as colony-forming units per gram (CFU/g). All measurements were performed in triplicate.

For identification, a 10 g portion of green mussel (*P. viridis*) muscle tissue was aseptically excised and homogenized with 225 mL of sterile peptone water, and the homogenate was incubated at 37 °C for 24 h to allow bacterial growth. Following enrichment, portions of the culture were streaked onto selective media for preliminary isolation. *E. coli* was screened on MacConkey and Eosin Methylene Blue (EMB) agar, with pink colonies on MacConkey and metallic green colonies on EMB selected as presumptive *E. coli*. For *Salmonella* and *Shigella*, 5 g of tissue was blended with 90 mL sterile saline and incubated at 37 °C for 16–20 h, after which a portion of the culture was transferred to Rappaport-Vassiliadis (RV) medium and incubated at 42 °C for 24 h to selectively enrich *Salmonella*. Enriched cultures were streaked onto Xylose Lysine Deoxycholate (XLD) agar, and colonies displaying characteristic morphology, red with black centers for *Salmonella* and red without black centers for *Shigella*, were selected and further confirmed using Triple Sugar Iron (TSI) agar slants based on slant/butt colour changes, gas production, and hydrogen sulfide generation. For presumptive *Vibrio cholerae* identification, a portion of enriched samples was streaked onto Thiosulfate Citrate Bile Salts Sucrose (TCBS) agar, with yellow colonies selected as presumptive *V. cholerae*. The final identification was done based on the PCR-based method.

Representative colonies from selective media (MacConkey/EMB for *E. coli*, XLD/TSI for *Salmonella/Shigella*, and TCBS for *Vibrio* spp.) were selected based on morphology, purified, and subjected to species-specific PCR assays using primer sets described in previous studies (Table 1). Colony PCR targeted invA (*Salmonella* spp.), ipaH (*Shigella* spp.), uidA (*E. coli*), and toxR (*V. cholerae*). DNA templates were prepared using the crude boiling method. PCR reactions were carried out in a 25 μL volume containing standard reagents and appropriate negative controls. The amplification protocol included initial denaturation at 95 °C for 5 min, followed by 35 cycles (94 °C for 30 s, gene-specific annealing for 45 s, 72 °C for 1 min) and a final extension at 72 °C for 7 min. Amplified products were visualized on 1.5% agarose gel, and bands of expected sizes (approximately 284 bp for invA, 620 bp for ipaH, 147 bp for uidA, and 779 bp for toxR) were considered positive. Only isolates showing both characteristic colony morphology and the correct PCR amplicon size were recorded as confirmed.

2.4. Toxic heavy metals and trace elements analysis

The edible tissues of *P. viridis* were separated using a stainless-steel knife, thoroughly washed with tap water, rinsed three times with deionized water, and oven-dried at ~70 °C until a constant weight was achieved. The dried tissues were ground to a fine powder using a carbide mortar and pestle, stored in plastic vials inside a desiccator, and 0.1 g portions were pressed into pellets with a pellet maker (Specac Ltd., UK). The pellets were preserved in polyethene bags for analysis by Energy Dispersive X-ray Fluorescence (EDXRF) spectroscopy (Thermo Fisher Scientific; Ecublens SARL, Switzerland) at the Atmospheric & Environmental Chemistry Laboratory, Atomic Energy Center, Dhaka. Elemental analysis was performed by irradiating the pellets with an X-ray beam, and the emitted characteristic X-rays were detected using a Peltier-cooled Silicon Drift Detector (resolution ≤140 @ MnKα, 200 Kcps). AXIL software was used for qualitative and quantitative determination (Rahman et al., 2019; Rakib et al., 2021; Jolly et al., 2022). The method was validated with certified reference material (IAEA-350 tuna fish homogenate) and quality control checked with CRM TORT-2 to ensure accuracy and precision (Maheen et al., 2022).

2.5. Statistical analysis

All statistical analyses were performed in R (version 4.4.2; R Development Core Team, 2024), with data processing and visualization performed using the tidyverse package (Wickham et al., 2019). Two datasets were analyzed: (i) microbial concentrations, including TVB, PSS-BC, PVB, and PGN-CC, and (ii) toxic heavy metals and trace elements concentrations, including chromium (Cr), manganese (Mn), iron (Fe), nickel (Ni), copper (Cu), zinc (Zn), arsenic (As), selenium (Se), mercury (Hg), and lead (Pb). Explanatory factors included depuration time, salinity, and mussel size, with replicas treated as a random intercept where appropriate. Descriptive statistics (mean, SD, SE, range) were computed for each microbial and metal variable using dplyr

Table 1
PCR primer sets used for molecular confirmation of pathogenic bacterial isolates from green mussel (*Perna viridis*) muscle during depuration experiment.

Pathogenic bacteria	Gene marker	Primer name	Primer sequence (5′–3′)	Amplicon size (bp)	Reference
Salmonella spp.	*invA*	Forward Reverse	GTGAAATTATCGCCACGTTCGGGCAA TCATCGCACCGTCAAAGGAACC	~284	Rahn et al., 1992
Shigella spp.	*ipaH*	Forward Reverse	GTTCCTTGACCGCCTTTCCGATACCGTC GCCGGTCAGCCACCCTCTGAGAGTAC	~620	Sethabutr et al., 2000
Escherichia coli	*uidA*	Forward Reverse	AAAACGGCAAGAAAAAGCAG ACGCGTGGTTACAGTCTTGCG	~147	Bej et al., 1991
Vibrio cholerae	*toxR*	Forward Reverse	CCT TCG ATC CCC TAA GCA ATA C AGG GTT AGC AAC GAT GCG TAA G	~779	Rivera et al., 2001

(Wickham et al., 2023) and exported for tabulation. Normality and variance homogeneity were evaluated with rstatix (Shapiro–Wilk test: Kassambara, 2023) and car (Levene's test: Fox and Weisberg, 2019), supplemented by histogram and Q–Q plot visualization. Microbial data were strictly positive, right-skewed, and heteroscedastic; therefore, generalized linear mixed-effects models (GLMMs) with a Gamma distribution and log link were applied without transformation. Each microbial dataset was modeled separately using the glmer() function (lme4 package: Bates et al., 2015a, 2015b), with time, salinity, size, and their interactions as fixed effects, and replicas as a random intercept. Model significance was assessed via Type III Wald χ^2 tests (Anova, car) and likelihood ratio tests (drop1, stats)., Post hoc pairwise comparisons were performed using emmeans package (Lenth, 2024) using Bonferroni adjustment. Model fit was evaluated using AIC, BIC, and log-likelihood, while marginal and conditional R^2 values were computed using MuMIn (Bartoń, 2025). In addition, Type III ANOVA was applied to the same microbial datasets using identical fixed factors to provide a conventional fixed-effects comparison framework. However, given the non-normal data structure and presence of interaction terms, these ANOVA results were used for descriptive comparison only, and primary inference was based on the GLMM outputs.

Toxic heavy metals and trace elements analyses followed a similar framework but accounted for design limitations: the initial (0 h) sample represented ambient salinity conditions, while 15–30 psu treatments corresponded to 72 h depuration. Therefore, two complementary linear mixed-effects models (lmer using lme4 Bates et al., 2015a, 2015b; lme using nlme: Pinheiro et al., 2024) were used: (i) a salinity model treating salinity as a combined treatment factor (including the initial sample) and (ii) a time/size model comparing 0 h and 72 h while controlling mussel size. Fixed effects were tested via Type III ANOVA with Satterthwaite's approximation (lmerTest: Kuznetsova et al., 2017), and model fit was evaluated using AIC, BIC, log-likelihood, and R^2 indices (MuMIn). Post hoc pairwise contrasts (emmeans, Bonferroni) and CLD groupings were used to summarize significant differences. An additional

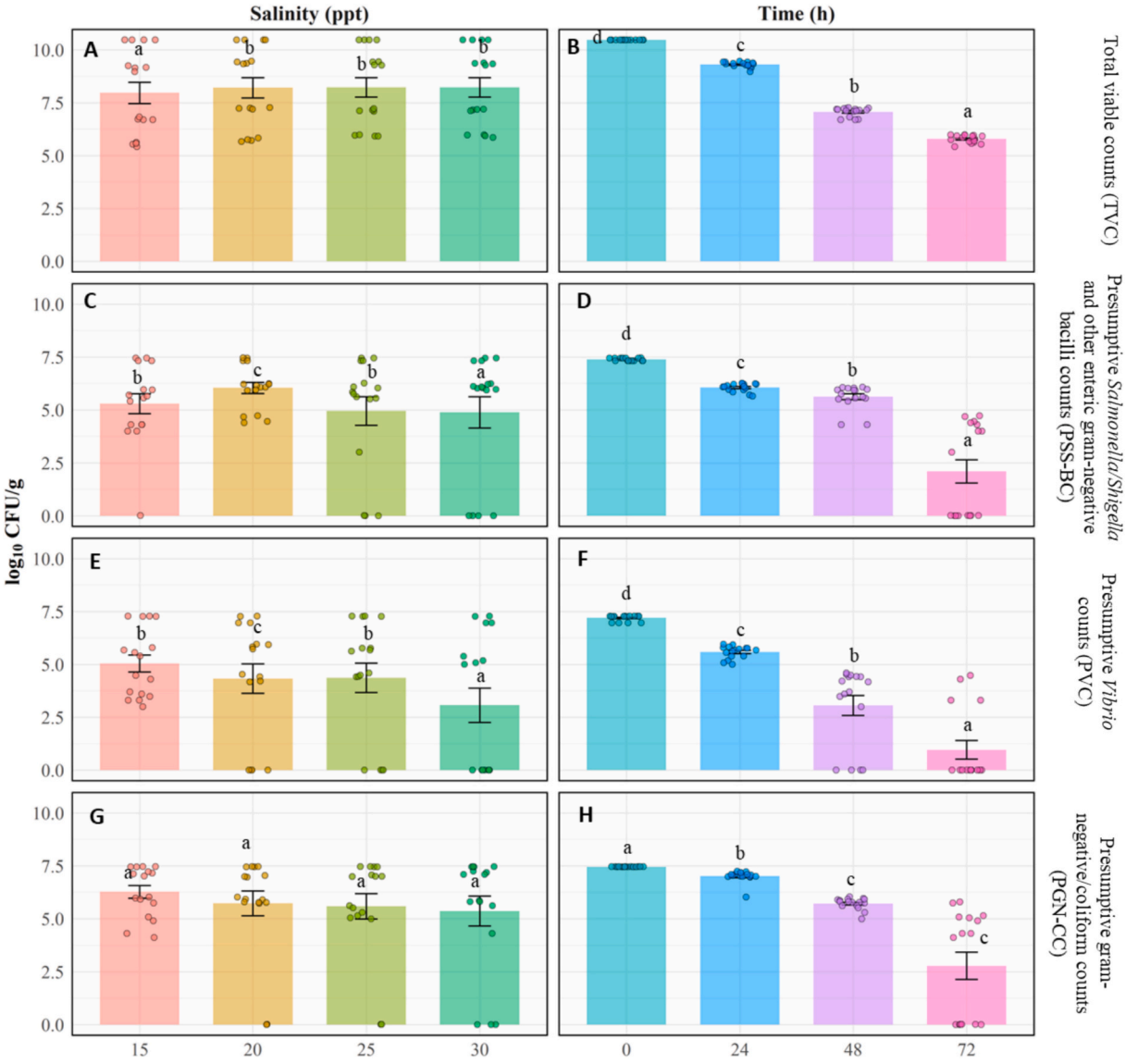

Fig. 2. Microbial concentrations (log_{10} CFU/g) in mussels (*Perna viridis*) across salinity (15, 20, 25 and 30 psu) and depuration time (0, 24, 48 and 72 h) for total viable bacterial counts (TVC), presumptive *Salmonella/Shigella* and other enteric gram-negative bacilli (PSS-BC), presumptive *Vibrio* counts (PVC), and presumptive gram-negative coliform counts (PGN-CC) using market-sized (MS = 45–60 mm) mussels. Bars show mean concentrations (± SE) from the Type III ANOVA main-effect comparisons of salinity (left panels) and depuration time (right panels). Different lowercase letters above the bars indicate significant pairwise differences among treatment groups ($\alpha = 0.05$, Bonferroni adjustment); shared letters denote non-significant differences ($p > 0.05$). Because subsequent GLMMs detected significant salinity × time interactions (see Fig. 3), these main-effect plots are presented only for comparison with the mixed-model results.

combined model evaluating Metal × Time Group effects was fitted in long format to quantify overall temporal changes across all ten metals. For robustness, non-parametric Wilcoxon rank-sum tests (0 h vs 72 h) with Benjamini–Hochberg correction were applied to each metal individually.

3. Results

3.1. Effects of salinity on microbial depuration

3.1.1. Total viable bacterial counts (TVC)

Type III ANOVA indicated that both depuration salinity (Fig. 2A) and time (Fig. 2B) had significant main effects on TVC ($p < 0.001$ for both factors), with their interaction also significant ($p < 0.001$), suggesting

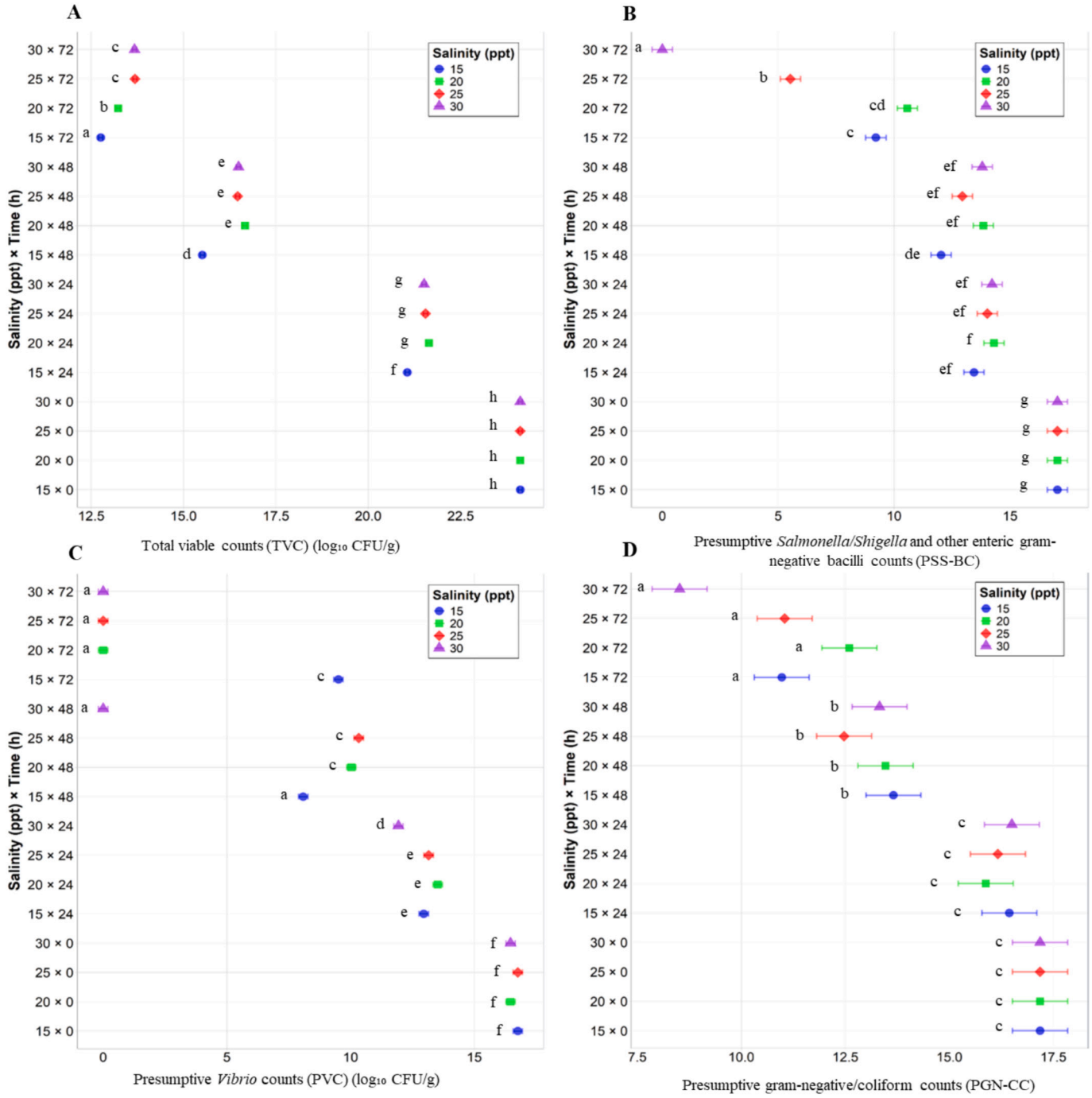

Fig. 3. Interaction effects of salinity and depuration time on (A) total viable bacterial counts (TVC, $\log_{10}$ CFU/g), (B) presumptive *Salmonella/Shigella* and other enteric gram-negative bacilli (PSS-BC, $\log_{10}$ CFU/g), (C) presumptive *Vibrio* counts (PVC, $\log_{10}$ CFU/g), and (D) presumptive gram-negative coliform counts (PGN-CC, $\log_{10}$ CFU/g) in mussels (*Perna viridis*). Points represent estimated marginal means ± standard errors derived from the generalized linear mixed-effects models (Gamma distribution with log link). Different lowercase letters denote significant pairwise differences among salinities within each depuration time (Bonferroni-adjusted $\alpha = 0.05$), whereas shared letters indicate non-significance ($p > 0.05$). For PGN-CC (D), no consistent salinity differences were detected; letters therefore compare times pooled across salinities. These interaction plots complement the main-effect results shown in Fig. 2 and illustrate how microbial reduction over time was influenced by salinity.

that bacterial reduction varied across salinity levels over time. However, when random effects were incorporated using generalized linear mixed-effects modeling (GLMM), the analysis revealed a highly significant effect of depuration time ($\chi^2 = 25{,}363.2$, df = 3, $p < 0.001$; Fig. 3A) and the interaction between salinity and time ($\chi^2 = 190.2$, df = 9, $p < 0.001$; Fig. 3A), whereas the main effect of salinity averaged over time was not significant ($\chi^2 = 0.0$, df = 3, $p = 1.0$). This difference between ANOVA and GLMM outcomes reflects the adjustment for replication structure and the time-dependent nature of salinity effects captured in the mixed model. The GLMM showed excellent fit (AIC = 2345.8; BIC = 2384.6; log-likelihood = −1154.9), with marginal $R^2 = 0.99$ and conditional $R^2 = 0.99$, indicating that nearly all variance was explained by the fixed and random effects. Estimated marginal means demonstrated a consistent and substantial decline in TVC with increasing depuration time across all salinity levels. Although salinity alone was not a significant predictor in the mixed model, its interaction with time revealed pronounced reductions in bacterial load, particularly at 25 and 30 psu. Pairwise comparisons confirmed statistically significant decreases from 0 to 72 h (Bonferroni-adjusted $p < 0.001$), and the interaction contrasts for salinity at each time point were also significant ($p < 0.001$), indicating that microbial reduction over time was enhanced under higher salinity. By 72 h, bacterial concentrations had dropped by more than four log units in high-salinity treatments, supporting the effectiveness of prolonged depuration.

3.1.2. Presumptive Salmonella/Shigella and other enteric gram-negative bacilli counts (PSS-BC)

Statistical testing using Type III ANOVA indicated strong effects of depuration of salinity (Fig. 2C) and time (Fig. 2D) on PSS-BC ($p < 0.001$), together with a significant interactive influence of the two variables. In contrast, when accounting for replication structure and random variability, GLMM indicated a significant effect of depuration time ($\chi^2 = 166.75$, df = 3, $p < 0.001$, Fig. 3B) and a significant interaction between salinity and time ($\chi^2 = 286.5$, df = 9, $p < 0.001$, Fig. 3B) on PSS-BC on XLD agar. However, salinity alone did not significantly influence PSS-BC levels ($\chi^2 = 0.0$, df = 3, $p = 1.0$, Fig. 3B). This difference reflects the influence of time-dependent salinity responses captured by the mixed model, which averages out in the simpler ANOVA framework. The GLMM showed excellent fit (AIC = 1780.8; BIC = 1819.6; log-likelihood = −872.4), with marginal and conditional R^2 values of 0.99, indicating that nearly all variability was explained by the fixed and random effects. Estimated marginal means demonstrated a progressive and pronounced decline in PSS-BC concentrations with increasing depuration time across all salinities. Although salinity alone was not a significant predictor, its interaction with time revealed strong differences in microbial reduction rates, particularly at 25 and 30 psu. Pairwise comparisons confirmed significant reductions between 0 and 72 h across all salinity levels (Bonferroni-adjusted $p < 0.001$). While baseline (0-h) bacterial counts were comparable among salinities, reductions were enhanced under elevated salinity. By 72 h, microbial concentrations at 30 psu had declined to nearly undetectable levels, underscoring the combined benefits of extended depuration and higher salinity for effective bacterial removal.

3.1.3. Presumptive Vibrio counts (PVC)

Both the Type III ANOVA (Fig. 2F) and GLMM analyses (Fig. 3C) identified depuration time as a key driver of change in PVC, with consistently strong statistical support ($p < 0.001$). While ANOVA also detected a significant salinity effect (Fig. 2E), this influence disappeared in the mixed model once the interaction with time and replication structure were included. The GLMM indicated that time ($\chi^2 = 1280.6$, df = 3, $p < 0.001$; Fig. 3C) and the salinity × time interaction ($\chi^2 = 2668.3$, df = 9, $p < 0.001$; Fig. 3C) together explained nearly all of the variability observed, whereas salinity alone was not significant ($\chi^2 = 2.47$, df = 3, $p = 0.4801$). Model diagnostics confirmed strong performance (AIC = 1335.8; log-likelihood = −649.9; $R^2m = R^2c = 0.9993$). Depuration consistently reduced *Vibrio* loads across all salinity treatments, with sharper declines emerging under higher salinity. The estimated means showed that bacterial concentrations fell steeply between 0 and 72 h, especially in the 25 and 30 psu groups. Pairwise contrasts (Bonferroni-adjusted $p < 0.001$) demonstrated that, despite similar baseline counts, high-salinity treatments produced the most pronounced reductions by the end of the experiment. By 72 h, *Vibrio* densities on TCBS agar had diminished by more than four log units at elevated salinities, underscoring the efficiency of combined time and salinity effects in depuration-driven microbial control.

3.1.4. Presumptive gram-negative/coliform counts (PGN-CC)

Type III ANOVA (Fig. 2H) and GLMM analyses (Fig. 3D) both identified depuration time as the dominant driver of PGN-CC reduction, while salinity (Fig. 2G) and the salinity × time interaction showed no significant effects. Likelihood-ratio tests from the Gamma-log GLMM confirmed a strong influence of time ($\chi^2 = 84.997$, df = 12, $p < 0.001$ 10^{-13}, Fig. 3D), but neither salinity ($\chi^2 = 15.256$, df = 12, $p = 0.228$, Fig. 3D) nor the interaction ($\chi^2 = 12.845$, df = 9, $p = 0.170$, Fig. 3D) contributed significantly to model fit. The model performed well (AIC = 1986.9; BIC = 2025.8; log-likelihood = −975.5), and both marginal and conditional R^2 values were 0.95. Estimated marginal means revealed a steady and pronounced decline in PGN-CC over time, irrespective of salinity. Pairwise comparisons showed significant reductions from 0 to 72 h (Bonferroni-adjusted $p < 0.001$), with the pattern following 72 h < 48 h < 24 h ≈ 0 h. Salinity contrasts within each time were uniformly non-significant, apart from a minor difference at 72 h (30 psu < 20–25 psu), which did not alter the overall interaction outcome. These results confirm that extended depuration time, rather than salinity level, was primarily responsible for bacterial clearance in mussels (Fig. 3D).

3.1.5. Effects of salinity on the detection of pathogenic bacteria

The depuration of naturally accumulated pathogenic bacteria in raft-cultured green mussels (*P. viridis*) was strongly influenced by salinity and exposure time (Table 2). At the start of the experiment (0 h), all four target bacteria, *Salmonella* spp., *Shigella* spp., *E. coli*, and *V. cholerae*, were detected across all salinity levels (15–30 psu). Depuration at low salinity (15 psu) was slower, with *Salmonella* and *Shigella* eliminated by 48 h, while *E. coli* and *V. cholerae* persisted until 72 h. At intermediate salinity (20 psu), both *Salmonella* and *Shigella* were completely depurated after 24 h, whereas *E. coli* and *V. cholerae* required longer, with complete elimination by 48–72 h. In contrast, higher salinity levels (25

Table 2
Effect of different salinity levels (15, 20, 25, and 30 psu) on the depuration of naturally accumulated pathogenic bacteria in raft-cultivated green mussels (*Perna viridis*). The depuration experiment was carried out for 72 h at room temperature (29 ± 1.5 °C) using market-size mussels (shell length: 45–60 mm). The detection of pathogenic bacteria during initial (0 h), 24 h, 48 h, and 72 h is quantitatively represented as present (✓) or absent (×).

Salinity (psu)	Time (h)	Sample size	*Salmonella* spp.	*Shigella* spp.	*Escherichia coli*	*Vibrio cholerae*
15	0	$n = 6$	√	√	√	√
15	24	$n = 9$	√	√	√	√
15	48	n = 9	x	x	√	√
15	72	n = 9	x	x	x	x
20	0	n = 6	√	√	√	√
20	24	n = 9	x	x	√	√
20	48	n = 9	x	x	x	√
20	72	n = 9	x	x	x	x
25	0	n = 6	√	√	√	√
25	24	n = 9	x	x	√	√
25	48	n = 9	x	x	x	x
25	72	n = 9	x	x	x	x
30	0	n = 6	√	√	√	√
30	24	n = 9	x	x	√	√
30	48	n = 9	x	x	x	x
30	72	n = 9	x	x	x	x

and 30 psu) markedly accelerated bacterial removal. At 25 psu, *Salmonella* and *Shigella* were absent by 24 h, and *E. coli* and *V. cholerae* were fully depurated by 48 h. At 30 psu, the highest salinity tested, depuration was even more rapid: *Salmonella* and *Shigella* were eliminated within the first 24 h, and *E. coli* and *V. cholerae* were undetectable by 48 h. These results indicate that elevated salinity substantially enhances depuration efficiency, with *Salmonella* and *Shigella* consistently removed faster than *E. coli* and *V. cholerae*.

3.2. Effects of body size on microbial depuration

3.2.1. Total viable bacterial counts (TVC)

Type III ANOVA model revealed body size ($p > 0.05$) has no influence but depuration time ($p < 0.05$) markedly reduced TVC loads (Fig. 4A). GLMM analysis also indicated a significant effect of depuration time ($\chi^2 = 520.64$, df = 3, $p < 0.001$) on TVC, while neither mussel size ($\chi^2 = 0.00$, df = 2, $p = 1.000$) nor the size × time interaction ($\chi^2 = 2.54$, df = 6, $p = 0.864$) was statistically significant. The model showed excellent fit (AIC = 2047.7, BIC = 2073.9, logLik = −1009.9), and the marginal and conditional R^2 values were both 0.99, indicating nearly all variation was explained by the fixed effects. Estimated marginal means revealed a marked decline in bacterial concentration over time. At 72 h, TVC had declined significantly across all size groups, though size had no independent or interactive effect. Pairwise comparisons confirmed significant reductions from 0 to 72 h ($p < 0.001$), supporting the efficacy of time alone in reducing total bacterial loads during depuration.

3.2.2. Presumptive Salmonella/Shigella and other enteric gram-negative bacilli counts (PSS-BC)

Type III ANOVA model revealed body size ($p > 0.05$) has no influence but depuration time ($p < 0.05$) markedly reduced PSS-BC loads (Fig. 4B). GLMM analysis revealed a significant effect of depuration time ($\chi^2 = 37{,}932$, df = 3, $p < 0.001$) and a significant interaction between size and time ($\chi^2 = 14{,}153$, df = 6, $p < 0.001$, Fig. 5A) on PSS-BC on XLD agar, while size alone was not significant ($\chi^2 = 0$, df = 2, $p = 1.000$). The model fit was strong (AIC = 1232.1, BIC = 1258.3, logLik = −602.1), with marginal and conditional R^2 values near 0.99, indicating high explanatory power of the fixed and random effects. The significant size × time interaction suggests that the pattern of bacterial reduction over time varied by mussel size, especially at the 48-h and 72-h marks. Post hoc comparisons indicated that small-sized mussels exhibited greater

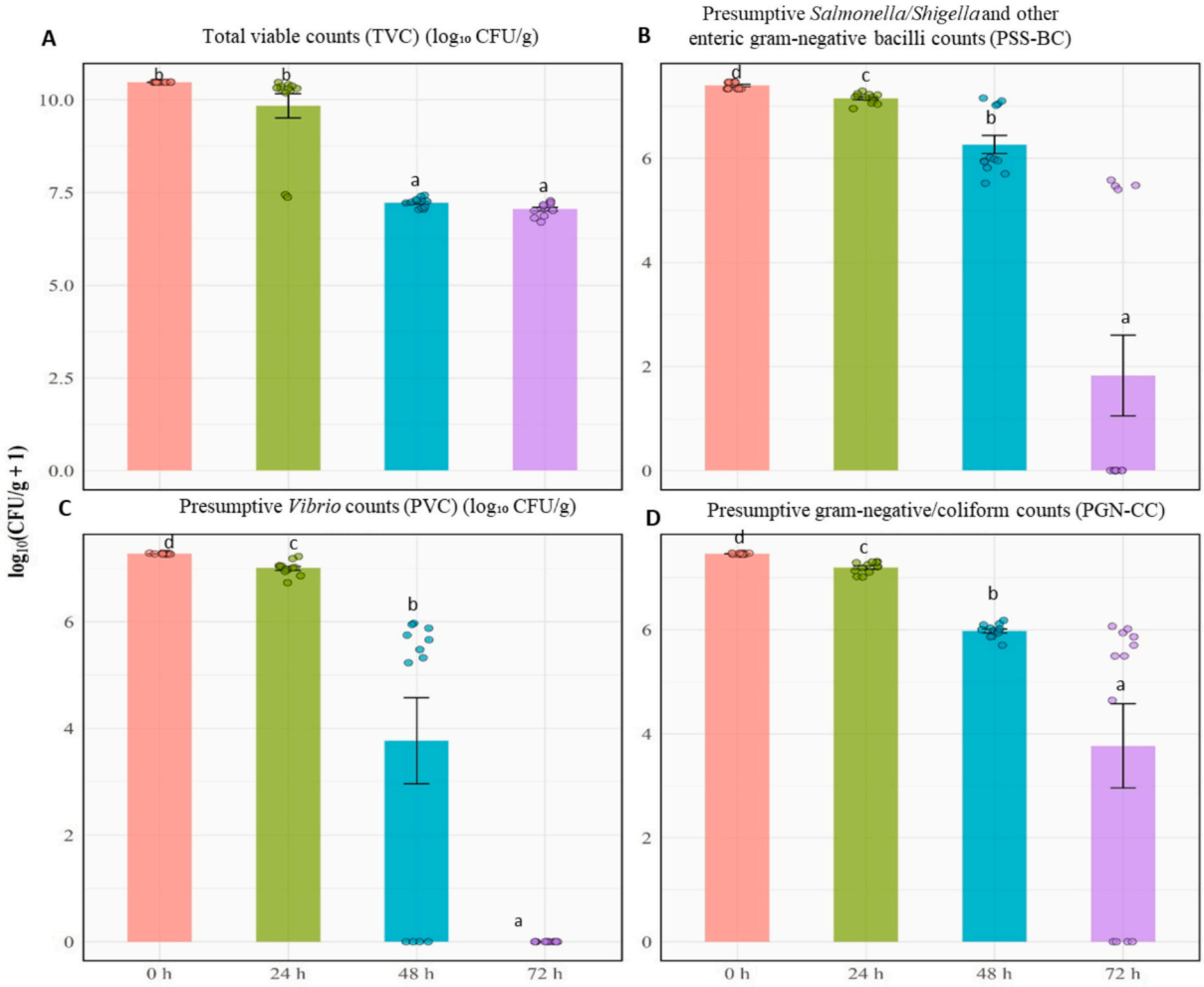

Fig. 4. Influence of depuration time (0, 24, 48 and 72 h) of size-based experiment of green mussels (*Perna viridis*) on microbial concentrations (log_{10} CFU/g) for total viable bacterial counts (TVC), presumptive *Salmonella/Shigella* and other enteric gram-negative bacilli (PSS-BC), presumptive *Vibrio* counts (PVC), and presumptive gram-negative coliform counts (PGN-CC). Bars show mean concentrations (± SE) from the Type III ANOVA main-effect comparisons of depuration time. Since the effects of mussel sizes, (small: 35–45 mm), medium (medium: 45–60 mm), and (large: > 60 mm), are non-significant ($p > 0.05$) based on the Type III ANOVA, the data are not presented here. Different lowercase letters above the bars indicate significant pairwise differences among treatment groups ($\alpha = 0.05$, Bonferroni adjustment); shared letters denote non-significant differences ($p > 0.05$). Because subsequent GLMMs detected significant salinity × time interactions (see Fig. 5), these main-effect plots are presented only for comparison with the mixed-model results. (For interpretation of the references to colour in this figure legend, the reader is referred to the web version of this article.)

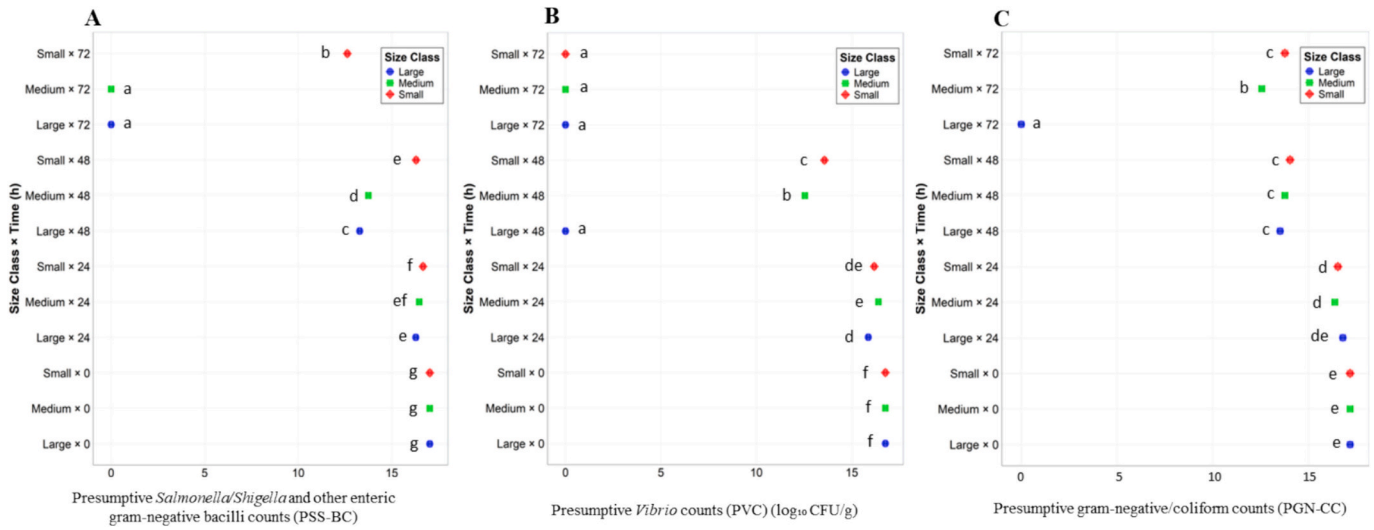

Fig. 5. Interaction effects of body size (small SS, medium MS and large LS) and depuration time (0, 24, 48 and 72 h) on (A) presumptive *Salmonella/Shigella* and other enteric gram-negative bacilli (PSS-BC, $\log_{10}$ CFU/g), (B) presumptive *Vibrio* counts (PVC, $\log_{10}$ CFU/g), and (C) presumptive gram-negative coliform counts (PGN-CC, $\log_{10}$ CFU/g) in mussels (*Perna viridis*). Points represent estimated marginal means ± standard errors derived from the generalized linear mixed-effects models (Gamma distribution with log link). Different lowercase letters denote significant pairwise differences among body size within each depuration time (Bonferroni-adjusted $\alpha = 0.05$), whereas shared letters indicate non-significance ($p > 0.05$). For total viable bacterial counts (TVC, $\log_{10}$ CFU/g), no interaction effects were detected. These interaction plots complement the main-effect results shown in Fig. 4 and illustrate how microbial reduction over time was influenced by body size.

reductions in PSS-BC during the later stages of depuration.

3.2.3. Presumptive Vibrio counts (PVC)

According to the Type III ANOVA, body size showed no significant influence ($p > 0.05$), while depuration time significantly decreased PVC concentrations ($p < 0.05$) (Fig. 4C). GLMMs indicated a significant effect of depuration time on PVC on TCBS agar ($\chi^2 = 54{,}810$, $df = 3$, $p < 0.001$), along with a significant size × time interaction ($\chi^2 = 17{,}238$, $df = 6$, $p < 0.001$, Fig. 5B), while the main effect of size was not significant ($\chi^2 = 0$, $df = 2$, $p = 1.000$). The model showed excellent fit (AIC = 977.5, BIC = 1003.7, logLik = −474.8), and both marginal and conditional R^2 values were above 0.999, indicating strong explanatory power from the fixed and random effects. Post hoc analysis of estimated marginal means (not shown here) revealed that large-sized mussels exhibited substantial reductions in PVC at 48 h and 72 h, whereas smaller size classes retained higher levels until the final point. The interaction effects were especially pronounced at 48 h, where small and medium-sized mussels showed significantly lower reductions compared to large-sized mussels. Notably, the depuration time of 72 h interaction effects were no longer significant for small-sized and medium-sized mussels, suggesting convergence of microbial loads across size classes by the end of the depuration period.

3.2.4. Presumptive gram-negative/coliform counts (PGN-CC)

Statistical analysis using Type III ANOVA demonstrated a non-significant effect of body size ($p > 0.05$) but a significant reduction in PGN-CC with increasing depuration time ($p < 0.05$) (Fig. 4D). GLMMs using a Gamma distribution with a log link revealed a significant main effect of depuration time on PGN-CC measured on MacConkey agar ($\chi^2 = 12{,}348$, $df = 3$, $p < 0.001$), as well as a significant interaction between size and time ($\chi^2 = 5483.5$, $df = 6$, $p < 0.001$, Fig. 5C). However, the main effect of size alone was not significant ($\chi^2 = 0.0$, $df = 2$, $p = 1.000$). The model fit was strong (AIC = 1384.6, BIC = 1410.8, logLik = −678.3), and both marginal and conditional R^2 values were > 0.998, indicating high model explanatory power. Pairwise contrasts (not shown) confirmed that microbial loads consistently decreased over time across all size classes. Only time 24 h showed a modest but statistically significant reduction ($p = 0.034$), while 48 h and 72 h exhibited highly significant reductions compared to baseline/initial (0 h) ($p < 0.001$). Notably, for small-sized mussels, time 48 h was significantly different from the reference/initial group ($p = 0.040$), indicating that small mussels had a delayed yet eventually effective microbial reduction capacity.

3.2.5. Effects of body size on pathogenic bacteria depuration

The depuration efficiency of pathogenic bacteria also varied with mussel body size at 30 psu salinity and room temperature (29 ± 1.5 °C) (Table 3). Small-sized mussels (SS) initially contained all four target bacteria. *Salmonella* and *Shigella* were eliminated by 48 h, whereas *E. coli* persisted until 24 h and *V. cholerae* until 24–48 h. Medium-sized mussels (MS) exhibited rapid depuration of *Salmonella* and *Shigella*, undetectable after 24 h, while *E. coli* and *V. cholerae* remained at 24 h but were fully depurated by 48 h. In large-sized mussels (LS), *Salmonella* and *Shigella* were absent by 24 h, *E. coli* persisted until 24 h, and *V. cholerae* was detectable until 24 h in some samples, with complete elimination of 48 h. Across all body sizes, the depuration of *Salmonella* and *Shigella* was consistently faster than that of *E. coli* and *V. cholerae*.

Table 3
Effect of body size (small SS, medium MS, and large LS) on the depuration of naturally accumulated pathogenic bacteria in raft-cultured green mussels (*Perna viridis*). Three size groups of mussels, small (SS: 35–45 mm), medium (MS: 45–60 mm), and large (LS: > 60 mm) were tested at 30 psu salinity for 72 h at room temperature (29 ± 1.5°C). The detection of pathogenic bacteria is quantitatively represented as present (✓) or absent (×).

Body size	Time (h)	Sample size	*Salmonella* spp.	*Shigella* spp.	*Escherichia coli*	*Vibrio cholerae*
SS	0	n = 6	√	√	√	√
SS	24	n = 9	√	√	√	x
SS	48	n = 9	x	x	√	x
SS	72	n = 9	x	x	x	x
MS	0	n = 6	√	√	√	√
MS	24	n = 9	x	x	√	√
MS	48	n = 9	x	x	x	x
MS	72	n = 9	x	x	x	x
LS	0	n = 6	√	√	√	√
LS	24	n = 9	x	x	x	√
LS	48	n = 9	x	x	x	x
LS	72	n = 9	x	x	x	x

3.3. Effects of salinity on toxic heavy metals and trace elements depuration

Salinity LMM detected strong main effects of toxic heavy metals and trace elements and salinity (ANOVA: metal $F_{9,281} = 89.50$, $p < 0.0001$; salinity $F_{4,281} = 10.08$, $p < 0.0001$). Model fit indices were AIC = 2778.76, BIC = 2837.26, logLik = −1373.38, with $R^2_m = R^2_c = 0.739$. Relative to the reference metal, Fe ($\beta = 127.55$, $p < 0.0001$), Zn ($\beta = 98.79$, $p < 0.0001$), Mn ($\beta = 25.81$, $p = 0.0003$), and Cu ($\beta = 20.13$, $p = 0.0043$) were higher; other metals did not differ from the intercept. Compared with initial habitat salinity (before depuration), concentrations were significantly lower at 15 psu ($\beta = -16.22$, $p = 0.0012$), 20 psu ($\beta = -21.64$, $p < 0.0001$), 25 psu ($\beta = -24.86$, $p < 0.0001$), and 30 psu ($\beta = -28.22$, $p < 0.0001$). Post hoc CLD showed initial (before depuration) forming a distinct, higher group, whereas 15–30 psu shared a common lower grouping, indicating effective reduction by 72 h across depuration salinities (Fig. 6A). Group-wise means (±SE) of different toxic heavy metals and trace elements during initial at 0 h and 72 h depuration are shown in Fig. 6B. The time LMM revealed highly significant effects of toxic heavy metals and trace elements ($F_{9,252} = 310.26$, $p < 0.0001$), time ($F_{1,28} = 72.98$, $p < 0.0001$), and their interaction ($F_{9,252} = 68.06$, $p < 0.0001$). The model explained over 91% of variance ($R^2_m = 0.911$, $R^2_c = 0.915$). Fixed-effect contrasts indicated substantial 72 h decreases for Fe (interaction $\beta = -185.98$, $p < 0.0001$) and a smaller but significant decrease for Zn ($\beta = -20.66$, $p = 0.038$), while most other elements showed negligible change in the mixed-model framework. Nonparametric Wilcoxon tests (0 h vs 72 h) corroborated significant reductions (BH-adjusted p-values) for Fe (p_adj_BH = 0.0004), Pb (0.011), Mn (0.025), Cu (0.0256), Hg (0.0418), and Zn (0.0459). Changes were not significant for Cr, Ni, As, or Se (all p_adj_BH > 0.05). These results, combined with the salinity findings, indicate that the 72 h depuration period was particularly effective for Fe and several

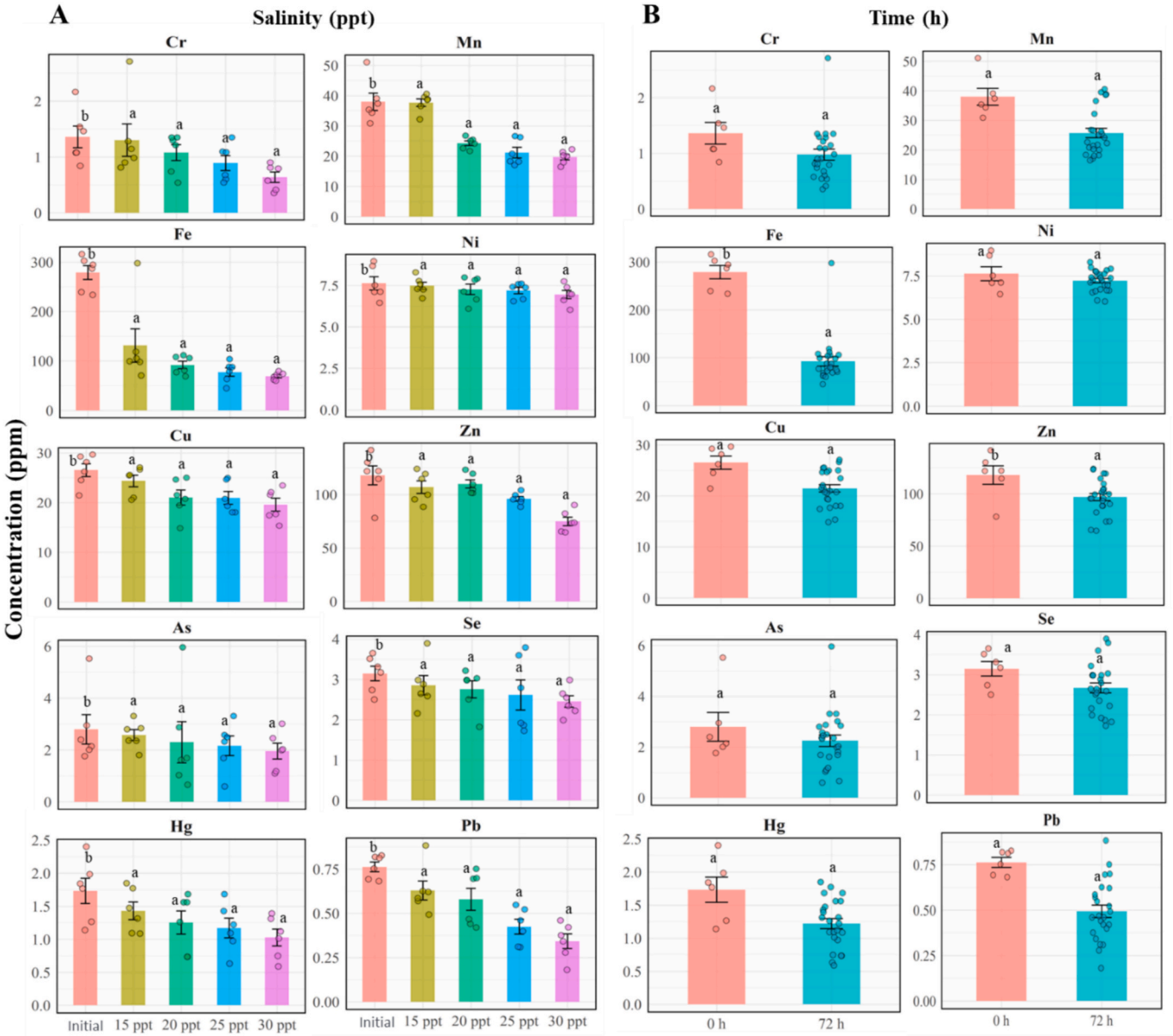

Fig. 6. Ten trace/toxic element (Cr, Mn, Fe, Ni, Cu, Zn, As, Se, Hg, and Pb) concentrations (ppm; dry matter basis) in mussels (*Perna viridis*) across salinity (15, 20, 25 and 30 psu, including habitat salinity as the initial sample) and depuration time (0 h and 72 h) using market size (shell length > 60 mm) mussels. Bars show mean concentrations (± SE) from the Type III ANOVA main-effect comparisons of salinity (left panels) and depuration time (right panels). Different lowercase letters above the bars indicate significant pairwise differences among treatment groups ($\alpha = 0.05$, Bonferroni adjustment); shared letters denote non-significant differences ($p > 0.05$).

other elements (Pb, Mn, Cu, Hg, Zn), while some elements exhibited limited or no temporal decline.

3.4. Effects of body size on toxic heavy metals and trace elements depuration

The individual LMMs indicated that mussel size had a strong and statistically significant effect on toxic heavy metals and trace elements concentrations across all ten analytes. The size effect was particularly prominent in chromium (Cr: $F_{5,30} = 16.53$, $p < 0.0001$), manganese (Mn: $F_{5,25} = 16.94$, $p < 0.0001$), iron (Fe: $F_{5,25} = 15.36$, $p < 0.0001$), copper (Cu: $F_{5,25} = 27.57$, $p < 0.0001$), zinc (Zn: $F_{5,30} = 15.28$, $p < 0.0001$), and lead (Pb: $F_{5,25} = 12.19$, $p < 0.0001$). Mussels classified as "initial medium" and "initial large" consistently exhibited higher concentrations for several elements compared to other size groups. For instance, Cu and Zn levels in "initial medium" mussels averaged 56.2 ppm and 140.4

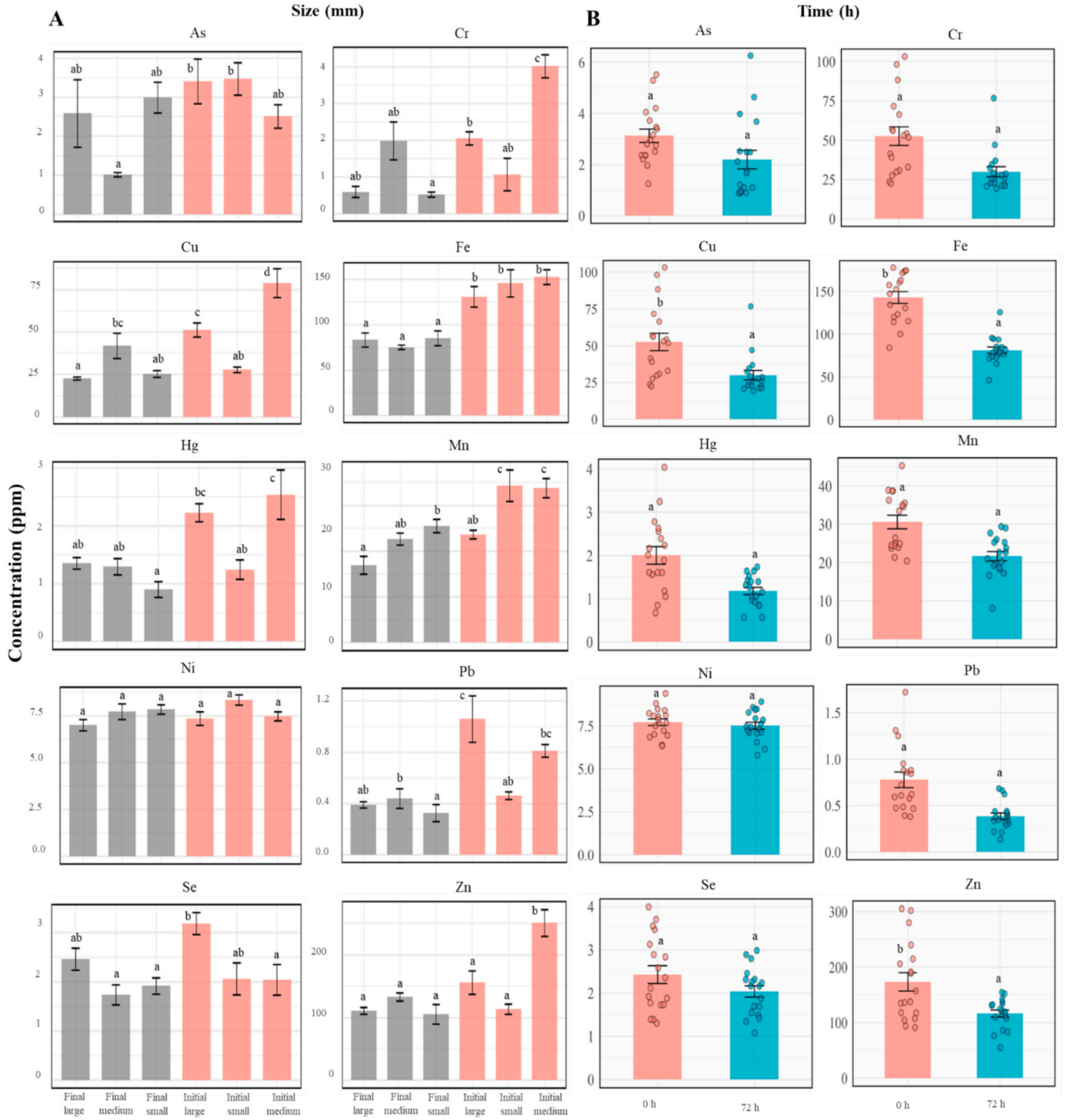

Fig. 7. Trace/toxic element concentrations (ppm) in mussels (*Perna viridis*) across body-size (SS, small-size = 35–45 mm; MS, medium-size = 45–60 mm; and LS, large-size >60 mm) and depuration time (0 and 72 h) for Cr, Mn, Fe, Ni, Cu, Zn, As, Se, Hg, and Pb using seawater salinity of 30 psu. Bars show mean concentrations (± SE) from the Type III ANOVA main-effect comparisons of different body size (left panels) and depuration time (right panels). Different lowercase letters above the bars indicate significant differences between treatment groups based on pairwise comparisons ($\alpha = 0.05$). Shared letters denote non-significant differences ($p > 0.05$).

ppm, respectively, which were significantly elevated relative to other size classes ($p < 0.001$). Similarly, Fe concentrations were substantially higher in "initial medium" ($\beta = 69.25$, $p < 0.0001$) and "initial small" ($\beta = 62.41$, $p < 0.0001$) mussels compared to the reference group (Fig. 7A).

Model fit diagnostics supported the robustness of these models, with marginal R^2 values ranging from 0.23 (Ni) to 0.72 (Cu). Conditional R^2 values incorporating random effects were slightly higher, particularly for Cu ($R^2c = 0.82$) and Mn ($R^2c = 0.75$), reflecting modest but detectable variability across replicate tanks. For Cr, As, Zn, and Se, the random intercept variance was near zero, suggesting minimal tank-level effects. In contrast, the fixed effect of depuration time (0 h vs 72 h) was not statistically significant in any of the individual toxic heavy metals and trace elements-specific LMMs, indicating that a 72-h depuration period did not result in measurable reductions in toxic heavy metals and trace elements concentrations when controlling mussel size. This lack of time effect held consistently across all elements, including Ni, As, Se, Hg, and Pb. Additionally, the size × time interaction term was dropped from all models due to rank deficiency, preventing interpretation of interaction effects, likely due to collinearity or missing combinations in the dataset (Fig. 7B).

However, when examining time effects using the combined model across all elements, a different pattern emerged. The Type III ANOVA revealed significant main effects of toxic heavy metals and trace elements ($F_{9,306} = 268.02$, $p < 0.0001$), time group ($F_{1,34} = 36.06$, $p < 0.0001$), and a significant metal × time group interaction ($F_{9,306} = 14.54$, $p < 0.0001$). Model fit for this global analysis was strong, with marginal $R^2 = 0.872$ and conditional $R^2 = 0.880$. Effect size analysis showed that mean concentrations for most metals decreased after 72 h of depuration, with the highest percentage reduction observed in Fe (−43.2%), Cu (−43.1%), Zn (−33.0%), Pb (−50.4%), Cr (−56.6%), and Hg (−41.0%). Other metals such as Mn (−29.1%), As (−29.8%), and Se (−16.1%) also showed moderate declines, though to a lesser extent. Nickel exhibited minimal reduction (−2.64%). Post hoc comparisons indicated that these reductions were statistically significant for Fe ($p < 0.001$), Cu ($p = 0.018$), and Zn ($p < 0.001$), with borderline significance in Mn ($p = 0.40$). The interaction terms suggest that the effect of depuration time is metal-specific, with some elements (e.g., Fe, Cu, Zn, Cr, Pb, Hg) responding more strongly to depuration, while others (e.g., Ni, As, Se) remained largely unaffected.

4. Discussion

Depuration efficiency in *P. viridis* is governed by the combined influences of salinity, duration, and body size, with elevated salinity and extended depuration time enhancing microbial clearance, while body size determines contaminant burdens but does not alter the overall elimination efficiency after 72 h. Toxic heavy metals and trace elements depuration is distinctly element-specific; essential metals (Fe, Cu, Zn) are rapidly regulated, Pb, Cr, and Hg exhibit notable reductions, whereas Ni, As, and Se persist, underscoring the necessity for integrated depuration protocols that optimize salinity, exposure duration, and size-class management to ensure shellfish safety.

4.1. Effects of salinity on microbial depuration

Salinity emerged as a critical factor influencing the efficiency of microbial depuration in mussels, although its effects were primarily expressed through interactions with time rather than as an independent variable. Bivalves, like osmoconformers, cannot regulate their internal osmotic balance (Shumway, 1977). Consequently, fluctuations in salinity directly influence their physiological performance, particularly pumping and feeding activity (Rodrick and Schneider, 1991). Effective depuration, therefore, requires maintaining salinity levels close to natural growing conditions, with the National Shellfish Sanitation Program (NSSP, 1990) recommending that differences should not exceed 20%.

The present study revealed that prolonged depuration time markedly reduced bacterial loads, while elevated salinity further enhanced this reduction. This pattern may be explained by two complementary mechanisms. First, prolonged depuration allows mussels to continuously filter water and expel contaminants from their digestive system. Second, higher salinity is likely to impose osmotic stress on bacteria, creating hyperosmotic conditions that may induce water efflux, cell shrinkage, and ionic imbalance. These changes can disrupt membrane integrity, impair energy metabolism, and interfere with macromolecule synthesis, potentially leading to bacterial inactivation. In addition, improved physiological performance at higher salinity may contribute to enhanced depuration efficiency, as optimal salinity conditions are known to increase scope for growth (SFG), filtration activity, and energy availability in *Perna viridis*, whereas low salinity can suppress clearance rates due to osmotic stress (Wang et al., 2011). The multi-log reductions observed over 72 h suggest that prolonged exposure to these conditions may exceed the adaptive capacity of most bacterial populations. Such synergy between depuration time and salinity likely represents a powerful strategy for enhancing microbial safety in bivalves (Rodrick and Schneider, 1991). These findings emphasize that salinity optimization during depuration is likely to be a critical factor for ensuring microbial safety in bivalve products, especially in tropical environments.

Similar depuration patterns have been reported in other bivalve species under controlled systems. Love et al. (2010) demonstrated significant declines in *E. coli* and *Enterococcus faecalis* in oysters and hard-shell clams, while Phuvasate and Su (2013) reported substantial reductions in *Vibrio parahaemolyticus* in *Crassostrea gigas* following extended depuration at higher salinities. Larsen et al. (2013, 2015) likewise found marked decreases in *V. parahaemolyticus* and *V. vulnificus* in *C. virginica* when maintained under salinities above 25 psu. The results from the present study correspond closely with these findings, confirming that *P. viridis* achieves efficient microbial clearance when depurated for at least 72 h under high salinity conditions. Since mussel filtration activity is known to vary with salinity and temperature (Rajesh et al., 2001; Riisgård and Larsen, 2025), the consistent reduction in bacterial load under these parameters suggests the physiological adaptability of *P. viridis* to optimized depuration conditions. In tropical and subtropical estuarine systems like the Bay of Bengal, controlled depuration under slightly elevated salinities may therefore represent a practical approach to enhancing the microbiological safety of green mussels (Rajesh et al., 2001).

An important observation in this study was the uneven rate of bacterial reduction among different microbial groups. Although *Salmonella–Shigella* and *Vibrio* spp. were effectively reduced to low or undetectable levels, coliforms persisted longer during depuration. This differential pattern may suggest that coliforms are more resistant to environmental stress or may have the ability to form biofilm-like clusters on gill or gut surfaces, offering protection from osmotic stress and water exchange (Leoni et al., 2017; Serratore, 2017). These findings align with earlier reports showing that coliforms are often poor predictors of pathogen removal, as their persistence does not always correlate with the elimination of true pathogens (Leoni et al., 2017; Serratore, 2017). Conversely, Chinnadurai et al. (2023) reported faster reductions of coliforms under certain system conditions, implying that species-specific physiology, water quality, and depuration setup influence clearance efficiency. Thus, while traditional depuration is generally effective for reducing microbial loads, the survival of certain indicator bacteria demonstrates the complexity of microbial dynamics within bivalve depuration systems.

Currently, European Commission Regulation 2285/2015 bases shellfish safety evaluation exclusively on *E. coli* as an indicator of faecal contamination. This approach does not account for naturally occurring pathogens such as *V. parahaemolyticus*, which are of increasing concern in shellfish safety monitoring. Further studies are therefore required to assess the reliability of natural pathogenic Vibrios as alternative or complementary indicators. Such efforts could help to address data gaps

in pathogen prevalence across production areas and inform the development of specific safety criteria (Suffredini et al., 2014). As an alternative strategy, regulatory bodies may consider coliforms as indicators. However, their persistence during depuration suggests they reflect the adaptive role of resident microbiota with established physiological interactions in bivalves (Destoumieux-Garzon et al., 2020) and may not fully capture the risks posed by natural pathogens, underscoring the need for refined monitoring criteria to safeguard public health.

4.2. Effects of body size on microbial depuration

Like salinity, another crucial parameter in the depuration process is the age and body size of the animals subjected to depuration (Richards, 1988). Before depuration, the concentrations of different groups of bacteria in small-sized (SS) *P. viridis* mussels were higher than those in medium-sized (MS) and large-sized (LS) mussels. Several studies have highlighted the role of age and body size in the accumulation of microbes in bivalve mollusks' soft tissues (Lopez-Joven et al., 2011). In our study, LS reached European Commission safety limits within 48–72 h, with all counts reduced to zero or non-detectable levels, a key safety indicator. In contrast, small-sized (SS) and medium-sized (MS) mussels took longer to reach safety limits. However, studies on other bivalve mollusks, such as the Pacific oyster, *C. gigas*, have shown that age and body size had no significant impact on the depuration of faecal coliforms (Phuvasate and Su, 2013).

The greater reduction of different groups of bacterial loads in large-sized (LS) mussels may be attributed to their higher filtration activity. According to Metcalf et al. (1979), the size of bivalve mollusks impacts the volume of water pumped through their gills, with larger individuals pumping more water. This increased pumping activity may influence both the rate of bioaccumulation and the efficiency of contaminant removal during depuration. The enhanced filtration efficiency in larger mussels may result from a higher gill surface area to body size ratio and greater physiological demand. Accordingly, harvesting strategies may consider size-related differences in depuration efficiency, although this was not directly tested in the present study. The convergence of microbial loads across mussel size classes by 72 h, particularly for presumptive *Vibrio* counts (PVC), suggests that extended depuration periods can mitigate initial size-related differences in bacterial clearance efficiency. This temporal convergence implies that while smaller mussels may experience rapid initial reductions in bacterial loads due to their higher mass-specific filtration rates, larger mussels may achieve comparable reductions over time owing to their sustained absolute filtration capacity (Marescaux et al., 2016; Cranford et al., 2011). The delayed yet effective microbial reduction observed in small-sized mussels (SS) at 48 h further suggests the role of size-related physiological differences in influencing the efficiency of depuration, rather than its ultimate efficacy. These findings highlight that the efficiency of bacterial clearance is largely governed by depuration duration, allowing for a gradual but substantial reduction in bacterial loads over time. The observed temporal patterns reflect the intricate interactions between bacterial type, mussel size, and depuration duration, emphasizing the complexity of microbial depuration in bivalve mollusks (Marescaux et al., 2016).

4.3. Effects of salinity on toxic heavy metals and trace elements depuration

Salinity of the aquatic environment plays a critical role in governing the bioaccumulation of toxic heavy metals and trace elements in bivalve mollusks (Kumar et al., 2015; Yin and Wang, 2017). While this relationship is well documented, comparatively little attention has been given to the reverse process, depuration of toxic heavy metals and trace elements. In contrast, the influence of salinity on microbial reduction during depuration has been extensively studied (Phuvasate and Su, 2013). Only a limited number of investigations have addressed toxic heavy metals and trace elements elimination in bivalves during depuration, and these did not explicitly examine salinity as a determining factor (Çağlak et al., 2020; Yang et al., 2020). The comparatively low depuration efficiency of *P. viridis* at 15 psu relative to higher salinities (25–30 psu) suggests that ionic strength and osmotic gradients may influence metal release through both physiological and physicochemical pathways. Bivalves maintained at lower salinities (15 psu) are likely to experience physiological stress, which can suppress filtration and ingestion rates, thereby limiting depuration capacity (Rajesh et al., 2001). Supporting this, *Mytilus edulis* exposed to 15 psu demonstrated a significant decline in heart rate, reflecting impaired physiological function under reduced salinity conditions (Bakhmet et al., 2005).

Not all toxic heavy metals and trace elements responded equally, underscoring differences in binding chemistry and detoxification pathways. The marked reductions of Fe, Zn, Mn, Cu, Pb, and Hg indicate that these elements are relatively more labile or accessible for elimination. By contrast, the persistence of Cr, Ni, As, and Se may reflect stronger tissue binding or slower turnover rates, which may limit depuration efficiency within a 72 h timeframe. This variability is consistent with earlier findings that depuration is often element-specific, with essential trace elements showing more dynamic regulation than non-essential or toxic elements (Rainbow, 2002).

The observed reduction of Fe during depuration may be associated with homeostatic regulation mechanisms, including metallothioneins, ferritin, and transport systems that modulate intracellular metal pools (Baird et al., 2006). Similarly, decreases in Zn and Cu are consistent with their regulated physiological roles (Barreira et al., 2024), although the exact pathways were not directly assessed in this study. Zinc declined more rapidly at lower salinity, which may be linked to regulatory adjustments and redistribution processes. Previous studies have reported rapid Cu elimination in bivalves under controlled conditions, although such mechanisms were not explicitly examined here (Saed et al., 2004; Pan and Wang, 2009). In contrast, Pb depuration was less efficient, while oysters accumulated Pb more slowly than Hg and Cd; faster elimination has been documented in certain species such as *Pinna nobilis* (Jebali et al., 2014) and cockles, which achieved 86.5% removal within 24 h at 35 psu (Firdaus et al., 2020). Overall, these findings suggest that while Cu and Fe are efficiently regulated, Pb clearance is more variable, reflecting species- and salinity-specific differences (Chinnadurai et al., 2022; Fukunaga and Anderson, 2011).

The overall effectiveness of salinity-controlled depuration supports its utility as a practical approach in shellfish sanitation protocols. Evidence from both experimental studies and industry practices suggest that medium-sized mussels maintained at salinities of 25–35 psu for 48–72 h under moderate temperatures can achieve substantial reductions in bioaccumulated metals (Chinnadurai et al., 2022). Nonetheless, the limited elimination of As and Cr remains a challenge and may be related to their strong tissue binding, complex speciation, and possible retention within metabolically less active compartments, thereby reducing clearance rates (Yap and Al-Mutairi, 2025; Zhao et al., 2021). Arsenic is of particular concern given the toxicity of its inorganic forms, which are often difficult to mitigate under conventional depuration conditions. Similarly, chromium's strong affinity for cellular proteins and its slow turnover rate may contribute to its persistence during treatment. These constraints suggest that extended depuration periods or complementary strategies, such as pH modification, chelating agents, or targeted pre-harvest management, could enhance removal efficiency and support compliance with international food safety regulations (European Commission, 2005).

4.4. Effects of body size on toxic heavy metals and trace elements depuration

Besides environmental factors such as temperature, salinity, and water treatment, the body size of bivalves may also significantly influence depuration efficiency. Previous studies have shown that the accumulation of toxic heavy metals and trace elements in soft tissues is

strongly size-dependent (Lee et al., 1998), yet little attention has been given to how body size influences these elements elimination during depuration. In this study, freshly harvested mussels of different size classes (SS, MS, LS) contained both essential trace (Fe, Cu, Zn, Mn, Cr, Se) and non-essential toxic (Pb, Hg, As, Ni) elements, with Mn, Ni, and As exceeding safety levels (Table 4). Depuration for 72 h reduced metal levels across all sizes, though As remained above the safe limit in SS mussels. This may reflect their higher initial As burden, indicating that smaller individuals may require a longer depuration period. Physiological differences may help explain these patterns. Larger bivalves pump more water through their gills, which could enhance contaminant removal. Since depuration efficiency is closely linked to filtration and physiological activity (Richards, 1988; Jones et al., 1992), size is likely a critical determinant. Supporting this, LaTouche and Mix (1982) found that depuration efficiency in *M. edulis* increased with body size. Similarly, Chinnadurai et al. (2022) observed that Pb levels in SS clams and mussels remained above safety limits after 48 h, suggesting that smaller bivalves may require longer depuration times.

The extent of toxic heavy metals and trace elements reduction varied across size classes, likely reflecting physiological factors such as clearance rate (Wen-Xiong and Fisher, 1996), metabolic activity (El-Shenawy, 2004), and gill surface area and filtration capacity (Riisgård et al., 2018). Larger mussels, with greater tissue biomass, tend to bioaccumulate more metals but may depurate less efficiently due to slower turnover and reduced surface area-to-volume ratios, whereas smaller mussels may more readily eliminate surface-adsorbed contaminants (Cossa et al., 1980). However, the lack of a consistent size × time interaction across individual models suggests that depuration efficiency is not strongly modulated by body size over short-term periods. This finding indicates that while size influences absolute metal concentrations, the rate of depuration appears relatively consistent across size classes during the 72-h experimental timeframe. This pattern suggests that short-term depuration processes are primarily governed by metal-specific biochemical mechanisms rather than size-dependent physiological differences, which may become more pronounced over longer depuration periods where tissue turnover and metabolic differences have greater opportunity to manifest.

The combined analysis showed that depuration was highly element-specific: Fe (−43.2%), Cu (−43.1%), and Zn (−33.0%) exhibited substantial reductions, consistent with homeostatic regulation through transport proteins and binding molecules; Pb (−50.4%) and Cr (−56.6%) showed pronounced elimination, which might be associated with metallothionein binding and detoxification pathways (Baudrimont et al., 2003); and Hg decreased significantly (−41.0%) possibly related to its strong affinity for sulfhydryl groups (Ajsuvakova et al., 2020; Wu et al., 2024). In contrast, Mn (−29.1%), As (−29.8%), and Se (−16.1%) showed only moderate declines, while Ni (−2.64%) remained largely unaffected, which may indicate strong binding or sequestration in compartments inaccessible to short-term depuration (Gagné et al., 2007). These findings suggest that depuration efficiency is jointly determined by organismal physiology and metal-specific biochemical interactions, with essential metals benefiting from regulatory mechanisms (Chandrapalan et al., 2021) and non-essential metals exhibiting variable elimination depending on their chemical affinities and tissue distribution (Le et al., 2023).

4.5. Implications for food safety

Pathogenic bacteria, including *Salmonella* spp., *Shigella* spp., *Escherichia coli*, and *Vibrio cholerae* were initially detected in all samples but declined progressively during depuration, becoming completely undetectable after 48–72 h at salinities ≥25 psu, and across all body sizes, suggesting that controlled salinity and sufficient depuration time are effective in improving microbiological safety. In terms of toxic heavy metals and trace elements, concentrations of toxic elements such as Pb, Hg, and Cr decreased substantially during 72 h of depuration (see Table 4), and essential trace elements (Fe, Cu, Zn, Mn) remained within acceptable limits, staying below the international thresholds set by WHO, FAO, EU, FDA, and other regulatory bodies (see Table 5). However, total arsenic (As) concentrations, while declining during depuration (from ~0.71 $mg{\cdot}kg^{-1}$ at 0 h to ~0.50 $mg{\cdot}kg^{-1}$ at 72 h), remained above the reference benchmark of 0.3 $mg{\cdot}kg^{-1}$. It is important to emphasize that these measurements reflect total arsenic, whereas food safety regulations and risk assessments typically consider only inorganic arsenic (iAs), the more toxic fraction. In bivalves, inorganic arsenic usually constitutes only a small proportion of total As, which may indicate that the actual health risk may be limited. Collectively, these findings suggest that green mussels from the Bay of Bengal, when subjected to 72 h of salinity-optimized depuration, are likely safe for human consumption with respect to microbial pathogens and most toxic heavy metals and trace elements, though further monitoring of inorganic arsenic and toxins is recommended to ensure full compliance with food safety standards.

5. Conclusion

This study demonstrates that depuration efficiency in *Perna viridis* is primarily governed by exposure time, with salinity exerting a significant interactive effect on microbial removal. Optimal depuration (72 h at 25–30 psu) achieved near-complete elimination of pathogenic bacteria

Table 4
Mean concentrations of trace/toxic elements (mg/kg, on dryweight basis) in the green mussel (*Perna viridis*) at 0 h and 72 h of depuration under varying salinity levels (15 psu, 20 psu, 25 psu, and 30 psu) and body size categories (SS = 35–45 mm; MS = 45–60 mm; LS ≥ 60 mm) at room temperature (29 ± 1.5°C).

Sample Category	Time (h)	Concentration (mg/kg)									
		Trace elements						Toxic elements			
		Mn	Fe	Ni	Cu	Zn	Se	Cr	As	Hg	Pb
Salinity (psu)											
Initial	0	9.73	71.42	1.95	6.79	30.20	0.81	0.35	0.71	0.44	0.19
15	72	9.65	33.65	1.91	6.24	27.38	0.73	0.33	0.66	0.37	0.16
20	72	6.21	23.58	1.86	5.38	28.14	0.70	0.28	0.59	0.30	0.15
25	72	5.42	19.89	1.84	5.36	24.59	0.67	0.23	0.55	0.29	0.11
30	72	5.04	17.73	1.78	5.01	19.17	0.63	0.16	0.50	0.26	0.09
Body Size (mm)											
SS	0	8.79	37.29	2.13	7.10	29.08	0.52	0.27	0.89	0.32	0.12
SS	72	6.52	21.79	2.00	6.47	26.94	0.49	0.13	0.77	0.23	0.09
MS	0	8.65	39.03	1.97	20.16	64.29	0.52	1.03	0.64	0.65	0.21
MS	72	5.79	19.26	1.91	10.71	33.99	0.45	0.51	0.26	0.33	0.11
LS	0	6.04	33.45	1.88	13.10	39.89	0.81	0.52	0.87	0.57	0.27
LS	72	4.33	21.31	1.79	5.78	28.35	0.63	0.15	0.66	0.35	0.09

Table 5
Human health risk threshold limits for trace/toxic element concentrations in bivalve shellfish and seafood according to different international food safety standards.

Trace Elements	Threshold concentration (mg/kg)								
	WHO/ JECFA	EC	MFR	FSSAI	FAO	FDA/US	Health Canada	FSANZ	Japan MHLW
Mn	1	–	–	–	–	–	–	–	–
Cr	–	–	–	–	12	13	–	–	–
Fe	100	–	–	–	–	–	–	–	–
Ni	2	–	–	1.5	–	–	–	–	–
Cu	3	–	30	30	30	–	–	–	–
Zn	50	–	100	50	–	–	–	–	–
As	–	–	–	–	–	–	0.3	–	–
Hg	–	0.5	–	0.5	0.5	1	0.5	0.5	0.3
Se	–	–	–	–	–	–	–	–	1.2
Pb	2	1.5	2	2.5	–	–	–	–	–

Here, all threshold concentrations are expressed in mg/kg dryweight. Values represent permissible limits for bivalve shellfish, except where specifically indicated for seafood (Cr: 12 mg/kg, FAO; Cr: 13 mg/kg, FDA/US Health Canada).
World Health Organization (2020).
European Commission (2006).
Malaysian Food Regulation (1985).
Food Safety and Standards Authority of India (2011).
Food and Agriculture Organization and World Health Organization (2002).
U.S. Food and Drug Administration. (2024).
Health Canada (2005).
Food Standards Australia New Zealand (2023).
Ministry of Health, Labour and Welfare (Japan) (2020).

and substantial reductions in several toxic heavy metals and trace elements (Fe, Cu, Zn, Pb, Hg, and Cr), whereas Ni, As, and Se showed limited responsiveness. Body size influenced initial contaminant levels but did not affect final depuration outcomes within 72 h. These findings provide an evidence-based basis for optimizing depuration protocols under tropical conditions to improve seafood safety. However, the persistence of certain elements, particularly arsenic, highlights the need for further investigation into element speciation and longer-term depuration strategies. Future research integrating physiological, molecular, and environmental approaches would help refine depuration practices and enhance their applicability in commercial aquaculture systems.

Declaration of generative AI in scientific writing

During the preparation of this work, the authors used ChatGPT in the writing process to improve the readability and language of the manuscript. After using this tool/service, the authors reviewed and edited the content as needed and took full responsibility for the content of the published article.

CRediT authorship contribution statement

Md Asaduzzaman: Writing – original draft, Visualization, Supervision, Project administration, Methodology, Funding acquisition, Formal analysis, Data curation, Conceptualization. **Khandakar Zakir Hossain:** Writing – original draft, Methodology, Formal analysis, Data curation. **Sabrina Jahan:** Writing – review & editing, Methodology, Investigation, Formal analysis, Data curation. **Israt Jahan:** Writing – original draft, Investigation, Data curation. **Kanij Fatema Ety:** Methodology, Formal analysis, Data curation. **Md. Ramzan Ali:** Writing – review & editing, Resources, Formal analysis, Data curation. **Md Nahiduzzaman:** Writing – review & editing, Resources, Project administration, Funding acquisition. **Yeasmin Nahar Jolly:** Writing – review & editing, Methodology, Investigation. **Shirin Akter:** Writing – review & editing, Resources, Methodology. **Mohammad Sadequr Rahman Khan:** Writing – review & editing, Project administration, Funding acquisition. **Md Moshiur Rahman:** Writing – review & editing, Visualization, Software, Formal analysis, Data curation.

Declaration of competing interest

The authors declare that they have no known competing financial interests or personal relationships that could have appeared to influence the work reported in this paper.

Acknowledgements

This work was conducted as a part of the research plan of the Bangladesh Academy of Sciences- United States Department of Agriculture (BAS-USDA) Endowment 5th phase project implemented by Chattogram Veterinary and Animal Sciences University through a collaborative agreement with BAS (F 127). We would like to thank the director and other staff of the BAS-USDA Endowment Program for providing funding for this research work. A partial funding support was also received from the Enhanced Coastal Fisheries in Bangladesh II (ECOFISH II) project of the WorldFish activity particularly for the microbial count study. We also thank the staff of the Oceanography Laboratory, Department of Marine Bioresource Science, Chattogram Veterinary and Animal Sciences University, for helping with oyster sampling and parameter analysis.

Data availability

Data will be made available on request.

References

Ajsuvakova, O.P., Tinkov, A.A., Aschner, M., Rocha, J.B.T., Michalke, B., Skalnaya, M.G., Skalny, A.V., Butnariu, M., Dadar, M., Sarac, I., Aaseth, J., Bjørklund, G., 2020. Sulfhydryl groups as targets of mercury toxicity. Coord. Chem. Rev. 417, 213343. https://doi.org/10.1016/j.ccr.2020.213343.

Anacleto, P., Maulvault, A.L., Barrento, S., Mendes, R., Nunes, M.L., Rosa, R., Marques, A., 2013a. Physiological responses to depuration and transport of native and exotic clams at different temperatures. Aquaculture 408 (409), 136–146. https://doi.org/10.1016/j.aquaculture.2013.05.035.

Anacleto, P., Maulvault, A.L., Chaguri, M., Pedro, S., Nunes, M.L., Rosa, R., Marques, A., 2013b. Microbiological responses to depuration and transport of native and exotic clams at optimal and stressful temperatures. Food Microbiol. 36, 365–373. https://doi.org/10.1016/j.fm.2013.07.002.

Asaduzzaman, M., Rahi Noor, A., Rahman, M.M., Akter, S., Hoque, N.F., Shakil, A., Wahab, M.A., 2019. Reproductive biology and ecology of the green mussel *Perna viridis*: a multidisciplinary approach. Biology 8 (4), 88. https://doi.org/10.3390/biology8040088.

Asaduzzaman, M., Nahiduzzaman, M., Chowdhury, M.T.H., Rahman, M.M., Mamun, A. A., Hossain, M.M., 2025a. Advancing low-trophic extractive mariculture (LTEM): Strategies for a thriving blue economy in Bangladesh. Mar. Policy 173, 106557. https://doi.org/10.1016/j.marpol.2024.106557.

Asaduzzaman, M., Mohiuddin, M., Rahman, M.M., Kabir, I.E., Nahiduzzaman, M., 2025b. Ecology intersects with mariculture: how cultivation depth and site-specific environmental factors shape growth and nutritional profile of green mussels (*Perna viridis*). Reg. Stud. Mar. Sci. 81, 103981. https://doi.org/10.1016/j.rsma.2024.103981.

Baird, S.K., Kurz, T., Brunk, U.T., 2006. Metallothionein protects against oxidative stress-induced lysosomal destabilization. Biochem. J. 394, 275–283. https://doi.org/10.1042/bj20051143.

Bakhmet, I.N., Berger, V.J., Khalaman, V.V., 2005. The effect of salinity change on the heart rate of *Mytilus edulis* specimens from different ecological zones. J. Exp. Mar. Biol. Ecol. 318 (2), 121–126. https://doi.org/10.1016/j.jembe.2004.11.023.

Bánfalvi, G., 2011. Cellular Effects of Heavy Metals, 1st ed. Springer, Dordrecht. https://doi.org/10.1007/978-94-007-0428-2. pp. XIV, 348.

Barreira, J., Chen, L., Silva, M., 2024. Copper and zinc isotope systematics in different bivalve species: implications for biomonitoring. Mar. Pollut. Bull. 198, 115842. https://doi.org/10.1016/j.marpolbul.2024.116177.

Bartoń, K., 2025. MuMIn: Multi-model Inference. R package version 1.48.11. Available online: https://CRAN.R-project.org/package=MuMIn.

Bates, D., Mächler, M., Bolker, B., Walker, S., 2015a. Fitting linear mixed-effects models using lme4. J. Stat. Softw. 67, 1–48. https://doi.org/10.18637/jss.v067.i01.

Bates, D., Maechler, M., Bolker, B., Walker, S., Christensen, R.H.B., Singmann, H., Bolker, M.B., 2015b. Package 'lme4'. Convergence 12 (1), 2.

Baudrimont, M., Andrès, S., Durrieu, G., Boudou, A., 2003. The key role of metallothioneins in the bivalve Corbicula fluminea during the depuration phase, after in situ exposure to Cd and Zn. Aquat. Toxicol. 63 (1), 89–102. https://doi.org/10.1016/s0166-445x(02)00134-0.

Bej, A.K., Dicesare, J.L., Haff, L., Atlas, R.M., 1991. Detection of *Escherichia coli* and *Shigella* spp. in water by using the polymerase chain reaction and gene probes for uid. Appl. Environ. Microbiol. 57 (4), 1013–1017.

Bonneris, E., Perceval, O., Masson, S., Hare, L., Campbell, P.G., 2005. Sub-cellular partitioning of Cd, Cu and Zn in tissues of indigenous unionid bivalves living along a metal exposure gradient and links to metal-induced effects. Environ. Pollut. 135 (2), 195–208.

Çağlak, E., Karsli, B., Koral, S., 2020. The effect of depuration on metals, bacteria, and nutrition in *Venus verrucosa* from the Aegean Sea: Benefit and risk for consumer health of Warty Venus. J. Aquat. Food Prod. Technol. 29 (6), 577–591. https://doi.org/10.1080/10498850.2020.1774691.

Chae, M.J., Cheney, D., Su, Y.C., 2009. Temperature effects on the depuration of *Vibrio parahaemolyticus* and *Vibrio vulnificus* from the American Oyster (*Crassostrea virginica*). J. Food Sci. 74, M62–M66. https://doi.org/10.1111/j.1750-3841.2008.01031.x.

Chandrapalan, T., Aimukhanov, A., Kistaubayeva, A., 2021. Functional significance and physiological regulation of essential trace elements in fish. Rev. Fish. Sci. Aquacult. 30 (4), 470–489. https://doi.org/10.1242/jeb.238790.

Chinnadurai, S., Mohamed, K.S., Venkatesan, V., Sharma, J., Kripa, V., 2014. Depuration of bacterial populations in the Indian backwater oyster *Crassostrea madrasensis* (Preston, 1916): effects on surface and bottom held oysters. J. Shellfish Res. 33, 409–414. https://doi.org/10.2983/035.0330.0200.

Chinnadurai, S., Campos, C.J.A., Geethalakshmi, V., Kripa, V., Mohamed, K.S., 2021a. Baseline health risk assessment of trace metals in bivalve shellfish from commercial growing areas in the estuaries of Ashtamudi and Vembanad (Kerala, India). Environ. Sci. Pollut. Res. https://doi.org/10.1007/s11356-021-15284-5.

Chinnadurai, S., Elavarasan, K., Geethalakshmi, V., Kripa, V., Mohamed, K.S., 2021b. Evaluation of static and flow-through depuration system on depuration of naturally contaminated farmed edible oyster *Crassostrea madrasensis* (Preston, 1916). Aquaculture 545, 737141. https://doi.org/10.1016/j.aquaculture.2021.737141.

Chinnadurai, S., Elavarasan, K., Geethalakshmi, V., Kripa, V., Mohamed, K.S., 2022. Temperature, salinity, and body-size influences depuration of heavy metals in commercially important edible bivalve mollusks of India. Chemosphere 307, 135879. https://doi.org/10.1016/j.chemosphere.2022.135879.

Chinnadurai, S., Elavarasan, K., Geethalakshmi, V., Kripa, V., Mohamed, K.S., 2023. Development of a depuration protocol for commercially important edible bivalve mollusks of India: ensuring microbiological safety. Food Microbiol. 110, 104172. https://doi.org/10.1016/j.fm.2022.104172.

Cossa, D., Bourget, E., Pouliot, D., Piuze, J., Chanut, J.P., 1980. Geographical and seasonal variations in the relationship between trace metal content and body weight in *Mytilus edulis*. Mar. Biol. 58 (1), 7–14. https://doi.org/10.1007/bf00386873.

Cranford, P.J., Dowd, M., Grant, J., MacDonald, B.A., 2011. Bivalve filter feeding: variability and limits of the mechanistic filtration model. J. Shellfish Res. 30 (1), 141–150.

Destoumieux-Garzon, D., Canesi, L., Oyanedel, D., Travers, M.A., Charrière, G.M., Pruzzo, C., Vezzulli, L., 2020. *Vibrio*–bivalve interactions in health and disease. Environ. Microbiol. https://doi.org/10.1111/1462-2920.15055.

El-Shenawy, N.S., 2004. Heavy-metal and microbial depuration of the clam *Ruditapes decussatus* and its effect on bivalve behavior and physiology. Environ. Toxicol. 19 (2), 143–153.

Engwa, G.A., Ferdinand, P.U., Nwalo, F.N., Unachukwu, M.N., 2019. Heavy metal toxicity in humans. In: Poisoning in the Modern World: New Tricks for an Old Dog, p. 77.

Esposito, M., Canzanella, S., Danese, A., Pepe, A., Gallo, P., 2022. Essential and non-essential elements in razor clams (*Solen marginatus*, Pulteney, 1799) from the Domitio Littoral in Campania (southwestern Tyrrhenian Sea, Italy). Toxics 10 (8), 452.

Eti, K.F., Tasnim, R., Ferdous, A., Mohiuddin, M., Hossain, M.N., Rahman, M.M., Asaduzzaman, M., 2026. Environmental fingerprints of cultivation site and depth: Variation in shell shape and coloration of the green mussel (*Perna viridis*) from the southeast coast of the Bay of Bengal, Bangladesh. Aquac. Fish. 11 (4), 740–756. https://doi.org/10.1016/j.aaf.2026.01.003.

European Commission, 2005. Commission regulation (EC) no 2073/2005 on microbiological criteria for foodstuffs. Off. J. Eur. Union. https://doi.org/10.2903/j.efsa.2010.1452. L 338/1-L 338/26.

European Commission, 2006. Commission regulation (EC) no. 1881/2006 setting maximum levels for certain contaminants in foodstuffs. Off. J. Eur. Union L 364, 5–24. https://eur-lex.europa.eu/legal-content/EN/TXT/?uri=CELEX%3A02006R1881-20220701/ (accessed 11 October 2025).

FAO, 2016. Species Fact Sheets *Perna Viridis* (Linnaeus, 1758). Food and Agricultural Organization of the United Nations, Rome, Italy. https://www.fao.org/fishery/en/aqspecies/2691/en/ (accessed 23 September 2025).

Fernández, B., Albentosa, M., 2019. Insights into the uptake, elimination and accumulation of microplastics in mussel. Environ. Pollut. 249, 321–329.

Firdaus, A.R., Mubarak, A.S., Tjahjaningsih, W., 2020. The effect of depuration on lead levels of the cockles anadara sp. by using activated carbon as a filter. In: IOP Conf. Ser. Earth Environ. Sci., pp. 1–8. https://doi.org/10.1088/1755-1315/441/1/012036.

Food and Agriculture Organization, World Health Organization, 2002. Explanatory note on heavy metals. In: JECFA Monographs, vol. 1, pp. 19–25. https://www.fao.org/3/y1579e/y1579e03.htm/ (accessed 24 October 2025).

Food Safety and Standards Authority of India, 2011. Food Safety and Standards (Contaminants, Toxins and Residues) Regulations. Retrieved from. https://www.fssai.gov.in/ (accessed 13 October 2025).

Food Standards Australia New Zealand, 2023. Food Standards Code: Maximum Levels of Contaminants and Natural Toxicants. Retrieved from. https://www.foodstandards.gov.au/code/ (accessed 16 October 2025).

Fox, J., Weisberg, S., 2019. An R Companion to Applied Regression, third ed. Sage, Thousand Oaks, CA. Available online: https://www.john-fox.ca/Companion/. (accessed 12 July 2022).

Fukunaga, A., Anderson, M.J., 2011. Bioaccumulation of copper, lead and zinc by the bivalves *Macomona liliana* and *Austrovenus stutchburyi*. J. Exp. Mar. Biol. Ecol. 396, 244–252. https://doi.org/10.1016/j.jembe.2010.10.029.

Gagné, F., Blaise, C., Pellerin, J., Gauthier-Clerc, S., 2007. Ecotoxicological effects of primary-treated urban wastewaters on the freshwater mussel *Elliptio complanata*. Comp. Biochem. Physiol. C Toxicol. Pharmacol. 145 (4), 542–550. https://doi.org/10.1016/j.cbpc.2007.01.019.

Garrett, D.O., Longley, A.T., Aiemjoy, K., Yousafzai, M.T., Hemlock, C., Yu, A.T., Luby, S. P., 2022. Incidence of typhoid and paratyphoid fever in Bangladesh, Nepal, and Pakistan: results of the Surveillance for Enteric Fever in Asia Project. Lancet Glob. Health 10 (7), e978–e988. https://doi.org/10.1016/s2214-109x(22)00119-x.

Health Canada, 2005. Maximum Levels for Chemical Contaminants in Foods. https://www.canada.ca/en/health-canada/services/food-nutrition/food-safety/chemical-contaminants/maximum-levels-chemical-contaminants-foods.html/ (accessed 16 September 2025).

Hoque, N.F., Shakil, A., Sultana, F., Wahab, M.A., Rahman, M.J., Nahiduzzaman, M., Asaduzzaman, M., 2021. Feasibility study of green mussel *Perna viridis* farming in the southeast coast of the Bay of Bengal of Bangladesh. J. Indian Soc. Coastal Agric. Res. 39 (2). https://doi.org/10.54894/jiscar.39.2.2021.111862.

Jannatun, N.J., Mia, M., Jion, M., Islam, M.S., Ali, M.M., Siddique, M.A., Ibrahim, S.M., Pal, S.C., Costache, R., Malafaia, R., Islam, A.R., 2023. Pollution trends and ecological risks of heavy metal (loid)s in coastal zones of Bangladesh: a chemometric review. Mar. Pollut. Bull. 191, 114960. https://doi.org/10.1016/j.marpolbul.2023.114960.

Jebali, J., Chouba, L., Banni, M., Boussetta, H., 2014. Comparative study of the bioaccumulation and elimination of trace metals (Cd, Pb, Zn, Mn and Fe) in the digestive gland, gills and muscle of bivalve *Pinna nobilis* during a field transplant experiment. J. Trace Elem. Med. Biol. 28, 35–41. https://doi.org/10.1016/j.jtemb.2013.12.001.

Jolly, Y.N., Surovi, S.A., Rahman, S.M.M., Kabir, J., Akter, S., Mamun, K.M., Rahman, A., 2022. A probabilistic-deterministic approach towards human health risk assessment and source apportionment of potentially toxic elements (PTEs) in some contaminated fish species. Biol. Trace Elem. Res. https://doi.org/10.1007/s12011-022-03274.

Jones, H.D., Richards, O.G., Southern, T.A., 1992. Gill dimensions, water pumping rate and body size in the mussel *Mytilus edulis* L. J. Exp. Mar. Biol. Ecol. 155, 213–237. https://doi.org/10.1016/0022-0981(92)90064-H.

Kassambara, A., 2023. Rstatix: Pipe-Friendly Framework for Basic Statistical Tests. R package version 0.7.2. Available online: https://CRAN.R-project.org/package=rstatix.

Kumar, V., Sinha, A.K., Rodrigues, P.P., Mubiana, V.K., Blust, R., De Boeck, G., 2015. Linking environmental heavy metal concentrations and salinity gradients with metal accumulation and their effects: a case study in 3 mussel species of Vitória estuary and Espírito Santo bay, Southeast Brazil. Sci. Total Environ. 523, 1–15. https://doi.org/10.1016/j.scitotenv.2015.03.139.

Kuznetsova, A., Brockhoff, P.B., Christensen, R.H.B., 2017. LmerTest package: tests in linear mixed effects models. J. Stat. Softw. 82, 1–26. https://doi.org/10.18637/jss.v082.i13.

Larsen, A.M., Scott Rikard, F., Walton, W.C., Arias, C.R., 2013. Effective reduction of *Vibrio vulnificus* in the Eastern oyster (*Crassostrea virginica*) using high salinity

depuration. Food Microbiol. 34, 118–122. https://doi.org/10.1016/j.fm.2012.11.009.
Larsen, A.M., Rikard, F.S., Walton, W.C., Arias, C.R., 2015. Temperature effect on high salinity depuration of *Vibrio vulnificus* and *V. parahaemolyticus* from the Eastern oyster (*Crassostrea virginica*). Int. J. Food Microbiol. 192, 66–71. https://doi.org/10.1016/j.ijfoodmicro.2014.09.025.
LaTouche, Y., Mix, M., 1982. The effects of depuration, size, and sex on trace metal levels in bay mussels. Mar. Pollut. Bull. 13 (1), 27–29. https://doi.org/10.1016/0025-326X(82)90494-5.
Le, T.H., Truong, T., Tran, L.T., Nguyen, D.H., Pham, T.P.T., Ng, C., 2023. Antibiotic resistance in the aquatic environments: the need for an interdisciplinary approach. Int. J. Environ. Sci. Technol. 20 (3), 3395–3408.
Lee, B.G., Wallace, W.G., Luoma, S.N., 1998. Uptake and loss kinetics of Cd, Cr and Zn in the bivalves *Potamocorbula amurensis* and *Macoma balthica*: effects of size and salinity. Mar. Ecol. Prog. Ser. 175, 177–189. https://doi.org/10.3354/meps175177.
Lenth, R.V., 2024. Emmeans: Estimated Marginal Means, aka Least-Squares Means. R package version 1.10.5. Available online: https://CRAN.R-project.org/package=emmeans.
Leoni, F., Chierichetti, S., Santarelli, S., Talevi, G., Masini, L., Bartolini, C., Rocchegiani, E., Naceur Haouet, M., Ottaviani, D., 2017. Occurrence of *Arcobacter* spp. and correlation with the bacterial indicator of faecal contamination *Escherichia coli* in bivalve molluscs from the Central Adriatic, Italy. Int. J. Food Microbiol. 245, 6–12. https://doi.org/10.1016/j.ijfoodmicro.2017.01.006.
Lewis, M., Rikard, S., Arias, C.R., 2010. Evaluation of a flow-through depuration system to eliminate the human pathogen *Vibrio vulnificus* from oysters. J. Aquacult. Res. Dev. 1, 1–6. https://doi.org/10.4172/2155-9546.1000103.
Lopez-Joven, C., de Blas, I., Ruiz-Zarzuela, I., Furones, M.D., Roque, A., 2011. Experimental uptake and retention of pathogenic and nonpathogenic *Vibrio parahaemolyticus* in two species of clams: *Ruditapes decussatus* and *Ruditapes philippinarum*. J. Appl. Microbiol. 111, 197–208. https://doi.org/10.1111/j.1365-2672.2011.05024.x.
Love, D.C., Lovelace, G.L., Sobsey, M.D., 2010. Removal of *Escherichia coli*, *Enterococcus fecalis*, coliphage MS2, poliovirus, and hepatitis A virus from oysters (*Crassostrea virginica*) and hard shell clams (*Mercinaria mercinaria*) by depuration. Int. J. Food Microbiol. 143, 211–217. https://doi.org/10.1016/j.ijfoodmicro.2010.08.028.
Maheen, M., Mehnaz, Y.N., Jolly, A.K.M., Alam, Rashidul, Kabir, Jamiul, Akter, Shirin, Mamun, Khan M., Rahman, Arafat, Islam, Md Mahfuz, 2022. Prediction of hazardous effect of heavy metals of point source wastewater on fish (*Anabas cobojius*) and human health. Biol. Trace Elem. Res. https://doi.org/10.1007/s12011-022-03378-1.
Malaysian Food Regulation, 1985. Food Regulations 1985 (P.U. (A) 437/85). http://faolex.fao.org/docs/pdf/mal27305.pdf/ (accessed 16 September 2025).
Marescaux, J., Falisse, E., Lorquet, J., Van Doninck, K., Beisel, J.N., Descy, J.P., 2016. Assessing filtration rates of exotic bivalves: dependence on algae concentration and seasonal factors. Hydrobiologia 777 (1), 67–78. https://doi.org/10.1007/s10750-016-2764-0.
Martinez-Albores, A., Lopez-Santamarina, A., Rodriguez, J.A., Ibarra, I.S., Mondragon, A.D.C., Miranda, J.M., Cepeda, A., 2020. Complementary methods to improve the depuration of bivalves: a review. Foods 9 (2), 129.
McGuire, M., Stevely, J., 2009. Invasive Species of Floridas Coastal Waters: The Asian Green Mussel (Perna viridis). the Florida Sea Grant College Program with support from the NOAA, U.S. Department of Commerce, USA. https://doi.org/10.32473/edis-sg094-2009, 3 p.
Metcalf, T.G., Mullin, B., Eckerson, D., Moulton, E., Larkin, E.P., 1979. Bioaccumulation and depuration of enteroviruses by the soft-shelled clam, *Mya arenaria*. Appl. Environ. Microbiol. 38, 275–282. https://doi.org/10.1128/aem.38.2.275-282.1979.
Ministry of Health, Labour and Welfare (Japan), 2020. Standards for the Specifications and Standards for Food, Additives, etc. https://www.jetro.go.jp/ext_images/en/reports/regulations/pdf/foodext2010e.pdf/ (accessed 16 September 2025).
Mokrani, A., Li, J.A., Li, Q., Liu, S., 2025. Toward understanding mechanistic regulation of body size and growth control in bivalve mollusks. Rev. Aquac. 17 (1), e12962.
Muniain-Mujika, I., Girones, R., Lucena, F., 2000. Viral contamination of shellfish: evaluation of methods and analysis of bacteriophages and human viruses. J. Virol. Methods 89, 109–118. https://doi.org/10.1016/s0166-0934(00)00208-1.
National Shellfish Sanitation Program (NSSP), 1990. Manual of Operations, Part II: Sanitation of the Harvesting, Processing and Distribution of Shellfish. Public Health Service, US Food and Drug Administration.
Oranusi, S., Effiong, E.D., Duru, N.U., 2018. Comparative study of microbial, proximate and heavy metal compositions of some gastropods, bivalve and crustacean seafood. Afr. J. Clin. Exp. Microbiol. 19 (4), 291–302.
Pan, K., Wang, W.X., 2009. Biodynamics to explain the difference of copper body concentrations in five marine bivalve species. Environ. Sci. Technol. 43, 2137–2143. https://doi.org/10.1021/es802888u.
Pasinszki, T., Prasad, S.S., Krebsz, M., 2023. Quantitative determination of heavy metal contaminants in edible soft tissue of clams, mussels, and oysters. Environ. Monit. Assess. 195 (9), 1066.
Phuvasate, S., Su, Y.C., 2013. Impact of water salinity and types of oysters on depuration for reduction of *Vibrio parahaemolyticus* in Pacific oysters (*Crassostrea gigas*). Food Microbiol. 34, 287–292. https://doi.org/10.1016/j.foodcont.2013.01.025.
Phuvasate, S., Chen, M.H., Su, Y.C., 2012. Reductions of *Vibrio parahaemolyticus* in Pacific oysters (*Crassostrea gigas*) by depuration at various temperatures. Food Microbiol. 31, 51–56. https://doi.org/10.1016/j.fm.2012.02.004.
Pinheiro, J., Bates, D., R Core Team, 2024. Nlme: Linear and Nonlinear Mixed Effects Models. R package version 3.1-166. Available online: https://CRAN.R-project.org/package=nlme.
Power, U.F., Collins, J.K., 1990. Elimination of coliphages and *Escherichia coli* from mussels during depuration under varying conditions of temperature, salinity, and food availability. J. Food Prot. 53, 208–212. https://doi.org/10.4315/0362-028x-53.3.208.
R Development Core Team, 2024. R: A Language and Environment for Statistical Computing, Version 4.4.2. R Foundation for Statistical Computing, Vienna, Austria. Available online: https://www.r-project.org/ (accessed 10 June 2025).
Rahman, M.S., Hossain, M.S., Ahmed, M.K., Akther, S., Jolly, Y.N., Akhter, S., Kabir, M.J., Choudhury, T.R., 2019. Assessment of heavy metals contamination in selected tropical marine fish species in Bangladesh and their impact on human health. Environ. Nanotechnol. Monit. Manage. 11, 100210. https://doi.org/10.1016/j.enmm.2019.100210.
Rahn, K., De Grandis, S.A., Clarke, R.C., McEwen, S.A., Galan, J.E., Ginocchio, C., Gyles, C.L., 1992. Amplification of an *invA* gene sequence of *Salmonella typhimurium* by polymerase chain reaction as a specific method of detection of *Salmonella*. Mol. Cell. Probes 6 (4), 271–279.
Rainbow, P.S., 2002. Trace metal concentrations in aquatic invertebrates: why and so what? Environ. Pollut. 120, 497–507. https://doi.org/10.1016/s0269-7491(02)00238-5.
Rajagopal, S., Venugopalan, V.P., Velde, G.V.D., Jenner, H.A., 2006. Greening of the coasts: a review of the *Perna viridis* success story. Aquat. Ecol. 40, 273–297. https://doi.org/10.1007/s10452-006-9032-8.
Rajesh, K.V., Mohamed, K.S., Kripa, V., 2001. Influence of algal cell concentration, salinity and body size on the filtration and ingestion rates of cultivable Indian bivalves. Indian J. Mar. Sci. 30, 87–92.
Rakib, M.R.J., Jolly, Y.N., Enyoh, C.E., Khandaker, M.U., Hossain, M.B., Akther, S., Alsubaie, A., Raheem, A., Almalki, S.A., Bradley, D.A., 2021. Levels and health risk assessment of heavy metals in dried fish consumed in Bangladesh. Sci. Rep. 11, 14642. https://doi.org/10.1038/s41598-021-93989w.
Richards, G.P., 1988. Microbial purification of shellfish: a review of depuration and relaying. J. Food Prot. 51, 218–251. https://doi.org/10.4315/0362-028x-51.3.218.
Riisgård, H.U., Larsen, P.S., 2025. Effect of temperature on filtration in the blue mussel, Mytilus edulis—our present understanding. J. Mar. Sci. Eng. 13 (11), 2033. https://doi.org/10.3390/jmse13112033.
Riisgård, H.U., Larsen, P.S., Pleissner, D., 2018. Allometric equations for maximum filtration rate in blue mussels *Mytilus edulis* and importance of condition index. Helgol. Mar. Res. 68 (2), 193–198. https://doi.org/10.1007/s10152-013-0377-9.
Rivera, I.N., Chun, J., Huq, A., Sack, R.B., Colwell, R.R., 2001. Genotypes associated with virulence in environmental isolates of Vibrio cholerae. Appl. Environ. Microbiol. 67 (6), 2421–2429.
Rodrick, G.E., Schneider, K.R., 1991. Vibrios in depuration. In: Otwell, W.S., Rodrick, G.E., Martin, R.E. (Eds.), Molluscan Shellfish Depuration, pp. 115–125. https://doi.org/10.1201/9781351074810-10.
Saed, K., Ismail, A., Omar, H., Kusnan, M., 2004. Heavy metal depuration in flat tree oysters *Isognomon alatus* under field and laboratory conditions. Toxicol. Environ. Chem. 86, 169–177. https://doi.org/10.1080/02772240400007039.
Saritha, K., Mary, D., Patterson, J., 2015. Nutritional status of green mussel *Perna viridis* at Tamil Nadu, Southwest Coast of India. J. Nutr. Sci. https://doi.org/10.4172/2155-9600.s14-003.
Serratore, P., 2017. Supply chain of the molluscan shellfish: overview of key food safety issues. Madridge J. Food Technol. 2, 99–108. https://doi.org/10.18689/mjft-1000115.
Sethabutr, O., Venkatesan, M., Yam, S., Pang, L.W., Smoak, B.L., Sang, W.K., Isenbarger, D.W., 2000. Detection of PCR products of the *ipaH* gene from *Shigella* and enteroinvasive *Escherichia coli* by enzyme-linked immunosorbent assay. Diagn. Microbiol. Infect. Dis. 37 (1), 11–16.
Shumway, S.E., 1977. Effect of salinity fluctuation on the osmotic pressure and Na^+, Ca^{2+}, and Mg^{2+} ion concentrations in the hemolymph of bivalve mollusks. Mar. Biol. 41, 153–177. https://doi.org/10.1007/BF00394023.
Shumway, S.E., Koehn, R.K., 1982. Oxygen consumption in the American oyster *Crassostrea virginica*. Mar. Ecol. Prog. Ser. 59–68. https://doi.org/10.3354/meps009059.
Strubbia, S., Schaeffer, J., Besnard, A., Garry, P., Desdouits, M., Guyader, F.S., 2020. Metagenomic to evaluate norovirus genomic diversity in oysters: impact on hexamer selection and targeted capture-based enrichment. Int. J. Food Microbiol. 323, 108588. https://doi.org/10.1016/j.ijfoodmicro.2020.108588.
Suffredini, E., Mioni, R., Mazzette, R., Bordin, P., Serratore, P., Fois, F., Piano, A., Cozzi, L., Croci, L., 2014. Detection and quantification of *Vibrio parahaemolyticus* in shellfish from Italian production areas. Int. J. Food Microbiol. 184, 14–20. https://doi.org/10.1016/j.ijfoodmicro.2014.04.016.
Taib, A.M., Madin, J., Ransangan, J., 2016. Density, recruitment and growth performance of Asian green mussel (*Perna viridis*) in Marudu Bay, Northeast Malaysian Borneo, three years after a massive mortality event. Songklanakarin J. Sci. Technol. 38 (6), 631–639.
Tantanasarit, C., Babel, S., Englande, A.J., Meksumpun, S., 2013. Influence of size and density on filtration rate modeling and nutrient uptake by green mussel (*Perna viridis*). Mar. Pollut. Bull. 68 (1–2), 38–45.
U.S. Food and Drug Administration, 2024. Fish and Fishery Products Hazards and Controls Guidance. https://www.fda.gov/food/seafood-guidance-documents-regulatory-information/fish-and-fishery-products-hazards-and-controls/ (accessed 28 September 2025).
Wang, Y., Hu, M., Wong, W.H., Shin, P.K.S., Cheung, S.G., 2011. The combined effects of oxygen availability and salinity on physiological responses and scope for growth in the green-lipped mussel *Perna viridis*. Mar. Pollut. Bull. 63, 255–261. https://doi.org/10.1016/j.marpolbul.2011.03.030.
Wen-Xiong, W., Fisher, N.S., 1996. Assimilation of trace elements by the mussel *Mytilus edulis*: effects of diatom chemical composition. Mar. Biol. 125 (4), 715–724. https://doi.org/10.1007/bf00349254.

Wickham, H., Averick, M., Bryan, J., Chang, W., McGowan, L.D.A., François, R., Yutani, H., 2019. Welcome to the Tidyverse. J. Open Source Softw. 4 (43), 1686. https://doi.org/10.21105/joss.01686.

Wickham, H., François, R., Henry, L., Müller, K., Vaughan, D., 2023. Dplyr: A Grammar of Data Manipulation. R package version 1.1.4. Available online: https://CRAN.R-project.org/package=dplyr.

World Health Organization, 2020. Cadmium – JECFA. In: WHO Food Additives Series, vol. 84. https://apps.who.int/food-additives-contaminants-jecfa-database/Home/Chemical/1376/ (accessed 22 September 2025).

Wright, A.C., Fan, Y., Baker, G.L., 2018. Nutritional value and food safety of bivalve molluscan shellfish. J. Shellfish Res. 37 (4), 695–708.

Wu, S., Wang, L., Zhang, P., El-Aty, A.M.A., Zeng, H., Mu, P., Wang, H., Chen, M., Duan, J., 2024. The toxicity of mercury and its chemical compounds: molecular mechanisms and environmental and human health implications. ACS Omega 9 (5), 5092–5118. https://doi.org/10.1021/acsomega.3c07047.

Yang, S.C., Lin, C.H., Aljuffali, I.A., Fang, J.Y., 2017. Current pathogenic *Escherichia coli* foodborne outbreak cases and therapy development. Arch. Microbiol. 199 (6), 811–825. https://doi.org/10.1007/s00203-017-1393-y.

Yang, C., Liu, Q., Meng, X., Cao, L., Liu, B., 2020. Depuration of cadmium from *Chlamys farreri* by ZnSO4, EDTA–Na2 and sodium citrate in short time. Chemosphere 244, 125429. https://doi.org/10.1016/j.chemosphere.2019.125429.

Yap, C.K., Al-Mutairi, K.A., 2025. Depuration kinetics of potentially toxic metals (Hg, Co and Cr) in *Perna viridis*: implications for biomonitoring, environmental management, and planetary health. J. Fish. 13 (1), 131202. https://doi.org/10.17017/j.fish.751.

Yin, Q., Wang, W.X., 2017. Relating metals with major cations in oyster *Crassostrea hongkongensis*: A novel approach to calibrate metals against salinity. Sci. Total Environ. 577, 299–307. https://doi.org/10.1016/j.scitotenv.2016.10.185.

Zhao, Y., Liu, X., Chen, M., 2021. Bioaccumulation and biotransformation of inorganic arsenic and chromium in marine bivalves. Chemosphere 268, 129312. https://doi.org/10.1016/j.chemosphere.2021.130270.